VOL. 22, NO. 1 • JANUARY 1983

Microwaves & RF

A HAYDEN PUBLICATION

The evolution of mm-wave synthesizers

. . . eases complex impedance measurements



AUTOMATION: Power device testing/Transmission and return-loss measurements/Industry action to improve ATE standards **INSTRUMENTATION:** Electrically short dipoles **DESIGN:** New DBS receiver uses coplanar waveguide/A 600-W, 2-to-30-MHz MOSFET amplifier

CONTENTS: Page 6

Microwaves & RF

JANUARY 1983 • VOL. 22, NO. 1



about the cover

A limiting factor in the accurate evaluation of millimeter-wave networks—the lack of high-frequency signals with low phase noise—has been overcome with the advent of a series of frequency synthesizers capable of 26.5-to-110-GHz swept operation. Quiet Impatt oscillators provide the clean signals. (Photograph courtesy of Hughes Aircraft Co., Electron Dynamics Div., and the A. W. Briggs Advertising Agency.)

p. 103

departments

15 Feedback
17 Editorial
49 R&D Roundup
62 For Your Personal Interest
134 Infocenter
136 Looking Back
136 Looking Ahead

news

39 **Coplanar waveguide may lead to inexpensive DBS TVROs.** Three 12-GHz receivers from Comsat Laboratories could make it happen.

31 ARFTG streamlines round-robin calibration program . . . **42** Philips develops HF-based NMR system to speed medical diagnosis in humans . . . **42** Alpha shifts emphasis . . . **44** New facility handles VORTAC antenna upgrade . . . **44** $2.75 million awarded to "Centers of Excellence" . . . *45 Over-the-horizon radar detailed at IEE Radar '82 conference . . . **47** Millimeter-wave telescope to explore the universe . . . **54** Free trade is AEA objective for '83 . . . **61** Pave mover proves formidable . . . **61** Wasp flies alone

19 The Front End • **53** Financial News • **56** People • **60** On The Agenda

design features

64 **ATE Systems Offer Versatile Accuracy.** Edward Cernek, Jr., of TRW Semiconductors, Inc., compares the use of automatic and manual test systems for semiconductor evaluation.

72 **New Transition Expands Options For SSS Users.** Israel Galin, of Aerojet ElectroSystems Co., details a new waveguide-to-suspended-stripline transition.

74 **Analyzing Short Dipoles With Nonlinear Loads.** Motohisa Kanda, of the National Bureau of Standards, presents two nontraditional techniques, one analytical and one numerical.

80 **Automated System Eases Loss Measurements.** Dr. Peter Lacy and Ivan Andres, from Wiltron, unveil a technique for measuring transmission and return loss using coaxial air lines.

89 **Four MOSFETs Deliver 600 W Of RF Power.** H.O. Granberg, of Motorola Semiconductor Products, presents an amp design that doesn't rely on power combiners and splitters.

94 **Design Considerations For Deep-Space Transmitters.** In part 2 of *Deep-Space Laser Communications,* Morris Katzman, of The Aerospace Corp. , shows how transmitters operate at high data rates.

product technology

103 **Millimeter-Wave Synthesizers Come Of Age.** In this month's cover feature, Ken Y. Ishikawa and Chung-Ta Hsieh, of Hughes Aircraft, introduce a broadband millimeter-wave frequency synthesizer.

112 **Analyzing The Needs Of RF Signal Generation.** Mark Capra, of Hewlett-Packard, details the requirements of RF test signals . . . Features—**114** Miniature attenuators provide economical DC-to-26.5-GHz coverage . . . **119** Directional components aid the new breed of signal sources . . . **124** Stand-alone system calibrates power sensors

*121 New Products • **131** Application Notes • **133** New Literature

* *Domestic Editions Only*

ATE Systems Offer Versatile Accuracy

The choice between a manual and an automatic semiconductor test setup usually depends on the type of measurements to be performed. This guide explains when it is advantageous to rely on the versatility of an ATE system.

Edward Cernek, Jr., Senior Engineer, TRW Semiconductors, Inc., 14520 Aviation Blvd., Lawndale, CA 90260.

AUTOMATIC test systems for semiconductors have grown in sophistication as a result of the ever-increasing demands for more complex test routines and greater productivity. They are now able to verify product performance prior to shipments at higher and higher operating frequencies and power levels. They can perform test sequences that include multiple frequencies, levels, and bias conditions. These systems (see Fig. 1) also perform clerical duties such as binning, matching, and serialization of parts. In comparison, manual test setups are still restricted to testing at single power levels and frequencies.

It should be remembered, however, that automated test systems are not merely automatic manual setups; some of the instrumentation is unique to an automatic test area. Examples are the error-corrected vector measurements impractical for manual testing because of the time element involved. Keep in mind that before an automatic test system is constructed, it is important to know whether a need for it exists. RF power transistor testing, for instance, is constrained by the following details:

- Test fixtures are very specialized and are often supplied by a customer, precluding the use of automatic insertion equipment.
- The test rate is limited by the instrumentation and the time for the device under test (DUT) to thermally stabilize. It is not limited by the processor speed.

On the other hand, if accuracy is an important criterion, then an ATE system is the clear choice, even though it may not always be the faster of the two systems.

A few examples can illustrate how the speed of the systems differ. In the first case, a device is tested manually, at one drive level, one supply voltage, and one frequency. The equipment is calibrated by a technician before the test. All the operator has to do is to insert the DUT (an action which will also apply the collector bias) and check the instruments for proper performance. The tolerance margins are high enough so that even a glance at the instruments will reveal if the unit is acceptable. A typical test rate under these conditions is 300 devices per hour. In contrast, the ATE system will test about 180 devices per hour when following the same test sequence. The ATE will perform these simple tests with the same exacting accuracy as it does much more complex tests. The second case features a device tested at two frequencies, two supply voltages, and a variety of input and output conditions. Each unit must be serialized, data-logged, and classified for insertion phase and gain so that it can be marked appropriately later on. The ATE system will run about 80 units an hour, and give the operator the bin codes for the units



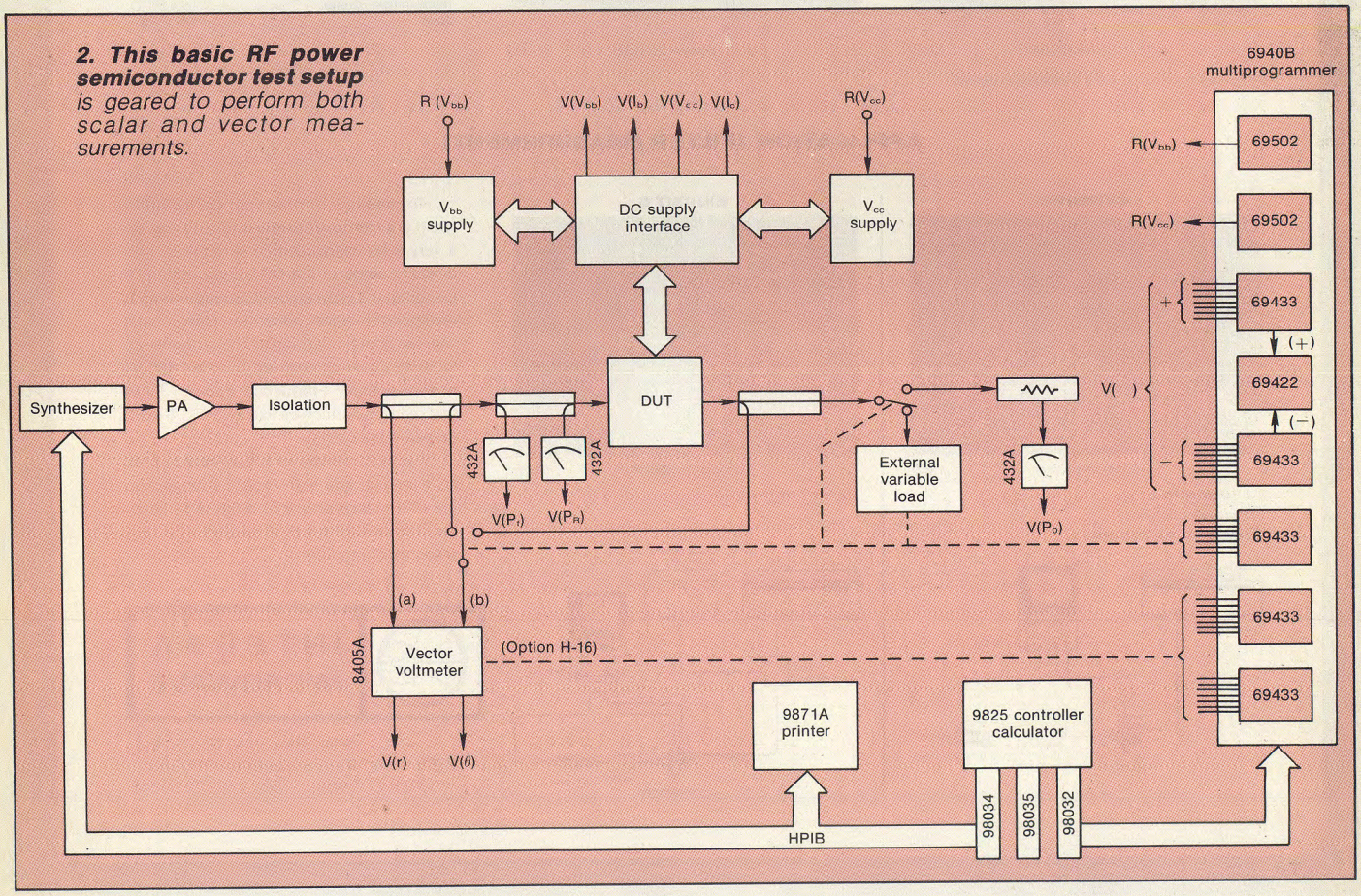
1. The author instructs a technician *on the procedure for running a semiconductor test. This particular ATE system will test devices as high as 512 MHz.*

tested. The manual test setup would only be able to test about five units per hour under these conditions.

The clerical duties performed by an ATE setup, such as binning and serialization, often seriously hinder an operator's productivity, not to mention the fact that they are subject to transcription error. Once the complexity of a test procedure has exceeded a certain threshold, the operator's effectiveness drops and errors increase, especially when that operator is testing a number of different parts during the course of a day. The ATE takes a great deal of tedium away from the operator by performing these chores.

An important part of any test setup is the semiconductor test fixture. In many cases, more than one fixture may be used, and the readings obtained by each will differ to some extent when testing the same device. It is extremely difficult, if not impossible, to construct test fixtures for RF power transistors that are similar enough

(continued on p. 67)



2. This basic RF power semiconductor test setup *is geared to perform both scalar and vector measurements.*

for the differences to be negligible. Some kind of correction must be determined and applied.

The performance of RF power semiconductors is very load dependent. When it is possible to fine tune the load side of the test fixture for optimum performance, the VSWR of the load is not important. Then, the primary concern is knowing the coupling coefficient to the output power meter. Once this fairly frequency-independent coupling characteristic is known, the system can be used at different frequencies without recalibration. When it is not possible to tune the test fixture's load side, the lowest possible VSWR is crucial for testing success.

Another parameter that is important when the input side of the test fixture can't be tuned is the measurement of reflected power. The objective, in this case, is to obtain and maintain a given device input impedance. The reflected power specification, in conjunction with a fixed-impedance matching structure, is a way of placing a boundary around the acceptable variations in device input impedance.

A directional coupler is used to determine the reflected power. Provided that the test specifications are not very restrictive, the directivity of the coupler is not critical. In this situation, a "max-flat" coupler, which is designed to maintain a relatively constant coefficient of coupling over a given bandwidth, can be used to minimize frequency-dependent calibration difficulties. When the test specifications are restrictive, a "reflectometer" coupler is required. It is designed to maximize directivity over a given bandwidth. (Design tradeoffs in this kind of device usually mean increased coupling variations.) With this coupler, calibration factors must be determined and applied. If the test accuracy requirements exceed a certain point, then error correction procedures must be used. These call for the utilization of vector measurements and the determination of a two-dimensional matrix with complex coefficients for each frequency of interest. Reflected power can usually be calculated from vector measurements analyzed in conjunction with a complex matrix.

Another consideration in the establishment of a test setup is the power supply: RF power semiconductors are very sensitive to power-supply voltage variations. Saturated power output varies approximately as the square of the supply voltage. For example, a transistor loaded to produce 50 W of saturated output power when operated from a 12-V supply will exhibit a supply voltage sensitivity of about 8 W/V. The corresponding supply current is 8 A. Voltage drops occur in the wiring between the supply and the test fixture. Remote sensing techniques must be applied carefully because moderate levels of RF energy in the immediate vicinity may cause problems for the power supply's internal regulation circuitry.

High-current power supplies typically up-program much faster than they down-program, especially under no-load conditions. Care must be taken when varying the supply voltage to the DUT. One way is to switch in a pull-down resistor during the programming of the ATE setup.

Choosing a controller

The choice of a system controller is probably the most important factor in the long-term success of an ATE system. These systems are typically developed and maintained by the engineering staff, rather than by a computer staff. Therefore, if engineers build their own controllers, they must be ready to develop and support the software as well as the hardware. Unless this approach is the only way to achieve the test objectives, it should be avoided. If a controller is to be purchased, the choice is between two basic categories: a general purpose unit or a ROM-resident interpreter. Using even a small general-purpose computer requires a working knowledge of the various software utilities (text editor, compiler, linker, and file management system) and the discipline of a computer professional to keep the software maintained, updated, and flexible. Despite these drawbacks, this approach is more versatile. It permits assembly-language coding for fast routines and high-level-language coding for areas where speed is less critical. A ROM-resident interpreter, on the other hand, is bound by the instruction set that has been implemented and is generally slower in execution and I/O than a general-purpose computer. Still, the software is easier to develop and maintain, especially for engineers who have a limited computer background. The interpreter approach is a good first choice if the other factors are within acceptable limits, since RF power ATE systems are primarily limited in their test rate by the speed of the instrumentation.

Creating the interface

There are a number of ways to connect the controller to the test instrumentation. Two popular approaches are the IEEE-488 (GPIB) interface bus and the "multiprogrammer," an I/O expander. The former requires that each instrument connected to the bus have interface circuitry built into it, in addition to the circuitry needed for its measurement functions. Virtually all of the interface hardware design is done by the equipment manufacturer. Communication between the instruments and the controller is usually in the form of ASCII characters that can be written to and read from the instruments by the controller within the framework of existing high-level languages such as BASIC.

For older instruments, the bus capability must be retrofit. This sometimes results in a rather limited control capability. Some controls, such as rotary switches, are often difficult to replace without seriously affecting an instrument's performance. As a consequence, a great many retrofit conversions tend to supply more data-gathering capability than control capability. In contrast, new instruments are designed with automation in mind. A single bus command can cause these units to execute a complex series of measurements and return a thoroughly "digested" result. For example, the following "HPL" program fragment might cause a model 1980B programmable oscilloscope (Hewlett-Packard Co.) to measure and store 501 time points of data and average 64 measurements at each time point:

```
wrt 728 "DGS1"          (1)
```

This fragment shows how the bus approach focuses on convenience and control. Its weaknesses are higher costs and lower reliability. The costs are higher simply because the interface circuitry is built into each instrument. Reliability is lower because connectors are used rather than soldered contacts. This is particularly true as the number of instruments on the bus increases.

It's possible to automate older, pre-bus instruments by using a multiprogrammer, that is, a card cage connected to the controller. Such a cage can contain a variety of different

(concluded on p. 70)

cards (printed-circuit boards designed to perform relatively simple functions). For example, a card might be an analog-to-digital converter (ADC) or a digital-to-analog converter (DAC), or it might provide a programmable resistance value or some number of programmable relay contacts. Each card can be independently addressed by the controller. Thus, a simple test system can be automated by the addition of a controller and a multiprogrammer containing an appropriate number of cards.

The multiprogrammer approach is relatively inexpensive, although the software is more difficult to write and the language used must be capable of low-level operations. The programmer may need access to certain physical registers in the controller. The complexities of this system can be readily seen in the programming language. For example, the following "HPL" subroutine (Eq. 2) might cause a model 69422A ADC (Hewlett-Packard Co.) to perform a measurement; the 12-bit, 2's complement result is then converted to a voltage value.

```
"ReadV":moct;wtb 9,170260,
50000,170240;wti 0,11;wti 4,50000
band(rdi 4,7777)→pl; mdec; otdpl pl;
ret .0005(pl-4096(pl>2047))          (2)
```

The software consequences of each approach are roughly equivalent if the hardware configuration is stable, as is the case for most production-oriented ATE systems. Initial efforts are needed to develop a "driver" routine that can be referenced elsewhere in the system. Once this is accomplished, the realities of the physical interface become invisible. For example, communication with a power-supply driver routine is in terms of volts rather than in terms of an internal code—the bit and byte activity is invisible.

ATE in action

A typical RF power semiconductor ATE system is shown in Fig. 2. It tests devices that operate at supply voltages as high as 35 V, supply currents as high as 30 A, output levels as high as 100 W, and frequencies ranging from 100 to 512 MHz.

Scalar RF measurements are performed with model 435 thermal power meters (Hewlett-Packard). These measurements can be done at a relatively high speed if the reflection accuracy requirements are modest. The directional coupler is a model 3020 dual directional device (Narda Microwave). It is a reflectometer type and is located electrically close to the test fixture, so the degradation of the intrinsic directivity of the coupler is minimized. A short piece of high-quality coaxial cable with type-N connectors is used to hook up the test fixture. (The term "high quality" here refers to the stability of the electrical properties of the cable when it is flexed or physically manipulated, not necessarily to its loss.) The magnitude of the directivity error can be determined under these conditions of stability and appropriate guard bands instituted.

Vector measurements are performed with a model 8405 vector voltmeter (Hewlett-Packard) using a special remote option (H-16). This is an economical way to perform vector measurements below 1 GHz and under CW conditions. The directional coupler used in the vector measurements can be located anywhere on the input side of the system. Still, it is a good idea to begin with the best intrinsic measurement capability possible. The usefulness of the error correction matrix depends upon a set of components with electrical properties unchanged by time. For these vector measurements, the interconnections are made with semirigid coaxial cable, since a mechanically stable configuration is essential.

A model 9825B desktop controller (Hewlett-Packard) of the interpreter type was chosen for the standard controller. The HPL language is execution- and memory-efficient, and has numerous instructions for control and measurement applications. In addition, an engineer who has briefly studied FORTRAN or BASIC can understand the HPL programs in about a week and write simple test routines in another week.

Data acquisition is transparent in all systems. Data is recorded on tape cartridges and may be transmitted to a larger computer through a modem at any time. Large data-base management is performed by a minicomputer or mainframe computer. Data acquisition and error correction are carried out by the desktop computers, while administration and analysis are performed by the mainframe.

The software has been written with human interaction in mind. Operators are prompted at various points in the test process when their intervention is required. Responses are checked for their validity, and appropriate messages are issued in the event of an error. Most difficulties are handled by the operator, although a few require supervisor-level assistance. Fortunately, little engineering involvement is needed since diagnostic software identifies most failures that have occurred more than once.

The interface includes both an I/O expander (the Hewlett-Packard model 6940B multiprogrammer) and the IEEE-488 bus. The I/O expander is used for most functions: resistive power supply programming, multiplexed ADC for analog signals (power-supply voltages and currents, power-meter recorder outputs, and vector voltmeter magnitude and phase), and relay contacts for various switching functions. The GPIB is used to drive the frequency synthesizer and printer.

By using multiple identical controllers as a feature in the ATE system, as well as a backup system, downtime has been reduced to an hour in many cases. It is also true that most systems are capable of manual operation if the situation warrants it. In short, there are many advantages to the establishment of an ATE system, especially when the test procedure is one that is already becoming too complicated for a manual test area. ●●

New Transition Expands Options For SSS Users

The increasing popularity of printed components using suspended stripline on dielectric substrates has created a need for new methods to couple from waveguide to suspended stripline.

Israel Galin, Senior Technical Staff Specialist, Aerojet ElectroSystems Co., 110 W. Hollyvale St., Azuza, CA 91702.

PRINTED components, especially those using suspended stripline on dielectric substrates (SSS), are receiving increasing consideration in millimeter-wave applications. Since millimeter-wave measurement systems are constructed in waveguide, the use of SSS has created a need for efficient transitions between waveguides and SSS-printed components. Unfortunately, the availability of such transitions has been lacking.

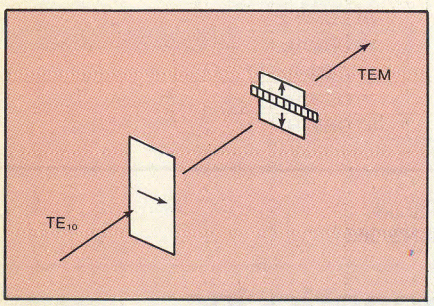
The literature on transitions from waveguides to microwave integrated circuits contains descriptions of several techniques, including ridge, Van Heuven and probe types. A basic difference between the various techniques is the orientation of the mode-coupling region, where the transition is made from the dominant TE_{10} waveguide mode to the TEM mode in the printed circuit. The variety of transitions available insures that appropriate techniques can be found for differing applications. This has not been true for waveguide-to-SSS transitions, for which only transitions of the probe type have been reported.[1-4]

This article describes a new wideband and compact technique for waveguide-to-SSS transition that is particularly attractive for millimeter-wave applications.

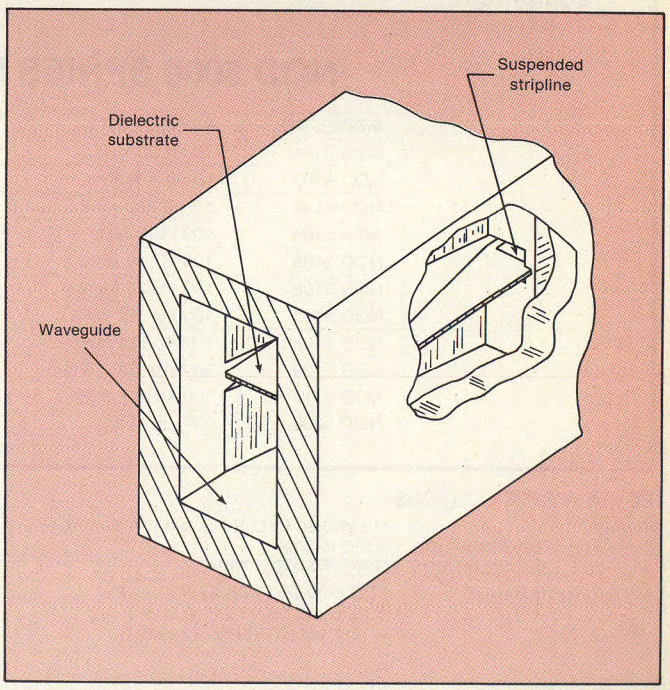
The new transition technique employs a structure along the propagation path inside the waveguide to create a region in which the mode propagating is gradually changed from TE_{10} to TEM. The electrical field in the waveguide is symmetrically split, and the two portions are gradually rotated in opposite directions until each has changed direction by 90 degrees. At this point, the main portions of the E-field have been transferred from the TE_{10} mode of the waveguide to the TEM mode of the SSS (Fig. 1).

Mechanical characteristics

To accomplish this electrical transition, two identical, gradually tapered ridges are built on the inside of the narrow walls of the waveguide (Fig. 2). A dielectric substrate is positioned in the middle of the waveguide, bridging its broad walls (along the E-field). This substrate has a gradually tapered ridge printed on one side of the dielectric, while the other side of the dielectric is stripped of any metallization. The printed ridge is constructed to complement the two ridges built on the narrow walls. At the



1. The concept of the new transition *splits the E-field and rotates the components 90 degrees.*



2. Mechanically, the transition employs a dielectric substrate *positioned between two tapered ridges.*

plane where the tapered ridges reach half the waveguide height, the narrow-wall ridges abruptly bridge the opposite wide walls of the waveguide. At this same plane, the printed ridge is cascaded with the printed transmission line.

A prototype design

An experimental transitions structure based on this technique has been built and tested (Fig. 3). Two transitions, separated by a suspended-stripline line, were cascaded to obtain a symmetrical waveguide-to-stripline-to-waveguide section.

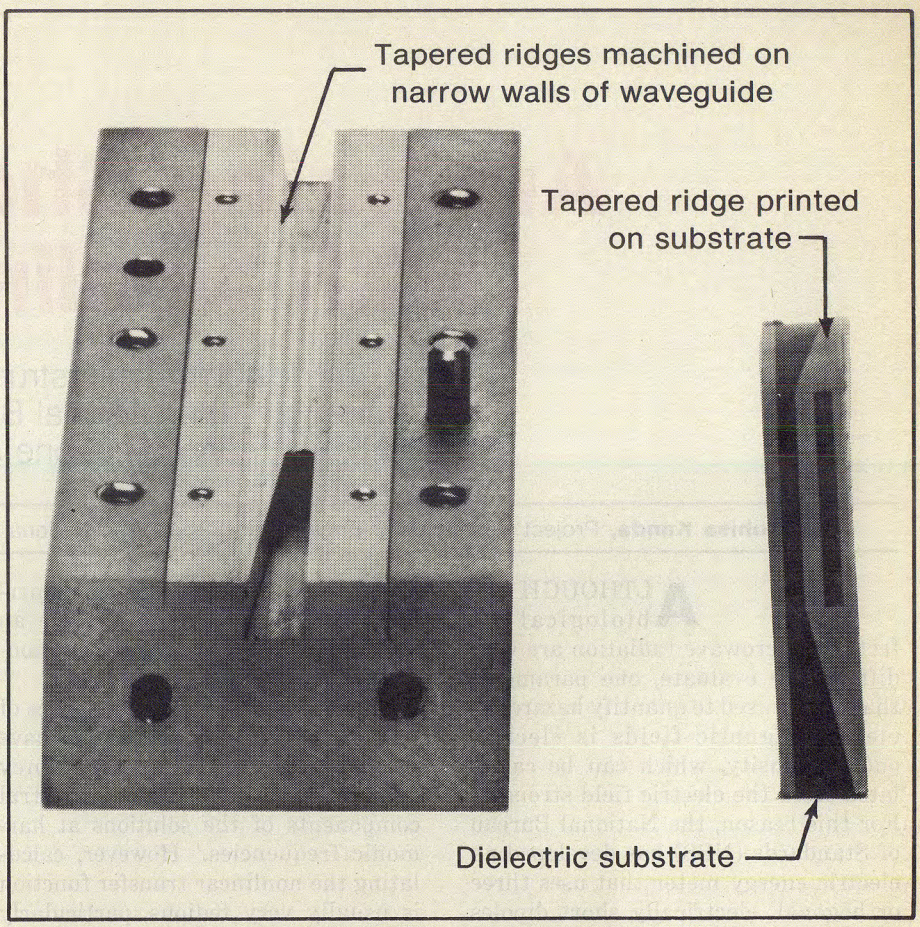
The prototype was designed to operate at K-band (26.5 GHz to 40.0 GHz) and used a CuFlon substrate with a dielectric constant of $\epsilon_r = 2.2$ and a thickness of 0.005 in. in conjunction with a WR-28 waveguide. The choice of material and thickness was influenced by a desire to scale the transition, eventually, into the G-band (140 GHz to 220 GHz), which would require a scale factor of approximately five (or 200 GHz ÷ 40 GHz). Since the thinnest copper-plated CuFlon available is 0.001-in. thick, a thickness of 0.005 in. was required for the "low-frequency" K-band prototype. A low dielectric constant was chosen to maintain a low filling factor for the dielectric in the suspended-stripline channel.

The choice of the dimensions of the suspended-stripline channel, 0.140 × 0.070 in., was guided by the desire to suppress waveguide modes and to insure practical dimensions for structures designed for higher frequencies.

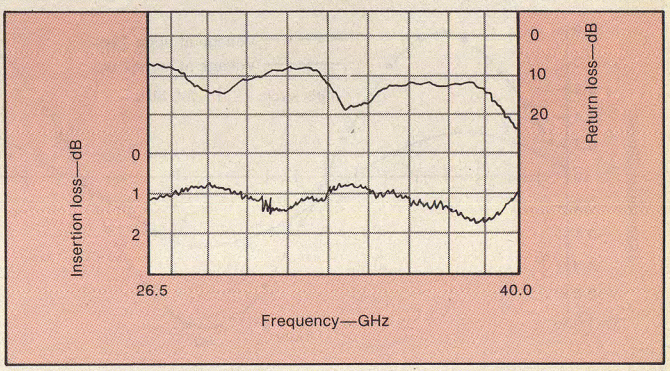
A 1-in. suspended-stripline, 50-ohm line was located in the suspended channel. The width of the line was derived by assuming a transmission-line strip in a channel with an $E_{eff} \approx 1$. As stated earlier, the suspended line bridges the transitions.

The printed, tapered sections of the two transitions were chosen to be 0.65 in. long, approximately 1.5 times the λ_g in the waveguide in the middle of the K-band, and the estimated minimum length required for a smooth transition from TE_{10} to TEM. The printed, tapered sections were of the same length as the complementary taper along the narrow walls of the waveguide.

The prototype transition's performance was measured from an input to an output waveguide (Fig. 4). The maximum transmission loss in a bandwidth from 26.5 GHz to 40 GHz was found to be less than 2.0 dB and, in fact, was less than 1.0 dB in most of the band. That total loss included the loss in the 50-ohm suspended-stripline section as well as in the two transition regions. Since the estimated loss in the suspended stripline was 0.4 dB, the loss for each transition was less than 0.8-dB maximum (less than 0.3 dB in most of the band). The return loss for the prototype device was measured at better than 10 dB, which provided a VSWR of 2:1. ●●



3. This photo shows half a waveguide (narrow wall at bottom) *to illustrate how the tapered ridges are machined onto the broad walls. The dielectric substrate is shown separately.*



4. The insertion loss shown includes an estimated 0.4 dB *in a suspended stripline and losses in each of two transitions.*

References

1. R.H. Knerr, "A New Type of Waveguide-to-Stripline Transition," *IEEE Transactions*, MTT-16 (March 1968).
2. D. Rubin and A.R. Hislop, "Design Techniques for Suspended Substrate and Microstrip," *Microwave Journal* (October 1980).
3. G. Glance and R. Trambarylo, "A Waveguide-to-Suspended-Stripline Transition," *IEEE Transactions*, MTT-21 (February 1973).
4. P.T. Parrish, A.G. Cardiasmenos, and I. Galin, "A 94-GHz Beamlead Balanced Mixer," *IEEE Transactions*, MTT-29 (November 1981).

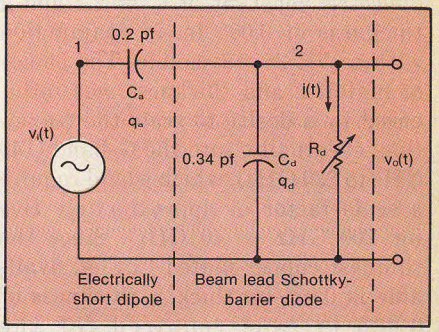
Analyzing Short Dipoles With Nonlinear Loads

In designing an instrument to measure electric field strength, the National Bureau of Standards used two nontraditional techniques, one analytical and one numerical.

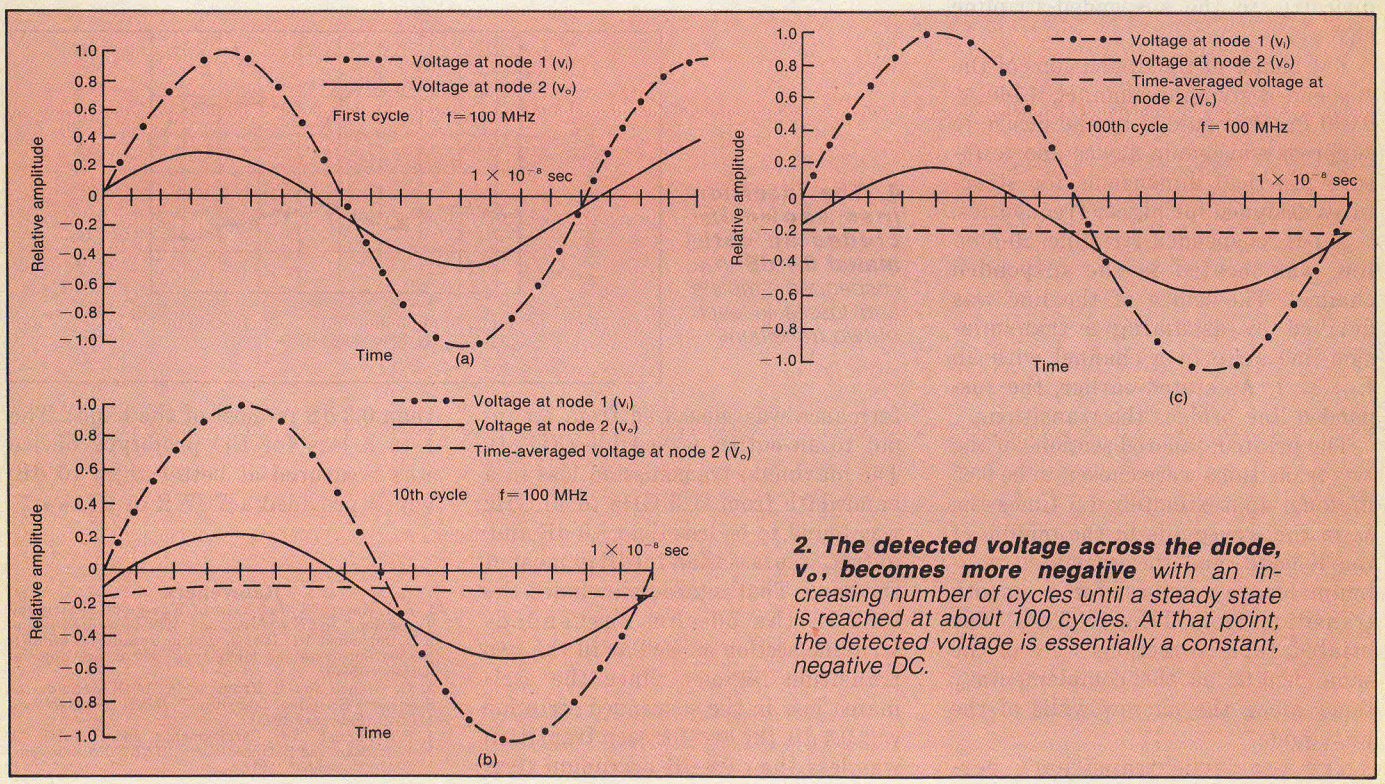
Motohisa Kanda, Project Leader, Nat. Engineering Laboratory, National Bureau of Standards, Boulder, CO 80303.

ALTHOUGH the biological effects of microwave radiation are very difficult to evaluate, one parameter that can be used to quantify hazardous electromagnetic fields is electric energy density, which can be calculated from the electric field strength. For this reason, the National Bureau of Standards (NBS) has developed an electric energy meter that uses three orthogonal, electrically short dipoles with diode detectors between the arms of the dipoles. In the process, two techniques, one analytical and one numerical, were developed to analyze an electrically short dipole with a nonlinear load.

Traditionally, the characteristics of an antenna with a nonlinear load have been analyzed in the frequency domain by considering the spectral components of the solutions at harmonic frequencies.[1] However, calculating the nonlinear transfer function is usually very tedious, particularly when the circuit model of the nonlinear load is very complex and the



1. A short dipole with a nonlinear, diode load can be represented *by the Thévenin's equivalent circuit diagrammed above.*



2. The detected voltage across the diode, v_o, becomes more negative *with an increasing number of cycles until a steady state is reached at about 100 cycles. At that point, the detected voltage is essentially a constant, negative DC.*

nonlinearity is great. Thus, most recent analyses of antennas with nonlinear loads have used time-domain techniques, as do the procedures described below.

The analytical technique used by NBS solves the first-order, nonlinear, time-domain differential equation in terms of Anger functions. The numerical technique uses a time-stepping, finite-difference process to obtain the numerical solution to the differential equation, with the nonlinear effect caused by the diode solved by a conventional iteration method. The use of the numerical solution provides an insight into the effects of nonlinear loads on antennas and permits consideration of certain problems that are too complicated to be treated by an analytical technique.

Setting up a Thévenin equivalent

Figure 1 shows the Thévenin's equivalent circuit for the dipoles with the nonlinear load. The equivalent was derived by using the frequency-domain concept for the effective length and the driving point impedance of an electrically short dipole without a nonlinear load. Note that the nonlinear load selected for the model is a beam-lead Schottky barrier diode, which is represented in simplified form by the parallel combination of a linear capacitance, C_d, and a nonlinear resistance, R_d.

The dipole portion of the circuit includes C_a, the equivalent driving point capacitance of the dipole, and $v_i(t)$, the induced, open-circuit voltage at the dipole terminal, which is given by:

$$v_i(t) = e_{inc}(t) \times h_e \qquad (1)$$

where e_{inc} is the normal, incident electric field strength and h_e is the effective length of the dipole. For an electrically short dipole ($wh < 1$, where w is the free-space wave number and h is half the physical length of the dipole), C_a and h_e are given in farads by:

$$C_a = \frac{4\pi\epsilon_o h}{(\Omega - 2 - \ell n\ 4)} \qquad (2)$$

and in meters by:

$$h_e = \frac{h\ (\Omega\text{-}1)}{2\ (\Omega - 2 + \ell n\ 4)} \qquad (3)$$

In these formulas, ϵ_o is the free-space permittivity in farads/meter and Ω is the antenna thickness factor, $2\ \ell n\ (2h/a)$, where a is the antenna's radius in meters.

The nonlinear resistance of the diode, R_d, can be described by its V-i characteristics:

$$i(t) = I_s\ (e^{\alpha v_o(t)} - 1) \qquad (4)$$

where i(t) is the current in amperes; $v_o(t)$ is the voltage across the diode junction; I_s is the saturation current, which is assumed to be 2×10^{-9} A; and:

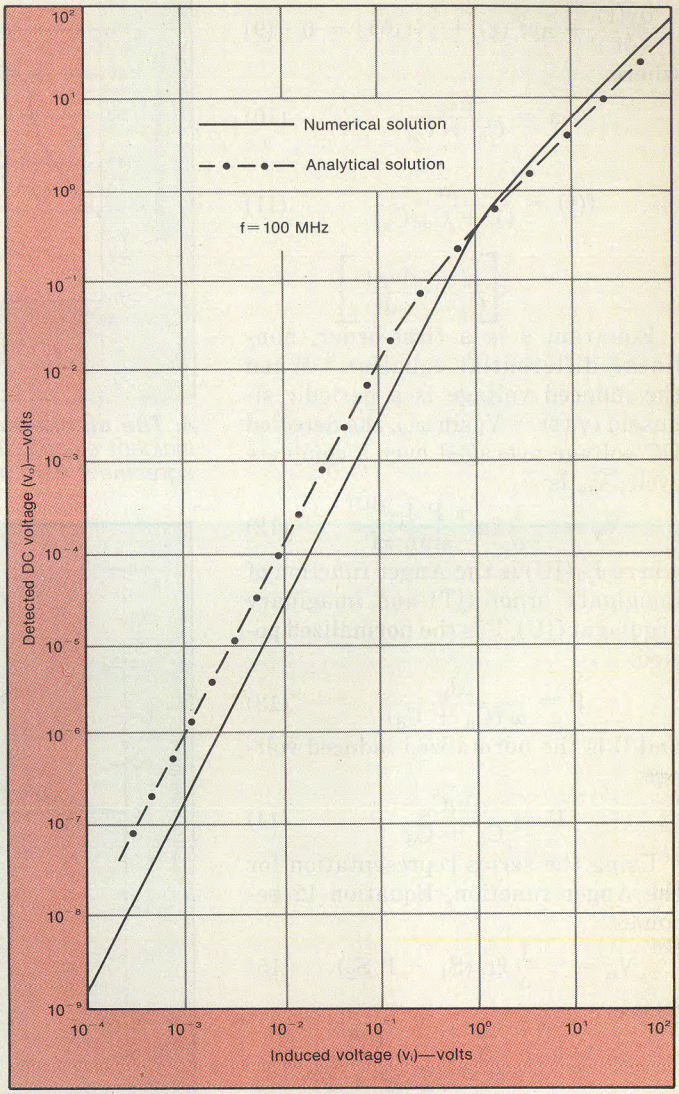
$$\alpha = \frac{q}{nkT} \approx 38V^{-1}$$

where q is the electronic charge (1.6×10^{-9} coulomb), n is the diode ideality factor (~ 1.05), k is Boltzmann's constant (1.38×10^{-23} J/K) and T is the temperature ($\sim 290°K$).

The linear capacitance of the diode, C_d, is a combination of the junction capacitance, C_j, and the package capacitance, C_p. The value of C_d varies from diode to diode and is very difficult to determine. For the purposes of this discussion, C_d is assumed to be 0.34 pF for the beam-lead Schottky barrier diode. In a more elaborate model, C_j is a nonlinear function of the built-in potential, V_b:

$$C_j(V) = \frac{C_j(O)}{\left(1 - \frac{V}{V_b}\right)^{1/2}} \qquad (5)$$

for a step junction. The package capacitance generally remains constant.



3. The "knee" in the dipole-diode response curve represents *the break point between square-law response ($v_i < 1$) and proportional response ($v_i > 1$). The agreement between the numerical and analytical techniques was quite good.*

The analytical technique

Using the Thévenin equivalent circuit described above, the voltage equation and corresponding current equation of the dipole-diode combination can be stated as:

$$v_i(t) + \frac{q_a(t)}{C_a} = \frac{q_d(t)}{C_d} = v_o(t) \qquad (6)$$

$$\frac{dq_a(t)}{dt} + \frac{dq_d(t)}{dt} + i(t) = 0 \qquad (7)$$

where q_a and q_d are the charges on C_a and C_d, and i(t) is the current through the nonlinear resistance, R_d.

Substituting:

$$y(t) = e^{\alpha v_o(t)} \qquad (8)$$

(continued on next page)

in Equation 6, provides:

$$\frac{dy(t)}{dt} + ay^2(t) + y(t)f(t) = 0 \quad (9)$$

where:

$$a = \frac{\alpha I_s}{C_a + C_d} \quad (10)$$

$$f(t) = \frac{\alpha}{(1 + C_d/C_a)} \quad (11)$$

$$\times\left[\frac{I_s}{C_a} + \frac{dv_i(t)}{dt}\right]$$

Equation 9 is a first-order, nonlinear differential equation.[2] When the induced voltage is a periodic sinusoid ($v_i(t) = V_i \sin \omega t$), the detected DC voltage averaged over a complete cycle, $\overline{V}_o$, is:

$$\overline{V}_o = -\frac{1}{\alpha} \ln \frac{\pi P J_{jT}^{(jU)}}{\sinh \pi P} \quad (12)$$

where $J_{jT}(jU)$ is the Anger function of imaginary order (jT) and imaginary argument (jU), P is the normalized period:

$$P = \frac{\alpha I_s}{\omega (C_a + C_d)} \quad (13)$$

and U is the normalized induced voltage:

$$U = \frac{\alpha V_i C_a}{C_a + C_d} \quad (14)$$

Using the series representation for the Anger function, Equation 12 becomes:

$$\overline{V}_o = -\frac{1}{\alpha} \ln (S_1 - P S_2) \quad (15)$$

where:

$$S_1 = 1 + \sum_{\substack{m=1 \\ \text{even}}}^{\substack{\infty \\ k=2 \\ \text{even}}} \frac{U^m}{\frac{m}{\pi}(k^2 + P^2)} \quad (16)$$

and:

$$S_2 = \sum_{\substack{m=1 \\ \text{odd}}}^{\substack{\infty \\ k=1 \\ \text{odd}}} \frac{U^m}{\frac{m}{\pi}(k^2 + P^2)} \quad (17)$$

At high frequencies, where $P << 1$, a small induced voltage provides:

$$V_o = -\frac{\alpha}{4}\left[\frac{V_i}{1 + C_d/C_a}\right]^2 \quad (18)$$

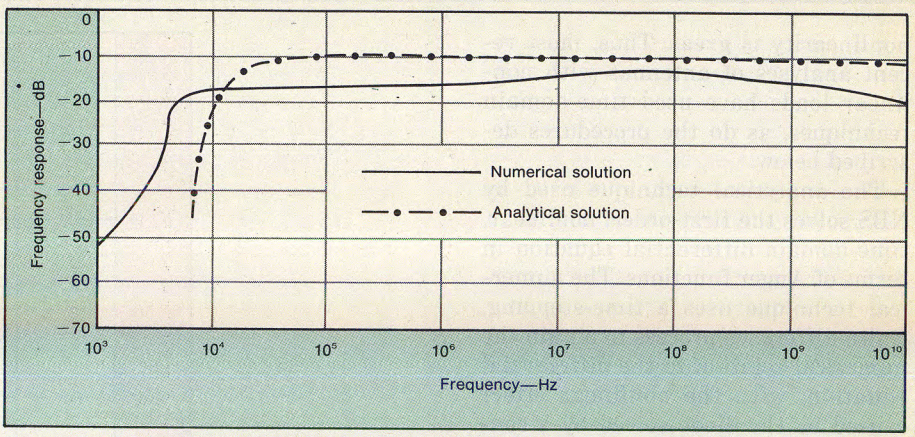
and a large induced voltage gives:

$$V_o = -\frac{V_i}{1 + C_d/C_a} \quad (19)$$

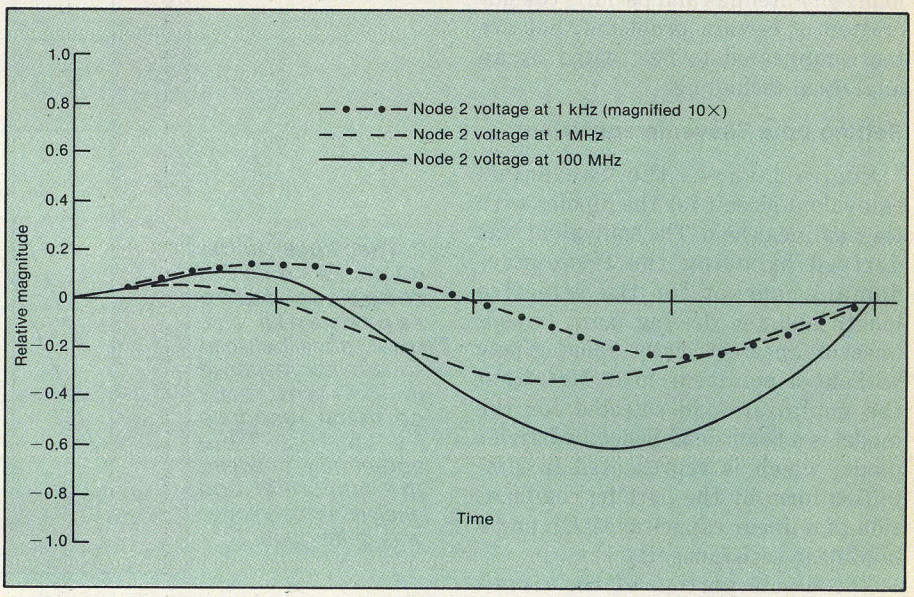
Equation 18 shows that for a small induced, steady-state voltage, V_i, the output DC voltage, V_o, is a square-law function of V_i. On the other hand, Equation 19 shows that for a large V_i, the output DC voltage is proportional to V_i.

The numerical technique

The basics of the time-stepping, difference-equation technique that was used to solve the network in Fig. 1 are discussed below.[3]



4. The dipole-diode combination's transfer function was plotted *for a normal, incident electric field strength of 1 V/m², and the two solutions showed excellent agreement from about 10 kHz to several GHz.*



5. The lower the frequency of the induced voltage, *the less negative skew exhibited by the detected voltage. This characteristic may explain the sharp dropoff below about 10 kHz in Fig. 4.*

First, the elements of the circuit are converted into resistance-current-source equivalent networks using the nodal equation method. For instance, in a regular R, L, C circuit:

$$v_n = Ri_n \quad (20)$$

$$i_{n+1} = C\frac{v_{n+1} - v_n}{\tau} \quad (21)$$

$$v_{n+1} = L\frac{i_{n+1} - i_n}{\tau} \quad (22)$$

where τ is a time-sampling interval.

Once an initial v_o or i_o is given, v_1 and i_1, v_2 and i_2, etc., can be determined. An iterative approach is used to handle the nonlinear equations that result from nonlinear elements. Given a nonlinear system f(i, v), the solution of f(i, v) = 0 yields the system response.

The procedure is described below.

First, f(i, v) is expanded at an initial solution:

$$\begin{bmatrix} i^o \\ v^o \end{bmatrix}$$

That is:

$$f(i, v) = f(i^o, v^o) + j\left[f(i, v)\right]\begin{bmatrix} \Delta i^o \\ \Delta v^o \end{bmatrix} \quad (23)$$

where j is the Jacobian of f:

$$j = \begin{bmatrix} \frac{\partial f_1}{\partial i_1} & \cdots & \frac{\partial f_1}{\partial v_{n+m}} \\ \vdots & & \vdots \\ \frac{\partial f_{n+m}}{\partial i_1} & \cdots & \frac{\partial f_{n+m}}{\partial v_{n+m}} \end{bmatrix} \quad (24)$$

Now, f(i, v) = 0 determines:

$$\begin{bmatrix} \Delta i^o \\ \Delta v^o \end{bmatrix}$$

as:

$$j\left[f(i^o, v^o)\right]\begin{bmatrix} \Delta i^o \\ \Delta v^o \end{bmatrix} = -f(i^o, v^o) \quad (25)$$

And the solution of:

$$\begin{bmatrix}\Delta i^o \\ \Delta v^o\end{bmatrix}$$

updates the initial value of:

$$\begin{bmatrix} i^o \\ v^o\end{bmatrix}$$

via:

$$\begin{bmatrix} i^{n+1} \\ v^{n+1}\end{bmatrix}=\begin{bmatrix} i^n \\ v^n\end{bmatrix}+\begin{bmatrix}\Delta i^n \\ \Delta v^n\end{bmatrix} \quad (26)$$

The operation is repeated for n = 0, 1, . . . until:

$$\begin{bmatrix}\Delta i \\ \Delta v\end{bmatrix}$$

is sufficiently small.

Results of solutions

Figures 2a, 2b, and 2c show the time-domain waveforms of the first, 10th, and 100th detected sinusoids for a 100-MHz input voltage. Note that the nonlinearity of the diode causes the detected voltage to start in the negative polarity. This characteristic is more pronounced in succeeding waveforms until the 100th sinusoid, where the response is essentially steady-state. Thus the diode's nonlinearity results in a time-averaged detected voltage that is a constant, negative DC.

The agreement between the analytical and numerical solutions was quite good, as indicated in Fig. 3, which shows the detected DC voltage from the dipole-diode combination as a function of the induced voltage. The breakpoint for the change from square-law performance to proportional response occurs at about 0.1 volt.

The transfer functions of the dipole-diode combination derived from the two techniques also agree well (Fig. 4). The transfer function was defined as the ratio of the detected DC voltage, V_o, to the amplitude of the induced voltage, V_i, expressed in dB when $e_{inc} = 1\ V/m^2$. This definition results in a square-law response. The two functions agree within 8 dB from about 10 kHz to several GHz.

The discrepancy between the two functions below 10 kHz may be due to insufficient time-averaging in the numerical solution. That is, the numerical solution may require additional iterations at very low frequencies to insure proper convergence.

Figure 5 can explain the sharp cutoff that both transfer functions exhibit below 10 kHz. The lower the frequency of the induced voltage, the less negative skew to the detected voltage.

Since the analytical and numerical solutions agree so well, the technique selected for a specific project can be determined by practical considerations. One advantage of the analytical technique is that the solution is given in the closed form and is very easy to evaluate. It would be very difficult, if not impossible, however, to find the closed-form solution for the nonlinear differential equation for a much more complex antenna model, which might include a nonlinear capacitance and linear inductance in addition to a linear capacitance and nonlinear resistance. If so, the numerical solution—using the time-stepping, difference-equation technique—will provide an accurate time-domain solution for more general nodal equations. ••

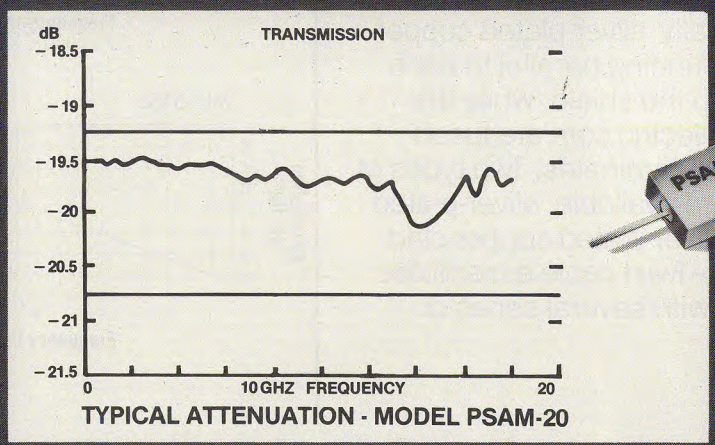
References

1. N. Wiener, *Nonlinear Problems in Random Theory*, MIT Press, Cambridge, MA (1959).
2. M. Kanda, *IEEE Transactions on Antennas and Propagation*, Vol. AP-28, No. 1, pp. 71-78 (January 1982).
3. D.A. Calahan, *Computer-Aided Network Design*, revised ed., McGraw-Hill, New York (1972).

Designer's Choice

Drop-In Attenuator

1 to 30 dB • DC to 18 GHz

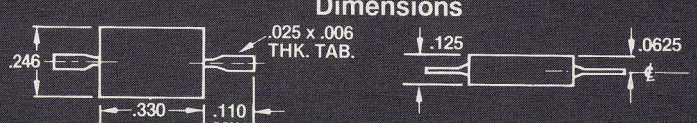


TYPICAL ATTENUATION - MODEL PSAM-20

Attenuation Accuracy: 1 dB to 10 dB ±0.5 dB
11 dB to 30 dB ±0.75 dB

VSWR: D|C to 12.4 GHz: 1.30 Max
12.4 to 18.0 GHz: 1.50 Max

Dimensions



FINISH: CASE & LEADS GOLD PLATED
PER MIL-G-45204

For Additional Information – Call TOLL FREE – (800) 221-0357

KDI PYROFILM

60 S. Jefferson Road, Whippany, N.J. 07981 • (201) 887-8100 • TWX (710) 986-8220

P83-4

Automated System Eases Loss Measurements

Automated measurements of transmission loss and return loss are now possible at levels as high as 55 dB. One of the keys is the use of an *in situ* air line as an impedance calibration standard.

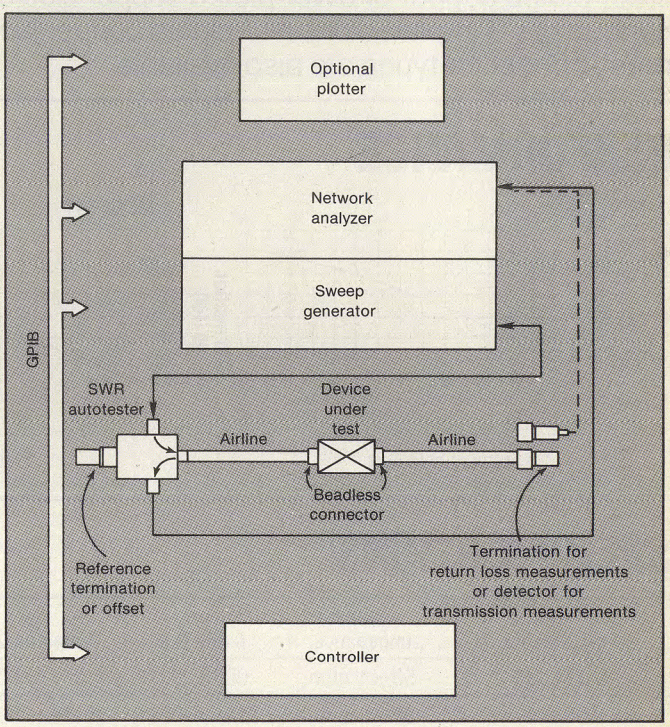
Dr. Peter Lacy, Chairman of the Board, and **Ivan Andres,** Product Manager for RF Analyzers and Microwave Components, Wiltron, 805 E. Middlefield Rd., Mountain View, CA 94042.

THE quest for improved precision in broadband microwave measurements has led to more accurate instrumentation, including better sweep generators and network analyzers, as well as the enhanced performance of passive components such as SWR bridges, detectors, terminations, and air-line impedance standards. In addition, more powerful computer controllers have simplified automated test setups. Still, two scalar measurements—transmission loss and return loss—have traditionally contained phase errors. Now, with the help of digital signal processing and finely crafted precision components, the automated network analyzer system of Fig. 1 can perform precise loss measurements automatically with error correction. The system is comprised of a sweep generator, a network analyzer, and the necessary passive components under the digital guidance of a desktop computer controller. The test setup can measure return losses as high as 55 dB from 1 to 17 GHz and can reduce phasor mismatch uncertainties when analyzing low and medium values of transmission loss. It owes its accuracy to a combination of digital filtering, a windowed Fourier transform, and a physical impedance standard (an air line).

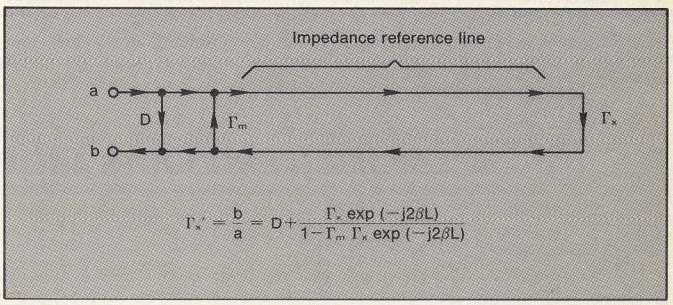
This system automates two return-loss measurement techniques: error averaging and ripple extraction. Both techniques involve digitizing a ripple waveform and normalizing it to a 100-percent reflection reference (a short at the unbeaded end of the air line). Following calibration, the test data is manipulated by the computer using an algorithm which includes a Kaiser-Bessel digital filter and a Fourier transform.

Theory behind system

In order to better understand the theory behind the air line system, it's useful to examine an equivalent reflectometer model, such as the one shown in Fig. 2. The impedance reference line is shown only as a line of length, L. Unknown impedance Γ_x, is placed at the far end of the line. The measurement equation shows that



1. The "air-line" system ties a sweep generator and network analyzer to a computer controller *for completely automated measurements of transmission and return-loss from 1 to 17 GHz.*



2. This reflectometer acts as a model for the air-line system *and, together with the measurement equation shown, illustrates the workings of the new test setup.*

output Γ_x of the reflectometer has a directivity term (D), a linear fractional term with Γ_x, line length L, and the test port match, Γ_m. Initiating a swept-frequency measurement causes the two phasors on the right-hand side of the equation to rotate with respect to frequency. These expressions contain the frequency-sweep data that are essential to the digital-processing method.

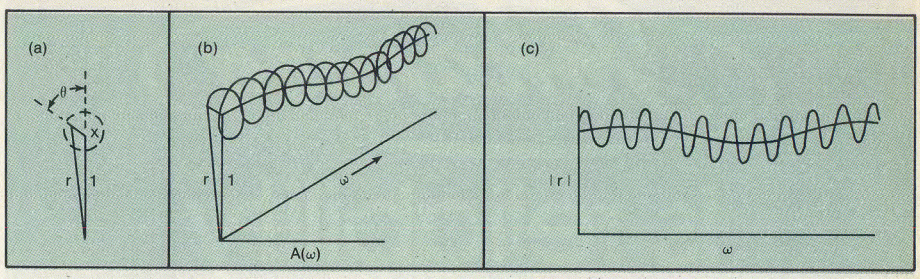
Figure 3 shows the phasor responses encountered during this swept-frequency measurement. In the diagram, (a) illustrates the phasor sum (r) of a unit reference vector and an unknown (x) at an angle θ with respect to the reference phasor. As the frequency changes, the phasor will rotate about the dotted locus. Diagram (b) shows the perspective of this phasor when it is plotted on the frequency axis (ω), and around the helix axis A(ω). Here the average value of A is unity and the magnitude of A(ω) contains all the frequency-sensitive parameters of the system as well as the other intrinsic, slowly varying instrumental quantities. Thus, the magnitude of r is given by:

$$|r| = A\sqrt{1+x^2+2x\cos\theta} \qquad (1)$$

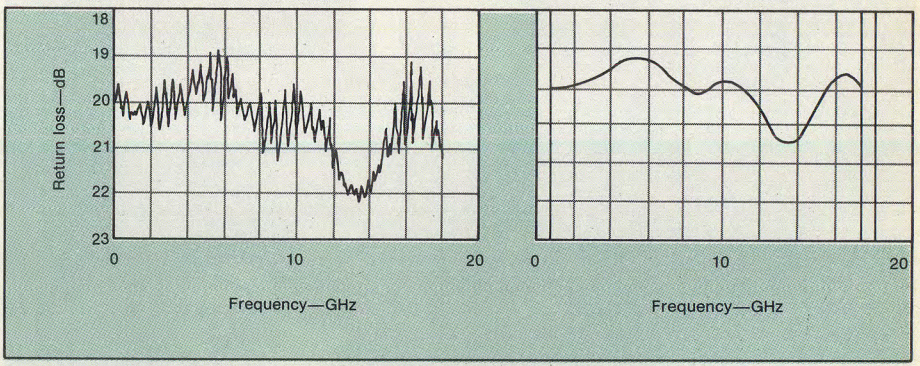
For the data processing used in the air-line system, the magnitude (and not the square) of the phasor is used. This is because the squared form contains a cross product of the unknown rotating value r and the reference magnitude, which can be other than unity. In the magnitudinal form, the sinusoidal quantity x is independent of the reference phasor value.

In both the error-averaging and the ripple-extraction data-processing

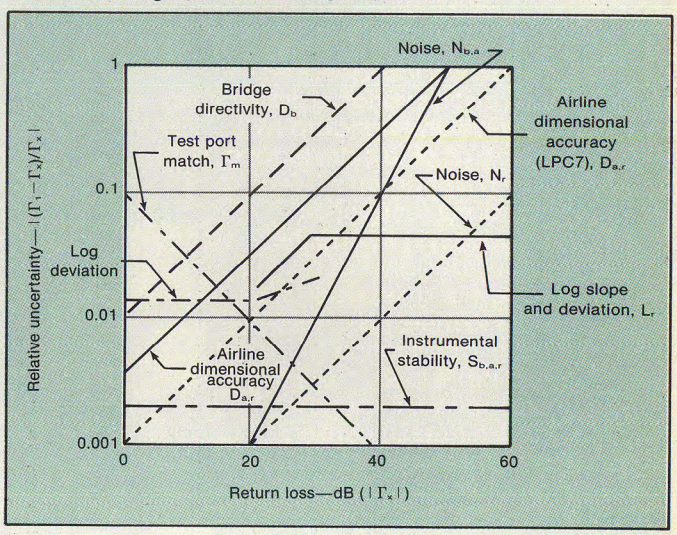
(continued on next page)



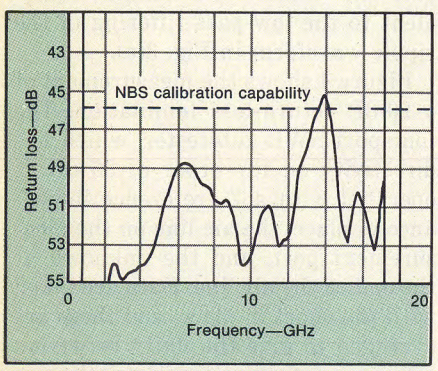
3. The response of phasors in reaction to swept frequencies *is shown as (a) the phase sum; (b) the perspective of the phasor, r, versus frequency (ω), with a helix axis A(ω); and as (c) magnitude |r| versus frequency, A(ω).*



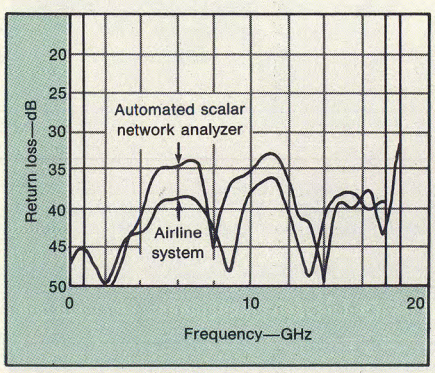
4. This measurement of a 20-dB return-loss termination *is shown as (left) raw sweep reflection data and as (right) error-averaged processed data.*



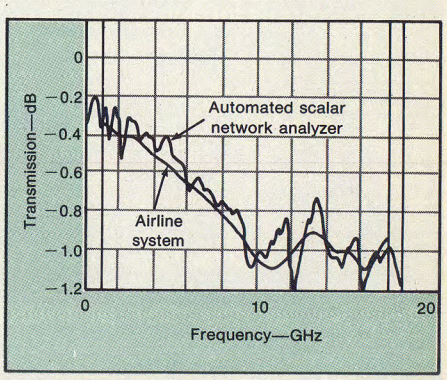
5. These reflection coefficient uncertainty factors *have been collected as a log-log plot of relative uncertainty versus diminishing $|\Gamma_x|$.*



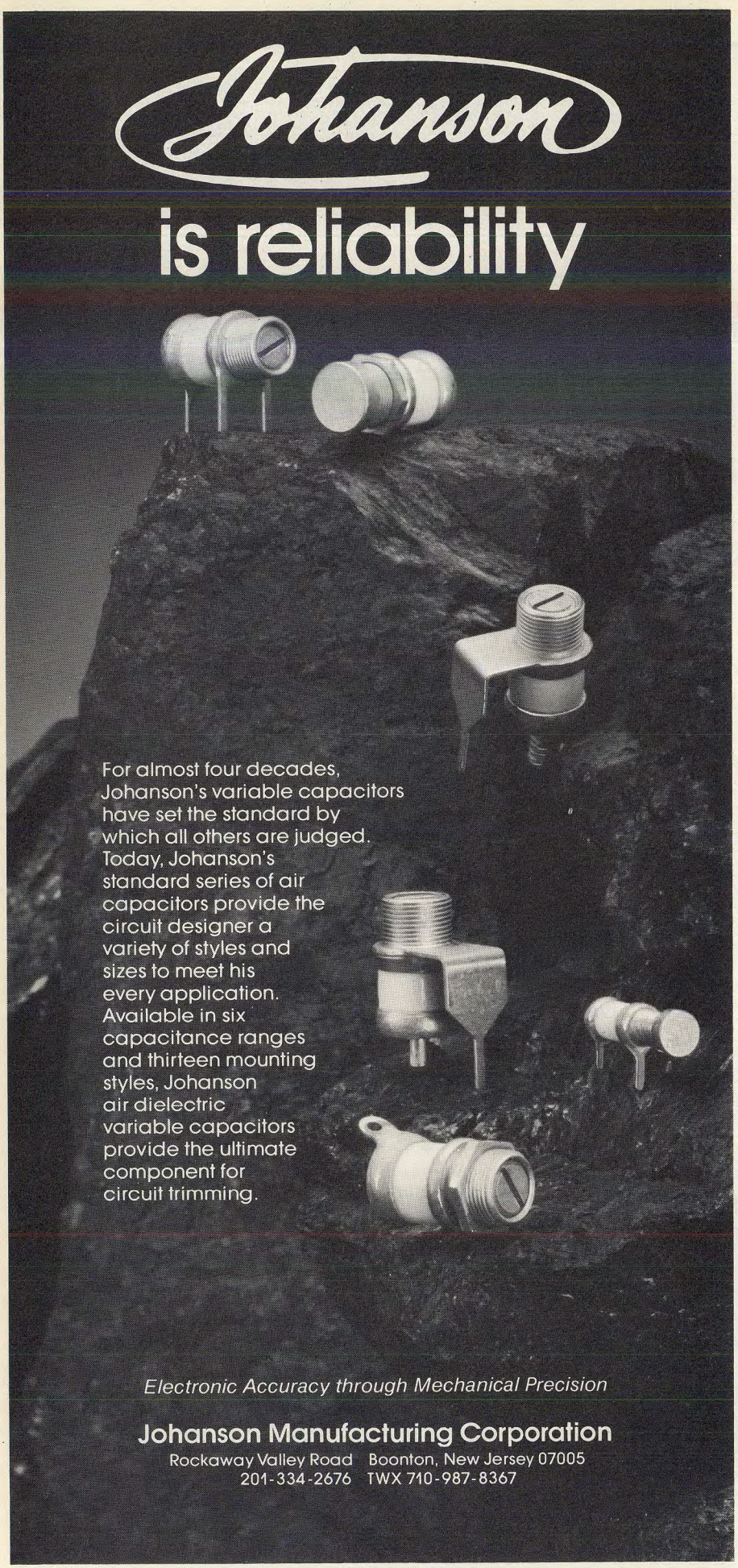
6. The return-loss measurement accuracy *of the new system exceeds that of the National Bureau of Standards' precisely calibrated ANA.*



7. Improvements up to 5 dB *can be made on the new system over the capabilities of a conventional automated scalar network analyzer.*



8. These PIN-diode switch measurements *show how the system reduces impedance mismatch errors for low-transmission-loss measurements.*



READER SERVICE NUMBER 58

AUTOMATED SYSTEM

(continued from p. 81)

techniques, a short is placed at the measurement port for calibration. Unprocessed data is taken across the measurement frequency range with the measurement function Γ_x' equal to:

$$\Gamma_x' = A(\omega) = D - \frac{\exp(-j2\beta L)}{1+\Gamma_m \exp(-j2\beta L)} \quad (2)$$

where β is $\frac{2\pi}{c}$, and L is the length of the coax line.

Error-averaging explained

In the error-averaging method, the magnitudes of $|D|$ and $|\Gamma_m|$ are approximately 0.01 and 0.06. The format of Eq. 2 shows that, relative to the unity reflection reference, D rotates in a positive direction while Γ_m (which dominates the two terms) rotates in a negative direction. It is in the use of this technique that the value of $A(\omega)$ is determined. This is the normalization term that will be divided into the subsequent measurement resultant.

At this point, the DUT is connected to the test port and error averaging provides the value for $A(\omega)\ |\Gamma_x|$. The processed data from the calibration provides the normalization data. After the unknown Γ_x is run and processed, the resultant ratio will simply be the value of $|\Gamma_x|$ with the phasor errors D and Γ_m effectively eliminated. In a further program step, the quadratic error magnitudes are obtained and used for second-error suppression. In this procedure, it is important that both D and Γ_m be less (6 to 8 dB less) than the reflection being measured.

In error averaging, the ripple pattern is observed through an RF frequency window that extends above and below the frequency under consideration. Errors are then averaged over the window in a manner equivalent to the low-pass filtering of the ripple waveform in Fig. 3(c).

Figure 4 shows the measurement of a 20-dB return-loss temination. The four-port SWR autotester, which has directivity on the order of 36 dB, is operated with a Z_0 reference impedance in place, the air line on the measurement port, and the unknown at the end of the air line. Data are taken with the short in place, and these are averaged to give the unity reflection reference information. Then, the unknown is applied at the test port, and a frequency sweep is made. The directivity of the SWR autotester is re-

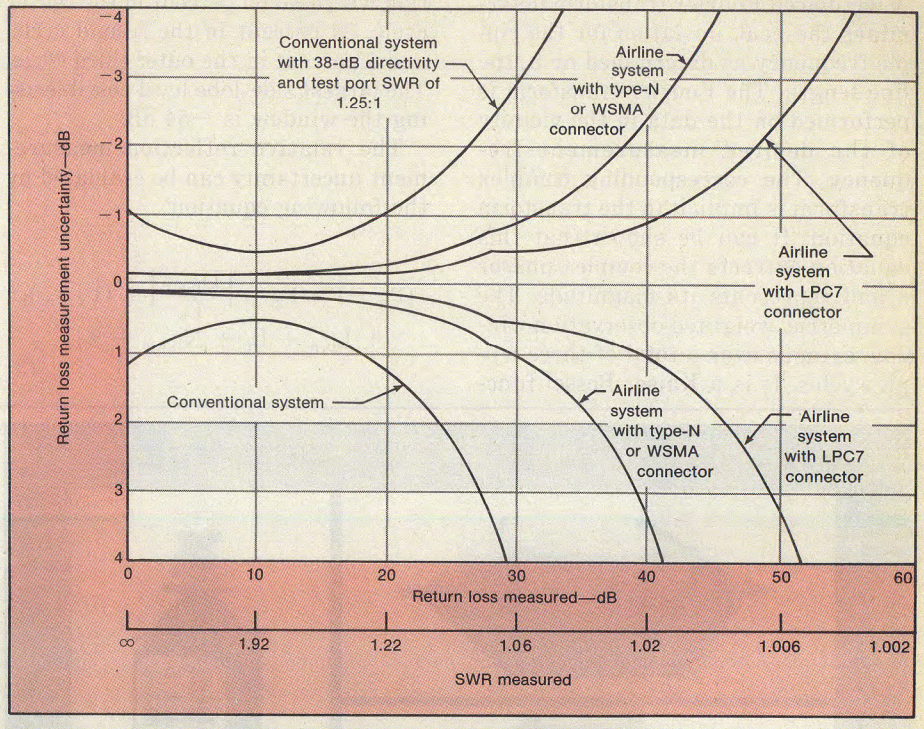
sponsible for a measurement uncertainty of about 1 dB. This is subsequently removed by the digital low-pass filtering of the raw-sweep reflection data. The processed sweep data are then referenced to the previous calibration sweep, and the resulting data are plotted in Fig. 4(b).

Ripple extraction

In ripple extraction, the short-circuit calibration is again performed with an "offset" termination differing from Z_0 on the reference port of the four-port SWR autotester. A value of 0.1 (for 20-dB return loss) is typically used for |D|. This value will dominate, but this latter factor will initially contribute a second-order correction term. The local ripple amplitude, $A(\omega)$ $|\Gamma_x(\omega)|$ is then normalized using the short-circuit calibration reference data.

The same window used for error averaging is also used to view the ripple waveform and to extract the characteristic sinusoid or ripple variation.

(continued on next page)



9. This analysis of the return-loss measurement uncertainty *takes into account the different types of coaxial connectors that are used with test instrumentation.*

WAVEGUIDE
Terminations

PRICE: Unbeatable from $79.00
(Series 200X: Quantity 10–24)
DELIVERY: Stock to 30 days
CALL: 516/420-9000

Struthers waveguide terminations are offered in three standard power ranges PLUS intermediate power levels specifically designed for satellite communication applications. PLUS unconditional guarantees assured by a tight, independent quality-control system. PLUS 25 years experience in the manufacture and design of MIL Spec microwave components.

To find out more about Struthers complete product line, write or call for comprehensive catalog. Let our engineering staff review your particular requirements.

HIGH POWER
Series J202

MEDIUM POWER
Series K202

LOW POWER
Series 200

QPL Series

- Frequency Range 1 to 40 GHz
- 1 Watt to 3 Kilowatts
- Low VSWR, typically <1.05
- Finned and unfinned units
- No forced air cooling required
- QPL approved models
- Unconditionally guaranteed

&
MAGIC "T" HYBRIDS
Series M352

Struthers®
Struthers Electronics Corporation, 4 Dubon Court, Farmingdale, NY 11735 • 516/420-9000 • TWX 510-224-6112
READER SERVICE NUMBER 59

AUTOMATED SYSTEM EASES LOSS MEASUREMENTS *(continued from p. 83)*

A windowed Fourier transform determines the peak deviation for the ripple frequency as determined by L, the line length. The Fourier transform is performed on the data in the vicinity of the desired measurement frequency. The corresponding complex transform is implicit in the transform equation. It can be shown that this equation extracts the complex phasor x and represents its magnitude. The symmetric, weighted observation window extends over a total of three ripple cycles. It is a Kaiser-Bessel function weighted 65 percent in the center cycle, 30 percent in the second cycle, and 5 percent in the outer third cycle. The largest side-lobe level possible using the window is −54 dB.

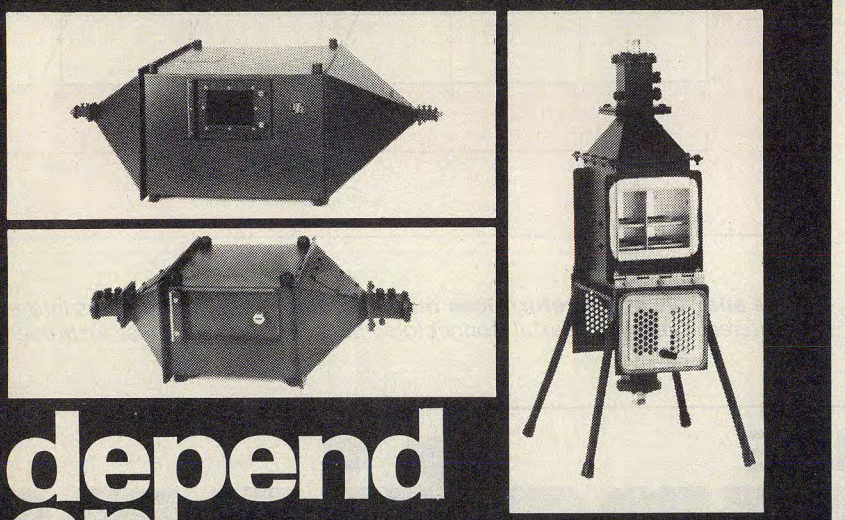
The relative reflection measurement uncertainty can be evaluated by the following equation:

$$|(\Gamma'_x - \Gamma_x)/\Gamma_x| = \left|\frac{D_{b,a,r}}{\Gamma_x}\right| + (|\Gamma_x\,\Gamma_m|)_b + L_{b,a} + L_r + N_{b,a,r} + S_{b,a,r} \quad (3)$$

Six terms appear in this equation:

- The first involves directivity ($D_{b,a,r}$), with the subscripts denoting bridge (b), error averaging (a), and ripple extraction (r). The term D_b stands for conventional bridge directivity, and $D_{a,r}$ is the dimensional accuracy of the airline.
- The second term (enclosed in parentheses) applies only to the conventional bridge reflectometer. Error averaging and ripple extraction will eliminate this term.
- The third term, $L_{b,a}$, applies to reflectometer-bridge and error-averaging methods and concerns the deviation from the true logarithmic response by the log amplifier. The log deviation exhibits a ripple response with equal amplitudes over 0 to 20 dB of the return-loss range and increasing above 20 dB.
- The fourth term applies only to the ripple-extraction method. It includes the effect of the slope of the log amplifier's frequency response.
- The fifth term is the noise contribution ($N_{b,a,r}$). This is a fluctuation around the best indicated measurement value, except at the lowest levels (highest return loss) where it biases the measured level toward a lower value of return loss (RL). The term $N_{b,a}$ has a +2 slope that is associated with square-law detection, while N_r has a +1 slope that is due to the homodyne action that results from the detection of a small unknown present with the larger signal value introduced by the offset termination on the bridge. At a 50-dB RL, $N_{b,a}$ has a value of unity, and then intersects N_r at the operating point of the offset bridge (20-dB RL).
- The last term is instrumental stability ($S_{b,a,r}$) and is set at the constant value of 0.002 for ±0.02 dB-accuracy. The log-log plot of relative uncertainty versus diminishing $|\Gamma_x|$ which is shown in Fig. 5 allows a wide range of parameters to be portrayed with straight-line error contributions. This uncertainty chart also illustrates that $|D_b| = 0.01$ and $\Gamma_m = 0.1$ for a high-performance reflection bridge.

For return-loss values from 0 to 30 dB, performed via the error-averaging method using the low-pass digital filter, the effects of D and Γ_m are virtually eliminated, but the logarithmic response $L_{b,a}$ dominates at low values and the dimensional accuracy D_a dominates at the high values. At higher values of return loss, noise will ap-



depend on ifi: Precision design TEM test chambers for accurate and broadband EMC testing

IFI's precision design and construction allows accurate E-Field generation within ± 1 db.

Each cell is equipped with a hinged access door that provides clearance for insertion of test objects, and transition panels for easy cable entry.

Larger cells can be supplied with integral E-Field Sensors, for direct readout in volts per meter.

Model CC-108—This test cell, with an operating range of DC to 800 MHz, offers an efficient means of obtaining broadband E-Field measurements in a compact, bench top application.

Model BC-100—This portable cell, specifically designed for medical and biological testing, provides a means of generating extremely high E-Fields up to 1GHz.

Model CC-103—The TEM Cell that has set industry standards, permits fully controlled testing at high E-Field levels with a moderate amount of input power.

Applications
- EMC/Susceptibility Testing
- Calibration of Field Intensity Meters
- Research & Development Applications
- Testing & Calibration of Power Density Probes

Benefits
- Cost Effective Alternative to a Full Size Screen Room
- Portable Shielded Enclosure for Lab Testing
- Protection from Hazardous Radiation During High E-Field Tests
- Useful for both Susceptibility and Emissions Measurements

"Also Depend of IFI for Broadband Amplifiers, E-Field Sensors and EMC Test Equipment"

ifi **INSTRUMENTS FOR INDUSTRY, INC.**
151 Toledo Street
Farmingdale, N.Y. 11735
(516) 694-1414

READER SERVICE NUMBER 60

pear, although its effects can be disregarded due to the filtering effects N_a of both error averaging and ripple extraction.

For return-loss values of greater than 25 dB, the windowed discrete Fourier transform (ripple extraction) is used. Errors that contribute to the air-line dimensional accuracy D_r and to the logarithmic slope and deviation term L_r dominate here. When an offset termination of 20 dB is used on the four-port SWR autotester, the average value of the ripple extraction histogram is −25 dBm. Note that the noise floor is 60 dB below the reference level created by this 20-dB offset termination. Thus, if a return loss of 40 dB is being measured, the signal-to-noise ratio will be 40 dB.

All the error contributions of Fig. 4, when applied to the appropriate modes, provide the overall performance previously shown in Fig. The combination of an *in situ* air-line as the impedance reference, the beadless LPC-7 connector (laboratory precision connector, compatible with GPC-7 or APC-7) at the reference port, and a good signal-to-noise ratio give this reflection measurement system substantial advantages over the traditional error-corrected phasor automatic network analyzers (ANAs).

Component analyses

For the purpose of evaluating the effectiveness of the test system, several difficult but typical measurements were undertaken on terminations, adapters, PIN-diode switches, and coaxial cable connectors. Figure 6 shows the results of a return-loss measurement made on a 50-ohm coaxial termination. The acquired data, in fact, exceed the National Bureau of Standards' 46-dB uncertainty limit. The NBS technique is based on the use of a very carefully calibrated ANA that employs directional couplers, a tuned receiver, and computer error-correction to achieve the 46-dB accuracy figure. The air-line system, on the other hand, takes advantage of an impedance standard (an unbeaded section of the air line) with return-loss capability that exceeds that of the NBS network analyzer by a significant margin. The return loss of the air line can be calculated by making precise dimensional measurements of the device's physical geometry. When three reference airlines were physically measured by NBS, they found their return-loss to be greater than 60 dB. Even when translated conservatively, this represents a limit which is at least a 9-dB improvement over the NBS system.

The second component tested was the coaxial adapter. It is sometimes assumed that this component doesn't introduce significant impedance discontinuities, although a glance at Fig. 7 will show how dangerous this assumption can be. Note that the return loss (and hence, the SWR) changes in a fairly unpredictable manner with respect to frequency. Precision GPC-to-WSMA adapters were measured, first with an automated scalar network analyzer (ASNA) and then with the air-line system. For the latter measurements, two air lines were used. They served to terminate both sides of the adapter in a near-ideal 50-ohm impedance. With the unbeaded ends of these air lines connected to the adapter, the device

(concluded on next page)



At Q-bit, we add Power Feedback™ technology to all our hybrid amplifiers.

We put more in . . . so you get more out! From the QBH-101 to the QBH-360, all Q-bit amplifiers utilize **Power Feedback™** technology, resulting in high reverse isolation and excellent input/output return loss. For example, check these specs:

QBH-110 @ 15 VDC

FREQ. MHZ	INPUT VSWR	GAIN (dB)	PHASE (deg.)	ISOLATION (dB)	OUTPUT VSWR
5.000	1.28	15.22	-177.1	-41.32	1.08
50.000	1.21	15.13	167.7	-40.30	1.05
100.000	1.20	15.14	153.7	-39.08	1.06
150.000	1.20	15.12	140.1	-37.71	1.06
200.000	1.20	15.09	126.1	-36.33	1.06
250.000	1.21	15.07	112.3	-35.12	1.07
300.000	1.21	15.06	98.6	-34.04	1.08
350.000	1.20	15.10	84.9	-33.08	1.08
400.000	1.19	15.14	71.0	-32.26	1.10
450.000	1.17	15.21	56.7	-31.53	1.12
500.000	1.14	15.29	42.1	-30.88	1.15

POWER: 15 VDC, 25 mA
INTERCEPT: 3rd ORDER 24.0 dBm, @ 240 MHz
NOISE FIGURE: 2.0 dB, @ 70 MHz
2nd ORDER 35.0 dBm, @ 240 MHz
2.3 dB, @ 500 MHz 1 dB COMPRESSION: 10.5 dBm, @ 240 MHz

Call or write:
311 Pacific Avenue, Palm Bay, FL 32905 • (305) 727-1838 TWX (510) 959-6257

Q-bit Q-bit Corporation

READER SERVICE NUMBER 61

under test is isolated, thereby reducing measurement uncertainty.

At certain frequencies, there was a difference of as much as 5 dB between measurements made on the two systems. This only emphasizes the effects of directivity errors on a conventional ASNA system. The newer system, with its air-line technology and digital-signal processing, suppresses these errors.

Transmission-loss analysis of a PIN-diode switch is another difficult task. Since it is a low-loss measurement on a device with poor input/output matches, it is extremely sensitive to errors due to interaction with the source and detector mismatches. Conventional ASNAs utilizing detectors with SWRs of 1.2:1 (a 19-dB return loss) can give measurements of questionable accuracy, with typical mismatch errors of 0.5 dB peak to peak. The air-line system, on the other hand, permits this measurement to be made more accurately (Fig. 8). Errors can be reduced to about 0.1 dB peak to peak.

Cable assemblies are a basic element of composite microwave systems. The measurement of cable connector reflections when placed on the end of a short cable has generally been impractical. Fortunately, the air-line system not only makes these practical, but also makes it possible to determine the precise effect that the addition of a right-angle bend (or an adapter) can have on the cable-assembly return-loss characteristics.

The return-loss measurement accuracy of the air-line system has been summarized in Fig. 9. The air-line system reduces uncertainty for every type of connector over a return-loss range of 0 to 55 dB. Conventional automated network analyzer techniques cannot match this, even with difficult-to-obtain 38-dB directivity components.

When using a system such as the air-line setup, measurements on devices with rapidly changing spectral response characteristics (i.e., greater than approximately one ripple every 5 GHz) should be made with caution. The software digital filtering will smooth out any rapidly occurring peaks and troughs, sometimes resulting in misleading information. For example, when similar filter data are compared on the air-line system and on an ASNA, the ASNA will reveal true return-loss peaks while the former system will smooth out these peaks to present an averaged value. In this case, an ASNA is a more valid measurement system. A good practice is to check these spectral response characteristics on an ASNA before analyzing them on the air-line setup.

●●

Acknowledgments

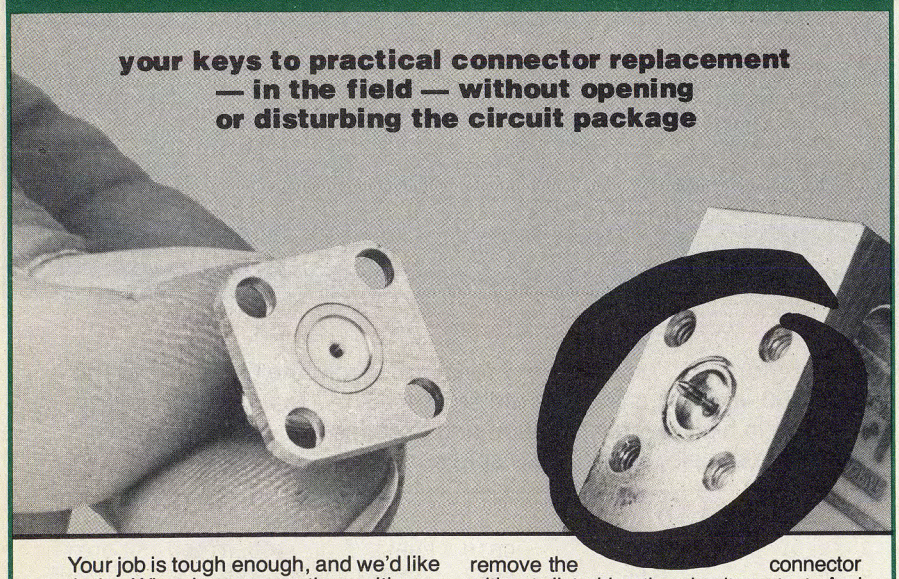
The authors wish to thank Mr. Christian Staeger of the Swiss PTT for his ideas on measurement theory and practice as they apply to cable connector interfaces. Mr. Robert Huenemann of Wiltron also made valuable contributions, including the preparation of the Option P1 software.

References

1. P.D. Lacy and W.A. Oldfield, "Precision Swept Reflectometer," *Microwave Journal* (April 1973).
2. D.L. Holloway and P.I. Somlo, "Origin of High-Resolution, Swept Frequency Reflectometry," *Microwave Journal* (August 1973).
3. P.D. Lacy, D.E. Dunwoodie, W.L. Baxter, and W. Oldfield, "An Easy-to-Use Method for Measuring Small SWRs to Better Than Computer-Aided Accuracy Levels," *Wiltron Technical Review No. 8* (September 1978).
4. P.D. Lacy and W. Oldfield, "Calculable Physical Impedance References in Automated Precision Reflection Measurement," *IEEE Transactions on Instrumentation and Measurement*, (December, 1980).
5. P.D. Lacy, "Phasor Error Correction using Air-lines with the Automated Scalar Network Analyzer," *Proc. European Microwave Conference* (1981).

Interchangeable transition pins:

your keys to practical connector replacement — in the field — without opening or disturbing the circuit package



Your job is tough enough, and we'd like to help. What better way than with our interchangeable transition pin connectors. The pins slip-fit into the connector and are soldered to the circuit. So you can remove the connector without disturbing the circuit contact. And that means in-the-field connector replacement is a sweetheart instead of a heartache. *Even on hermetic packages.*

And if that one advantage isn't enough to make life easier, we've got four more for you. *Our SMA flange connectors with interchangeable pins also:*

- *Increase package design options*
- *Assure mechanical integrity for improved electrical performance*
- *Simplify testing procedures*
- *Reduce inventory costs*

Of course these connectors meet all applicable specifications of MIL-C-39012. We'd like to say a lot more about these unique connectors. About their simplicity, practicality and economy. And if you'd care to listen, get in touch soon for full technical details or applications assistance.

EMC TECHNOLOGY, INC.
1971 OLD CUTHBERT ROAD
CHERRY HILL, NEW JERSEY 08034
Phone: (609) 429-7800 • TWX: 710-896-0193

Authorized distributors and technical sales representatives in all major metropolitan areas.

EMC TECHNOLOGY is a full line MIC product manufacturer. Our products include SMA connectors, terminations, attenuators, resistors and DC blocks for stripline, microstrip and SMA coax.

READER SERVICE NUMBER 62

Four MOSFETs Deliver 600 W of RF Power

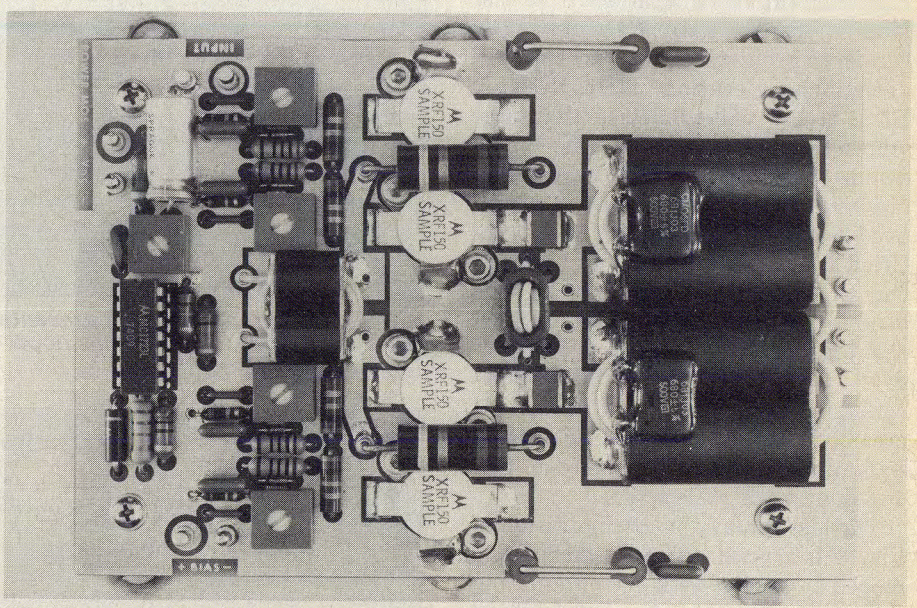
Amplifiers capable of providing 600 W of RF output power usually rely heavily on power combiners and splitters. There is a better way, and it only requires four MOSFETs and some standard circuit elements.

H. O. Granberg, Principal Staff Engineer, Motorola Semiconductor Products, Inc., 5005 East McDowell Rd., Phoenix, AZ 85008.

WHEN an application requires 600 W of RF power at 2 to 30 MHz, visions of power combiners usually come to mind. Combiners and splitters permit a great many solid-state devices to be coupled for high power levels, but with considerable signal loss and added cost. There is a way, however, to combine only four MOSFET transistors to achieve 600 W without the need of even one power combiner.

The resulting amplifier circuit is capable of operating at an efficiency of 50 percent.

Figure 1 shows the unique push-pull parallel circuit. It uses four MRF150 RF power FETs that can be paralleled at relatively high power levels. This technique is considered impractical for bipolar transistors because of low input impedance. In a common-source amplifier configuration, a power FET has approximately five to ten times higher input impedance than a comparable bipolar transistor in a common emitter circuit. The output impedance in both cases is determined by the DC supply voltage and power level. The limit to the number of FETs that can be paralleled is dictated by physical, rather than electrical, considerations. The mutual inductance between the drains is the most critical aspect, and limits the upper frequency range of operation. The magnitude of these losses is related to the impedance levels involved, and becomes more serious at lower supply voltages and higher power levels. Since the minimum mounting distance of the transistors is limited by the package size, the only real improvement would be a multiple die package. For higher frequency circuits, these mutual inductances could be used as part of the matching network, although they would seriously limit the bandwidth of the amplifier. (This is a technique that is popular with many VHF bipolar designs.)



***1. Good heat dissipation is required** in the 600-W RF amplifier because of the physical proximity of the four MOSFETs, which will generate 200 to 300 W of heat.*

There is another thing to be considered when paralleling FETs: If the unity gain frequency of the device is sufficiently high, an oscillator will be created, where the paralleling inductances together with the drain and gate capacitances will form resonant circuits. Feedback is obtained through the drain-to-gate capacitance, which results in a 360-degree phase shift in a frequency region somewhat higher than the amplifier's bandwidth. These oscillations may not be directly noticed in the amplifier output, but may have high amplitudes at the drains. This condition can be cured by isolating the paralleling inductance, which consists of the DC blocking capacitances (labelled C7 through C10 in the schematic diagram of Fig. 2) and their wiring inductances from the gates. Low-valued noninductive resistors that do not appreciably affect the system gain can be used for this purpose.

Building the amp

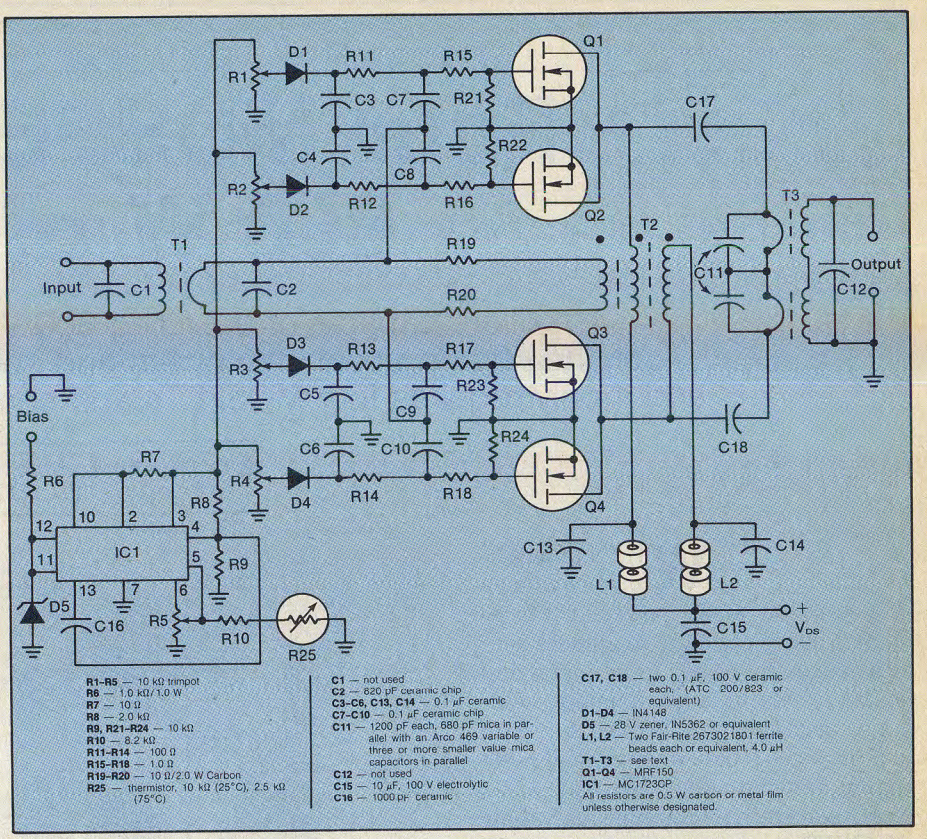
The total number of circuit elements needed for the 600-W amplifier is given in Fig. 2. Supply voltages of 40 to 50 VDC can be used, depending on linearity requirements. The bias for each device is independently adjustable; therefore, no matching is required for the gate threshold voltages. Since the power gain of a MOSFET is largely dependent on the drain bias current, only transconductance (com-

(continued on next page)

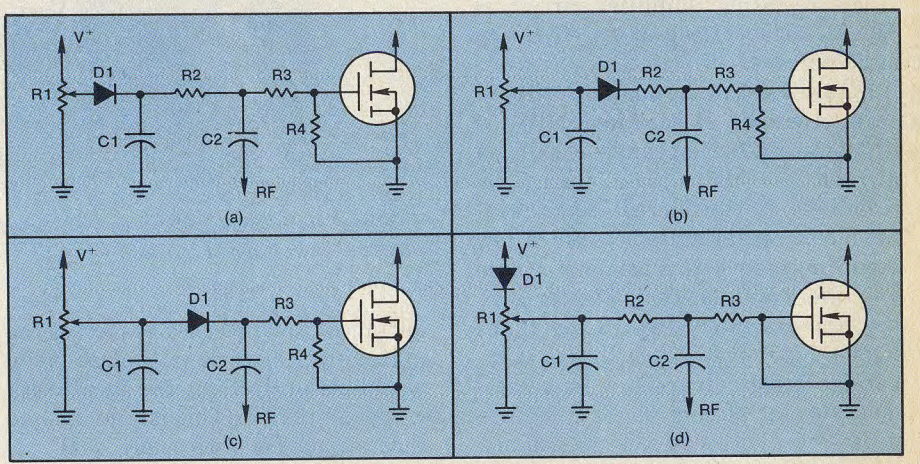
monly, g_m) matching within ±10 percent is required. The circuit board was designed to permit the several biasing configurations shown in Fig. 3. In configuration (a), which is used in the amplifier described here, diode D1 prevents positive voltage being fed back to the bias source in the event of a drain-gate short in one of the FETs. This serves to protect the other three devices from gate overvoltage. The C1-R2 combination establishes an RF shunt from the gate to the ground (mandatory for circuit stabilization). Resistor R4 could also be used for this purpose, but it would have a relatively low value, resulting in unnecessarily high current being drained from the bias supply. Normally, R4 is only a DC return to ground, required by the one-directional operation of D1. Resistor R3 is a low-valued device that prevents parasitic oscillations. Variations (b) and (c) in Fig. 3 are basically alike, except for R2, which can be used to control the amount of RF rectified by D1. In addition to blocking the DC in one direction, D1 can be used for proportional biasing in which the bias voltage increases with RF drive. This allows the initial idle current to be set to a low value, increasing the system efficiency. Gate Q trimming in circuits (b) and (c) of Fig. 3 is done with resistor R4.

The last remaining configuration of Fig. 3 is circuit (d), in which D1 is moved in series with R1 eliminating R4. The value of R1 must be high enough to prevent destruction from a drain-gate short. The common bias here is derived from integrated circuit element IC1 (part number MC1723CP), which provides both line and load regulation. The line voltage regulation is defeated when the voltage to the power input falls below 24 VDC. In this case, the bias input can be used for automatic level control (ALC) shutdown or as part of a linear ALC control. The regulator output voltage is adjustable from 0.5 to 0.9 VDC with resistor R5 (Fig. 2), which can be permanently set between 7 and 8 VDC. This voltage is also controlled by the combination of R10 and R25 of Fig. 2. Element R25 is a thermistor, and is tied to the heatsink for bias temperature compensation.

Referring to Fig. 2, the input from T1 is fed to the gates through C7-C10 and R15-R18. Input matching is initially done at the high end of the amplifier's bandwidth (30 MHz). In contrast to a bipolar push-pull circuit, in which the base-to-base impedance varies with the class of operation, the gate-to-gate impedance of a common-source FET circuit is always twice that from gate to ground. In this case, where two FETs are in parallel on each side of the circuit, the gate-to-gate impedance equals the gate-to-ground impedance of one device. Analysis of the amplifier circuit, via Smith-chart data, has shown this to be 3.45 ohms.



2. This schematic diagram presents a complete listing of all the circuit elements needed *to assemble the power amplifier. Note the parallel, push-pull configuration of the transistors.*



3. Four biasing arrangements are possible. *The configuration in (a) has been chosen for the amplifier described in the text.*

The effects of resistors R11 through R14 and R21 through R24 are minimal and can be disregarded in any circuit evaluation. Considering the standard integers for T1's impedance ratio, a value of 9:1 appears to be the closest (at 50 ohms) with that element's 5.55 ohms impedance for the secondary. This would set the values of R15 through R18 at 2.0 ohms. Using these resistances, there would be a resulting 3.5-dB gain loss and about 1 W would be dissipated in each resistor. For

(continued on p. 93)

these reasons, it was decided to reduce the values of the resistors to 1 ohm, and trim the values of C1 and C2 to achieve the lowest possible VSWR. As a tradeoff, the VSWR will peak slightly at frequencies between 15 and 20 MHz, but will still remain below 2.0:1.

Negative feedback is derived from a winding in T2 through resistors R19 and R20. Its purpose is to equalize the load impedance for T1 and reduce the amplifier's gain at low frequencies. Since the gate-to-source capacitance of a MOSFET is fairly constant with frequency, the amount of feedback voltage required is inversely proportional to its reactance. This function should be more or less linear, unless the inductive reactance of T1 is too low, or if resonances occur somewhere in the circuit. Computer analysis was not performed on the negative feedback system[1]; rather, a simple approach was taken[2] in which the gain difference between 2 and 30 MHz was used to determine the feedback voltage required to equalize the voltages of the secondary of T1 at these frequencies. Given an input impedance of 45 ohms at 2 MHz, and a feedback source delivering 15 VDC (rms), the values of R19 and R20 should be about 10 ohms each.

Designing output transformers

A ferrite toroid or a two-hole balun-type core can be used for T2. The use of relatively low permeability material with a high Curie temperature is recommended, since the minimum inductance requirement for the DC feed winding is less than 2μH. Depending on the material, T2 can run at temperatures from 200 to 250°C, and the wire insulation must be able to withstand this much heat. Several different output transformer configurations (T3) were tried, including the transmission-line types of Fig. 4. Although these particular types are difficult to make, they have the advantage of permitting low-permeability, low-loss ferrite material to be used with multiple-turn windings. Because of the high power levels of the amplifier, heat in the output transformer was a major problem. High-permeability materials, required in the metal-tube and ferrite-sleeve transformers, could not be used because of their higher losses and low Curie temperatures. On the other hand, low permeability cores with larger cross-sectional areas were not

(concluded on p. 120)

MSC INTRODUCES SIEMENS SOLID STATE MICROWAVE PRODUCTS

Presenting...

The SMR Series of DIELECTRIC RESONATOR MATERIAL

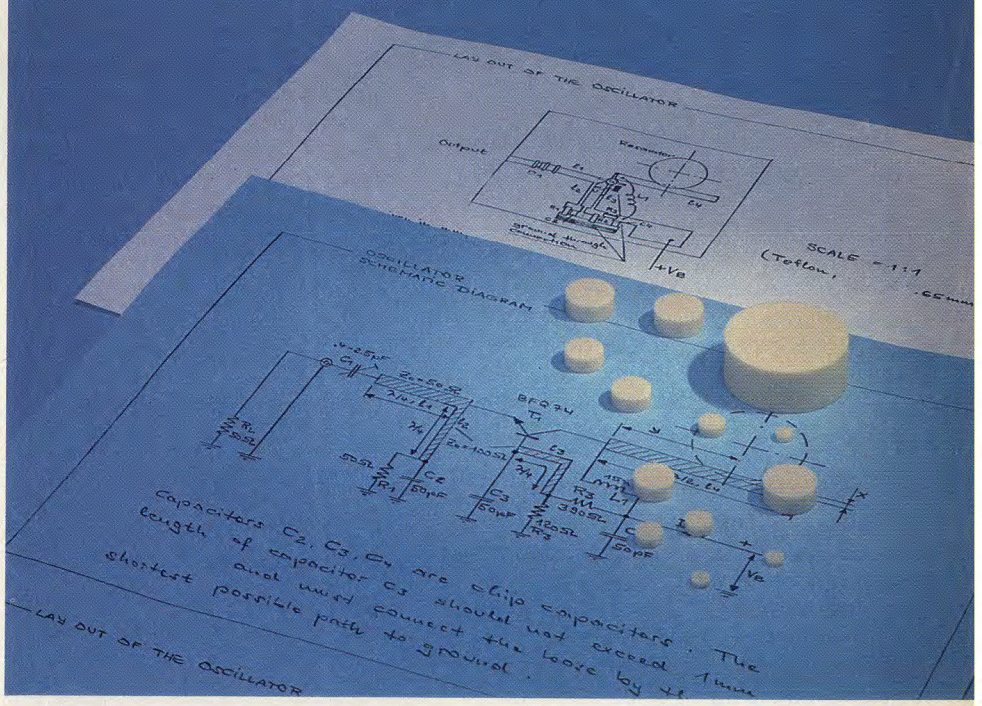
The Siemens line of Dielectric Resonators combine high Q with excellent temperature stability. These features in addition to their tuning capability assures direct applications in *microwave oscillators* and *filters*. Resonators are currently available for applications from 2–15 GHz.

Center frequency and temperature coefficients can be changed to meet your design requirements. Application notes are available for oscillator designs at 4 GHz and 10 GHz.

ELECTRICAL CHARACTERISTICS

Part Number	SMR 95100	SMR 95060	SMR 95040
Center Freq. (GHz)	10.0	6.0	4.0
Dielectric Constant	38.5	38.5	38.5
Temp. Coefficient (ppm/°C)	1.0	1.0	1.0
Q Factor	5000	6670	10,000
Diameter × Height (mm)	5.0 × 2.0	9.0 × 3.5	13.0 × 5.0

Contact MSC regarding additional information on our Dielectric Resonator products.



MSC MICROWAVE SEMICONDUCTOR CORP.
A Siemens Company
100 School House Rd., Somerset, N.J. 08873 (201)469-3311 TWX(710)480-4730 TELEX219929

READER SERVICE NUMBER 67

Part 2: Deep-Space Laser Communications

Design Considerations for Deep-Space Transmitters

By using low power and very narrow pulse widths, laser transmitters for deep-space communication systems can operate at extremely high data rates.

Morris Katzman, Project Engineer, The Aerospace Corp., 2350 East El Segundo Blvd., El Segundo, CA 90245.

THE first part of this series (*Microwaves & RF*, December, p. 70) discussed the design of optical receivers for deep-space communications. The point was made that, if the receiver was sensitive enough, a laser transmitter with low efficiency could be used successfully. The laser transmitter's contribution to the overall system is the generation of very narrow, high-peak-power pulses that make high data rates practical.

There are basically four source candidates for a laser transmitter: GaAs diode lasers, GaAs-diode-pumped Nd:YAG devices, GaAs-diode-pumped doubled Nd:YAG sources, and CO_2 lasers. Their main characteristics are presented in the table.

Diode lasers are small, rugged, and relatively efficient, but available only over a limited frequency range (wavelengths of about 0.8 to 1.7 μm). In their favor is their long potential lifetimes (about 10^5 hrs). They can even be modulated directly. The fly in the ointment is that they have limited power per diode, leading to the use of arrays and complicated power combination schemes. At present, single-diode lasers produce only about 15 mW for off-the-shelf systems and about 100 mW in the laboratory. Another problem is that the lifetimes projected by researchers have not been demonstrated because of the difficulty of performing accelerated life studies on solid-state devices. When diode devices have been tested, they have shown wavelength shifts as much as 8 Å after only 600 hrs at 40°C.

GaAs-pumped Nd:YAG lasers avoid such beam-combining headaches. Unfortunately, the electrooptical equipment that modulates these sources, by rotating the plane of polarization via a Pockel cell, is fairly elaborate. This is essentially the case for both types of Nd:YAG devices, whether fundamental (1.064-μm wavelengths) or doubled (0.532-μm wavelengths).

Increased power and higher data rates will be available when effective power-combining techniques are developed. One method involves using passive fiber-optic circuitry. Another combines diode arrays in a frequency-division multiplexer.

Lasers based on CO_2 are considerably different from the other types of laser sources. Solid-state lasers are electron injected or optically pumped (Nd:YAG), while the CO_2 sources are pumped by gas discharge—in effect, by the collisions between electrons and gas molecules. Because of this, CO_2 lasers are essentially gas-discharge tubes with the usual reliability problems caused by vacuum seals, cathodes, and anodes. Nevertheless, DC-pumped CO_2 lasers have been

Characteristics of principal laser sources

Laser type	Operating wavelength (μm)	Overall transmitter efficiency (%)	Laser oscillator efficiency (%)	Lifetime
GaAs	0.89	1	5 to 10	Laboratory >40,000 hrs extrapolate to 10^5 hrs[1]
Nd:YAG	1.06	0.5	0.4 to 1	Established by laser pump diode array
Nd:YAG (with doubled frequency)	0.532	0.4	0.8	Established by laser pump diode array
CO_2	10.6	0.7[2]	10 to 15	Problem areas: CO_2—CO reaction, seals, and anode and cathode; RF excitation solves many of these problems

1. M. Ettenberg and H. Kressel, "The Reliability of Al(Ga) as CW Laser Diodes," *IEEE Journal of Quantum Electronics*, Vol. QE-16, p. 186 (February 1980).

2. J. H. McElroy, et al, "CO_2 Laser Communication Systems for Near Earth Space Applications," *Proceedings of the IEEE*, Vol. 65, p. 246 (February 1977).

operated in a laboratory environment for over 10,000 hrs. Yet, there can be lifetime problems, since CO_2 is a reactive gas and tends to go to carbon monoxide with time. Attempts to overcome the inherent life-limiting mechanisms have met with some success by replacing the DC discharge (and internal anode and cathode) with an external RF pump. These devices promise lifetimes as high as 50,000 hrs.

Heterodyne detection requires the use of critically aligned local oscillator and signal fields on the mixer crystal surface (in the receiver). In CO_2 laser sources, these detectors must be cryogenically cooled. Radiative cooling might be one way to cool the detectors; mercury cadmium telluride detectors currently operate at 150°K. These detectors are adequate for many situations.

Designing a new transmitter

A new design concept is being developed which uses a laser diode to generate the low-power pulses, isolation to prevent signal regeneration, and Nd:YAG power amplifiers for gain. Although the sketch that was shown in Fig. 1 (see *Microwaves & RF*, December, p. 71) presents two amplifier sections, this number will vary according to power requirements. An advantage of this kind of design is that a family of transmitters can be produced for different system needs and power requirements.

This method was made possible by the use of GaInAsP diodes that provide output in the Nd:YAG fluorescent band, 7 Å wide and centered at a wavelength of 1.064 μm (at oscillating bandwidths of 0.1 Å). Temperature control allows fine tuning within the band, with a sensitivity of about 2.5 Å/°C.

Isolation is needed in this setup to make the amplifier unidirectional, so maximum gain can be achieved without oscillation. For the optimum overall gain, the loop gain within each section should be kept below unity (gain × reflectivity ≤ 1). Thus, for a gain of 30 dB, the reflectivity at the ends must be less than 0.001. This can be achieved with antireflection coatings and/or Brewster-angle end surfaces. Active optical isolation will probably not be necessary.

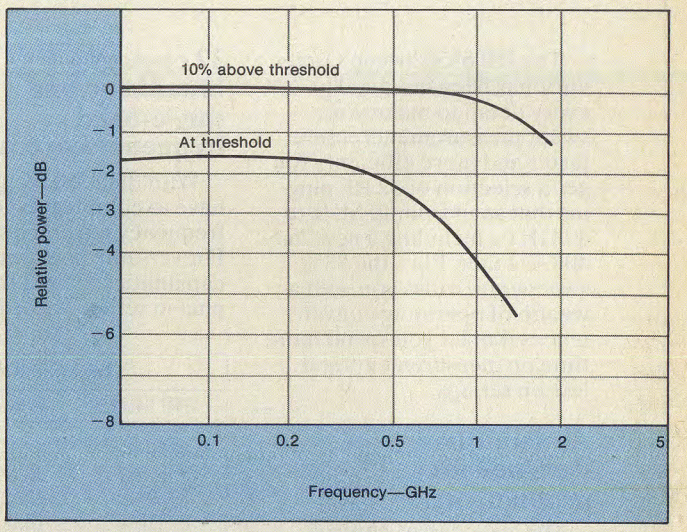
The Nd:YAG band is relatively insensitive to temperature variation (about 0.3 Å/°C). Also, it is homogeneously broadened, which means that the diode output doesn't have to be positioned in the exact center of the gain curve in order to deplete all of its stored energy.

Modulating the source

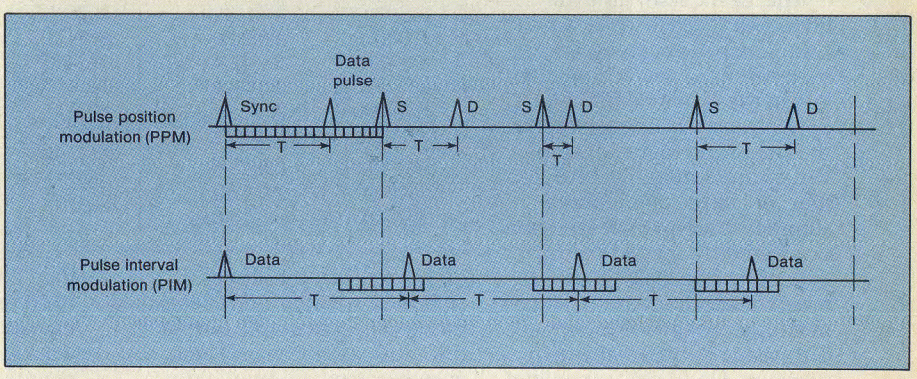
GaAs diodes can be modulated simply and directly over a wide modulation frequency range from near DC to 1 GHz, although only at very low output powers. Figure 2 shows laser diode output as a function of modulation frequency for two conditions, 10 percent above threshold (top) and at threshold (bottom).

There are basically three control methods that form the basis of laser modulation: "Q" switching, mode locking, and opening and closing the resonator output port (cavity dumping). Q switching made the development of range-measuring systems possible despite the extremely low efficiencies of ruby lasers. Modulating the Q of the resonator cavity boosts peak power levels by orders of magnitude. It can

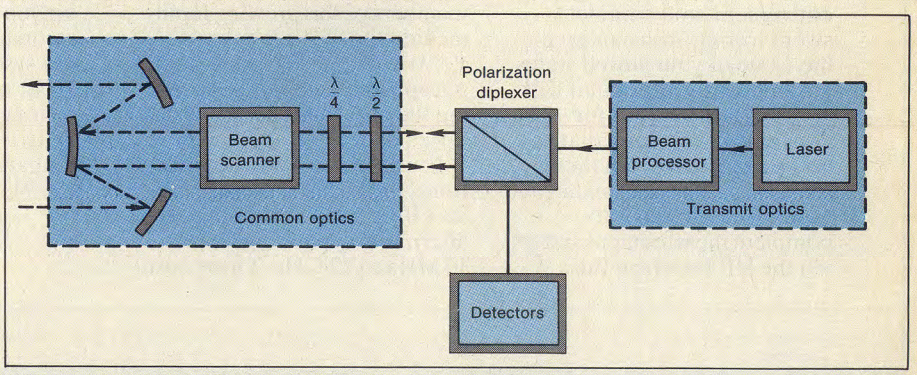
(concluded on p. 98)



***2. The relative power of an optical signal decreases** as the modulation frequency increases beyond 0.5 MHz.*



***3. Pulse position modulation (PPM) and pulse interval modulation (PIM)** differ in PPM's use of a synchronizing pulse.*



***4. The use of a half-wave plate** in the common optics of a transmit-receive system permits the polarization plane to be switched by 90 degrees.*

 (continued from p. 95)

be done by electrooptical modulation or by rotating one mirror of the Fabry-Perot resonator.

Mode locking occurs when the Q is modulated at the critical frequency of c/2L, where c is the speed of light and L is the length of the optical cavity.

The third control method, opening and closing the resonator, can be achieved by polarizing the radiation in the cavity. The preferred polarization sense is transmitted through the cavity while the other polarization is suppressed. By electrooptically rotating the plane of polarization at the required instant, the preferred polarization is reflected out of the cavity (i.e., the port is opened). This permits pulses to be generated at controllable time locations, and at pulse repetition frequencies up to a multimegahertz rate. The input beam is polarized in one element, rotated (or not rotated) in the next element, and passed (or absorbed) in the third element. The result is pulse-position modulation (PPM).

Pulse-position modulation should soon be practical at increasingly higher rates, and pulses as narrow as 76 picoseconds have already been achieved under laboratory conditions. Since commonly used laser wavelengths are in the micrometer range, while resonators operate at wavelengths of tens of centimeters, there is a dimensional relationship between the laser and resonator of about 10^5. Because of this ratio, many longitudinal (frequency) modes can be supported, and since pulse narrowing varies with the number of modes under the Nd:YAG fluorescent band, nanosecond and picosecond pulses are available.

Another modulation format, pulse-interval modulation (PIM), is actually a variation on pulse-position modulation. The two differ mostly in the use of a synchronous pulse (see Fig. 3). Pulse-position modulation employs a synch pulse to define a major time division, often called a "window." The window is divided into time slots that correspond to the particular data values being used. In PIM, there are no synch pulses and the window is defined by the first data pulse—basically, the data point is in the time interval between data pulses. Again, the window is divided into time slots to define the interval. To avoid ambiguity, the pulse width should not be large compared to the time slot.

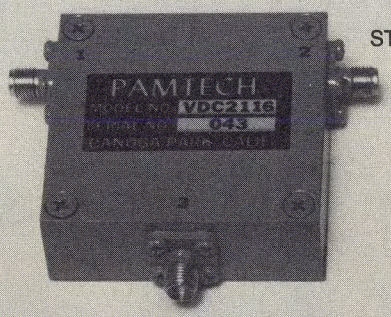
There are two major options to use when designing the optics section:

- reflective or refractive optics, and
- gimballed mirrors or gimballed telescopes for steering the light beam.

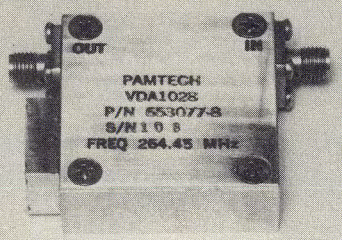
Refractive optics are simpler than reflective optics, but tend to be bulkier. For the latter, Cassegrain optics enable a single telescope to act as both transmitter and receiver. Diplexing can be performed via circularly polarized beams. Each lasercom can transmit one sense of polarization and receive the other. A circularly polarized beam changes to linear polarization when it passes through a quarter-wave plate; a half-wave plate will rotate the plane of polarization by 90 degrees. So, by using the half-plane plate through insertion and withdrawal, the receive and transmit polarization-planes can be switched (Fig. 4). Using these techniques, one station can transmit right-hand polarization and receive left-hand, while the other can transmit left-hand polarization and receive right-hand, acting much like a TR switch in a radar system. ••

PAMTECH

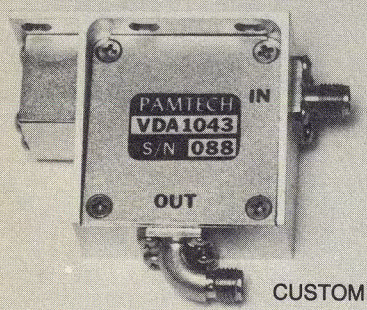
LUMPED-ELEMENT
Isolators • Circulators
10MHz-1000MHz



STANDARD



HI-REL

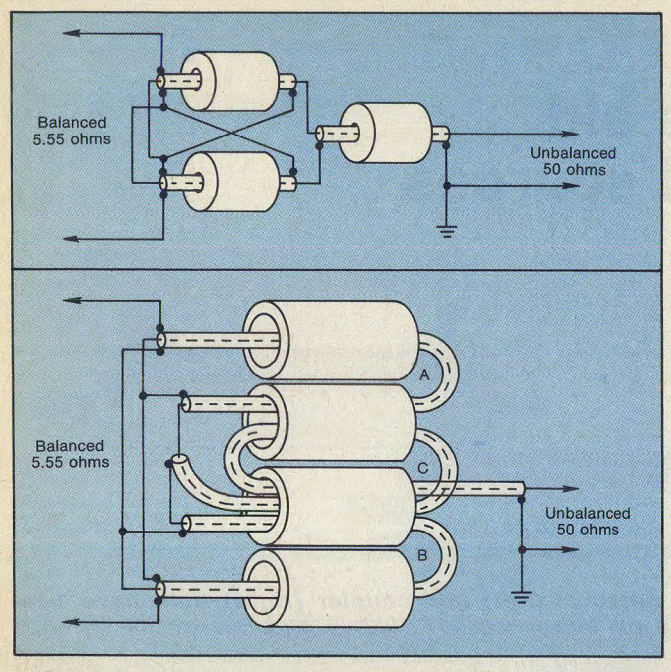


CUSTOM

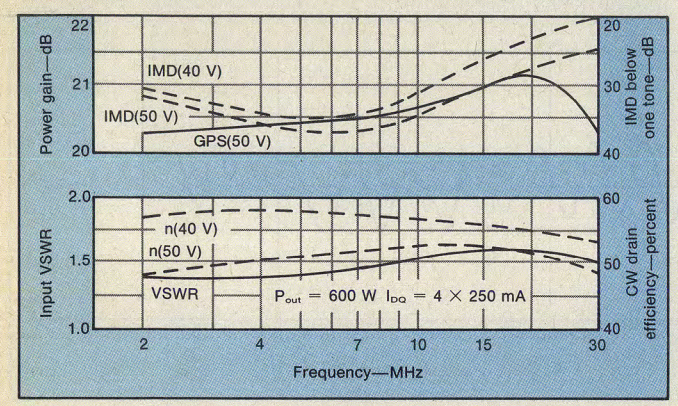
Reliability Through Quality
PAMTECH
PASSIVE MICROWAVE TECHNOLOGY
(213) 999-3110

8030 REMMET AVENUE #1, CANOGA PARK, CALIFORNIA 91304

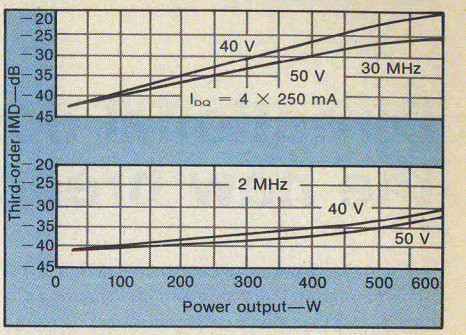
READER SERVICE NUMBER 69



4. The design of output transformer T3 *can be handled by a number of different approaches. Two transmission-line types are offered here.*



6. The power gain is at least 20 dB *over the full operating bandwidth, with an input VSWR that never exceeds 2.0:1.*



5. The third-order intermodulation distortion *reaches a peak when the amplifier is operated at full power at the high end of the bandwidth.*

the minimum inductance required for 2-MHz operation, two of these transformers, with low-permeability ferrite cores, were connected in series. Both have 9:1 impedance ratios. Alternatively, the secondaries can be connected in parallel with six turns in each, twice the usual number. Capacitor C11 must be able to withstand high RF currents, and must be soldered directly across the transformer primary connections. Regular mica or ceramic capacitors cannot be used, unless several smaller values are paralleled together.

Evaluating the performance

Due to the mechanical proximity of the four MOSFETs, the RF ground of the circuit board is poor, resulting in 1.0- to 1.5-dB gain loss at 30 MHz (see Fig. 5). One way to improve the ground plane is by connecting all the source leads together with a metal strap over the transistor caps. Another method places solder lugs under each one to the nearest source lead. In this case, the heatsink will double as the RF ground.

Although the third-order intermodulation distortion (IMD) is not exceptionally good (Figs. 5 and 6), the worst-case fifth-order products are −30 dB or less at all frequencies. As expected with FETs, the ninth- and higher-order products are at the −50-to-60-dB level. It is also apparent from Fig. 5 that the IMD does not increase at reduced power levels, as is common with bipolar amplifiers. The even-order output harmonic content depends largely on device balance, as is true of any push-pull circuit. The worst case occurs at low frequencies, where numbers like −30 to −40 dB for the second harmonic are typical. The highest third-harmonic amplitude of −12 dB is at carrier frequencies from 6 to 8 MHz. Of course, this performance can be improved through the use of a suitable harmonic filter.[3] The stability of the amplifier has been tested into a 3.0:1 load impedance mismatch at all phase angles. It was found to be completely stable, even at reduced supply voltages. In a MOSFET transistor, the ratio of the feedback capacitance to the input impedance is several times higher than that of a bipolar transistor (which reflects the distinction between common-source and common-emitter circuits). As a result, a properly designed FET circuit should be inherently more stable than a bipolar circuit, especially under varying load conditions.

Remember the heatsink

Special attention must be given to the heatsink of this amplifier, particularly in view of its operating power levels. With the 200 to 300 W of heat generated by the four transistors in a small physical area, heat conduction should be as efficient as possible. This can only be done with high-conductance material, such as copper. If aluminum is used for the heatsink, a copper heat spreader should be employed between the transistor flanges and the heatsink surface.

References

1. Motorola Semiconductor Products, Inc., Scottsdale, AZ, "Low-Distortion 1.6 to 30 MHz SSB Driver Designs," AN-779.
2. Motorola Semiconductor Products, Inc., Scottsdale, AZ, "A Two-Stage 1.0-kW Solid-State Linear Amplifier," AN-758.
3. H. Granberg, "MOSFET Power in the kW Level, *QST*, (December, January 1983).

Directional components aid the new breed of signal sources

Since signal sources up to 26.5 GHz are no longer uncommon, there is a need for precision components, such as directional couplers and detectors, that also work at these higher test frequencies. Such a need has led to the model 2610 10-dB directional coupler and the model 2610S directional detector (Fig. 1). Both have been designed to operate over the full 1-to-26.5-GHz bandwidth with insertion losses of only 1.6 dB and VSWRs of 1.5:1. The precision devices have been built for laboratory as well as production applications, such as broadband power monitoring or wideband power leveling of microwave signal sources.

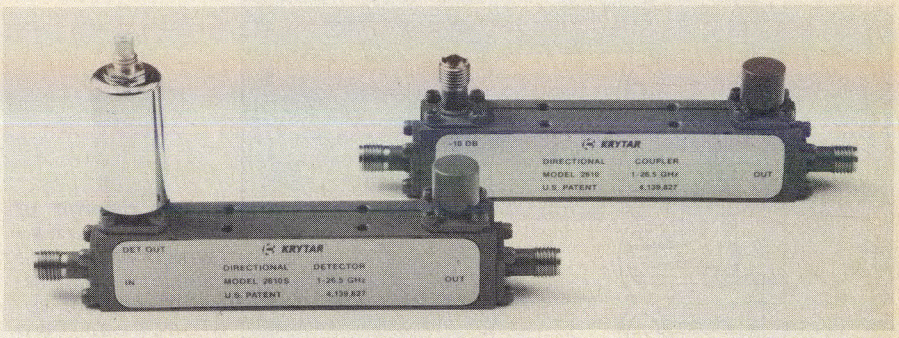
The directional coupler uses stripline construction to provide coupling (with respect to output) of 10 ± 1 dB with less than ± 0.6 dB ripple from 1 to 12.4 GHz and ± 0.8 dB over the full bandwidth (see Fig. 2). The coupler features a tapered line design laid out by a special computer-aided-design (CAD) program. An examination of the circuitry reveals offset coupled striplines set on three layers, with the coupled lines separated by a thin dielectric layer.

The directivity of the device is at least 14 dB from 1 to 12.4 GHz and a minimum of 12 dB over the remainder of the frequency range. The VSWR is no higher than 1.5:1 from 12.4 to 26.5 GHz, and improves to 1.35:1 for frequencies below 12.4 GHz. The insertion loss, while measured at 1.6 dB for frequencies above 12.4 GHz, falls to 1.1 dB below this point. The coupler has been rated to accept input powers up to 20 W on the average and 3 kW on peaks.

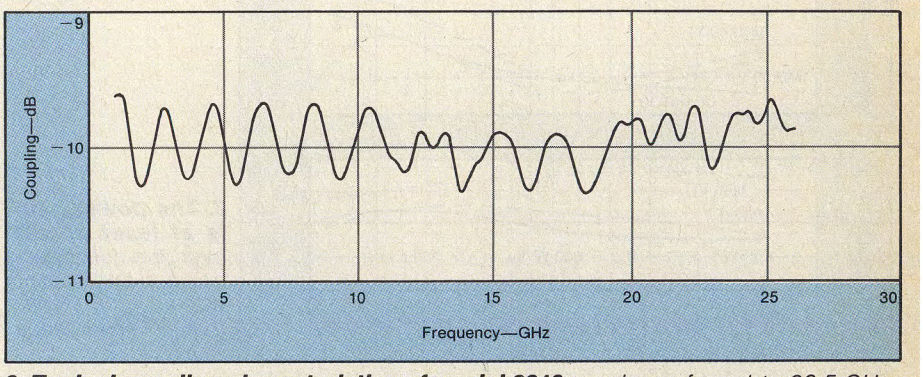
The directional detector features a frequency response which is within ± 0.7 dB from 1 to 12.4 GHz and ± 1.2 dB from 1 to 26.5 GHz. Figure 3 shows its output power-leveling capability. Its directivity is identical to that of the directional coupler, with similar characteristics for both VSWR and insertion loss. Although in many respects this device is a modified version of the directional coupler, the zero-bias Schottky detector unit has been mounted directly on the coupler's housing, rather than via an RF connector. This improves the ruggedness of the devices and minimizes frequency response ripple caused by coupler/detector VSWR interaction. The polarity of the detector's output is negative, and the unit has a low-level sensitivity of better than 40 μV/μW. The device has been rated for average inputs as high as 1 W.

Both coupler and detector use SMA-compatible 3.5-mm male or female coaxial connectors. The output of the detector is a female BNC or SMC jack. P&A: $825 (2610) and $1,250 (2610S); 4 wks. **Krytar, 1292 Anvilwood Ct., Sunnyvale, CA 94086. (408) 734-5999.**

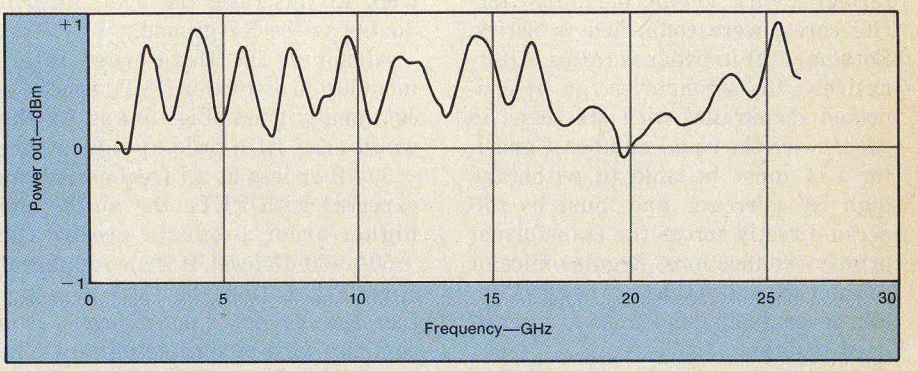
CIRCLE NO. 178



1. The directional detector (left) and coupler (right) both have 1-to-26.5-GHz bandwidths *with extremely good frequency responses over the full range.*



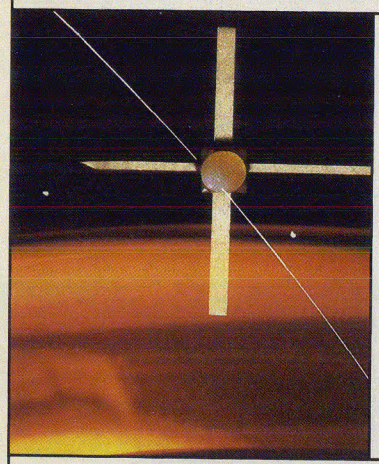
2. Typical coupling characteristics of model 2610 *are shown from 1 to 26.5 GHz.*



3. This broadband power-leveling performance *is made possible by the flatness of the coupler and the detector, and the absence of an extra connector.*

Microwaves & RF

FEBRUARY 1983 • VOL. 22, NO. 2



cover feature

89 **DBS expectations boost GaAs FET marketplace.** This month's cover feature, in our product technology section, analyzes Mitsubishi's plans to meet the high-volume semiconductor needs of DBS. (Artwork courtesy of Mitsubishi Electronics America, Inc., Sunnyvale, CA. Artwork produced by J-2 Marketing Services, Brea, CA.)

departments

13 Feedback
17 Editorial
53 R&D Roundup
66 For Your Personal Interest
118 Infocenter
120 Looking Back
120 Looking Ahead

news

28 **He takes over where the schools leave off.** Dr. Ralph Nash, a former NASA scientist, has transformed his basement into Adventure in Science, a learning center for children.

39 Innovative design marks new GaAs "foundry"
47 Tubes make strong showing at digital-oriented IEDM

19 The Front End • **57** Financial News • **62** On the Agenda • **64** People

design features

68 **Si Impatts Exhibit Low Noise At MM-Waves.** D.M. Brookbanks and colleagues, from Plessey Research Ltd., refute the theory that Impatt devices are too noisy for low-noise, LO applications.

74 **New GaAs Impatt Theory Explains MM-Wave Operation.** Glenn R. Thoren, from Raytheon's Missile Systems Div., tells how computer simulations demonstrate GaAs Impatt mm-wave operation.

80 **Improved IMD Measurements for GaAs Power FETs.** Paul M. White, of Raytheon, uses data on third-order intermodulation distortion to provide accurate determinations of GaAs FET linearity.

83 **Electrical Properties Govern Substrate Effectiveness.** Vijay Borase, from Materials Research Corp., focuses on the electrical properties of alumina and their implications for design.

product technology

91 **ISOFET Evolution Yields High-Power Devices.** Dick Moss, of Acrian, predicts ISOFETs will replace bipolars as high-power devices.

94 Single device is 40-W building block
*95 Mixer/preamplifiers are next on the road to integration
101 The first RF hand-pager?

*102 New Products • **115** Application Notes • **117** New Literature

* *Domestic Editions Only*

An engineer responds

To the Editor:

Close scrutiny of the remarks of Dean Watkins (*Microwaves & RF*, December, 1982, p. 16) on engineering careers reveals the following management program:

1. Work hard to get good young engineers into the company.
2. Shift productive engineers into management as they get older. (Since there is a practical limit to engineering salaries, it is the only way for them to earn more money.)
3. Provide no continuing education program. Get rid of older engineers who don't adapt to new technology and become obsolete.
4. Continually publicize that there is an engineering shortage and it is getting worse. State that your own company can recruit successfully to keep stockholders and customers satisfied.
5. Return to Step 1.

Richard G. Wiley
Senior Research Engineer
Syracuse Research Corp.
Merrill Lane
Syracuse, NY 13210-4080

Power-handling pulpit

To the Editor:

I have noted the changes proposed for *M&RF* and wish you well. There is much that needs to be said, and your initial articles are good. Your proposed list of issue themes also looks interesting.

In particular, Snapp's article on broadband RF amplifiers ("Practical Silicon MMICs Challenge Hybrids," *Microwaves & RF*, November, 1982, p. 93) drives home some points I first made in my 1962 book, *Handbook Of Transistor Circuit Design*. I have since extended these in several respects. Transistor transconductance is indeed a well-defined function of a transistor's output current, whereas transistor base input conductance is a function of the expression:

$$\text{Input conduct.} = G\,(\theta/\sinh\theta)\times(1-\cosh\theta)$$

where θ, which depends on minority carrier lifetime in the base, should approach zero. The first expression approaches unity in the limit, but the second has a leading θ^2 term. On the other hand, transconductance is a function of:

$$g_m = G\,(\theta/\sinh\theta)\,(\cosh\theta)$$

which has a limit value of unity. The G is present with both terms. (This is derived directly from Lo, et al, *Transistor Electronics*, published in 1955.) The transistor beta, which is a function of the ratio of transconductance to input conductance, is very sensitive to the value of θ.

The power-handling ability of all active devices, bipolar and field-effect transistors and electron tubes, is a function of the ratio of the effective device transconductance to its output current. The consequences of this have not been published anywhere.

I hope you will have the courage to invite and publish articles on controversial aspects of some of these subjects, as advancing the state of the art is critically dependent on such material getting a fair hearing.

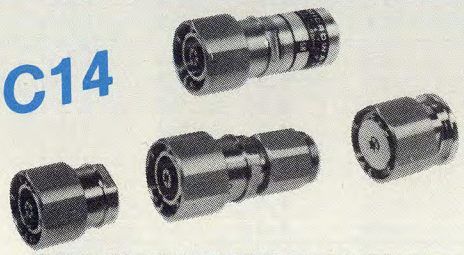
Best of luck.

Keats A. Pullen
2807 Jerusalem Rd.
Kingsville, MD 21087

14mm CONNECTORS, COMPONENTS, & INSTRUMENTS from MAURY

Now YOU HAVE A SOURCE!

MPC14



- HIGH PRECISION 14mm CONNECTOR DC to 8.5 GHz (EQUIV. TO GR900®).
- COMPREHENSIVE LINE OF PRECISION COMPONENTS AND INSTRUMENTS

MAURY High Precision MPC14 Connectors are for all practical purposes equivalent to GR900® connectors and are fully mating compatible. The connector body and center conductor are fabricated from tellurium copper and are gold plated. They employ a simplified eight tooth gear ring and an improved 1.00 hexagonal nut so that the junctions can be accurately torqued. An extensive line of components and instruments are available such as ANA calibration kits, sliding terminations, adapters, etc., which are partially summarized here. Also available are waveguide to coaxial adapters, tuners, etc. Send for complete details.

®GR900 is a trademark of General Radio Co.

CONNECTORS & ACCESSORIES

MODEL NO.	DESCRIPTION
2480A	Connector, Rigid Line (Equiv. GR900BT)
2480B	Connector, Panel Mnt w/nut - Rigid Line [1]
2480C	Connector, Panel Mnt w/out nut - Rigid Line [1]
2480D	Connector, Flexible Cable - MC214
2480E	Connector, Semi-rigid Cable - 0.325 dia.
2480L	Connector, Beadless (LPC14)
2480P	Panel Mount Kit for 2480A
2480R	Rotatable Centering Gear Ring
2498K	Tool Kit for 2480A, B, C
2498N	1.00 Hex Locking Nut (replacement kit).
2498T	Torque Wrench, 1.00 Hex.
A024	Connector Gage Kit.

ADAPTERS - COAXIAL TO COAXIAL

MODEL NO.	DESCRIPTION	FREQ. RANGE
2406C 2406D	MPC14 to N female, MPC14 to N male,	DC-8.5 GHz
2407A 2407B	MPC14 to APC3.5 female MPC14 to APC3.5 male	DC-8.5 GHz
2458A 2458B	MPC14 to LT female MPC14 to LT male	DC-5.0 GHz
2607	MPC14 to APC7	DC-8.5 GHz

COMPONENTS & INSTRUMENTS

MODEL NO.	DESCRIPTION
2450C	ANA Calibration Kit (HP8542B)
2450K	ANA Calibration Kit (HP8409B)
4096A	Direct Coupler, High Direct. 0.1 -0.6 GHz [2]
4096	Direct. Coupler, High Direct. 0.25-0.5 GHz [2]
4097	Direct. Coupler, High Direct. 0.5 -1.0 GHz [2]
4094	Direct. Coupler, High Direct. 0.75-1.5 GHz [2]
4091	Direct. Coupler, High Direct. 0.95-2.2 GHz [2]
4095	Direct. Coupler, High Direct. 1.5 -3.0 GHz [2]
4092	Direct. Coupler, High Direct. 1.7 -4.2 GHz [2]
4093	Direct. Coupler, High Direct. 3.7 -8.5 GHz [2]
4098A	Direct. Coupler, 300 watt, 10 to 400 MHz, 40 dB coupling
4098B	Direct. Coupler, 1000 watt, 10 to 300 MHz, 50 dB coupling
2401A	Sliding Termination, Bead Support, 0.9-8.5 GHz
2408	Sliding Termination, Beadless, 0.9-8.5 GHz
2404	Sliding Short, Bead Support, 0.9-8.5 GHz
2409	Sliding Short, Beadless, 0.9-8.5 GHz
2410A	Fixed Termination, DC-8.5 GHz
2415A	Fixed Short, Flat Plane
2415B	Fixed Short, Collet in Short Plane
2416B	Open Circuit
2403( )	Airlines, Bead Support [3]
2453( )	Reference Airlines, Beadless [3]
2454A	Airline 2-Port Standard Set [4]
MT7119A	Cryogenic (Cold) Termination (77°K)
MT7109A	Thermal (Hot) Termination (373°K)
2459A	Ambient Termination (295°K)

NOTES:
[1] Integral Flange-can't unscrew. 1.25 square with four 0.136 holes on 0.938 centers (inches)
[2] High Directivity greater than 42 dB (except Model 4093 - 37 dB min), 10 dB coupling factor secondary connector is N female.
[3] Eight models available, 30 cm to 3 cm lengths.
[4] VSWR values of 1.0, 1.1, 1.25, 1.5 and 2.0; 7.495 cm long.

See our New Catalog in Microwaves PRODUCT DATA DIRECTORY!

MAURY MICROWAVE CORPORATION
8610 HELMS AVE., CUCAMONGA, CA 91730, USA • TEL: 714-987-4715 • TWX: 910-581-3408

MSAT '83 Microwave Systems Applications Technology
SEE US AT...BOOTH 1006
MARCH 8-10, 1983
Sheraton Washington Hotel
Washington, D.C.

READER SERVICE NUMBER 10

Si Impatts Exhibit Low Noise At MM-Waves

Impatt devices, particularly silicon, were thought to be too noisy for low-noise, LO applications. That's not necessarily true at millimeter wavelengths.

D.M. Brookbanks, Group Leader, Two-terminal Microwave Device Research, **A.M. Howard**, Group Leader, Two-terminal Microwave Device Technology, and **M.R.B. Jones**, Senior Scientist, Plessey Research (Caswell) Ltd., Allen Clark Research Center, Caswell, Towcester, Northants, England.

IMPATT diodes have acquired a reputation for being noisy and thus unsuitable for low-noise, local oscillator (LO) applications. This was particularly true of silicon devices at lower microwave frequencies, but even the gallium arsenide devices were not good enough to oust the Gunn diode from its role as the choice for LOs.

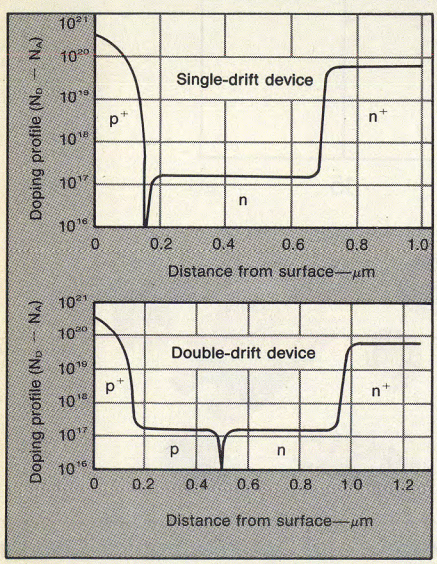
At millimeter wavelengths, however, the situation is quite different, since the Gunn diode's rapidly decreasing efficiency with increasing frequency leads to reduced output powers.[1] The use of the Impatt as an alternative LO then becomes quite attractive, particularly if many mixers are involved.

This article describes the noise performance achieved by silicon, millimeter-wavelength Impatt diodes. The devices were fabricated from uniformly doped, epitaxially grown silicon that was formed by the pyrolysis of silane at atmospheric pressure, using phosphine and diborane as the n- and p-type dopant gases. To minimize parasitic resistances, the substrates used were high-conductivity arsenic doped to minimize both the series resistance in the substrate and the contact resistance of the substrate metallization. Particular care was taken to obtain sharp interfaces and transition regions by minimizing autodoping and outdiffusion techniques described previously.[2]

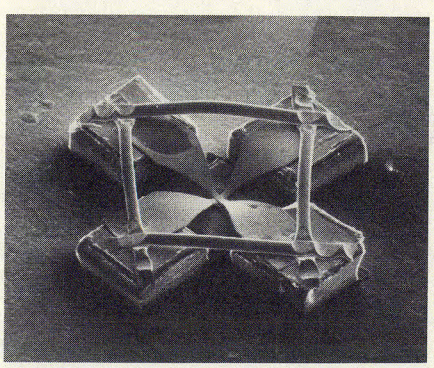
The layer structures were completed by either the diffusion or ion implantation of a boron-doped plus surface region having a very high surface concentration as contacts in the case of double-drift material and as abrupt junctions in the single-drift material. In the double-drift device, measurements indicated that the compensation region at the junction was less than 0.15-μm wide in an overall layer width of about 1 μm.[2] Figure 1 shows the doping profiles of both single- and double-drift W-band devices.

The contact metallization used for both faces was Cr/Pt/Au for high reliability, and the device diameters were typically 15 to 40 μm and 25 to 50 μm for the single- and double-drift devices, respectively. The overall thickness of the silicon was approximately 5 μm to minimize the parasitic resistance. In order to achieve this structure, an integral heatsink technology was employed, using gold as the heatsink material. This method of heatsinking resulted in the devices being thermally, rather than impedance, limited.

The device structure was completed by using a low-parasitic bonding geometry that incorporates four quartz blocks and two crossed low-impedance bonding tapes.[3] The overall structure is pictured in Fig. 2, which shows the ring of 25-μm wire connecting the quartz blocks and assisting in contact between the packaged device and the external circuit.



1. Noise measurements were made *on silicon Impatts with the doping profiles shown above.*



2. The structure of the devices used *included four quartz blocks and two low-impedance bonding tapes.*

RF characteristics

All of the results described in this article were obtained in resonant cap circuits using full-height waveguide. This type of circuit has proved to be ideal for the operation of relatively high-impedance Impatt devices because it can provide an optimum match at reasonable Q values, which provides high circuit efficiencies and

stable device operation, thus enabling the characteristics of the devices to be measured. The frequency was determined by the diameter of the cap, and the output power was maximized by the use of built-in E-H tuners and the waveguide short-circuit position.

As expected, the double-drift structures provided the highest efficiencies and powers because of their superior avalanche-zone characteristics and the reduced susceptance per unit area that arises from the presence of two drift regions. The best efficiencies achieved in the millimeter-wavelength range, shown in Fig. 3, confirmed the expected frequency independence of the efficiency of the silicon Impatt.[4]

The output power depended on the amount that junction temperature was allowed to rise, and the useful power outputs that could be obtained at junction temperature rises of 200°C were less than the state-of-the-art results.[5] The output was inversely proportional to the frequency, and powers in the W band could be as high as 200 mW for double-drift and 80 mW for single-drift devices at safe junction temperature rises.

These outputs, which are considerably greater than those achieved from Gunn devices, result simply from the increase in efficiency and are most useful at the high frequencies, where the efficiency difference between the Gunn and Impatt is the greatest.

The greater efficiency of the Impatt provides another important advantage: The device can be decoupled or "turned down" from its highest-power point to obtain improved oscillator stability. This capability has enabled low noise to be obtained at powers and efficiencies that are still well in excess of the Gunn diode's capability.

FM and AM noise measurements

The FM noise-measurement system used to evaluate the Impatts provides a direct measurement through a delay-line discriminator and a balanced-mixer detection system that feeds a wave analyzer via a low-noise amplifier.[6] The main advantage of a direct-detection system is that a highly stable LO is not necessary (unlike heterodyne noise-detection systems) and thus the system can be used over a broad bandwidth.

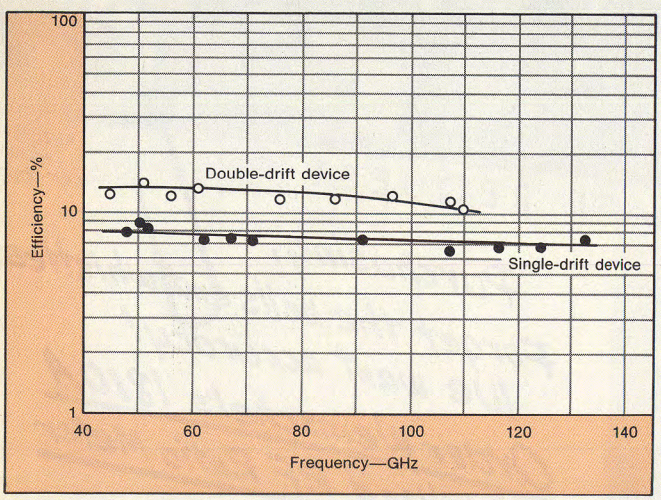
The bandwidth of the test bench, which is limited by the circulator used in the discriminator, is currently 80 GHz ±1.5 GHz. When measurements made on this system were compared with spectrum analyzer displays, good agreement was found for offset frequencies of 100 kHz to 1 MHz. This permits measurements to be made outside this narrow band around 80 GHz for assessment purposes.

However, the sensitivity of the system is limited by the power output of the oscillator under test, nonlinearities in the detectors, and the noise of the post-detection amplifiers. At 10 mW of RF power, the overall oscillator noise sensitivity is an RMS deviation of 4 Hz/$\sqrt{\text{Hz}}$ from 0 to 10 MHz. The noise test bench is calibrated by frequency modulating the oscillator under test in order to produce known side-band levels. It is at this point that the greatest error may occur, and the average of a number of measurements is necessary to insure an accurate calibration factor.

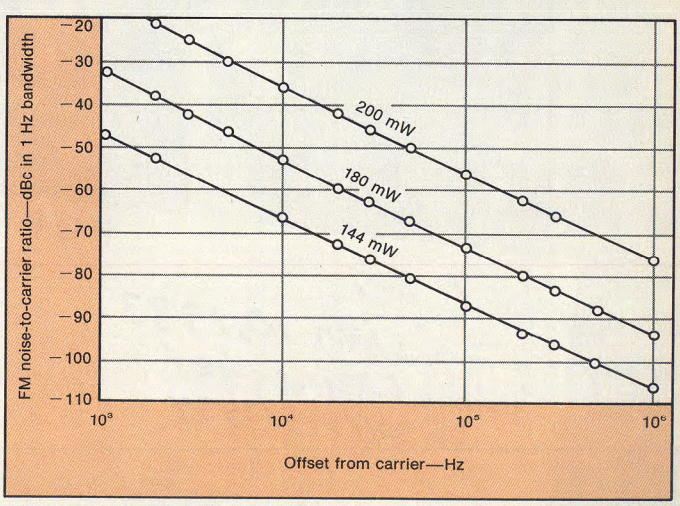
The FM noise measurements on a double-drift Impatt capable of 200 mW output power are shown in Fig. 4 as measured noise-to-carrier ratios. The slope of 6 dB/octave indicates that a white-frequency (constant-deviation) noise spectrum exists at offset frequencies greater than 1 kHz from the carrier. This usually is the case for Impatts, although measurements on single-drift devices have shown that some diodes exhibit deviations from this behavior to an f^{-1} characteristic at offset frequencies of 1 to 10 kHz. In general, single-drift devices exhibit noise-to-carrier ratios 5-to-10-dB worse than double-drift devices (for FM, 10 kHz) when operated under similar conditions.[7]

The RMS deviation of the device, shown in Fig. 4, remains constant ($\Delta f_{RMS} \approx 6\text{Hz}/\sqrt{\text{Hz}}$) as the output power is increased to 150 mW, but noise increases rapidly at power levels above 150 mW. At 200 mW the temperature of this device is beginning to rise above the safe junction temperature rise.

(continued on p. 71)



3. The efficiency of the devices tested *was independent of frequency in the millimeter-wavelength range. The double-drift devices exhibited better efficiency.*



4. Noise levels were found to increase *rapidly as power was increased above about 150 mW. Below 150 mW, the RMS deviation remained constant.*

The AM noise measurements were made by directly feeding the RF power into a single-ended detector and using a wave analyzer to measure the RMS noise voltage in a given bandwidth. The mixer conversion loss was measured by the DC variation of the RF power level, and the noise floor was estimated using a DC bias substitution method. The system detection limit was shown to be about −170 dBc at a 1-MHz offset.

Fig. 5 shows the measured AM noise of the diode. These measurements should be regarded as an upper limit for AM noise because this simple system has limited sensitivity. In addition, many factors may increase the measured AM noise above that of the oscillator. For example, since a typical Impatt oscillator may have AM and FM sensitivities of 1 to 2 mW/mA and 5 MHz/mA, the quality of the constant-current power supply is extremely important to insure that the supply does not contribute to the AM noise spectrum of the oscillator. FM noise spectra normally are not seriously degraded by power supply noise.

Noise behavior understood

The noise behavior of oscillators is reasonably well understood.[8,9] Theoretical expressions for the FM and AM noise of an oscillator are:

$$\Delta f_{RMS} = (f_0/Q_E)\,(kTBM/P_0)^{\frac{1}{2}} \quad (1)$$

$$(N/C)_{SSB}FM = (kTBM/P_0) \times [(S/2)^2 + (Q_E f_m/f_0)^2]^{-1} \quad (2)$$

$$(N/C)_{SSB}FM = \Delta f_{RMS}/2f_m \quad (3)$$

where:

$(N/C)_{SSB}AM$ = AM SSB noise-to-signal ratio

$(N/C)_{SSB}FM$ = FM SSB noise-to-signal ratio

f_0 = oscillation frequency

P_0 = oscillator power output

k = Boltzmann's constant

T = standard temperature, 290°K

f_m = modulation frequency (offset from carrier)

Q_E = external Q of the oscillator

B = measurement bandwidth

S = a measure of diode nonlinearity ($S = 2$ for max. output power)

M = noise measure of the oscillator

The noise measure, M, expresses the inherent noise performance of the active oscillator element relative to thermal noise. The main advantage of this quantity is that it does not vary with cavity-tuning conditions, unlike alternative noise units such as Δf_{RMS} or $(N/C)_{FM}$. However, care must be exercised if M is used to compare the noise performance of oscillators of different types. Because the output power is included in the formula for M, two oscillators exhibiting the same FM noise performance in terms of Δf_{RMS} or $(N/C)_{FM}$ may not demonstrate equivalence in M if there is a large difference in their power outputs.

This variation of FM noise with power output is more easily seen when plotting noise measure against normalized power output, as in Fig. 6, which compares devices taken from three process runs. In all cases observed to date, M has been flat up to about 75 percent of full output power. Because the external Q changes little in this region, the FM noise-to-carrier ratio is often a minimum in this area. This is also the most suitable operating point to insure a long life for the device because, as noted earlier, maximum power normally is obtained at unrealistic junction temperatures.

This relationship may in part explain the Impatt's reputation for poor noise characteristics. Published results on the basis of power and efficiency are almost always made near burnout, where the device is indeed noisy. There is a less than 10-percent reduction in efficiency at more conservative power levels compared to operation at the maximum power point.

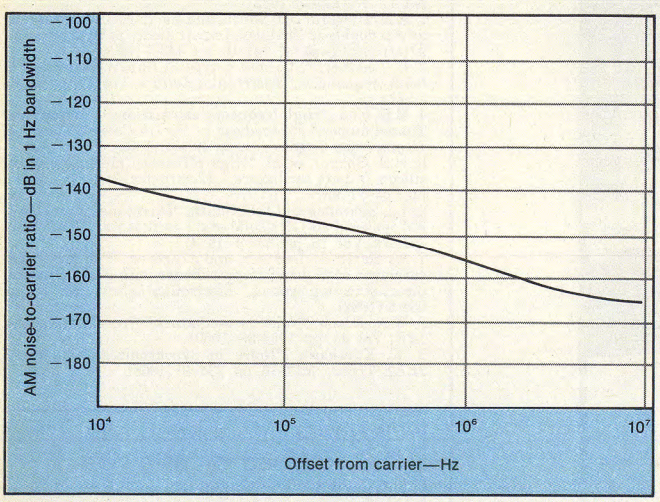
A typical spectrum of a device operating at 150 mW is shown in Fig. 7. The behavior of single-drift devices was very similar except that the higher noise-to-carrier ratios led to comparably greater noise measures.

Comparison with other devices

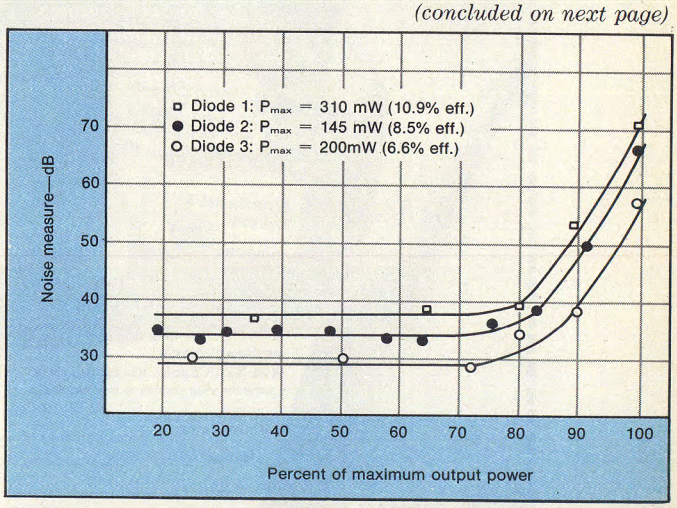
The noise measurements obtained in these tests are much lower than those normally associated with Impatt devices and, in fact, compare very favorably with Gunn diodes. Possible reasons for this improvement in noise measure and for the differences between single- and double-drift devices may be found in the mechanism that produces noise in an Impatt.

Because the generation of carriers in an Impatt is a result of impact ionization, the avalanche noise will be related to the statistical nature of the avalanche process, which leads to a constant-deviation FM noise. It can be shown that the magnitude of this

(concluded on next page)



5. The above AM noise measurement should be considered *an upper limit for the device, since the simple test system used had a limited sensitivity.*



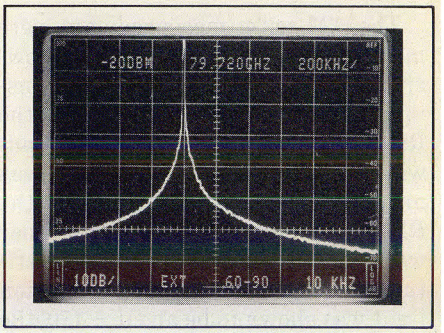
6. Measurements on devices taken from three process runs *showed that the noise measure was constant up to about 75-percent power, then increased rapidly.*

noise will be reduced if the number of ionizing events necessary for the generation of the current can be reduced. This is achieved in two ways in the millimeter-wave silicon Impatt. First, the increased peak field leads to both higher values and closer equality for the electron and hole ionization coefficients; second, the reverse saturation current is increased, thus reducing the carrier multiplication required. The same argument can be applied to the comparison of the single- and double-drift devices in that the presence of both carriers in the avalanche region of the double-drift device leads to reduced multiplication factors and, hence, less noise.

When comparing the noise performance of different devices, it is essential to define the role that the device is expected to fulfill. Noise measure is a useful figure of merit in that it provides a parameter by which different devices can be compared. The principal areas of interest fall into two categories: noise close to the carrier for Doppler-based systems and noise far from the carrier for LOs.

The Gunn diode probably will exhibit the lowest far-from-carrier noise; the noise measure for this device is typically 25 dB, compared with 27 to 37 dB for the Impatts in Fig. 6. Obviously, in the FM case, decoupling the Impatt to increase the Q value will assist in reducing the noise-to-carrier ratio so the Impatt can compete with the Gunn diode. For AM noise the noise-to-carrier ratio is not dependent on the circuit Q until very high offset frequencies of more than 2 GHz. In addition, noise-to-carrier ratios of −170 dBc/Hz will be adequate for most balanced-mixer applications, if the mixer has reasonable noise-rejection properties.

As the carrier is approached, the FM noise of both types of devices will increase at a rate of 6 dB/octave until offset frequencies of 1 MHz are reached. The f^{-1} flicker noise component of the Gunn diode then becomes significant, and its noise measure increases as the carrier is approached. This is in contrast to the Impatt, where this effect does not occur until 1 to 10 kHz from the carrier. Thus at 1 kHz from the carrier, the Impatt, with its 30-dB noise measure, can be much quieter than the Gunn diode, which has a noise measure of 45 to 50 dB. Comparing Fig. 6 with results from Gunn diodes[1] shows that noise-to-carrier ratios for the Impatt can be 15 dB better, and this with almost an order of magnitude more power.



7. A typical noise spectrum *for a double-drift device at 150 mW.*

The system designer, therefore, has a much wider choice of local oscillators for millimeter-wavelength systems than previously believed. The optimum device, be it Impatt or Gunn diode, will be closely related to the overall system design, and the selection process must take this into account. ●●

Acknowledgments

The authors wish to thank R.C. Jones for the supply of the epitaxial silicon wafers, S. Cotton and C.L. Sansom for device fabrication and bonding, and T.J. Simmons for the AM noise measurements. This work was supported in part by the Procurement Executive, UK Ministry of Defence, sponsored by DCVD.

References

1. I.G. Eddison and I. Davies, "Indium phosphide transferred electron oscillators for millimetre wave frequencies," *The Radio and Electronic Engineer*, Vol. 52, No. 11 (November 1982).
2. A.M. Howard, D.J. Smith, and J.J. Purcell, "Epitaxially grown double-drift silicon Impatt diodes at 60 to 90 GHz," *Electronics Letters*, Vol. 10, pp. 443-5 (1974).
3. D. Leistner, "Efficient p-type Si Impatt diodes for V-band frequencies," *Electronics Letters*, Vol. 17, pp. 635-6 (1981).
4. M.E. Elta, "High frequency calculations of Impatt and Tunnel diodes," *Proceedings of the 7th Cornell Electrical Engineering Conference*, pp 401-11 (1979).
5. H.S. Gokgor, et al, "High efficiency millimetre-wave silicon Impatt oscillators," *Electronics Letters*, Vol. 17, pp. 744-5 (1981).
6. T.J. Simmons and D.C. Smith, "Direct measurement of FM noise in 80 GHz solid-state oscillators," *Electronics Letters*, Vol. 18, pp. 308-9 (1982).
7. W. Harth, D. Leistner, and J. Freyer, "FM noise measurement of W-band Impatt diodes with a quasi-optical direct detection system," *Electronics Letters*, Vol. 18, pp. 355-6 (1982).
8. W.A. Edson, "Noise in oscillators," *Proceedings of the IRE*, Vol. 48, pp. 1454-66 (1960).
9. K. Kurokawa, "Noise in synchronized oscillators," *IEEE Trans.*, MIT-16, pp. 234-40 (1968).

Product information can be obtained by using the Reader Service Numbers listed by category in Infocenter.



New GaAs Impatt Theory Explains MM-Wave Operation

Skeptics once ruled them out, but GaAs Impatts remain the prime choice for power sources at millimeter-wave frequencies. Computer simulations show why they work so well.

Glenn R. Thoren, Section Manager, Millimeter Wave Transmitters and Systems, Antenna and Microwave Systems Dept., Raytheon Missile Systems Div., Hartwell Rd., Bedford, MA 01730.

UNTIL recently, the use of GaAs Impatt diodes was relegated to frequencies below 30 GHz because most designers considered the intrinsic response times of electrons too long to make these devices practical at higher frequencies. But such conventional wisdom has bowed to experimental evidence. Near 40 GHz, for example, GaAs Impatts have produced more than 3 W of CW power with an efficiency exceeding 21.4 percent. These devices offer slightly greater power and almost twice the efficiency of comparable silicon Impatts.[1]

This performance can be explained by a newly defined physical phenomenon—the delayed secondary avalanching (DSA) of minority carriers in the drift zone of the GaAs Impatt during large-signal operation.

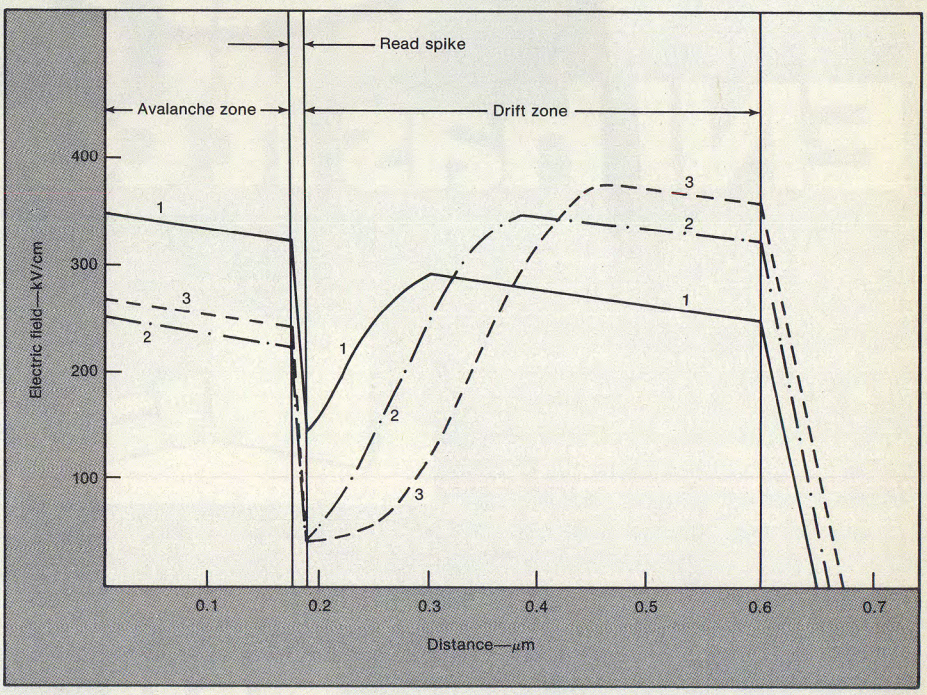
The very high density electron wave that propagates in these Impatts greatly perturbs the local electric-field profile in the drift zone and produces substantial avalanching of hole-electron pairs. If these DSA holes reenter the primary avalanche zone with the proper phase, they will enhance the diode's large-signal millimeter-wave performance. If they reenter at the wrong phase angle, the diode will shut off. These DSA effects have been simulated on a computer and correlated with experimental observations of efficiency, CW and pulsed power, and other variables in GaAs Impatt operation at millimeter-wave frequencies.

Secondary holes created

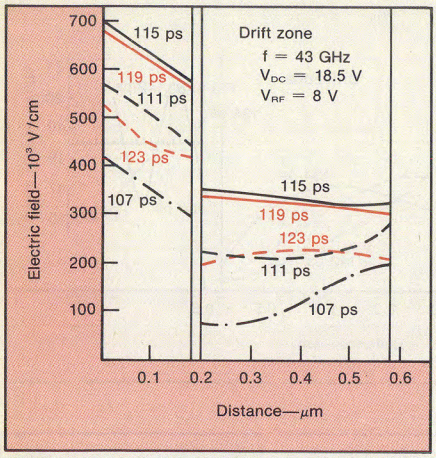
The DSA mode describes the large-signal operation of GaAs millimeter-wave Impatt diodes.[2] In the DSA mode, a substantial density of holes (minority carriers) is generated by impact ionization in the drift zone of the diode by the high local electric field and very high electron (majority carrier) density, which often exceeds 25kA/cm^2 (Fig. 1). These holes propagate back toward the primary avalanche zone and significantly influence the formation of the next electron wave.

The phase of the returning holes will determine if the DSA mode will enhance or limit the large-signal operation of the Impatt. The DSA holes are phased to act as an augmented saturation current that will activate the avalanching of the next electron wave to improve the injection angle and enhance the electron density. A computer simulation can model the DSA mode with both properly and improperly phased holes.[2,3]

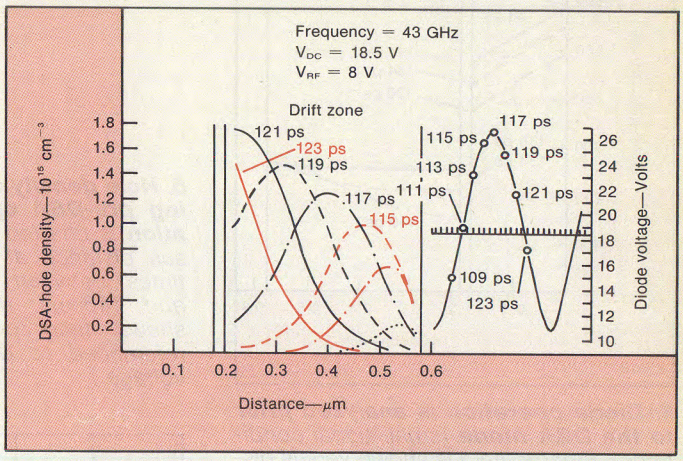
The computer simulation, a one-dimensional model in the time domain, solves Poisson's equation and the continuity equations for any particular diode and its bias conditions. In this way, the simulation derives the electric fields and the carrier densities within computational cells that divide the active region of the Impatt into many segments of equal width.



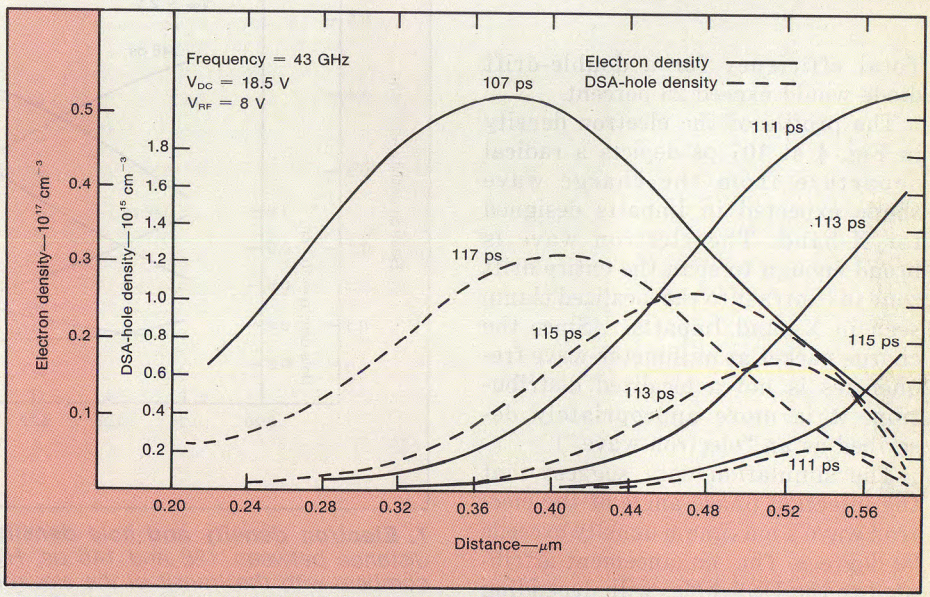
1. The electric-field profile of a GaAs Impatt diode *is represented schematically at three consecutive times (labeled 1, 2, and 3). The high density of electrons greatly perturbs the electric field and causes secondary avalanching primarily at the end of the drift zone.*



2. Electric field is shown versus distance for a GaAs Impatt during DSA-mode operation *at 107 ps, 111 ps, 115 ps, 119 ps, and 123 ps. The bias voltage is 18.5 V with an RF voltage of 8 V at 43 GHz.*



3. DSA-hole density for the diode *in Fig. 2 is shown against distance at 115 ps, 117 ps, 118 ps, 121 ps, and 123 ps. Inset at right shows the time points plotted against diode voltage.*



4. An expanded view of the electron and hole densities in the drift zone *(at 107, 111, 113, 115, and 117 ps) shows a radical departure from the compact packets in X-band devices. At millimeter-waves, the packets look more like waves.*

The ionization coefficients are calculated as functions of electric field within each cell for each increment of time. The multiplication factor for each carrier is computed for each time increment before the carriers are transferred to the next cell (with a predetermined saturated velocity).

The two examples described in the table illustrate the characteristics of DSA-mode enhancement. Case 1 shows the enhancement of the primary avalanching of the electron wave when a substantial number of properly phased DSA holes are present. Case 2 is an example of pre-DSA mode operation.

In Case 1, the Impatt is operating with a DC bias voltage, V_{DC}, of 18.5 V, and an RF voltage, V_{RF}, of 8 V at 43 GHz. Figures 2, 3, and 4 present the steady-state solutions to the explicit difference method used in the simulation. (The numbers next to each curve indicate the relative time of that simulation in picoseconds.)

Simulation indicates hole wave

In Case 1, the DSA-hole wave is formed during the interval between 111 ps and 115 ps (Fig. 3). The DSA-hole wave drifts toward the primary avalanche zone between 113 ps and 121 ps, and is entering the avalanche zone between 119 ps and about 125 ps. As the DSA holes propagate back toward the avalanche zone, they are multiplied in the high electric fields that exist in the drift zone.

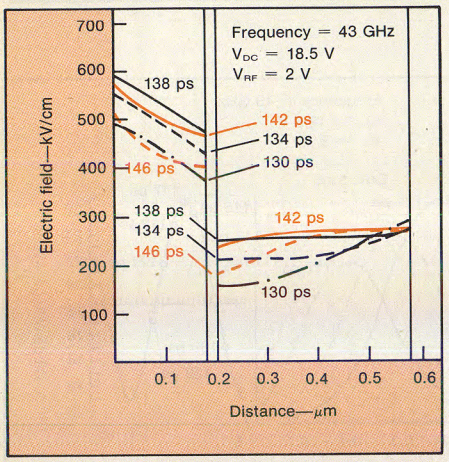
The additional electrons freed during the multiplication of the DSA-hole wave do not detract from the device efficiency, since their density is about 1×10^{15}/cm^3. A density at this level would comprise less than 2 percent of the current induced by the primary electron wave. Both high electric fields (200 to 400 kV/cm) and a large density of electrons in the primary electron wave are needed to generate a sufficiently large and coherent DSA-hole wave. The peak density of electron waves can exceed 5×10^{16}/cm^3 carriers or about 30 kA/cm^2. The electrons that are ionized in the drift zone merge with the electron wave and are collected along with it.

The DC-to-RF efficiency for this single-drift Read profile structure exceeds 14 percent in Case 1. Depending on the thickness and doping of the undepleted GaAs, the series resistance of the undepleted epitaxial material will degrade the efficiency.

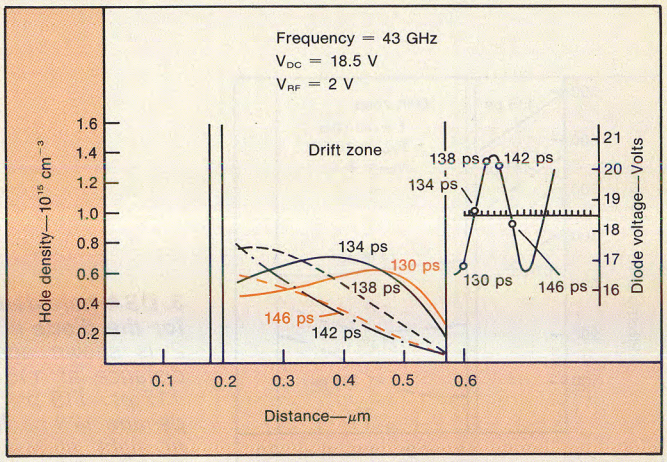
(continued on next page)

Delayed secondary avalanche examples

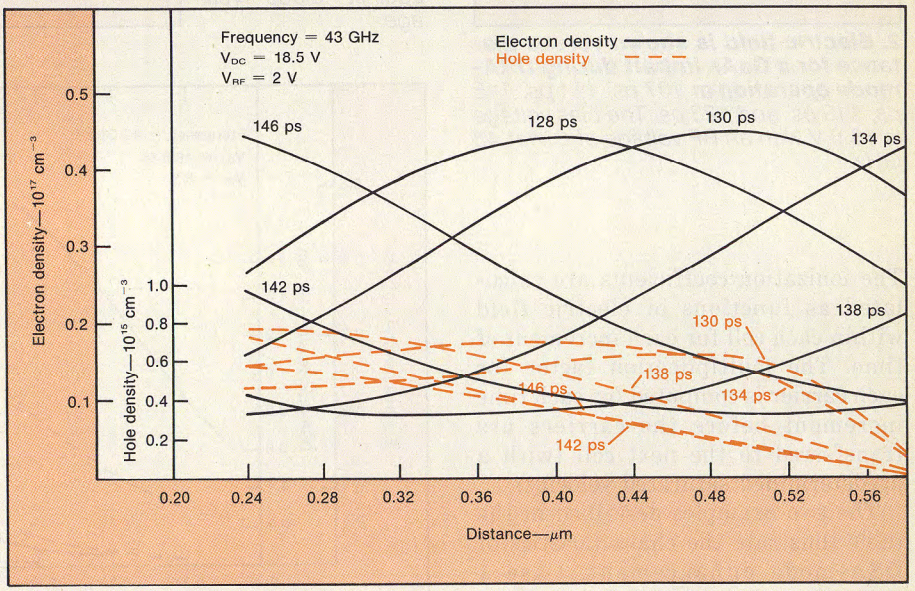
Case	Frequency (GHz)	DC voltage (Volts)	RF voltage (Volts)	Power out (mW)	Efficiency (%)
1	43	18.5	8	538	14.3
2	43	18.5	2	85	1.5



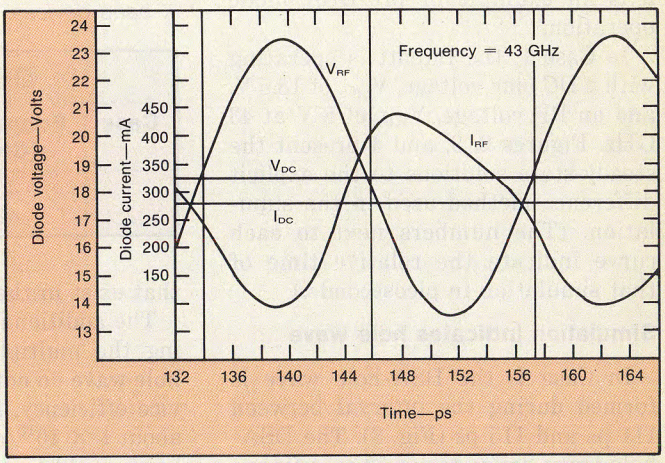
5. Diode operation is analyzed prior to the DSA mode *(small-signal conditions). Electric field is shown versus distance between 130 and 146 ps.*



6. Hole density during pre-DSA operation *is charted versus distance at five times between 130 and 146 ps. (Inset shows time points referenced to diode voltage.)*



7. Electron density and hole density for pre-DSA operation *is shown versus distance between 128 and 146 ps. High fields in the drift zone and buffer layer combine with the transit of the electron wave to produce a stream of DSA holes propagating back into the avalanche zone.*



8. Fourier analysis in the computer simulation *produced this plot of diode voltage and diode current versus time at 43 GHz. The computed DC current and voltage are shown as horizontal lines. The displacement current component is not shown.*

Total efficiency for a double-drift diode would exceed 25 percent.

The profile of the electron density in Fig. 4 at 107 ps depicts a radical departure from the charge wave shape expected in Impatts designed for X-band. The electron wave is broad enough to span the entire drift zone in contrast to the localized clump seen in X-band Impatts. (Since the charge packet at millimeter-wave frequencies is not a localized distribution, it is more appropriately described as an "electron wave.")

The simulation data suggest that the injection phase angle of the electron wave's maximum density exceeds 90 degrees. The enhancement attributed to the DSA holes will, depending on their phase, cause a peak in the electron density at some later time. This effect, which will improve the efficiency, is not apparent from the usual analysis based on the Read equation for Impatt operation.

If the RF voltage is increased without increasing the DC bias voltage, the electric field at the interface of the avalanche and drift zones may drop below 1 kV/cm. Consequently, carriers may be trapped in this region and either disturb the phasing of the DSA-hole wave or prevent the complete injection of the primary electron wave. The depression of the electric field can be seen at 107 ps in Fig. 2. Operating at a higher DC bias level will counter this limitation.

Case 2 depicts operation prior to the build up of the coherent DSA mode. The bias is V_{DC} = 18.5 V with V_{RF} = 2 V at 43 GHz. In this case, the diode exhibits an average DC conduction current of about 300 mA, with a minimum conduction current of 150 mA (the latter caused by continual avalanching in the diode). At these levels, such avalanching will severely degrade the efficiency during small-signal operation. However, it will also improve the response-time of the avalanche zone in GaAs by supplying a large quantity of mobile carriers to initiate avalanche and bridge the operation between the small-signal

(concluded on p. 78)

 (continued from p. 76)

state and the large-signal DSA mode.

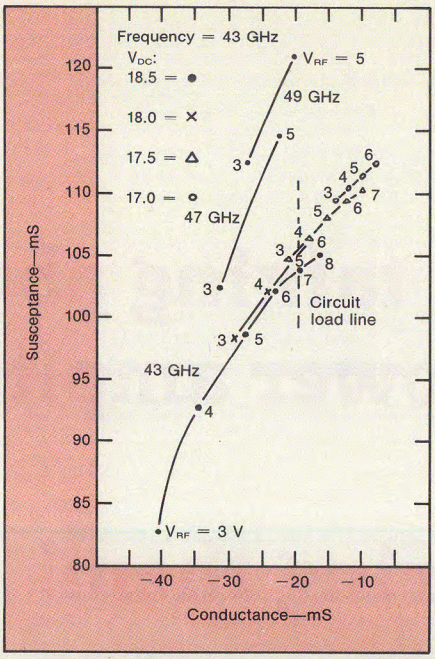
This mechanism will offset the long intrinsic response time limits that may exist in GaAs. Once the large-signal DSA mode is established, the efficiency degradation of the small-signal case is no longer a concern.

In Case 2 (Figs. 5, 6, and 7), the electric field remains high at the interface of the drift zone and the highly doped buffer layer. This high field results in a modulated spillover of the avalanche process into the drift zone. The transit of the electron wave and these high fields produce a stream of DSA holes propagating from the drift zone back into the avalanche zone throughout the cycle. The injection phase angle of the electron wave's peak density will be nearer to 90 degrees in this case. (For Case 1, the injection phase angle of the peak electron density exceeded 90 degrees when influenced by the DSA holes.)

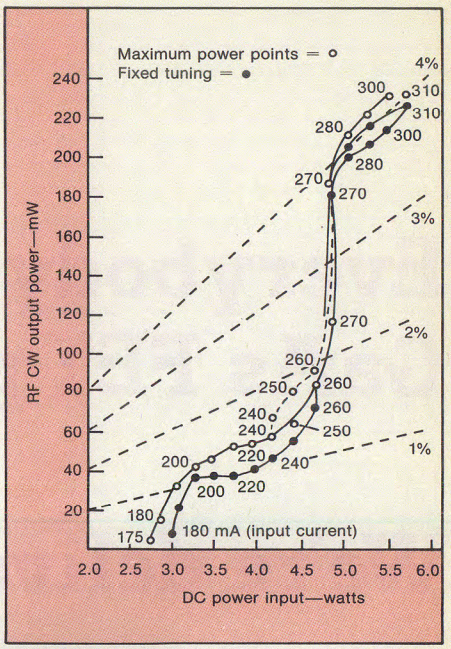
Figure 8 shows a typical example of the current induced by the conduction current associated with the electron wave. The displacement current component is not shown for this punch-through structure. The computed DC current and voltage are indicated as horizontal lines. The DC voltage bias is 18.5 V with V_{RF} = 5 V at 43 GHz.

By analyzing the data derived from a series of simulations, an admittance curve (Fig. 9) for the DSA-mode operation was determined over a range of DC bias voltage and RF voltage levels. The abrupt increase in power and efficiency that is observed experimentally for the DSA mode (Fig. 10 is typical, although this diode had a lossy, undepleted region) can be obtained from the simulation data. The intersection of the admittance curve with a circuit load line produces operating points that can be transferred to a curve of output power versus input power (Fig. 11). The anomalous rectification seen in Fig. 11 most likely results from the strong space charge feedback inherent in the DSA mode.

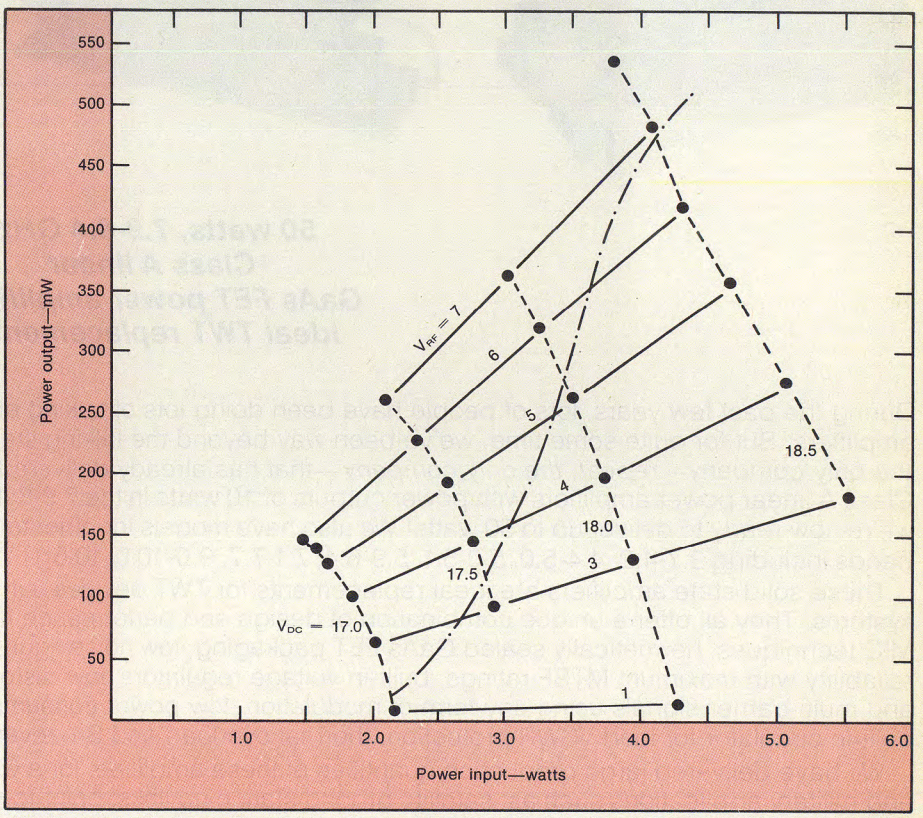
Using the physical dynamics of DSA-mode operation, an efficient and powerful GaAs Impatt can be designed for 94 GHz and may be the next power source for reliable millimeter-wave systems. There is, as yet, no apparent limitation on the carrier transport physics based on these results that would prevent GaAs Impatts from operating up to 100 GHz.●●



9. An admittance curve for DSA-mode operation *was derived by analyzing a series of simulations over a range of DC bias voltage and RF voltage levels.*



10. The simulation data confirms the abrupt increase in power and efficiency *that can be observed experimentally for the DSA mode.*



11. A plot of output power versus input power at 43 GHz and various bias voltages *shows the abrupt increase in efficiency as input power is increased and the diode enters the DSA mode.*

Acknowledgments

Dr. G. Conrad Dalman and Dr. Charles A. Lee provided technical expertise and support in developing the concepts of delayed secondary avalanching phenomena. Their expert assistance is gratefully acknowledged. The encouragement and support of Mr. John King was also greatly appreciated.

References

1. L.H. Holway, et al, "High Power Pulsed Avalanche Diodes," Raytheon Company Final Report to U.S. Air Force Avionics Laboratory, AFWAL-TR-80-1212, Contract #F33615-78-C-1499, p. 4 (February 1981).
2. G.R. Thoren, G.C. Dalman, and C.A. Lee, "Delayed Secondary Avalanche Effects in GaAs Millimeter-Wave IMPATT Diodes," *Electron Device Letters*, Vol. EDL-2, No. 1, pp. 10-13 (January 1981).
3. G.R. Thoren, "The Effects of Delayed Secondary Avalanche Phenomena on the High Efficiency Operation of GaAs Millimeter-Wave IMPATT Diodes," Ph.D. Thesis, School of Electrical Engineering, Cornell University (January 1981).

Improved IMD Measurements for GaAs Power FETs

A simplified presentation of data on third-order intermodulation distortion can provide more accurate determinations of GaAs FET linearity.

Paul M. White, Senior Engineer, Raytheon Co., Bearfoot Rd., Northborough, MA 01532.

THE linearity of microwave power amplifiers is an important performance consideration. Often a number of tradeoffs among linearity, power, gain, and efficiency must be considered to determine the suitability of a particular device or amplifier for a specific use. Linearity usually is characterized by third-order intermodulation distortion (IMD) measurements using a two-carrier input signal, but GaAs FETs are not well-behaved with respect to IMD, so the concept of a third-order intercept point for GaAs FET devices is of little value.[1,2]

For this reason, IMD for GaAs FETs customarily is specified at a particular gain-compression level. A more complete specification might include third-order IMD at a number of power input levels related to a particular gain compression. Although straightforward in concept, this procedure and the interpretation of its results often cause considerable misunderstanding. In fact, it is common for two engineers to hold completely different views on linearity based on the same set of measurements from a device.

This article describes how the conventional method of examining IMD data is prone to misinterpretation and suggests an alternate, more direct technique.

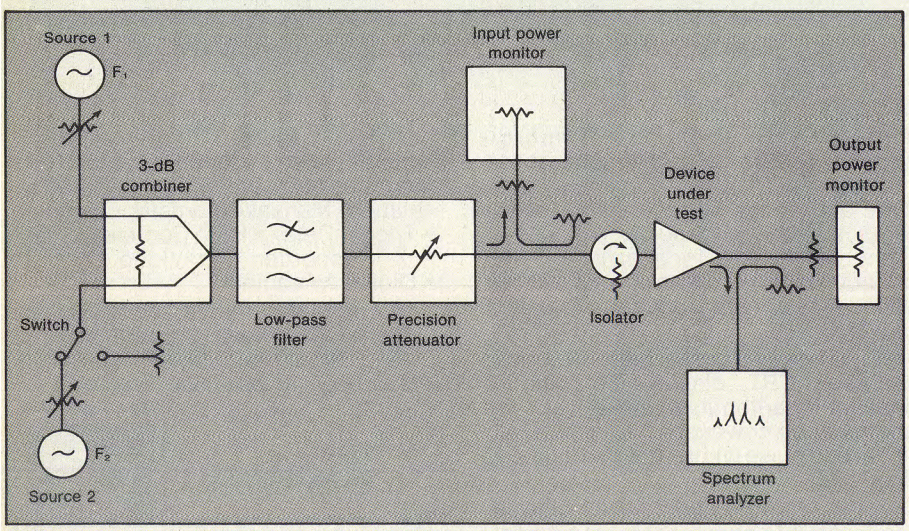
Single device or complete amp

A typical test setup for the complete measurement of third-order IMD and power-transfer characteristics is shown in Fig. 1. The device under test (DUT) can be a single FET in a test fixture with appropriately optimized matching circuits, or it can be a complete FET amplifier.

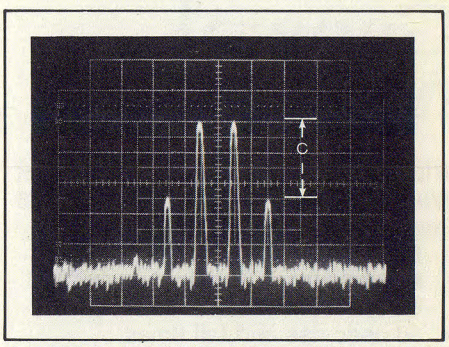
The test commences by recording the single-carrier power-transfer characteristic at a specified frequency, F_1, from small signal to saturation. If an accurate characterization of efficiency also is required, drain current, I_{ds}, should be recorded at each input power level, since I_{ds} typically varies with RF drive.

The third-order IMD measurements are then performed by switching in the second source at frequency F_2 (where $F_1 - F_2$ is typically a few MHz) and adjusting the amplitude of F_1. This is easily accomplished by viewing the sampled output on the spectrum analyzer. Figure 2 shows a typical display, in this case for a FET operating at 4.0 GHz with a carrier separation of $F_1 - F_2 = 2$ MHz.

The third-order intermodulation products at frequencies $2F_1 - F_2$ and $2F_2 - F_1$ are 2 MHz from each carrier. Third-order IMD is measured as the carrier-to-intermodulation power ratio, C/I, in dB or dBc, which is read directly from the spectrum analyzer. The complete characterization is performed by recording C/I and output power as a function of total two-carrier input power over the same



***1. This typical test setup can be used** to measure the third-order intermodulation distortion of either a single GaAs FET or a complete amplifier.*



***2. Third-order intermodulation distortion,** or the carrier-to-intermodulation power ratio (C/I), can be read from a spectrum analyzer display of the sampled output.*

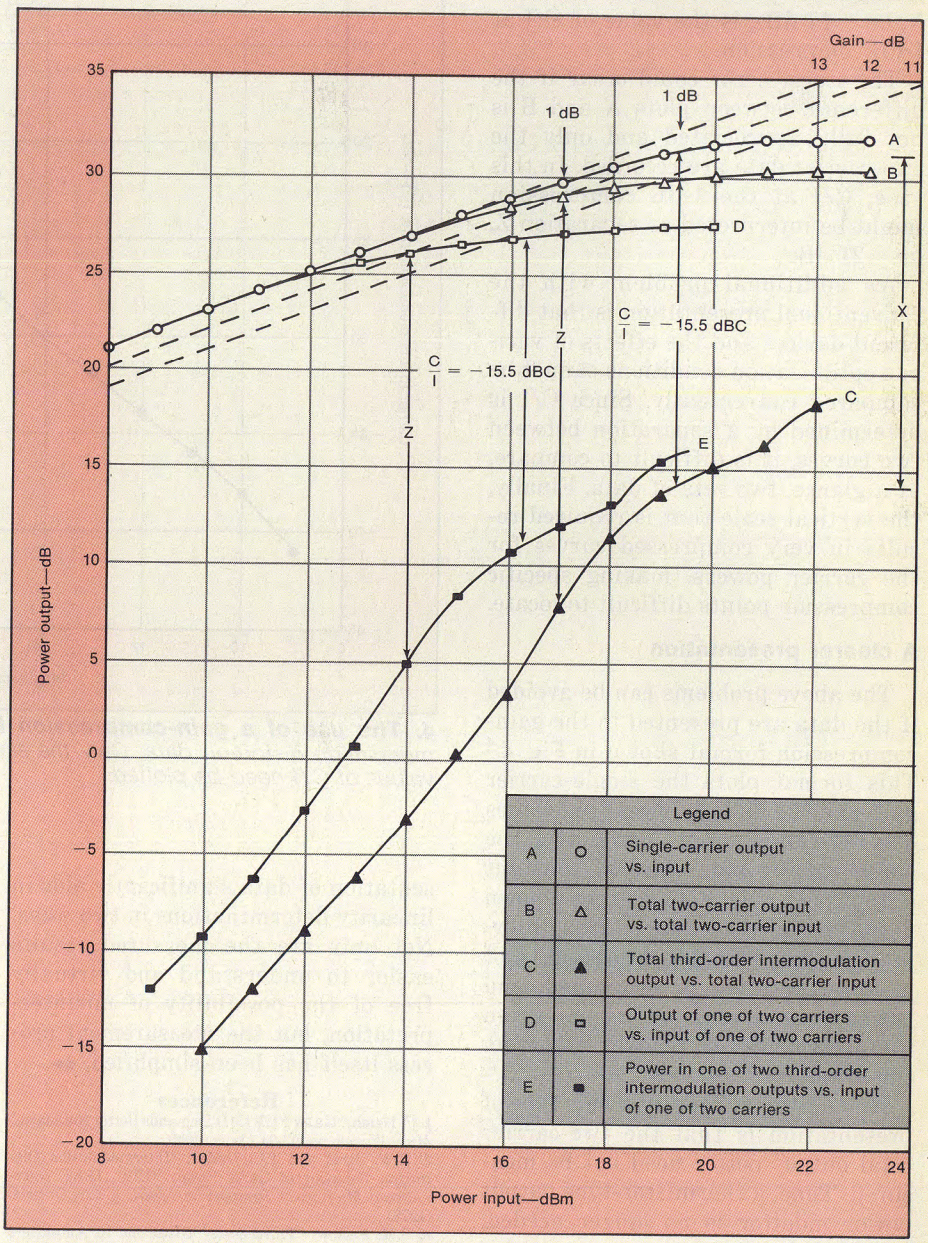
range used for the single-carrier measurements.

Input levels are best set using the precision attenuator to avoid any uncertainty regarding the response of the input power monitor to two signals. The power output monitor, however, must respond properly to the *total* power in the two signals, as a thermocouple or thermistor head does. Many types of detector heads are quite unsuitable, and their use is the first likely source of serious error.

Interpreting the results

A complete set of typical data for a 1-W power FET at 4.0 GHz is plotted in the conventional manner in Fig. 3, where the power outputs in dBm for the carriers and third-order intermodulation products are plotted against carrier input power. Note that three plots of carrier output power and two plots of intermodulation product output power are possible. Three plots of power-added efficiency against input power also can be constructed, but they have been omitted for clarity.

Plot A is the single-carrier power output versus the single-carrier power input—i.e., the first measurement called for. Plot B is the total power output versus the total power input for the two-carrier case, and plot C is the corresponding plot of total power output in the third-order intermodulation products. The earlier saturation of plot B compared to plot A is a fundamental property of RF amplifiers.[3] Plots D and E show the output power in one of the two carriers and in one of the two intermodulation products, respectively, versus the power input in one of the carriers. *(concluded on next page)*



3. A typical plot of data *for a 1-W power FET at 4.0 GHz includes three plots of carrier output power and two plots of intermodulation product output power. Data thus presented are prone to misinterpretation.*

Note that in this type of presentation the C/I ratio recorded from the spectrum analyzer is the separation between plot B and C or between D and E.

This conventional presentation, however, can be very ambiguous if the plots used are not precisely specified. For example, consider what could happen if C/I is specified loosely at 1-dB compression. This condition is correctly specified as C/I at a total of two-carrier input power equal to the single-carrier input producing 1-dB compression. The correct value in the example of Fig. 3 is −15.5 dBc. If only plots A and C are presented, however, it might be concluded that separation X, or −17 dBc, is the value of C/I at 1-dB compression.

The worst error could occur if the difference between plots A and B is not fully appreciated and only the two-carrier data are recorded. In this case, C/I at the 1-dB compression might be interpreted as separation Z, or −21 dBc.

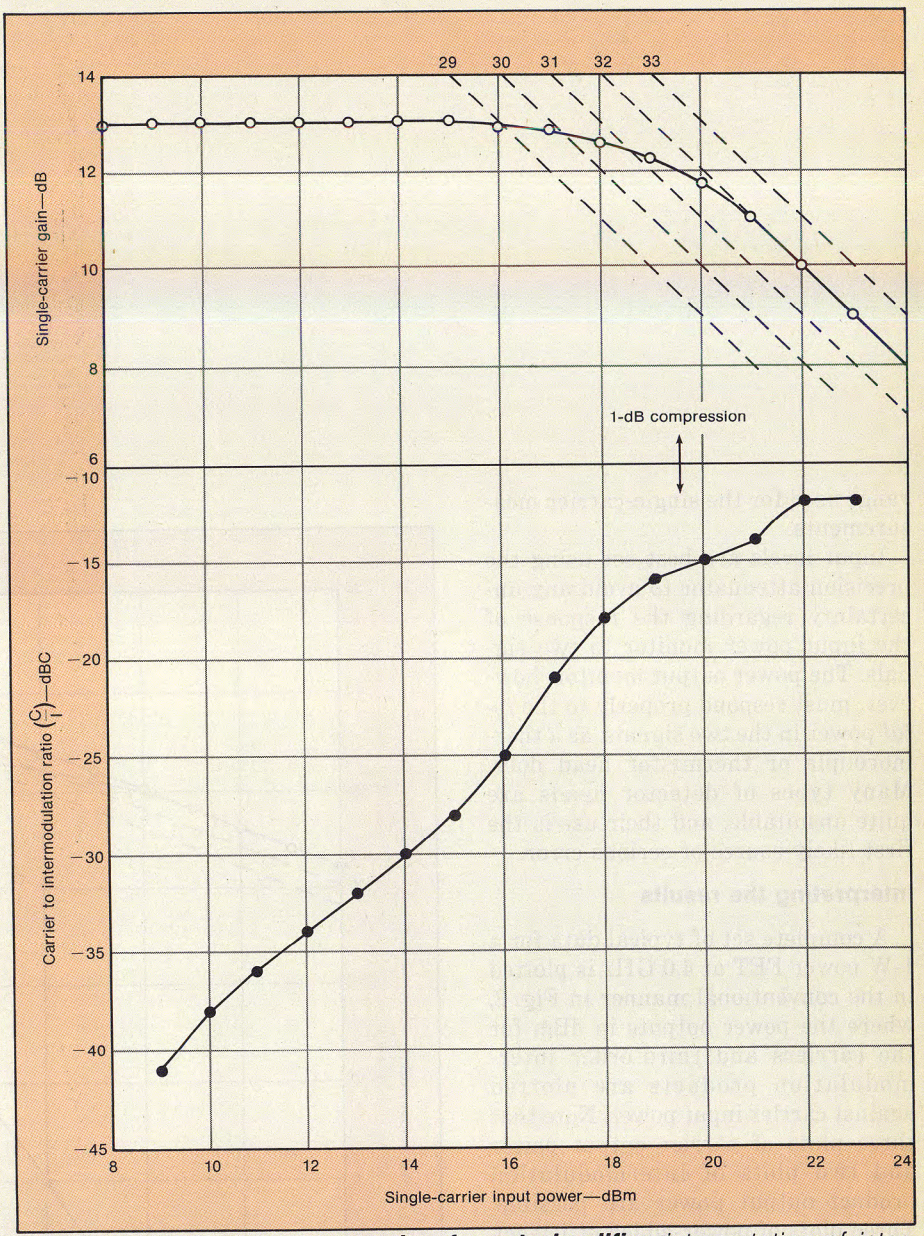
An additional problem with the conventional presentation is that different devices and the effects of various optimization conditions cannot be compared conveniently. Since C/I is determined by a separation between two curves, it is difficult to compare, at a glance, two sets of data. Finally, the vertical scale that is required results in very compressed curves for the carrier powers, making specific compression points difficult to locate.

A clearer presentation

The above problems can be avoided if the data are presented in the gain-compression format shown in Fig. 4.[4] This format plots the single-carrier gain and the directly measured values of C/I against input power. On the single-carrier plot, lines of constant output power lie at 45 degrees (shown dotted). Since no superfluous information is included, the possibility of misinterpretation is eliminated, and the correct value of C/I at any given compression can be read directly from the graph.

An additional benefit of this type of presentation is that the two-carrier total output power need not be measured. Thus, a thermistor-type output power monitor is no longer needed, provided that input powers are set using a precision attenuator.

This more straightforward presentation of data significantly aids in linearity determinations in two ways. Not only are the measured results easier to understand and virtually free of the possibility of misinterpretation, but the measurement process itself has been simplified. ••



4. The use of a gain-compression format simplifies *interpretation of intermodulation distortion data. Only the single-carrier gain and the directly measured values of C/I need be plotted.*

References

1. C. Hsieh, "GaAs FET IMD Demands Better Standard," *MicroWaves*, pp. 93-94 (June 1982).
2. E.W. Strid and T.C. Duder, "Intermodulation Distortion Behavior of GaAs Power FETs," *IEEE International Microwave Symposium Digest*, p. 135, Ottawa, (1978).
3. S.M. Perlow, "Third-Order Distortion in Amplifiers and Mixers," *RCA Review*, 37, p. 235 (1976).
4. J.A. Higgins and R.L. Kuvas, "Analysis and Improvement of Intermodulation Distortion of GaAs Power FETs," *IEEE Transactions*, MTT-28, No. 9 (1980).

Advertisers . . .
Products . . .
Literature . . .

Find them fast
in our
infocenter
(see p. 118)

Electrical Properties Govern Substrate Effectiveness

Substrates with fine-grained structures are essential for microwave applications because they guarantee consistent dielectric properties and resistivity.

Vijay Borase, General Manager, Ceramic Substrate Div., Materials Research Corp., Orangeburg, NY 10962.

THIN-FILM hybrid circuitry, which first appeared on glass substrates, is finding increased applications on aluminum oxide (alumina).

The early 94-to-96-percent alumina compositions, although well-suited to thick-film methods, lacked the uniformity of grain structure and the high degree of surface smoothness required for thin-film processing. Thin-film circuits on alumina did not come into prominence until a fine-grained substrate with a surface of 8 to 10 microinches, CLA (center line average), could be readily obtained.

Progress has continued in substrate manufacturing. Dimensional tolerances have improved and, with the introduction of 99-to-99.9-percent Al_2O_3, the as-fired surface finish of substrates has dropped to 4 microinches, CLA, and glazed surfaces are no longer required in most thin-film applications.

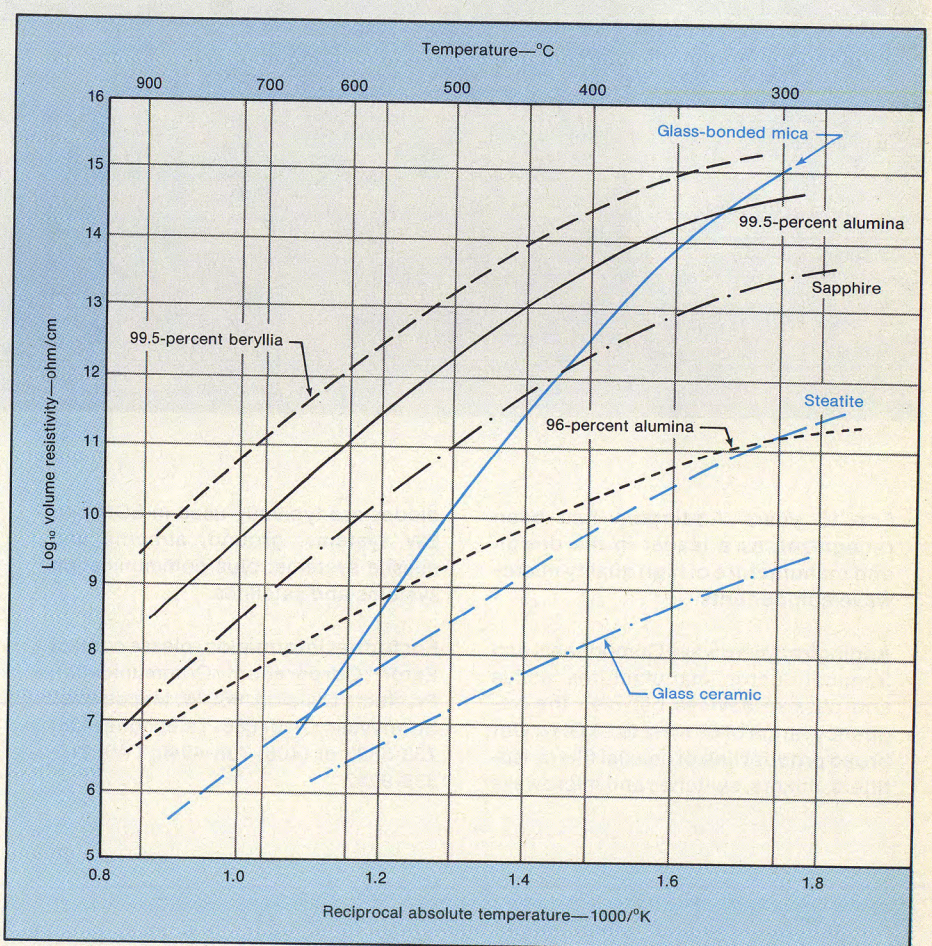
The term "hybrid," of course, refers to the marriage of two technologies in the finished circuit. For example, a hybrid may contain chip resistors, capacitors, or ICs in conjunction with a thin-film network. Mechanical or electrical bonding techniques attach the discrete devices to the thin-film.

In most hybrid applications, surface defects have less importance than strength, adhesion, scribability, and the flatness of the surface (camber).[1] High definition circuits, such as those combining fine-line resistor networks with discrete components, are exceptions. These require low defect densities and smooth, uniform surface texture.

In microwave integrated circuits (MICs) and microstrip, the impedance of the circuit must be matched to the remainder of the system. If the match does not exist, insertion losses will be caused by the power reflected at the impedance discontinuity.

MICs and microstrip circuits require substrates with consistent electrical properties, because the substrate actually becomes part of the circuit. The circuit is formed on one

(continued on p. 85)



1. Ceramic oxides, in general, are insulators at room temperatures *because of their large band gaps. Impurities or the presence of variable-valence cations can alter their conductivity.*

face of the substrate, and the other face is fully metallized to form an electrical ground plane. Microwave energy travels through the substrate from the circuit side to the ground plane.

In essence, such a configuration is a capacitor, and the dielectric constant and the substrate thickness dictate the capacitance value that determines the characteristic impedance. Therefore, once the circuit design is finalized, the dielectric properties and thickness of the substrate must remain constant.*

Cations alter volume resistivity

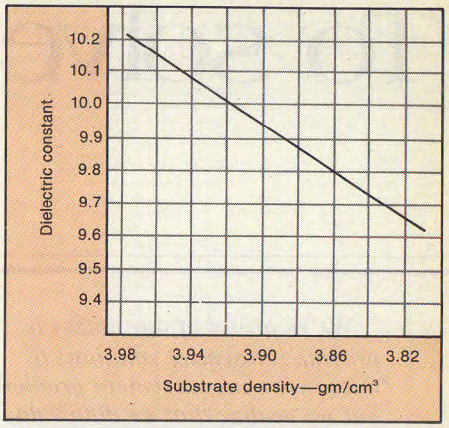
A study of resistivity as a function of temperature (Fig. 1) shows that, in general, ceramic oxides have large band gaps that make them insulators at room temperature.[2] Although conduction by mobile ions (except at high temperatures) is usually low, the presence of certain impurities or of cations of variable valence may impart electronic conductivity to the material. Even a small fraction of such cations can cause a drastically lowered resistivity, since the mobility of electrons is much greater than that of the ions.

The porosity of the substrate must also be considered. In polycrystalline materials, porosity always increases the resistivity. However, if the pores are filled with a secondary phase, the resistivity may increase or decrease depending on the composition and impurity levels.

Dielectric value set by matrix

In an alumina substrate, which is essentially a matrix composed of individual micron-size sapphire (aluminum oxide) grains, each grain differs from its neighbor only in crys-

(concluded on p. 88)



2. The density of the alumina ceramic affects its dielectric constant *according to the relationship shown in Eq. 3. This plot shows the linearity of the relationship.*

*In microstrip applications, extremely close tolerances in the physical dimensions of the substrate also avoid insertion losses. Because substrates are sometimes placed side by side to form a microstrip, alumina substrates often have to be ground to size. Spacing voids and irregular edges cannot be tolerated in these circuits.

Ceramics also support resistors

Resistor networks are another major use for ceramic substrates. In addition to the qualities outlined elsewhere, these networks require substrates that have good heat dissipation.

Usually, many identical networks are made at one time on a large substrate. The individual circuits, which can be smaller than 0.050 × 0.050 in. (with 0.0005-in. lines and spacings), are cut or scribed and snapped to size.

Analyzing resistor networks

For a uniform film thickness (t), and resistivity (ℓ), the sheet resistance is expressed by:

$$R_s = \frac{\ell}{t} \qquad (4)$$

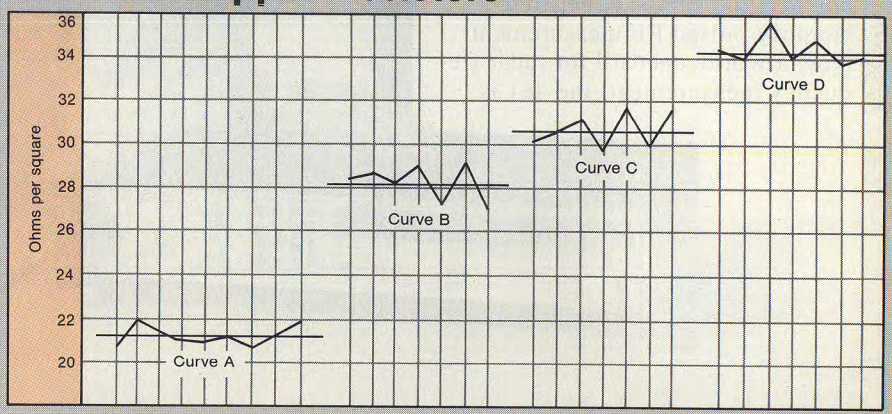
Sputtering conditions determine the film resistivity; the substrate morphology (in part) determines the film thickness. The typical resistor film will have a nominal thickness of 100 to 500 Å, or about 4 percent of a grain diameter. Obviously, the substrate appears very rough to a film this thin.

The morphology of the substrate affects the film thickness in two ways: (a) as the surface area increases, the mean film thickness decreases for a constant film volume; (b) deep grain boundary valleys result in film thickness variations throughout the film.

For a film with varying thickness, Eq. 4 is poorly defined, but the operational definition of the resistance of a square film section still applies. In most cases, when a film of uniform thickness is disturbed in such a way that thickness variations are introduced, the sheet resistance increases. Figure 3 shows the effect of surface roughness on sheet resistance (Ω/square). As the grain size and surface roughness decreased, the sheet resistance of the deposited tantalum film increased.[5] In addition, substrates that show larger sheet resistance values also exhibit large surface area.

Most stable resistor materials, such as tantalum nitride or nichrome, have low specific resistivity values. Therefore, the achievement of reasonable resistance values implies very thin films as well as very thin lines. Higher sheet resistivity in films is an advantage of smoother substrates. High resistance values become easier to achieve, and thin lines need not be as thin.

Finer grain size substrates have a uniform distribution of grains. This quality increases the reproducibility of the sheet resistivity of the film, thereby reducing trimming costs. Grain alignment during tape casting of as-fired substrates appears to have a significant effect on resistivity. Resistor manufacturers have noticed a difference between the sheet resistivity along the tape cast direction and that along the width. This effect seems to be more pronounced in evaporated films than in sputtered films. ●●



3. The sheet resistance of a deposited tantalum film increases as the grain size and surface roughness decreases. *Curve A shows the sheet resistance on glass substrates or polished alumina, Curve B on Al_2O_3 with 4-to-8-μm average grain size and 8-to-10-microinch surface roughness, Curve C on Al_2O_3 with 3-to-4-μm average grain size and 6-to-8-microinch surface roughness, and Curve D on Al_2O_3 with 1-to-2-μm average grain size and 2-to-4-μin. surface roughness.*

 (continued from p. 85)

tallographic orientation. The dielectric properties of sapphire (also known as α alumina) are not isotropic. Instead, the value of the dielectric constant varies with crystallographic direction and ranges between the extreme values of 11.55 (measured along the C or optic axis) to 9.34 (measured perpendicular to the C axis). The resultant matrix value is an average produced by the many contributions of the variously oriented crystallites.

For a perfectly random array of crystallites, the average value is 10.08. Tape process substrates,[1] however, all show a "preferred" orientation with all crystallites aligned with their C axes perpendicular to the surface of substrates made in this way. (The dielectric constant measured perpendicular to the substrate surface, the direction of the electric field, is more significant to microstrip applications.)

The residual porosity reduces the dielectric constant from the matrix value discussed above to some lower value. The exact value depends upon the degree of residual porosity or density of the ceramic. This dependence is given by the equation:[3]

$$E_2 = \left[\frac{E_1(1 - 3P) + 2E}{E_1 + (2 - 3P)E}\right] \quad (1)$$

In Eq. 1, E = the dielectric constant of the substrate, E_1 = the dielectric constant of the pores, E_2 = the matrix dielectric constant (which will depend on preferred orientation of the crystallites), and P = the volume fraction of the pores.

Since pores are essentially voids, their dielectric constant, E_1, has a value of unity. When a value is substituted for E_2 (10.22, for example, the value for MRC Superstrate at theoretical density), Eq. 1 can be rephrased to express E in terms of P:

$$E = 4.860 - 6.915P + 0.25\sqrt{(765.1)\,P^2 - 537.7P + 459.7} \quad (2)$$

Furthermore, P is related to the density by the formula:

$$P = \frac{\rho_o}{\rho} - 1 \quad (3)$$

In Eq. 3, ρ = the actual ceramic density, and ρ_o = the theoretical density (3.983). Using this equation, the dielectric constant can be plotted against the density of the alumina ceramic (Fig. 2).

So, two factors affect the dielectric constant of the ceramic: the preferred orientation of the alumina crystallites and the density of the material.

Fine-grained alumina ceramic exhibits a more random crystallite orientation than coarse-grained ceramic. The preferred orientation is hard to regulate and depends on process control during substrate manufacturing.

Control of dielectric constant and thickness to minimize insertion losses is very important in microwave applications, particularly those above 10 GHz.[4] In addition to its other drawbacks, a rough surface causes losses by scattering microwave energy. Large grains act as foreign particles and produce similar scattering. A large grain structure also implies a coarse distribution of residual porosity, i.e., bubbles in the material. These bubbles scatter microwave energy. ●●

References

1. V. Borase, "Substrates Influence Thin-Film Performance," *MicroWaves*, Vol. 21, No. 11, pp. 61 - 75 (October 1982).
2. L.I. Maissel and R. Glang, "Thin Film Substrates," (entry by Richard Brown), *Handbook of Thin Film Technology*, Ch. 6, McGraw-Hill, New York (1970).
3. W. Class, "Electrical and Chemical Requirements of High Alumina Substrates for Microstrip Applications," *Electronic Packaging and Production*, pp. 55-64 (March 1978).
4. A.R. Gerhard, "Measuring Dielectric Constant of Substrates for Microstrip Applications," *IEEE Trans. on Microwave Theories and Technology* (July 1976).
5. D.E. Peters and D.A. Rott, "Ceramic Substrates for ThinFilm Circuits," Western Electric Co., Inc., private communication.

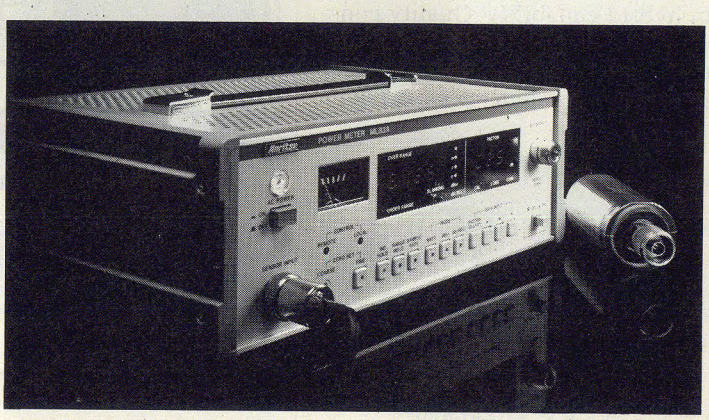
One Power Meter...No Peers

10MHz to 140GHz with a single instrument

The ML83A from Anritsu: It's the one instrument with no equal at measuring RF power over all frequency ranges from 10MHz to 140GHz. Simply by selecting from a variety of versatile sensors, you can use this single low-priced power meter to handle all your power measurement needs.

The ML83A Power Meter has the ample capabilities to make it the mainstay of your lab bench or production line. Each sensor has a thin-film thermocouple (or a diode) that provides a high degree of accuracy with excellent VSWR characteristics and temperature stability. And you'll appreciate such ML83A ease-of-use features as digital readout, self-calibration, and a handy analog meter for viewing output peaks. There's even a GPIB option for use in an automatic measurement system.

The ML83A. From the extensive Anritsu line of high-quality measuring instruments.



Anritsu

ANRITSU ELECTRIC CO., LTD.
OVERSEAS MARKETING DIVISION
10-27, Minamiazabu 5-chome, Minato-ku, Tokyo 106, Japan
Phone (03) 446-1111/Telex: 0-242-2353
Cable: ANRITDENKI TOKYO

Anritsu America, Inc.
128 Bauer Drive, Oakland, NJ 07436, U.S.A. Phone: 201-337-1111 Telex: 642-141 ANRITSU OKLD
Anritsu Europe Limited
Thistle Road, Windmill Trading Estate, Luton, Beds, LU1 3XJ, U.K. Phone: (STD0582) 418853 Telex: 826750 ANRSEU G
Anritsu Eletrônica Comércio Ltda.
Av. Passos, 91-8º Ander, 20.051-Rio de Janeiro-RJ, Brasil Phone: 221-6086, 224-9448 Telex: 2131704 ANBR

READER SERVICE NUMBER 73

ISOFET Evolution Yields High-Power Devices

The ISOFET transistor is a silicon power device with MOSFET-like power capabilities and potentially broad frequency bandwidths. Continued improvements in the basic design may lead to a 300-W FET.

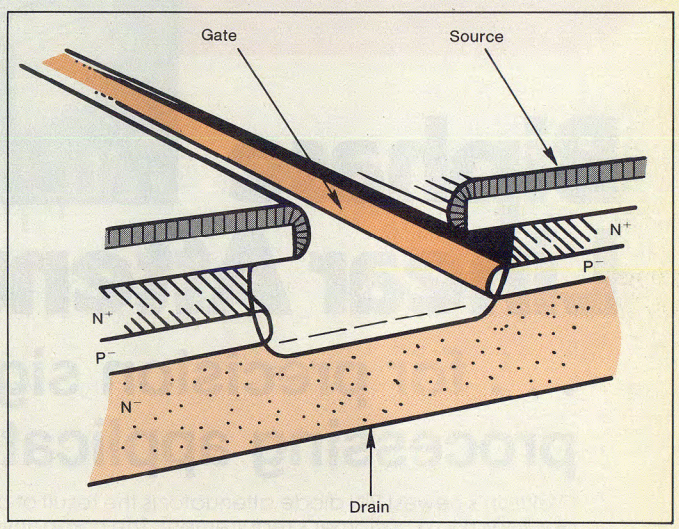
Dick Moss, Semiconductor Engineer, Acrian, Inc., 10060 Bubb Rd., Cupertino, CA 95014.

Solid-state power, once thought of as the sole domain of bipolars, now has a new silicon proponent: the ISOFET. The device promises to break the 125-W barrier that now marks the power ceiling for conventional silicon power bipolar transistors. And it will achieve these higher power levels without need of the intricate matching circuitry so familiar to bipolar designers.

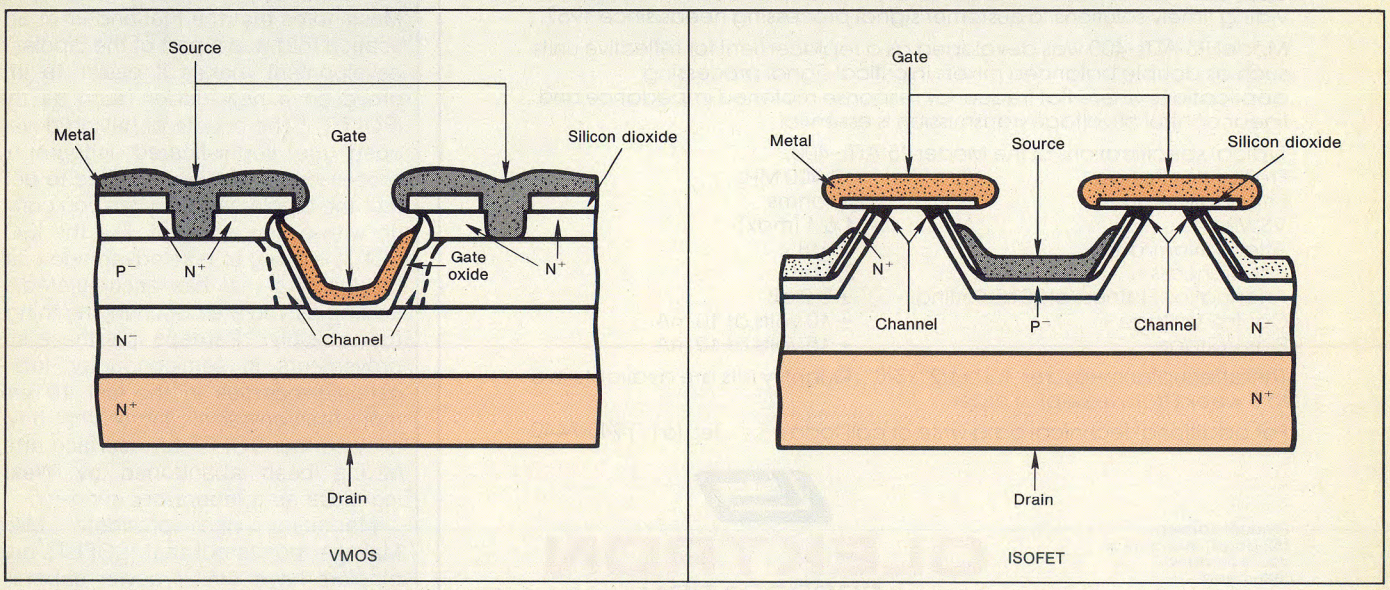
ISOFET technology is not new. It originated in a design developed by Westinghouse in the early 1970s. That device (Fig. 1) was created by etching silicon from beneath a silicon dioxide roof to shadow an evaporated metal that formed the gate. The fabrication process was too elaborate to consider the transistor a production-ready product; nevertheless, these laboratory devices operating with moderate power levels in the GHz range augured things to come.

The ISOFET that finally came out of the abandoned Westinghouse research is more or less a variation on a V-groove MOSFET (Fig. 2). While the VMOS features a recessed channel, the ISOFET uses an inverted VMOS pattern to place the channel closer to the surface of the device, where the electron mobility is higher. As a result, the power gain of the improved structure is typically 6 to 10 dB higher than available MOSFET designs, and the frequency coverage is typically four times as high, with f_T's up to 5 GHz now possible. The gate-to-drain capacitance of the ISOFET is typically about 1 pF. This is approximately one-fourth that of typical MOSFET devices, and accounts for the good input/output isolation of the new design. One of the keys to the device's low capacitance lies in its construction:

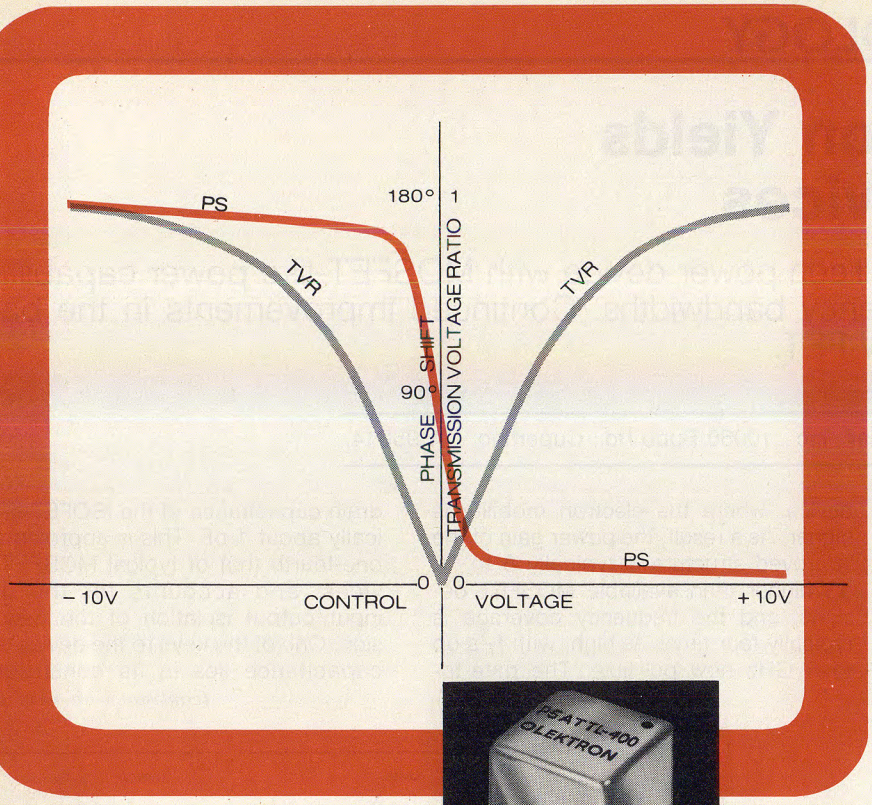
(continued on next page)



1. The original Westinghouse ISOFET was a shadow-isolated VMOS transistor. *It used a silicon dioxide roof to shadow an evaporated metal that formed the device's gate.*



2. The present-day ISOFET (right) represents a modified VMOS transistor (left). *The ISOFET's design basically involves inverting the VMOS's gate structure so that the gates are close to the surface, where the carrier mobility is higher. One direct result is higher-frequency performance, with f_T's as high as 5 GHz.*





Biphase Linear Attenuator

. . . for precision signal processing applications

Olektron's newest PIN diode attenuator is the result of an innovative approach to a customer's requirement. The company has been providing timely solutions to customer signal processing needs since 1967.

Model P5-ATTL-400 was developed as a replacement for reflective units such as double balanced mixers in critical signal processing applications where flat frequency response matched impedance and linear control of voltage transmission is essential.

Typical specifications of the Model P5-ATTL-400:

Frequency Range	10-400 MHz
Impedance	50 ohms
VSWR	1.6:1 (max)
Attenuation Range	40 dB
Insertion Loss	2.5 dB
Attenuation Flatness at 20 dB Setting	± 0.2 dB
Control Voltage	± 10 volts at 10 mA
Bias Voltage	± 15 volts at 10 mA

The attenuator measures 1/2"x1/2"x3/8". Quantity lots are available in 6 to 8 weeks from receipt of order.

For additional technical data write or call today. Tel. (617) 943-7440

Product catalog (52-page) available on your company letterhead.

OLEKTRON CORPORATION

61 Sutton Road/Webster, Mass. 01570

YOUR CHALLENGE IS OUR PROGRESS

READER SERVICE NUMBER 74

ISOFET EVOLUTION

(continued from p. 91)

since the channel is parallel to the surface, the gate length is shorter than normally found in conventional MOSFETs, on the order of 0.2 μm. The use of a metal gate, much quieter in noise characteristics than the polysilicon gates common in conventional high-power FETs, also enhances the high frequency performance of the ISOFET devices.

The new ISOFET transistors are close in topology to current GaAs FETs, except for the isolation structure. The fabrication process, which is similar to a procedure adopted by Siliconix in 1979 to pattern their VMOS transistors, makes use of a rotating planetary evaporation technique to fill the V-groove with evaporated metal. A major difference between standard FETs and the silicon ISOFETs is in the latter device's general lack of alignment problems. The ISOFET is constructed with a triple self-aligned process, whereas a typical GaAs FET uses interdigitated fingers that are difficult to align. The ISOFET is, in fact, a relatively simple device to fabricate, based on the number of mask sets needed in the processing. A typical VMOS requires as many as eight or nine

The quest fo

In the long run, the ISOFET will be facing off against the silicon bipolar transistor in the race for dominance of the power region lying at frequencies from a few megahertz up through 5 GHz. Ironically, the research of the last decade devoted to the development of the bipolar as a power device will have a great deal to do with the advancement of the ISOFET as a viable power semiconductor. Project engineer Dick Moss notes that the trial-and-error education that was a part of the bipolar's development makes it easier to improve on a new design such as the ISOFET: "The benefit of having developed the sophisticated lithography processes which were required to perfect the bipolar is that when you come up with a new concept, like the ISOFET, it is going to take advantage of all the learning that has accumulated—as long as you are not changing things too radically." Perhaps it is these improvements in semiconductor fabrication processes in the last 10 yrs. more than any single factor, that have allowed the ISOFET to resurface after having been abandoned by Westinghouse as a laboratory curiosity.

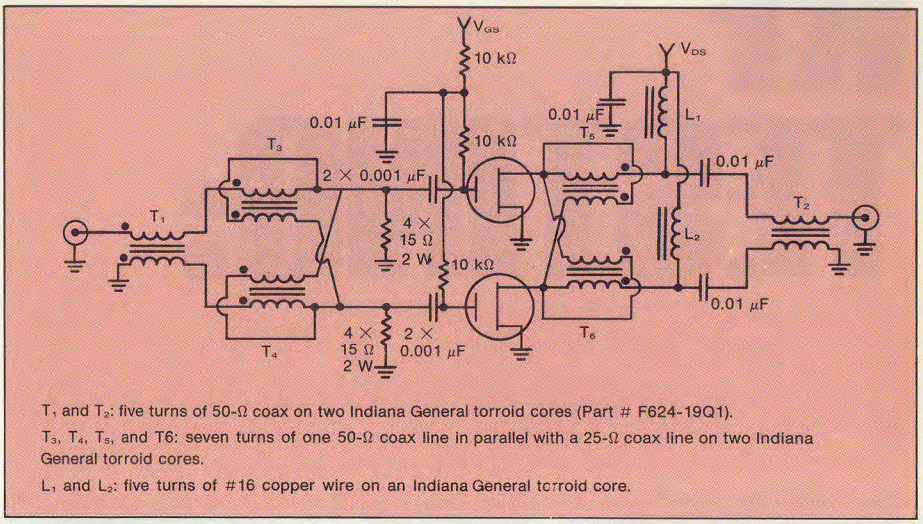
Marketing vice president Mike Malinger points out that ISOFETs and bipolars have similar power capabilities, but the ISOFET offers certain circuit-design advantages: "One of the

mask operations while the ISOFET can be constructed with five such steps. And the last step of the ISOFET process is a simple procedure performed basically to provide bond-wire access to the transistor's pads.

The development of the ISOFETs comes as a result of a thorough evaluation of the limitations of the VMOS technology. In addition, since most designers reach for bipolars when in need of VHF solid-state power, these semiconductors were also investigated. (For a comparison of how the ISOFET stacks up to the power bipolar, see "The quest for power: ISOFETs and bipolars.") The VMOS transistors were found to have excessively high feedthrough capacitances at the root of their high-frequency limitations. These capacitances couldn't be decreased without going to a new device structure. Another point in favor of changing the basic VMOS design was the opportunity to go to a topology with a shorter channel length, which would lead to a higher f_T frequency.

There was another hidden problem with the VMOS structure that needed to be overcome in the design of the ISOFET: the elimination of the parasitic bipolar which lies within the circuitry of the VMOS. Since the device is an N-P-N diffusion structure, an N-P-N bipolar transistor exists within the model of the semiconductor. When VMOS devices are driven to their maximum gain levels, competition will arise between what is the active area of the intended FET and the active area of the unwanted bipolar. If the VMOS is driven past its safe operating area (SOA), where the current

(continued on next page)



T_1 and T_2: five turns of 50-Ω coax on two Indiana General torroid cores (Part # F624-19Q1).

T_3, T_4, T_5, and T6: seven turns of one 50-Ω coax line in parallel with a 25-Ω coax line on two Indiana General torroid cores.

L_1 and L_2: five turns of #16 copper wire on an Indiana General torroid core.

3. This amplifier represents a typical example of what can be done with a pair of ISOFETs. *In this case, two 120-W devices are coupled in a fairly simple circuit.*

ower: ISOFETs and bipolars

inherent characteristics of a bipolar device is that you must stabilize it." Because of this requirement, the use of bipolars in power networks has traditionally required very elaborate tuning and matching circuits. Moss emphasizes that designing with the ISOFETs will be much simpler than what engineers have grown accustomed to with bipolars: "The FET inherently has good DC stability. Source biasing can often be done through a 1-Mohm resistor with the voltage provided from a fixed source—the FET will then stabilize with temperature. With the bipolar, you run into beta variations which must be compensated for by adding ballast resistors. And bipolars have the problem of their positive temperature coefficient: as the temperature increases, the device wants to thermally run away." In practical terms, Moss adds, the amount of power obtained from the ISOFETs is a more straightforward relationship of the number of devices used than is the case with bipolars: "Because of the need to back off bipolars in a power design, 1 plus 1 equals 1.6. If you use two 10-W bipolars, you are probably going to get about 16-W output. And the amount of circuit elements needed with the power bipolars is much greater than with the ISOFETs. You need input networks with the bipolar to split the power, drive the number of cells used in parallel, and then networks to combine the power. With the FETs, you could essentially build a 400-W amplifier with four 100-W devices, and not have to build four separate stabilizing circuits. All you really need are four 1-Mohm resistors."

Another circuit advantage the ISOFET has over the bipolar concerns input matching. Since the bipolar appears like a short circuit, a high-ratio impedance transformation must be made, which can lead to bandwidth problems. The bipolar requires compensation for its characteristic 6-dB/octave gain slope. Moss feels that a good deal of circuit manipulation has gone into bipolar networks in recent years: "System engineers have spent a good part of their time designing all kinds of gain-slope compensating networks to drive the low bipolar input impedances. These networks allow bipolars to work over broad bandwidths, even though there may be high VSWRs at the device's input." Since a FET looks like a very low-level capacitance, with a high input impedance, there is not the need for a great deal of gain-slope compensation, especially at the lower frequencies. As Moss explains: "You may have to do some compensation because of losses that occur with increasing frequencies, say for variations of 3 to 5 dB over several octaves, but it is nowhere like the compensation necessary with bipolars." Thus, the cost of circuitry for the ISOFET should prove to be less than that for an equivalent frequency bipolar.

Moss sees the ISOFET as one example of an evolving power technology: "Bipolar technology has been pushed to the limit. In contrast, the FET (ISOFET) process is a lot simpler, and can be conducted by more junior process people. The FET is just on the threshold of evolution, just reaching the beginning of its possibilities." Moss adds that the real advances in the next few years will be in power FETs rather than the already mature power bipolars: "A whole new generation of technology is going to allow the integration of matching filter networks with extremely broadband transistors and much higher power concepts. This technology also allows one to consider eliminating wire bonds, by turning the chip upside down so that the channel periphery area is on top of copper. In such a way, you can eliminate the need for BeO. There's no reason why we won't be looking at silicon FETs within the next two or three years that will be operating from 5 to 10 GHz." ●●

RF TESTING: COME WHERE THE POWER IS.



Power amplifiers to cover the widest range of rf testing requirements. Sub-octave to ultra-wideband response, and gain that's flat and reliable.

Take our popular Model 10W1000 as an example: This compact all-solid-state amplifier delivers a true 10 watts of linear power throughout a bandwidth of 1MHz to 1GHz—three extremely important decades of bandwidth in the rapidly expanding spectrum of rf testing. This is the huskiest combination of power and bandwidth available anywhere today.

AR amplifiers, from 1 watt to 10 kW, are unconditionally stable, immune even to worst-case load mismatch without damage to themselves or shutdown of the system. And the full bandwidth is instantly available—no tuning or system adjustments needed for continuous or automatic sweeping.

When you call AR, the chances are very good that we'll have whatever combination you seek—clean bandwidth, output power, linearity as needed, pulse capability—often in an amplifier about half the size of its nearest "competitor."



SEND FOR FREE BOOKLET

7333 © ar

ar AMPLIFIER RESEARCH

160 School House Road, Souderton, PA 18964
215-723-8181 • TWX 510-661-6094



READER SERVICE NUMBER 47

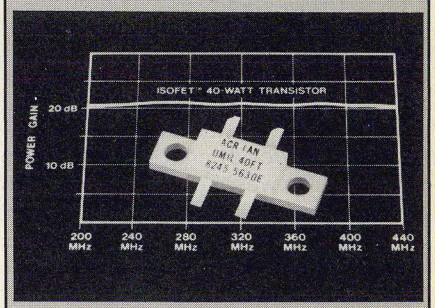
ISOFET EVOLUTION

(continued from p. 93)

across the body resistance of the device reaches a product of 0.6 V (which is the emitter-base junction voltage of the bipolar), the internal bipolar will turn on and burn out the FET. The ISOFET has been developed with shorter channels than VMOS devices, for higher operating frequencies, and with higher SOAs, for improved reliability. In fact, the ISOFET is capable of handling near-

(concluded on p. 113)

Single device is 40-W building block

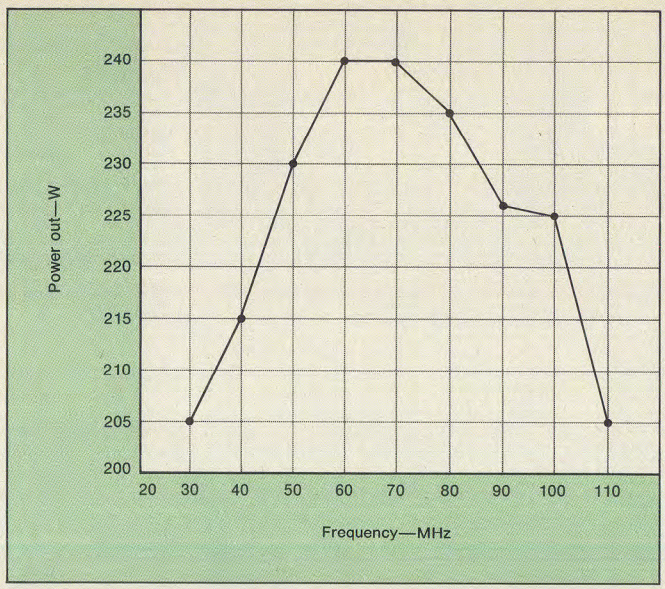


One of the newly introduced transistors that makes use of the ISOFET technology is the model UMIL40FT, a 40-W, broadband UHF device. The transistor consists of two ISOFET chips internally connected in a push-pull configuration. It is capable of providing 20-dB gain across the 200-to-440-MHz band.

This ISOFET is actually specified for the octave bandwidth from 200 to 400 MHz. It will deliver 40 W of power, flat within ± 0.5 dB, without gain sloping. Greater bandwidths are possible at reduced power levels. For example, at 30-W output, the device will operate from 20 to 500 MHz at ±1.5 dB.

The UMIL40FT has been designed for 2-to-30-MHz single sideband communications, AM/FM avionics/land communication, instrumentation, and broadband ECM in the 200-to-500-MHz range. In class-B operation, the device will reach its specified 40-W output level with about 800-mW drive (17-dB gain). When a requirement calls for low distortion, the transistor can be operated under class-A conditions. In this case, the 40-W output level is achieved with only 400-mW drive (20-dB gain).

Typical of the ISOFET design, the UMIL40FT can be biased very simply with a resistor. The device is very forgiving in regard to VSWR, and is capable of dissipating up to 100 W. The input impedance can be adjusted to 12.5, 25, or 50 ohms. P&A: $105; 3 to 4 wks. **Acrian, Inc., 10131 Bubb Rd., Cupertino, CA 95014. (408) 996-8522.** **CIRCLE NO. 231**



***4. The ISOFET amplifier's power output reaches levels as high as 240 W** at selected frequencies. The minimum gain across the bandwidth was 11.4 dB.*

infinite VSWRs without risk of damage from power backups. Another advantage that the ISOFET has over a conventional VMOS transistor is its higher transconductance (g_M)—two to three times higher for similar frequency bandwidths. The ISOFET makes greater use of its silicon material content than the VMOS, for higher gain-bandwidths than the older design.

In order to demonstrate the relative simplicity of designing with the ISOFETs, an amplifier was constructed using two VMIL120FT 120-W, 20-to-175-MHz devices (Fig. 3). The amplifier was operated from 30 to 110 MHz at power levels as high as 240 W at 60 to 70 MHz (see Fig. 4) and gain of at least 11.4 dB across the entire bandwidth. The power efficiency of the circuit was typically 63 percent. The amplifier was run from a 15-W input, a 7.5-A input current, and a drain-to-source voltage of 28 VDC. It required very simple matching compared to a twin bipolar circuit and showed a VSWR that only reached as high as 2.0:1 at the upper band edge.

Different frequency and power areas are currently being explored in ISOFET technology. One area will see the development of a 300-W transistor for 100-to-500-MHz operation in the not-too-distant future. In the 960-to-1216-MHz range, the objective is a 250-W device. As the technology is better understood, improvements will be made in the basic ISOFET device and more devices will be available for circuit and system use (see the product feature on p. 94). The bipolar may continue to be the prime candidate for low-frequency, high-power solid-state applications, but the ISOFET appears to be narrowing the gap in the race for power.●●

BOOKMARK

70 Years of Radio Tubes and Valves

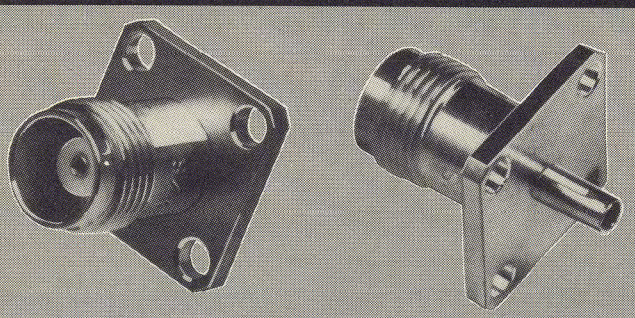
John W. Stokes

In 1880, Thomas Edison found that, under certain conditions, a current could be made to flow through a vacuum. Edison was able to construct devices demonstrating this phenomenon. For one of these devices, he received the first American electronics patent. Later, developments by the British engineer Sir Ambrose Fleming and the American inventor Lee De Forest led to the creation of the vacuum tube.

These developments and more are traced in John W. Stokes' delightful history of the radio tube. The vacuum tube was originally brought into being as a receiving device; it remained in that role for over a decade before it was found that a three-electrode tube could produce oscillations, and thus could be put to the task of transmitting CW radio signals.

All those who remember the RCA "Magic Eye" or the Philips "Magic Star" will enjoy reading *70 Years of Radio Tubes and Valves.* While it is true that many in our field still rely on tubes (such as TWTs) for high-power applications, the devices discussed in Stokes' book have largely been replaced by solid-state devices. This book offers a wonderful journey through one part of electronics history. (ISBN: 0-911572-27-9, 1982, 256 pp., $21.95.) **The Vestal Press Ltd., 320 N. Jensen Rd., Vestal, NY 13859.** ●● *JB*

18 GHz PTNC Flange Mount Connectors



Solitron/Microwave's new PTNC Flange Mount Connectors were designed especially for .085 and .141 semi-rigid cable. The 4055-0002 and 0003 connectors are constructed with gold-plated brass bodies; the 4055-6002 and 6003 with gold-plated stainless steel bodies. All have teflon insulators and beryllium copper contacts.

Typical specifications include:

FREQUENCY RANGE: DC to 18 GH_z

VSWR PERFORMANCE: $1.10 + .010 \times fGH_z$

INSERTION LOSS: $.05db \times \sqrt{fGH_z}$ (DC to 15 GH_z)

$.10db \times \sqrt{fGH_z}$ (15.1 to 18 GH_z)

All meet or exceed MIL-C-39012 requirements.

Contact us today for complete information.

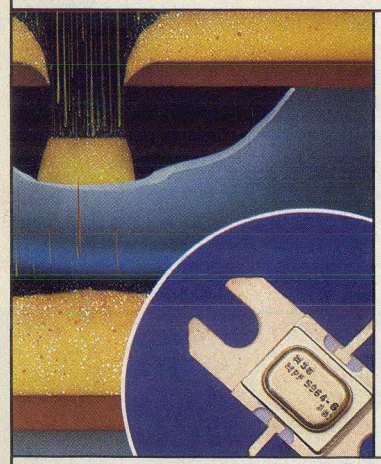
Solitron/Microwave

A Division of Solitron Devices, Inc.
Cove Road, Port Salerno, Florida 33492
Telephone (305) 287-5000 TWX: (510) 953-7500

READER SERVICE NUMBER 64

Microwaves & RF

MARCH 1983 • VOL. 22, NO. 3



cover feature

111 **One company's quest for solid-state power.** Microwave Semiconductor Corp. pursues true solid-state power through controlled materials research and self-aligned production techniques. (Artwork courtesy of MSC, Somerset, NJ 08873; produced by Wagner Graphics, Livingston, NJ 07039.)

departments

13 Feedback
17 Editorial
55 R&D Roundup
66 For Your Personal Interest
104 Bookmark
166 Infocenter
168 Looking Back
168 Looking Ahead

news

28 **Business use guarantees cellular radio success.** The "phone-in-every-car" predictions are optimistic, but not out of reach.

35 Alpha pegs growth on millimeter-wave technology . . . **39** UK scientists describe GaAs FET applications **46** Studies show VLF transmissions influence wave propagation . . . **48** Shared-spare won't be . . . **50** PIN-diode limiters picked for space applications

19 The Front End • **59** Financial News • **63** People • **64** On the Agenda

design features

69 **Installing 800-MHz Land-Mobile Communications.** Gregory M. Stone, a consulting engineer with Sachs/Freeman Associates, helps designers avoid common pitfalls.

78 **Graphic Design Of Feedback Amps.** Marina LeBrun, of Thomson-CSF, and Félix Perez, of Madrid University, use S-matrix parameters to choose the best circuit.

90 **US Navy Begins Shift To Digital Telemetry.** James Rieger and Paul Woodworth, of the Naval Weapons Center, introduce a new telemetry transmitter with TTL-compatible binary input.

94 **A Design Cure For Unstable Transistors.** David Rosemarin, of Microwave Semiconductor Corp., uses a "conjugate stability circle" to evaluate potentially unstable devices.

97 **Frequency Hopping Techniques Vary With Frequency.** Eric Ribchester, a senior designer of Racal's Jaguar series of military radios, explains equipment considerations for UHF, VHF, and HF bands.

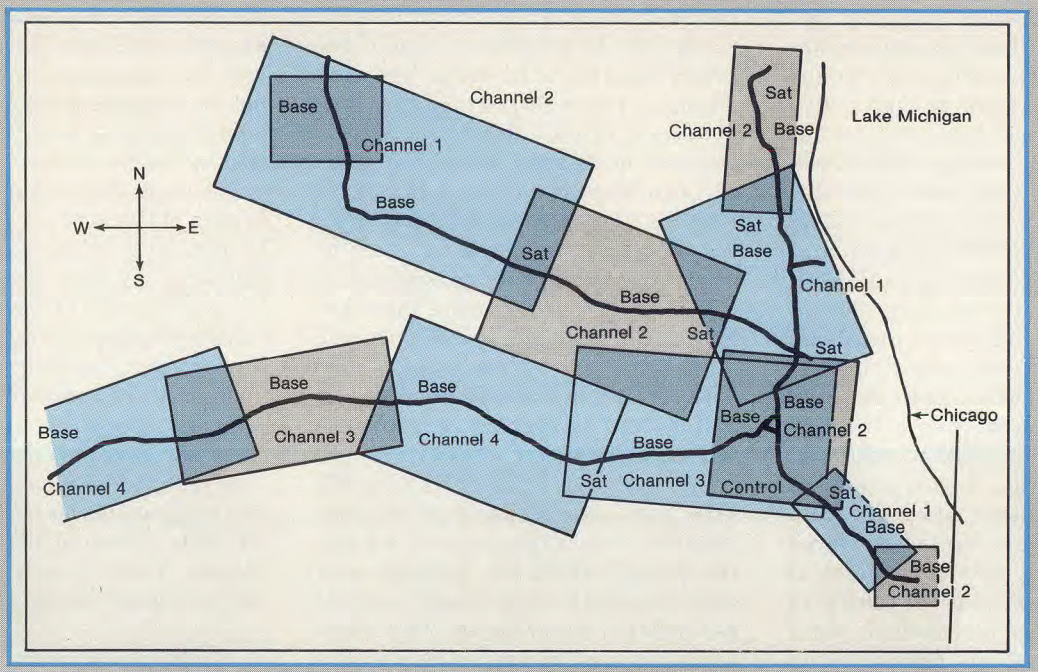
107 **Tubes In Space: Very Much Alive.** Henry G. Kosmahl, head of the microwave section at NASA's Lewis Research Center, argues that TWTs hold their own against solid-state devices in space.

product technology

121 **Radiation monitors measure potential health hazards.** These instruments allow investigators to check for unacceptable levels of nonionizing radiation.

131 **Band-reject filters suppress second harmonics.** Kurt E. Zublin and Behzad Moeen-Ziai, of Wavetek San Diego, filter unwanted harmonics . . . **145** **Determine the cost of temperature cycling.** James Wasson, of Ransco Industries, compares LN_2-cooled and mechanically refrigerated systems. **Features—138** SNA simplifies loss measurements from 10 MHz to 40 GHz . . . **163** NS20 system receives detector support

149 New Products • **162** Application Notes • **164** New Literature



1. This is a variation on a working 800-MHz system, *developed by Jack T. Watson for the Illinois State Toll Highway Authority.*

Installing 800-MHz Land-Mobile Communications

The difficulty of propagating 38-cm waves is just one of the pitfalls that confronts land-mobile communication engineers. Many of the design traps can be avoided by following the advice presented here.

Gregory M. Stone, Consulting Engineer, Sachs/Freeman Associates, Inc., 2970 Maria Ave., Suite 107, Northbrook, IL 60062.

THE 800-MHz band is an attractive alternative to the already congested 30-to-512-MHz area for land-mobile communications. Of course, the design of a working 800-MHz land-mobile system requires that a great many factors be evaluated, including aerial placement, noise-imposed limitations, and wave propagation.

Mobile communication aerials can be thought of as discontinuities in space that are used to couple orthogonally displaced electromagnetic energy to a detector system. The size of the conductor used in these aerials is crucial: the shorter it is, the less voltage is produced. This is an important point because aerials decrease in physical size at higher frequencies (shorter wavelengths), causing a reduction in the effective aperture of the antenna. The effective aperture or capture area of an aerial is related to the power gain by the following:

$$A = \lambda^2 G/4\pi \qquad (1)$$

where A is the effective aperture, λ is the wavelength (in meters), and G is the aerial numerical power gain above an isotropic source.

At 800 MHz, a half-wavelength dipole aerial has an aperture of about 0.018 m^2. An equivalent dipole for 450-MHz operation has an effective aperture of about 0.058 m^2. Thus, the dipole for the lower-frequency aerial has 3.22 times the effective aperture area of the 800-MHz aerial, and will absorb that much more energy than the 800-MHz unit.

Some of these wavelength-depend-

(continued on next page)

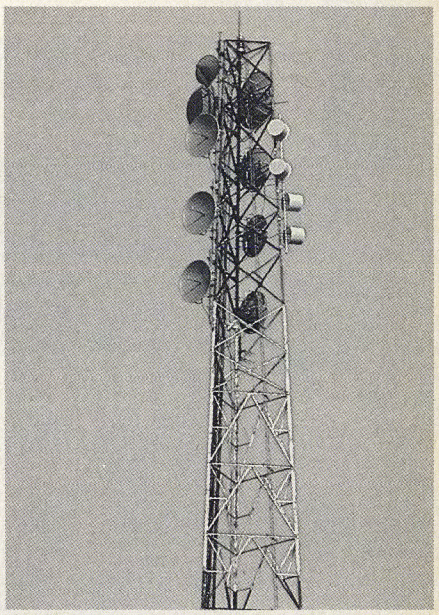
ent losses can be recaptured through the use of vertical beamwidth compression techniques. Still, caution must be advised when basing system design parameters on the use of gain-type vertical beamwidth compression mobile aerials in areas of high multipath signal concentration (such as large population areas with many buildings). Tests have shown that the mean aerial gain of a quarter-wavelength device is 0 dBd (dB gain with dipole reference).[1] When a 3-dBd collinear array was tested, it too showed unity gain and, in some instances, negative gain. In cities and heavily populated suburban locations, it is usually sufficient to use a modest-gain (1.2 dBd, 0.625/0.25-wavelength) aerial. In this way, a compromise in increased effective aperture and modest power gain can be achieved without causing excessive vertical beamwidth compression. Of course, in rural areas, where multipath is not a concern, 3-dBd aerials provide much in the way of increased effective aperture.

Since most cities have the largest structures at their cores and smaller buildings extending outwards, signal propagation, especially at shorter wavelengths, will be highly multipath in nature. The temptation exists to put a high-gain aerial at the top of the tallest building. Although this seems wise, vertical beamwidth compression concentrates much of the aerial's RF energy at the horizon outside of the prescribed area of coverage. This condition is often referred to as the "cone of silence" or the "umbrella effect." It becomes more apparent as the vertical beamwidth is increased. If the tall-building approach must be employed, a half-wavelength aerial can often be used with high-power transmitters to achieve better performance than possible with a collinear array. On the other hand, a collinear array, set up with the proper beam downtilt and null fill, can appreciably minimize the umbrella effect.

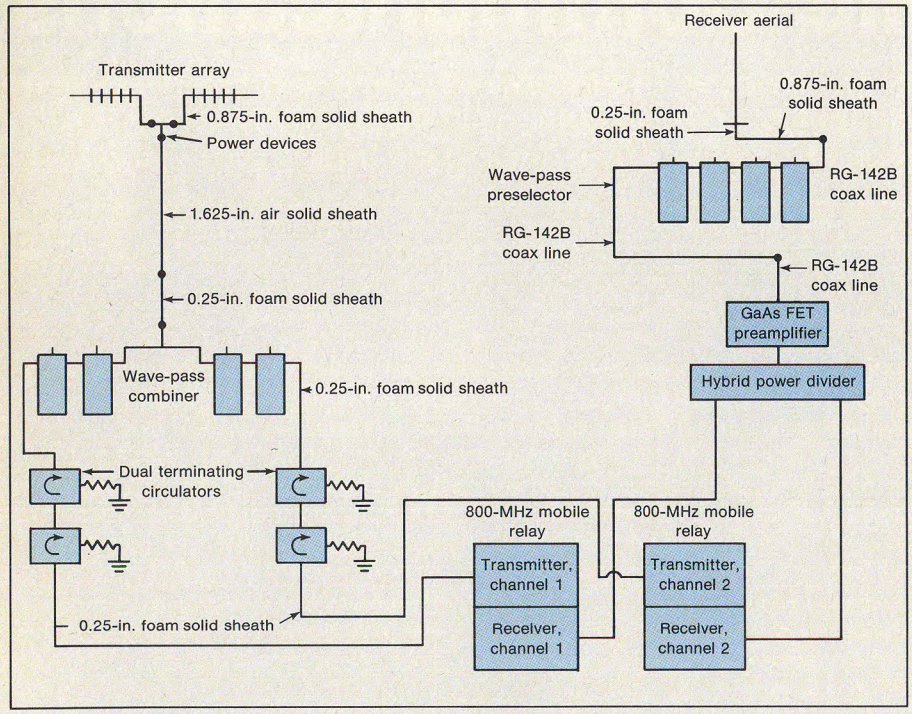
One way to cover a city with an 800-MHz land-mobile system is to locate satellite transmitter/receiver sites on the perimeters of the coverage area and use aerials with modest vertical beamwidth compression. This technique has seen success in mobile telephone applications. When these perimeter sites "look" into an urban area, multipath fill-in is exploited in order to cover a majority of that area's internal locations. A potential problem with this approach is the necessity of having all sides of the urban area covered. If this can't be achieved, low-signal areas will result where there is not enough multipath fill-in. In cases where losses in internal locations are severe, additional satellite receivers within that city's core may become necessary. An alternative coverage solution is to rely on omnidirectional aerials to cover adjacent suburban areas.

The areas that a land-mobile radio system must cover are rarely circular. In Fig. 1, a "ribbon" approach was developed by Jack T. Watson of the Illinois State Toll Highway Authority to sector base stations throughout the covered area. Parabolic reflectors previously were used to achieve full coverage. (See Fig. 2 for a schematic showing typical system components.)

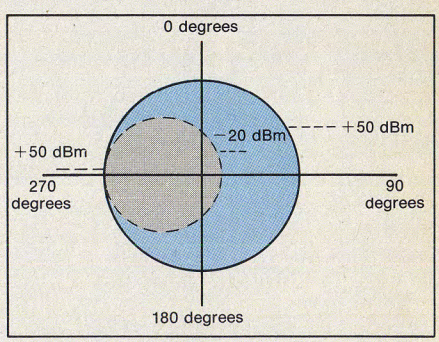
In order to develop sufficient effective radiated power (ERP) in the new 800-MHz system of Fig. 1, four seven-element Yagi-Uda aerials were mounted in a quad configuration. The ar-



3. Radomes can prevent array detuning, *which occurs when ice forms on the transmitter aerials.*



2. Cosystem interference can be controlled *by the use of separate receiver and transmitter aerials.*



4. An aerial's gain is always equal to or less than its directivity, *as this plot of omnidirectional and unidirectional patterns demonstrates.*

ray, which employs a fiberglass radome for protection from the detuning caused by ice loading (Fig. 3), is designed with half-wavelength H-plane spacing and 1.5-wavelength E-plane spacing, and has a forward gain of 14.5 dB over a half-wavelength dipole. Its 3-dB bandwidth is about 30 degrees in the E-plane and 46 degrees in the H-plane, with a 20-dB front-to-back ratio. Each Yagi-Uda aerial within the array has a power gain of 10 dBd; when aerials are stacked and phased, a theoretical 3-dB power gain from one aerial to another is achieved. Under ideal conditions, two of the aerials when stacked would provide a gain of 13 dBd, while four would produce 16 dBd. Of course, these optimistic theoretical limits are reduced somewhat by losses due to aperture coupling, harness attenuation, and signal loss due to the radome.

Certain misconceptions that complicate the design of an aerial setup should be cleared up. For one thing, microwave practice usually considers the gain reference source as isotropic; a better practice, however, is to use a half-wavelength dipole as a reference. It has a power gain of 2.15 dB over an isotropic source and is easier to work with. Care should always be taken when ascertaining the gain of an aerial and its reference. An aerial's gain is always equal to or less than its directivity (see Fig. 4). If both the omnidirectional and unidirectional patterns of an aerial are plotted, the signals at the 270-degree radial will be equal in magnitude. Don't fall into the "directivity-versus-gain" trap. If one assumes that an omnidirectional aerial is radiating at an effective power of +50 dBm, and this aerial is replaced with a unidirectional antenna having a major lobe center line at 270 degrees east of north with an ERP of +50 dBm, its power flux density at the 270-degree radial will be the same as the first aerial, although all other power radials will have less effective power.

Minimizing aerial coupling

The proper placement of aerials is instrumental in sidestepping the negative effects of aerial cross-coupling. For most cases involving horizontal displacement, the amount of cross-coupling can be calculated via free-space propagation formulas, or with the use of an illustrative example (such as Fig. 5). By referring to the figure, it's possible to find the ratio of the received spectral power to the radiated spectral power for antennas operating at a given wavelength (λ) and a known spatial displacement in free space (d):

$$\frac{P_2}{P_1} = \left(\frac{\lambda}{4d}\right)^2 G_1(\theta,\phi)\, G_2(\theta,\phi) \quad (2)$$

In Eq. (2), $G(\theta,\phi)$ is the function for aerial gain relative to an isotropic source. For a half-wavelength reference dipole, the gain function looks like:

$$G(\theta,\phi) = 1.64\, Gf(\theta,\phi) \quad (3)$$

where $f(\theta,\phi)$ is the spectral-power radiation pattern relative to the aerial's maximum gain and f_1 and f_2 are the phase relationships for the two antennas. Coupling losses between antennas can be found by the ratio:

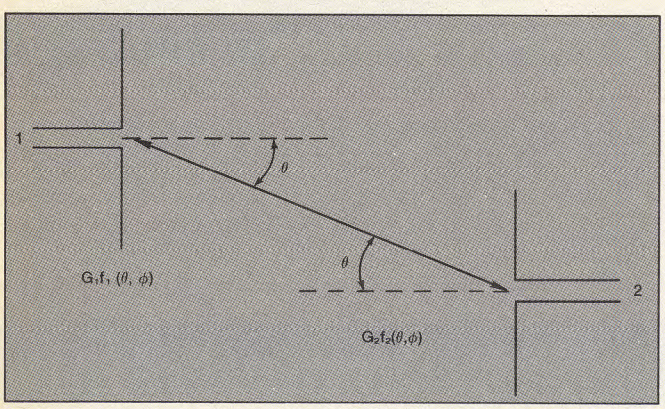
$$\frac{P_2}{P_1} = \left(\frac{0.13}{d/\lambda}\right)^2 G_1\, G_2\, f_1(\theta,\phi) f_2(\theta,\phi) \quad (4)$$

For an example using Eq. 4, see "How to reduce aerial cross-coupling."

Don't overlook noise

An old adage says that, as wavelength decreases in a communication system, the influence of man-made noise becomes less significant than the effects of internally generated detection-system noise products. Nev-

(continued on p. 74)



5. This aerial configuration can be used to calculate cross-coupling. *In the equations, G is the gain of an aerial relative to a half-wavelength reference dipole, and f(θ, φ) is the relative spectral power radiation pattern.*

How to reduce aerial cross-coupling

The best way to tackle a cross-coupling problem is to work out a real-life example. Let us assume that our system has two 800-MHz aerials separated by a distance of one wavelength. The aerials are offset by a 30-degree angle and each aerial has a power gain of 9 dBd. Since our intention is to use Eq.4 to cross-couple calculations, let us state the gain of the aerials in a numeric, nondecibel form: $G_1 = G_2 = 7.94$. Since both antennas will be assumed to be omnidirectional, their patterns do not involve the measure of θ, and the 3-dB vertical beamwidth can be safely written as 9 degrees. Therefore, the spectral power radiation for both antennas can be found by:

$$f_1 = f_2 = \frac{(\sin 9 \text{ degrees})}{(180 \text{ degrees})} = 0.00086$$

The values of declination and inclination can be determined, respectively, by:

f_1 (−30 degrees)
= 0.00086 (−30 degrees)
= 0.0258
f_2 (+30 degrees)
= 0.00086 (+30 degrees)
= 0.0258

For the ratio of the received to radiated spectral power, we employ Eq. 2:

$$\frac{P_2}{P_1} = \left(\frac{0.13}{1}\right)^2 (7.94)(7.94) \times (0.0258)(0.0258) = 7.09 \times 10^{-04} \log_{10} = 31.49 \text{ dB}$$

It is easy to show that the isolation between aerials will increase with separation distance. For example, if we increase the separation distance to 100 λ, the isolation becomes:

$$\left(\frac{0.13}{100}\right)^2 (7.94)(7.94)(0.0258)(0.0258) = 7.09 \times 10^{-08} \log_{10} = 71.49 \text{ dB}$$

By increasing the angle θ so that the aerials are collinear at this 100-λ spacing, even greater isolation can be achieved:

f_1 (−90 degrees)
= 0.00086 (−90 degrees)
= 0.00774
f_2 (+90 degrees)
= 0.00086 (+90 degrees)
= 0.00774

$$\frac{P_2}{P_1} = \left(\frac{0.13}{100}\right)^2 (7.94)(7.94) \times (0.00774)(0.00774) = 6.38 \times 10^{-09} \log_{10} = 81.94 \text{ dB}$$

Thus, it is clear that as the spatial displacement increases, the isolation between aerials increases (or, to put it differently, cross-coupling decreases). Collinear separation is also a valuable tool in minimizing the effects of cross-coupling. It should be noted, however, that isolation figures in excess of 75 to 80 dB are not truly realistic when both aerials are on the same structure. ●●

ertheless, a responsible system designer will not dismiss man-made noise quite so quickly. In a detection system, the effective spectral noise power density at the receiver's RF input port must be considered. This noise is generated by external means, such as the sun's EM energy, or man-made sources. The noise power, which is a function of the detection bandwidth, can be expressed in terms of the effective noise factor, f_A:

$$f_A = P_N/kT_0B = T_A/T_0 \qquad (5)$$

where P_N is the noise power (in W); k is Boltzmann's constant (1.38×10^{-23} J/K); T_0 is the system reference temperature (290°K); B is the effective detection system bandwidth (in Hz); and T_A is the effective aerial temperature in the presence of external noise (measured in °K). By referring to median noise values at 800 MHz,[2] urban man-made noise levels turn out to be 18 dB above the value of kT_0B; suburban levels are usually about 4 dB above the same reference level. In fact, some studies have shown that a mean noise figure ($10 \log_{10} f_A$) of 14 dB relative to kT_0B is common in areas of heavy automobile traffic.[3] The equivalent mean noise figure for a suburban area with moderate traffic is about 2 dB. Of course, too much noise adds up to a net reduction in detector sensitivity at 800 MHz.

Another factor that can limit the sensitivity of an FM detector is AM noise. Although it has not been reported as a significant problem at 800 MHz, and the limiter action of the FM detection process attenuates the amplitude of AM noise to a great extent, this type of impulse noise can "punch holes" in received signals and create a loss of information. Noise-blanker systems for AM noise will mask AM impulses to some degree, but will not solve the problem of associated signal losses.

With man-made noise wreaking havoc on 800-MHz land-mobile communications, the establishment of a usable detector level is important. In an area of heavy urban automobile traffic, a detector noise floor of 0.5 μV at 50 ohms is not unreasonable. Similarly, when traffic is moderate, a noise floor of 0.28 μV at the same impedance is recommended.

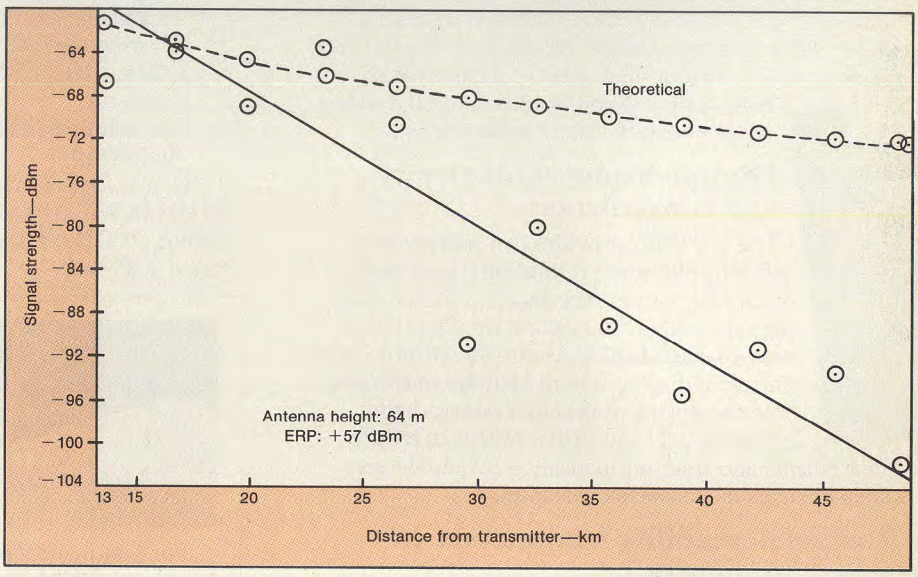
Overcoming multipath fading

The nature of RF-wave propagation at 800 MHz indicates that a received signal is the vector sum of incoming waves from all directions. Since the RF-wave propagation has displacement in both space and time, it is fair to assume that it is of a multipath type. Thus, wave cancellations and additions will occur, with resulting variations in signal amplitude. These variations are usually referred to as multipath or Rayleigh fading.

In areas of heavy multipath, fades as deep as 30 dB may occur. In fact, some studies have shown this level to be as high as 40 dB.[4] Under conditions of heavy multipath and multipath fading, the end result will be a reduction in the signal-to-noise ratio (SNR).

These variations in signal amplitude can be compensated for somewhat by applying decorrelation. Several techniques are available at 800 MHz, including spatial displacement, time displacement, and max-

(continued on p. 76)



6. Signal strength decreases as the distance from the transmitter increases, *but much faster than predicted by standard free-space attenuation formulas.*

Table 1: Signal losses for 30.4-m cable sections

Cable type	Loss (dB)
RG-213/RG-214	8.20
RG-58C	19.20
RG-142B	12.10
Andrew 0.25-in. FS1J50	6.00
Andrew 0.5-in. LDF4-50	2.30
Andrew 0.875-in. LDF5-50	1.40
Andrew 1.625-in. LDF7-50	0.79
Andrew 0.865-in. air HJ5-50	1.20
Andrew 1.625-in. air H57-50A	0.60

Table 2: A comparison of signal attenuation types

Type of loss (dB)	at 150 MHz	at 450 MHz	at 850 MHz
Free-space loss (relative to 150 MHz)	---	9.5	15.1
Bullington diffraction loss (relative to 150 MHz)	---	4.5	7.5
Urban noise (above kT_0B)	35.0	24.0	18.0
Suburban noise (above kT_0B)	20.0	9.0	3.0

imal ratio predetection. Spatial displacement is a simple means of producing decorrelation. A dual-aerial configuration with a spatial displacement of about 1.8 λ results in a correlation coefficient of less than 0.2—adequate signal decorrelation for most land-mobile setups.

Time decorrelation is available only to systems employing digital modulation. This technique is accomplished through the time transmission of data bits over a channel at intervals of time equivalent to the reciprocal of the baseband fading ratio. For effective operation, the time separation must increase as the fading rate decreases. The chief difference between the use of time and space methods is in their end results: space decorrelation will improve a system's SNR; time decorrelation will not, although it does permit the recovery of information which might otherwise be lost.

One way to modify standard spatial decorrelation involves placing satellite receivers throughout the area of coverage. Satellite sites are spatial displaced and configured so that, under most circumstances, the mobile signal will be received by several satellite receivers with a correlation coefficient of less than 0.2. This technique, known as satellite-receiver voting, is a combination of spatial and selection decorrelation practices. The end logic hardware is usually a comparator that selects the signal with the highest SNR or the lowest bit-error rate. Typically, such a system will employ three or more receivers throughout the area of coverage. This type of combination technique not only increases the overall SNR, but decreases mean propagation losses.

The third basic decorrelation method at 800 MHz is known as the maximal ratio predetection combining technique (MRPDC) which is a variation of signal cophasing. It works by weighting signals in the M branches of a system proportionately to their spectral noise-power ratios and the absolute signal voltage, cophasing their signals, and summing their outputs. For an MRPDC system to be effective, the power density present at each of the M branches must be decorrelated. Variable-gain RF amplifiers are usually employed at the branches. With predetection, it is usually required that the internal thermal noise be greater than the external ambient noise. The MRPDC system is a useful technique, although its effectiveness is compromised in areas of high RF noise levels, where the signals at each of the M branches may be highly correlated.

Defeating IMD

Intermodulation distortion (IMD) is another factor that can hinder the response of an 800-MHz land-mobile system. This complex noise can occur within detector-mixer circuits, at transistor junctions, at diode junctions, or even at corroded metal connectors at a transmitter aerial. The odd-octave difference products are the most harmful, since they fall within the operating bandwidth. Some of the methods used to combat IMD include elimination of the nonlinearity which is causing the problem (this is usually impractical), spatial displacement, aerial pattern shaping, RF shielding, the use of terminated circulators, and employing wave-reject or wave-pass filters. The goal of most of these approaches is the same: to reduce the magnitude of the IMD products by increasing system selectivity.

Squelching interference

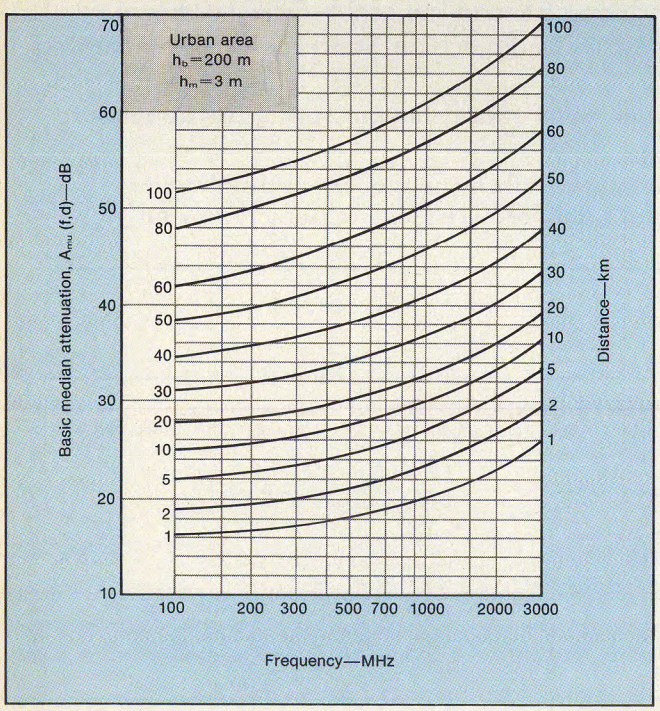
All RF transmission systems are subject to interference of either cosystem or non-cosystem nature. Cosystem interference originates within the system itself and includes transmitter spurious signals, sideband signals, modulation splatter, IMD, receiver desensitization, and signal imaging. Non-cosystem interference occurs outside of a given system and can be man-made noise, transmitter spurious, FM sideband signals, splatter, octave products, and IMD. For example, a receiver can be desensitized by an adjacent system's transmitter. To overcome interference, an adequate power budget must be set up so that reliable reception at some predetermined minimum level of quality is possible. Effective detector sensitivity is one of the key items in the power budget. Minimum-performance effective detector sensitivity values at 800 MHz for a system with a 12-dB SINAD (signal-plus-noise-plus-distortion/noise-plus-distortion) ratio, assuming a 10-kHz IF bandwidth, are −101 dBm (2 μV) under suburban conditions and −125 dBm (4 μV) under urban conditions.

A form of interference often overlooked is FM sideband noise. The use of RF filters at the detector will not adequately lower the level of this noise. The best approach is the employment of wave-pass cavity resonators at the transmitter (refer back to Fig. 2 for a system example).

Considering coax

Since coaxial transmission line is used in land-mobile systems, its effects must be evaluated when de-

(concluded on p. 150)



***7. These propagation-loss curves** were developed by Okumura for a base station at a height of 200 m.*

Graphic Design Of Feedback Amps

The use of graphic techniques employing S-matrix parameters can help designers choose the best feedback circuits for amplifiers.

Marina LeBrun, Thomson-CSF, Laboratoire Central De Recherches, Domaine De Corbeville, BP 10, 91401 Orsay, Cedex/France, and **Felix Perez,** Microwave Dept., ETSI, Madrid University, Madrid 3, Spain.

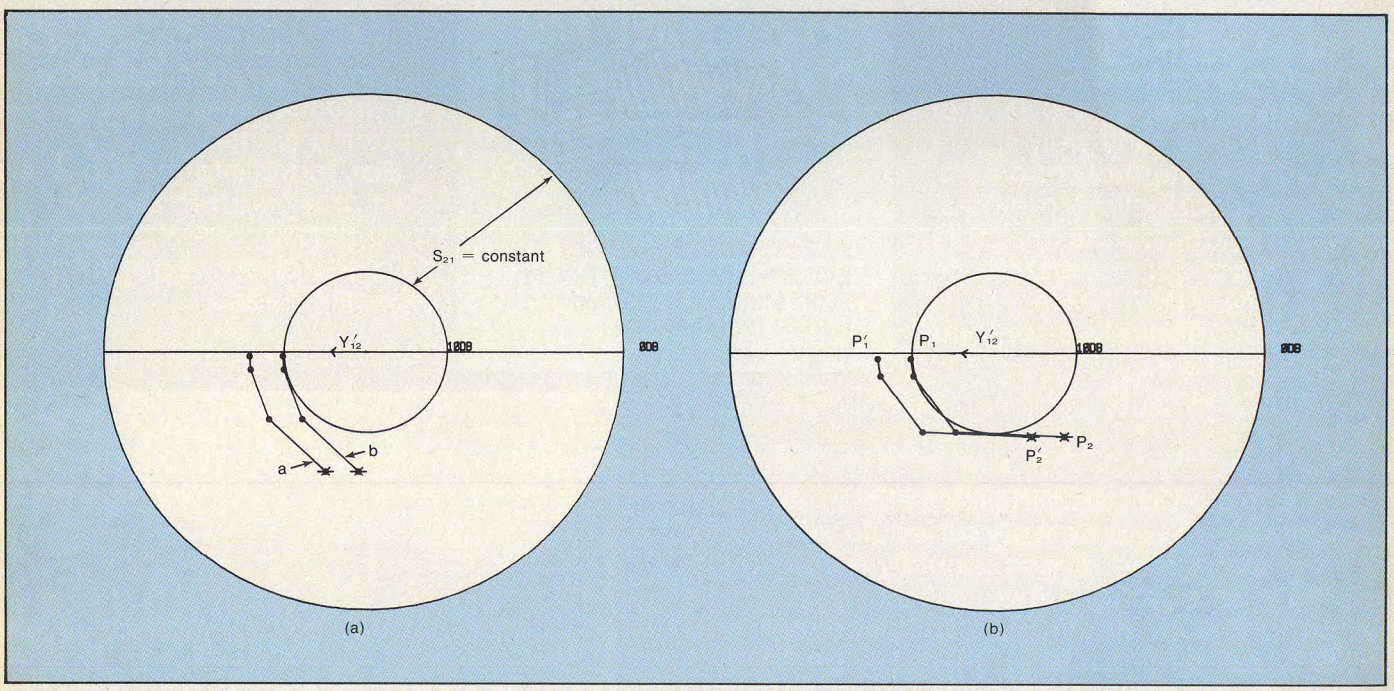
APPLYING feedback techniques to transistor amplifiers for use up to 1 GHz is well established,[1,2] but recent efforts have been made to extend these techniques to amplifiers at higher frequencies. Although computer-aided design (CAD) programs are available to calculate amplifier response after feedback is introduced, the choice of what type of feedback circuit to use is still left to the engineer. The graphic-design techniques discussed here should facilitate that choice by predicting the behavior of the gain or the input and output VSWR of a parallel feedback amplifier.

The use of graphic techniques in circuit design is not unusual; a Smith chart is an excellent example. But unlike a Smith chart, which relies on conformal mapping (a mathematical method), the technique presented in this article relies on the properties of the amplifier's matrix elements after feedback has been added.

Usually, the best way to handle parallel feedback is with Y parameters, but at high frequencies, S parameters and Smith charts are preferred. The conflict need not be a problem, however, since Y parameters can be used and the final results converted to S parameters. (See "Going from Y parameters to S parameters, and back," p. 81).

The Y parameters of a feedback amplifier, $[Y^f]$, are the sum of the amplifier's Y parameters, [Y], and the Y parameters of the feedback circuit, [Y']. That summation can be transformed to S parameters for the following analysis. Rather than look at the S_{ij} parameters themselves, we will examine the functions:

$$\frac{2}{S_{21}^f}, \frac{2S_{11}^f}{S_{21}^f}, \text{ and } \frac{2S_{22}^f}{S_{21}^f}$$



1. The vector $2/S_{21}$ plotted as a function of frequency will yield curved sections *shown in (a), although the sections will not be centered on the origin unless the gain, S_{21}, is flat over the bandwidth. Curve a shows the result of adding 200 ohms of resistive parallel feedback to curve b. Figure (b) shows the curves rotated in the fourth quadrant as a result of adding a series inductor before introducing feedback.*

It can be shown that:

$$\frac{2}{S_{21}^f} \cong \frac{2}{S_{21}} + Y_{12}' \times A \qquad (1)$$

$$\frac{2S_{11}^f}{S_{21}^f} \cong \frac{2S_{11}}{S_{21}} - Y_{12}' \times B \qquad (2)$$

$$\frac{2S_{22}^f}{S_{21}^f} \cong \frac{2S_{22}}{S_{21}} - Y_{12}' \times B \qquad (3)$$

where A and B are functions of S_{ij} and are, therefore, independent of the feedback circuit:

$$A = \left[1 - \frac{2 + S_{11} + S_{22}}{S_{21}}\right] \qquad (4)$$

$$B = \left[1 + \frac{1 - S_{11}S_{22} + S_{12}S_{21}}{S_{21}}\right] \qquad (5)$$

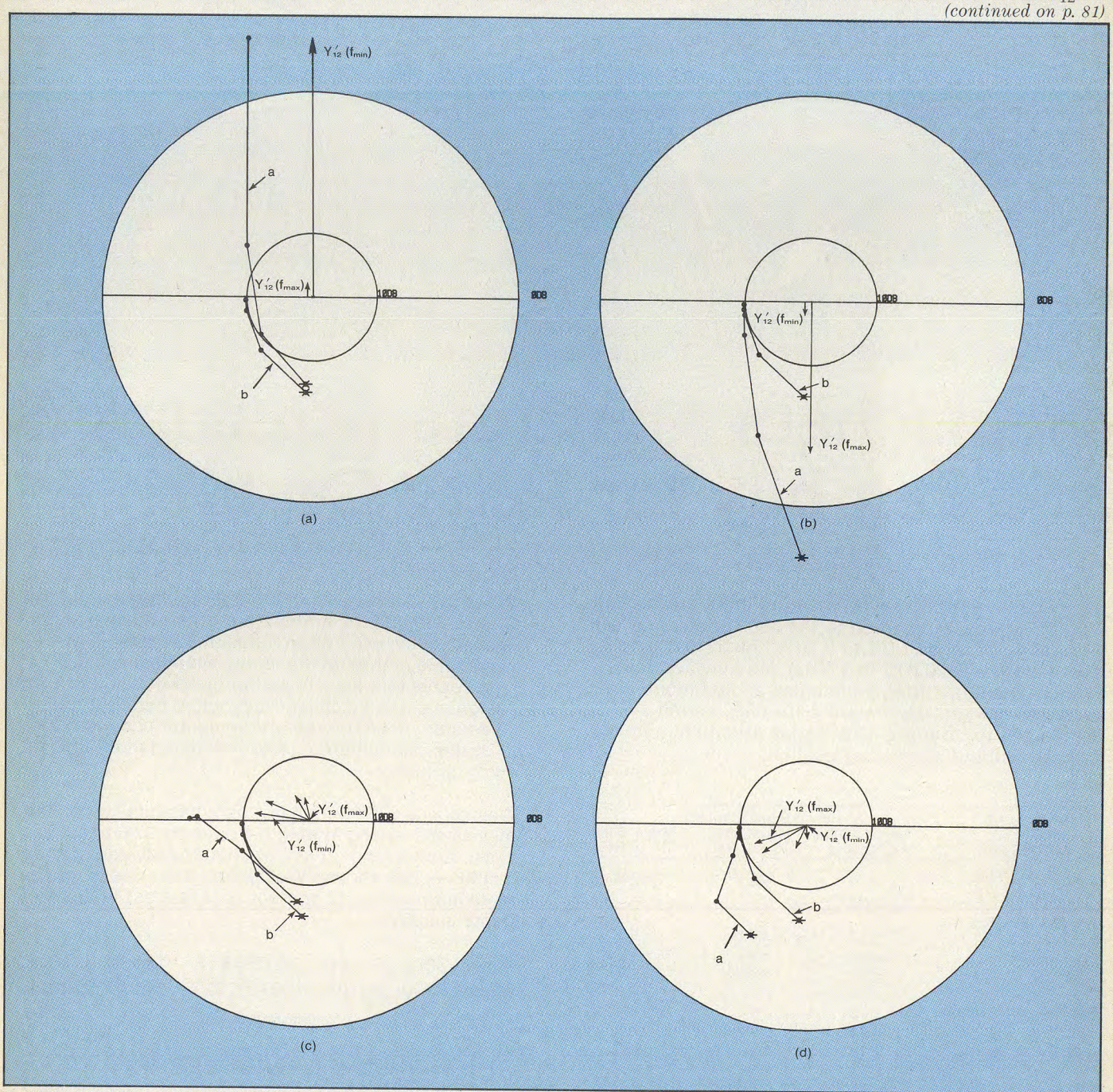
The only approximation needed to arrive at these relatively straightforward equations is that $Y_{21}' << Y_{21}$.

A graphical analysis

Equations 1, 2, and 3 are vector additions in the complex plane, so if the vector $2/S_{21}$ is plotted as a function of frequency on a polar chart, the result is a section of a curve. Figure 1a shows an example of such a plot. The circles centered on the origin are constant-gain curves, i.e., where S_{21} is constant. The plot of $2/S_{21}$ generally will not be centered on the origin. That would be the case only if gain S_{21} were flat over a specified bandwidth. This is what an engineer hopes to accomplish by using the feedback network. Graphically this means moving the plot onto a constant gain curve by adjusting vector $Y_{12}' \times A$ in Eq. 1.

In the simplest case, where the feedback network is a resistance, we can assume A = B = 1. Then $Y_{12}' =$

(continued on p. 81)



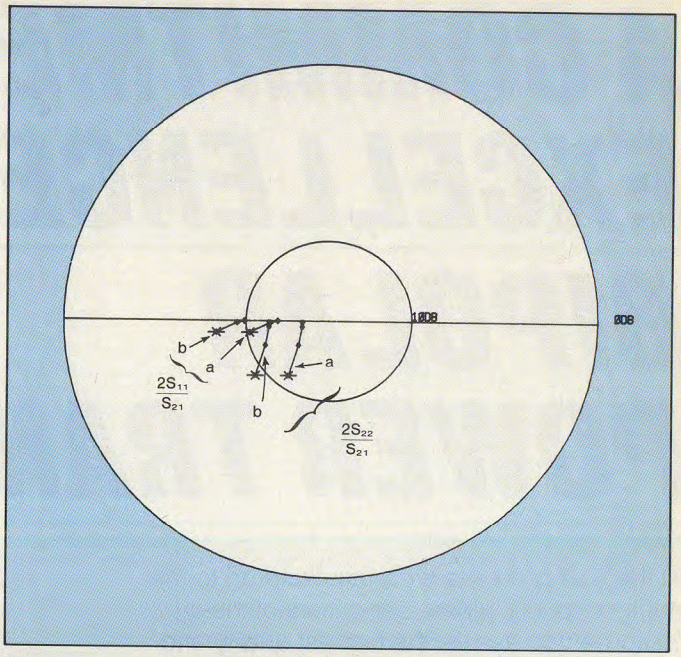
2. These curves show the effect of reactive feedback networks on the plot of $2/S_{21}$. *Pure inductive feedback will translate the curve upward on the polar plot (a); pure capacitive feedback will translate the curves downward (b). The amount of movement per unit reactance will be frequency dependent. In (c) and (d) the effects of combined resistive-reactive feedback are shown.*

$-Y'_{21} = -1/R$. Thus, for a resistive network, the vector (Y'_{12}) will fall on the negative side of the real axis and be independent of frequency. The vector addition (Eq. 1) will translate the curve toward the left side of the chart and, depending on which quadrant the $2/S_{21}$ vector falls in, will increase or reduce the value of S_{21}. That is, the feedback will be negative or positive. Figure 1b illustrates this.

A quick look at the $2/S_{21}$ curve will tell an engineer whether a feedback resistor will suffice for a particular application and, if so, what its value must be.

Reactive networks, of course, are more complicated. Pure inductance will produce a translation upward, and pure capacitance will produce a translation downward, but the amount of movement will depend on the frequency (see Figs. 2a and 2b).

Any series combination of passive components in a parallel feedback network can be treated similarly. Examples are shown in Figs. 2c and 2d.



3. Feedback will affect input and output impedance, *as shown in these plots of $2S_{11}/S_{21}$ and $2S_{22}/S_{21}$ without resistive feedback (curves b) and with resistive feedback (curves a).*

Impedance matching

The feedback network also will affect input and output impedance. In fact, if we continue to assume that A = B = 1, the vectors $2S_{11}/S_{21}$ and $2S_{22}/S_{21}$ are subject to the same translations as $2/S_{21}$, although in the opposite direction. Thus resistive feedback will translate these two vectors toward the center of the polar chart, where their modules are smaller. If $2S_{11}/S_{21}$ and $2S_{22}/S_{21}$ lie in the second and third quadrant, therefore, resistive feedback will improve the impedance match. If they lie in the first and fourth quadrant, resistive feedback will degrade the match (see Fig. 3). Similarly, reactive feedback will cause nonuniform vertical translations that will improve or degrade the impedance match, depending on the original location of the vectors.

In any case, the point is still valid: Even a quick look at a polar plot of the $2S_{11}/S_{21}$ and $2S_{22}/S_{21}$ curves will provide a designer with a good idea of what type and quantity of feedback are necessary to adjust the amplifier's VSWRs as desired.

Practical usage

We have used the approximation A = B = 1 to facilitate the explanation of graphic-design techniques, but in general, A and B (Eqs. 4 and 5)

(concluded on p. 86)

Going from Y parameters to S parameters, and back

A two-port network can be characterized by its short-circuit admittance matrix (Y matrix):

$$I_1 = Y_{11}E_1 + Y_{12}E_2$$
$$I_2 = Y_{21}E_1 + Y_{22}E_2$$
$$[I] = [Y] \times [E]$$

or by its scattering matrix (S matrix):

$$b_1 = S_{11}a_1 + S_{12}a_2$$
$$b_2 = S_{21}a_1 + S_{22}a_2$$
$$[b] = [S] \times [a]$$

In the S matrix, a and b are the incident and reflected "waves" at each port and are functions of port voltage, port current, and certain normalizing numbers (such as characteristic impedance).

The Y and S matrices are related as follows:[3,4]

$$Y_{11} = \frac{1 - \Delta S + S_{22} - S_{11}}{1 + S_{22} + S_{11} + \Delta S}$$

$$S_{11} = \frac{1 - \Delta Y + Y_{22} - Y_{11}}{1 + Y_{22} + Y_{11} + \Delta Y} \quad (1)$$

$$Y_{22} = \frac{1 - \Delta S + S_{11} - S_{22}}{1 + S_{22} + S_{11} + \Delta S}$$

$$S_{22} = \frac{1 - \Delta Y + Y_{11} - Y_{22}}{1 + Y_{22} + Y_{11} + \Delta Y} \quad (2)$$

$$Y_{12} = \frac{-2S_{12}}{1 + S_{22} + S_{11} + \Delta S}$$

$$S_{12} = \frac{-2Y_{12}}{1 + Y_{22} + Y_{11} + \Delta Y} \quad (3)$$

$$Y_{21} = \frac{-2S_{21}}{1 + S_{22} + S_{11} + \Delta S}$$

$$S_{21} = \frac{-2Y_{21}}{1 + Y_{22} + Y_{11} + \Delta Y} \quad (4)$$

$$\Delta Y = Y_{11}Y_{22} - Y_{12}Y_{21}$$

$$\Delta S = S_{11}S_{22} - S_{12}S_{21} \quad (5)$$

Note that the algebraic form of the transformation from Y to S is the same as that from S to Y. Thus, for a computer program, the transformation need be written only once. A "dummy" matrix A can be set up as the departure matrix, and a dummy matrix B can be set up as the arrival matrix. If a transformation from Y parameters to S parameters is desired, the Y matrix is loaded into the A matrix and the S matrix is given under the name of B. If a transformation from S to Y is needed, the S matrix is loaded into A. ••

must not be ignored. A designer can use the approximation, choose the type of feedback desired, and let a more complete CAD program complete the design. Or he or she can plot the actual correcting terms, $Y_{12}' \times A$ and $Y_{12}' \times B$, on the same polar chart to determine their effects on gain and impedance.

Either way, the graphic presentation will provide a good feel for the feedback elements needed to accomplish the design objective. Even when the approximation is used, the plots indicate a useful trend.

The other approximation made was that $Y_{21}' << Y_{21}$. If this is not valid, the advantage of plotting the three S vectors is reduced, and feedback effects will be harder to predict, although the graphics still will be helpful. In this case, Eqs. 1, 2, and 3 are not valid, and the entire matrix Y' must be used.

The above discussion concerns parallel feedback, but series feedback can be handled in a similar fashion, using the Z matrix instead of the Y matrix. In this case, the sign for the translation of the vector $2/S_{21}$ is the same as that for the vectors $2S_{11}/S_{21}$ and $2S_{22}/S_{21}$.

It is sometimes useful to modify the angular position of the vectors to obtain a positive feedback. This can be accomplished by adding an inductor in series with the amplifier's active element before introducing feedback. In this case, the chain matrix:

$$\begin{bmatrix} A & B \\ C & D \end{bmatrix}$$

is used to calculate the new Y- or S-matrix elements, and feedback is introduced as before.

Calculations required

One drawback of using this graphical-design technique is the need to calculate and plot the several vectors at a number of frequencies, with and without feedback. This task, however, can be handled by a desktop computer, which can be programmed not only to make the calculations but also to control a plotter.

The figures in this article were generated using a Commodore CBM 8032 computer and an HP-7220S plotter. Similar plots have been generated using a graphics terminal. A terminal has the advantage of speed and the ability to study a plot on the screen before deciding whether a printout is needed. However, the resolution of a plotter is better than that of a screen printout. ●●

References

1. E. Ulrich, "Use Negative Feedback To Slash Wideband VSWR," *MicroWaves*, pp. 66-9 (October, 1978).
2. F. Perez and V. Ortega, "A graphical method for the design of feedback networks for microwave transistor amplifiers: theory and applications," *IEEE Transactions MTT-29*, p. 1019 (October, 1981).
3. L. Weimberg, "Fundamentals of Scattering Matrices," *Electrotechnology*, pp. 55-72 (July, 1967).
4. R. Anderson, "S Parameter Technique for Faster, More Accurate Network Design," HP Application Note No. 95-1.

WAVEGUIDE
Terminations

PRICE: Unbeatable from $79.00
(Series 200X: Quantity 10–24)
DELIVERY: Stock to 30 days
CALL: 516/420-9000

Struthers waveguide terminations are offered in three standard power ranges PLUS intermediate power levels specifically designed for satellite communication applications. PLUS unconditional guarantees assured by a tight, independent quality-control system. PLUS 25 years experience in the manufacture and design of MIL Spec microwave components.

To find out more about Struthers complete product line, write or call for comprehensive catalog. Let our engineering staff review your particular requirements.

HIGH POWER
Series J202

MEDIUM POWER
Series K202

LOW POWER
Series 200

QPL Series

- Frequency Range 1 to 40 GHz
- 1 Watt to 3 Kilowatts
- Low VSWR, typically <1.05
- Finned and unfinned units
- No forced air cooling required
- QPL approved models
- Unconditionally guaranteed

&
MAGIC "T" HYBRIDS
Series M352

Struthers®
Struthers Electronics Corporation, 4 Dubon Court, Farmingdale, NY 11735 • 516/420-9000 • TWX 510-224-6112
READER SERVICE NUMBER 75

US Navy Begins Shift To Digital Telemetry

UHF has been used for some time in telemetry, but mostly in analog systems. New requirements and a new transmitter have led to adoption of digital techniques.

James Rieger, Electrical Engineer, and **Paul Woodworth**, Technician, Naval Weapons Center, China Lake, CA.

THE US Navy has been using UHF for telemetry since 1967, mostly in analog pulse-amplitude modulation (PAM) or as FM subcarriers (FM/FM). However, demands for greater accuracy, the availability of equipment, and the requirement for encrypted telemetry have recently caused a shift to new designs that use digital pulse-code modulation (PCM) formats. Unlike previous transmitters, the new units, made to specification MIL-T-85375(AS), have a transistor-transistor-logic-compatible (TTL) binary input rather than an analog input.

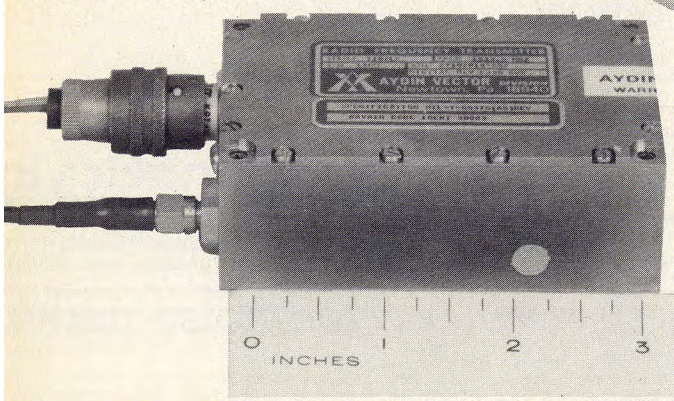
Deviation of the transmitted frequency for a "one" or a "zero" is factory fixed, as is the rate of change from the upper to the lower frequency. The term "center frequency" is no longer accurate, because the transmitter passes through what would be called the center frequency only instantaneously, and no possible input can cause the center frequency to be produced on a steady-state basis.

Telemetry systems for missiles, aircraft, and high-speed sleds use 1-MHz channels between 1435 and 1535 MHz and between 2200 and 2290 MHz, as well as other channels when required. For some uses, wideband channels of 3 or 5 MHz are assigned. A typical transmitter puts out between 2 and 5 W and measures 8 to 12 cu. in. Transmitters built to the new specification (Fig. 1) are similar in size and identical in connector layout to those made for analog inputs to specification AS-1990C, which has been in use since 1969. Each year, the government uses several thousand such transmitters, made by five manufacturers.

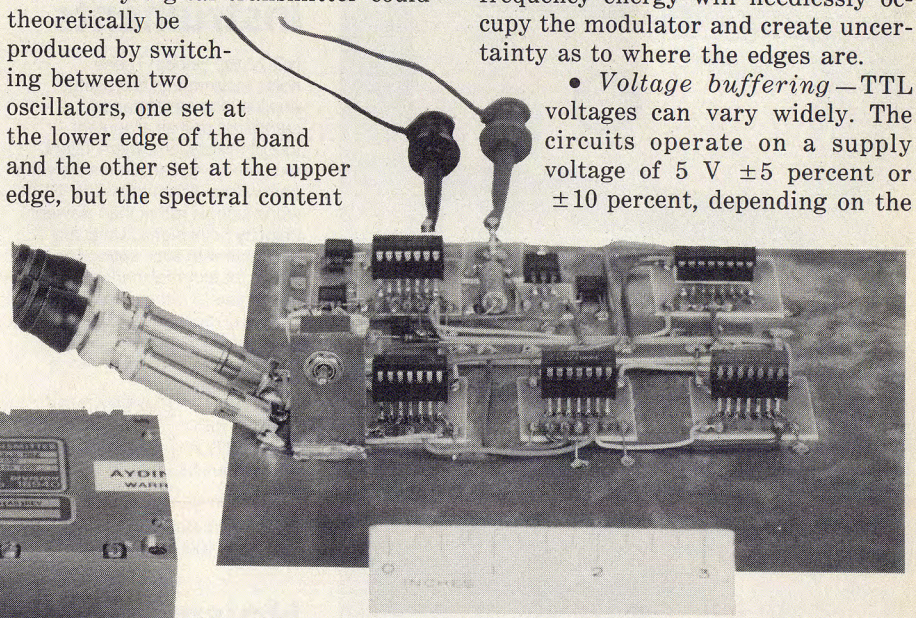
Processing the input

A binary digital transmitter could theoretically be produced by switching between two oscillators, one set at the lower edge of the band and the other set at the upper edge, but the spectral content of such a signal would be very large. Hence, the modulator actually used in the digital transmitter is linear, so the transmitter gradually changes from one frequency to the other at a rate determined by an internal premodulation filter. When such a linear input is used and the input is a standard TTL system, as would be found at the output of a multiplexer or the output of an encryption device that is fed by the multiplexer, a number of things must be done to the signal before the transmitter sees it:

- *Deglitching*—A TTL signal may have rough edges, ringing, etc., on its leading and trailing edges. If these aren't removed, a lot of high-frequency energy will needlessly occupy the modulator and create uncertainty as to where the edges are.
- *Voltage buffering*—TTL voltages can vary widely. The circuits operate on a supply voltage of 5 V ±5 percent or ±10 percent, depending on the



1. New digital telemetry transmitters *are similar to older analog units in size and connector layout.*



2. This TTL generator and randomizer *was built to test the digital telemetry transmitters.*

family, which produces a level of uncertainty itself. The actual level of a zero can be anything from 1.4 V on down, and the level of a one can be 2.4 V on up. These voltages will depend on power-supply voltage, and will vary mainly with temperature and component age as well as from unit to unit and with loading.

• *Voltage offsetting*—The two stabilized voltages for the one and the zero are typically offset and scaled to provide symmetrical modulation of the transmitter, usually ±1 V or so.

• *Low-pass filtering*—Low-pass filtering rounds off the edges of the pulses to remove higher-frequency components that contribute little to reception of the digital data but increase the occupied spectrum. Typically, the filter's cutoff frequency is about 0.7 times the bit rate, assuming a nonreturn-to-zero format.

All these functions are performed by the premodulation filter unit.

An analog transmitter must also be characterized by a specified bandwidth, distortion, linearity, monotonicity, and other requirements not germane to digital systems. Thus, the digital transmitter, in which the premodulation processing and modulator are combined, eliminates the need for an external box, as well as testing for characteristics required by analog systems.

The introduction of encryption to a digital telemetry system presents a few theoretical problems, and helps solve a few others. A typical telemetry signal involves repeating values that change very little and, worse yet, are often zero. That adds DC components to the signal, changing what the receiver considers to be the center frequency. As a result, an automatic frequency control can't be used to correct for drift. Introducing encryption also places limits on how well the occupied spectrum of the transmitter can be known.

Spectrum occupancy, however, is of great concern to frequency managers, even though interchannel spacing is fixed. Designers are concerned with sideband energy as much as 60 dB down from the carrier as well as the points that contain 99 percent of the signal energy. While a signal alternating between one and zero requires the widest bandwidth, a randomized PCM signal requires a smaller spectrum, although it will have some specific structure. Moreover, any signal randomized by an encryption device will have the least bandwidth. This is because the random signal has as many transitions (from one to zero and vice versa) as an alternating signal since the bit that follows a zero is equally likely to be a one or another zero, while an alternating signal requires a transition between each bit.

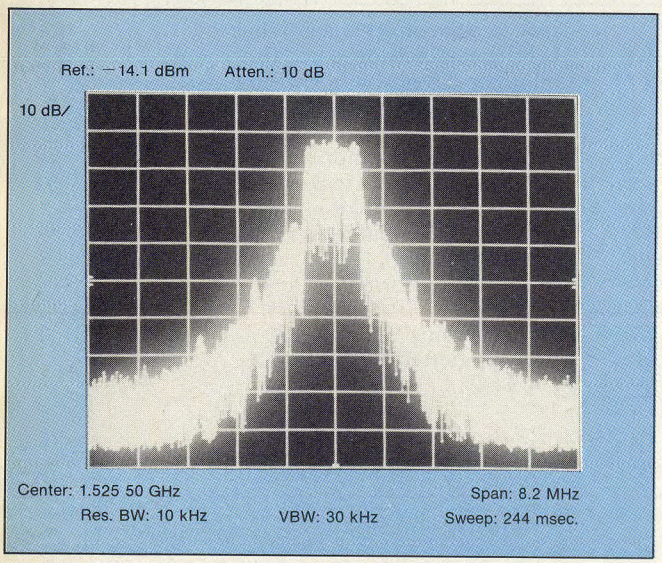
For test purposes, a circuit was built with variable bit rates and two outputs (Fig. 2). The two outputs consisted of an alternating one-zero sequence (corresponding to a square wave at half the bit rate) and a pseudorandom pattern that resembles a more realistic signal. Spectral responses of the transmitter for the two test signals are shown in Figs. 3 and 4.

For a digital transmitter, these signals are symmetrical with respect to the channel center, which is the average between the one and zero state, but the unmodulated carrier *level* (not the frequency) is attained with a sustained zero or one at the input, neither of which is at the center of the channel. Unencrypted PCM falls between the bandwidths for alternating and random patterns, but exactly where is unpredictable.

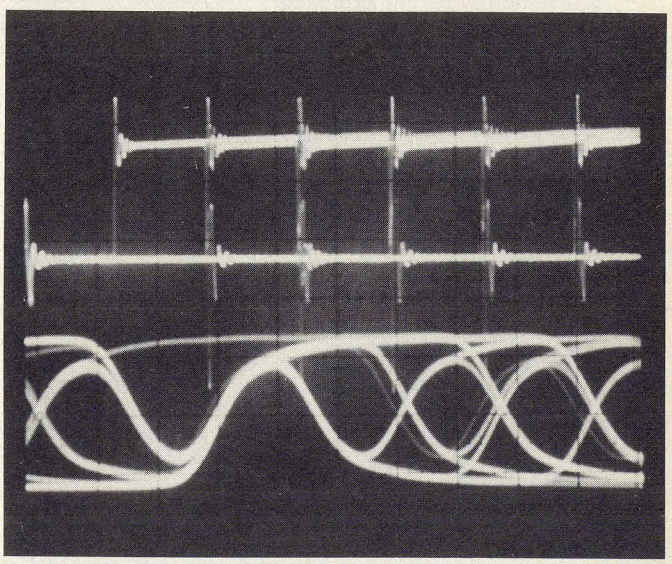
Transmitters for analog inputs are characterized for a specific center frequency tolerance, and symmetrical modulation is assumed. However, no tolerances are placed on deviation sensitivity, making center frequency measurement impossible when asymmetrical waveforms are transmitted.

With a digital transmitter, the center frequency is taken as the average of the steady-state one and zero conditions, and deviation symmetry is guaranteed. Deviation is fixed at the factory, as is the corner frequency of the internal premodulation filter. These parameters are selected to allow a frequency deviation in kHz of ±35 to ±40 percent of the bit rate in kbit, although other deviation ratios are possible. Thus a 350-kHz deviation transmitter is used for bit rates in the 850 kbit to 1 Mbit/s range.

Initial tests of the digital transmitters produced to date indicate that the units function as expected. ••



***3. Spectral output of the transmitter is** shown with an 886-kbit/s random input and ±350-kHz deviation.*



***4. Transmitter output** is shown compared with a 1-Mbit/s random PCM TTL input signal and ±350-kHz deviation.*

A Design Cure For Unstable Transistors

The traditional procedure for analyzing transistor stability is effective but complicated. A new technique develops a "conjugate stability circle" on a Smith chart as a simpler means of studying unstable devices.

David Rosemarin, R&D Engineer, Microwave Semiconductor Corp., 100 School House Rd., Somerset, NJ 08873.

THE traditional method of transistor instability analysis is based on the conditions established for inherent stability. According to these conditions, a device is inherently stable if its input and output resistances are positive for any passive terminations. This is equivalent to saying that the input and output reflection coefficients are presented by the following values:

$$|S_{11}'| < 1 \quad (1)$$

$$|S_{22}'| < 1 \quad (2)$$

From these equations, Smith chart input and output stability circles can be derived.

Under these familiar stability conditions, the output stability circle is drawn on a Smith chart that represents the load reflection coefficient (Γ_L) plane. After a specific level of power gain is selected, the corresponding power gain circle is then drawn on a Smith chart, and a desired load reflection coefficient is selected at a point on the circle which is outside the region of instability.

Following this, a source reflection coefficient, Γ_S, is chosen. Provided that the input circuit can be conjugately matched, the source reflection coefficient can be calculated by:

$$\Gamma_S = (S_{11}')^* \quad (3)$$

where S_{11}' is the input reflection coefficient and $(S_{11}')^*$ is the conjugate of the input reflection coefficient. To determine whether this particular source reflection coefficient is acceptable, an input-circuit stability circle must be drawn. As in the case of the output circuit circle, the input reflection coefficient refers to stable operation when it does not fall in or near the unstable region of the input circle.

Because two separate planes are involved, the calculations behind the inherent stability technique are tedious. Furthermore, this method, while adequate, does not let a designer quickly see all the conditions for stability (or instability).

New method is clear

The technique described here is based on the development of a different stability circle (see the figure). It shows the contour of the output reflection coefficient, Γ_L, which is acceptable for conjugate input matching. When this circle, together with the power gain circles, is drawn on the Γ_L-plane, the conditions for stability are apparent without need of any further calculations.

The development of the conjugate stability circle begins by defining a few necessary terms. Let the determinant of the scattering-parameter S-matrix be represented by Δ, which is equal to:

$$\Delta = S_{11}\,S_{22} - S_{12}\,S_{21} \quad (4)$$

The complex variables C_1 and C_2, which must be defined in order to locate the centers of the gain and stability circles, respectively, can be given by:

$$C_1 = S_{11} - S_{22}^*\,\Delta$$
$$C_2 = S_{22} - S_{11}^*\,\Delta \quad (5)$$

The stability factor, K, is generally presented as:

$$K = \frac{1 - |S_{11}|^2 - |S_{22}|^2 + |\Delta|^2}{2\,|S_{12}\,S_{21}|} \quad (6)$$

but, for simplification, let us make the substitutions:

$$E_1 = |S_{11}|^2 - |\Delta|^2$$
$$E_2 = |S_{22}|^2 - |\Delta|^2 \quad (7)$$

and:

$$G_1 = 1 - |S_{22}|^2$$
$$G_2 = 1 - |S_{11}|^2 \quad (8)$$

so that Eq. 6 can now be written as:

$$K = \frac{G_i - E_i}{2\,|S_{12}\,S_{21}|} \quad (9)$$

where i = 1 or 2.

Now, armed with these factors, it is possible to find the center of the stability circle. It is at:

$$R_2 = \frac{2\,|S_{12}\,S_{21}|\,K}{|C_2|^2 - |E_2|^2}\,C_2^* \quad (10)$$

The radius of this circle can be written as:

$$\rho_2 = \frac{|S_{12}\,S_{21}|^2}{|C_2|^2 - |E_2|^2} \quad (11)$$

In order to evaluate this circle alongside the inherent stability circle, the inherent stability circle's characteristics are presented here. The output stability circle has a center at:

$$R_2 = \frac{1}{|E_2|} C_2^* \quad (12)$$

and a radius of:

$$\rho_2 = \frac{|S_{12}\, S_{21}|}{|E_2|} \quad (13)$$

Similarly, the input stability circle has a center at:

$$R_1 = \frac{1}{|E_1|} C_2^* \quad (14)$$

and a radius of:

$$\rho_1 = \frac{|S_{12}\, S_{21}|}{|E_1|} \quad (15)$$

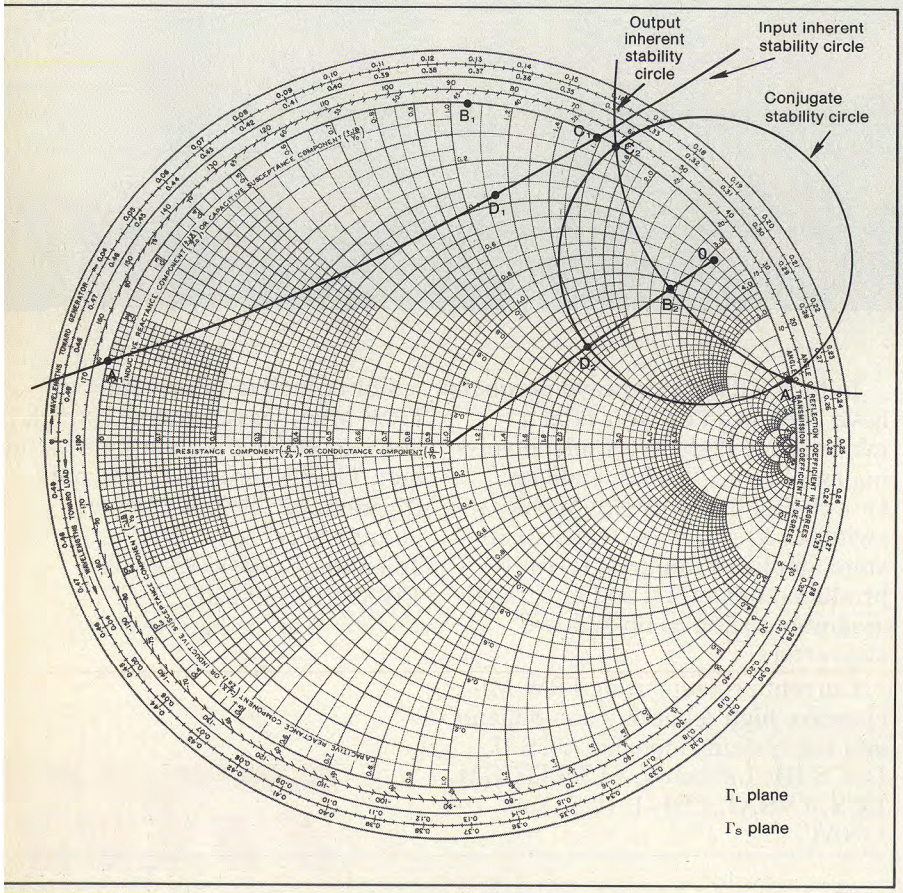
Looking at Eqs. 10 and 12, it's apparent that the centers of both output stability circles are on the same radius vector C_2^*. By further mathematical analysis (which will not be presented here) it can be shown that both circles intersect the circumference of the Smith chart at the same point. This is demonstrated in the example above. It can also be shown that the conjugate stability circle coincides with a power gain circle for a given specific operating power level:

$$G_{pm} = 2K \left| \frac{S_{21}}{S_{12}} \right| \quad (16)$$

The significance of Eq. 16 lies in the fact that it presents a higher maximum stable gain (MSG) than that represented by the traditional relationship for that parameter:

$$MSG = \frac{|S_{21}|}{|S_{12}|} \quad (17)$$

The difference between Eqs. 16 and 17—the factor 2K—indicates that it is possible to operate a two-port device over a greater range than previously accepted, and still maintain stable conditions. ••



The Smith chart contains important information, *in the form of the conjugate stability circle, that can simplify the manipulation necessary for the establishment of stability conditions.*

Surveying the stability of a bipolar

How well does the new conjugate stability technique work? An RF bipolar transistor operating at +6 VDC, 3 mA, and 200 MHz was evaluated for stability. Its S-parameters showed the following magnitudes and phase angles:

$S_{11} = 0.61\angle -65$ degrees
$S_{12} = 0.05\angle +61$ degrees
$S_{21} = 5.4\angle +122$ degrees
$S_{22} = 0.82\angle -18$ degrees

The center of the conjugate stability circle was located at

$$R_2 = 0.920\angle 36.076 \text{ degrees}$$

with a radius of:

$$\rho_2 = 0.426$$

The center of the output stability circle was located at:

$$R_2 = 1.602\angle 36.076 \text{ degrees}$$

with a radius of:

$$\rho_2 = 0.817$$

Finally, the center of the input inherent stability circle could be found at:

$$R_1 = 9.540\angle 115.142$$

The radius for this circle was:

$$\rho_1 = 8.953$$

Refer to the figure to make use of this information. Points A_2, B_2, and C_2 on the output inherent stability circle are transformed to points A_1, B_1, and C_1 on the source reflection coefficient plane. In this case, arc $A_1B_1C_1$ satisfies the condition:

$$|\Gamma_s| = 1$$

It can be shown that points A_2, D_2, and C_2 on the output conjugate stability circle easily transform to points A_1, D_1, and C_1 on the input inherent stability circle. Since the region that is outside the conjugate stability circle can be conjugate-matched at the input, there is no need to draw an input plane since all the necessary information is included on the output plane. ••

Frequency Hopping Techniques Vary With Frequency

VHF and UHF frequency-hopping equipment can work at fairly high data rates in uncluttered spectrums. But HF designs must deal with different restrictions, including the whims of the ionosphere.

Eric Ribchester, Technical Director, Racal-Tacticom Systems Ltd., 472 Basingstoke Rd., Reading RG20QF, England.

THE specific characteristics of the three frequency regimes commonly used for battlefield communications—HF (1.6 to 30 MHz), VHF (30 to 88 MHz), and UHF (225 to 400 MHz)—affect the manner in which frequency hopping can be applied in these particular bands. This article summarizes these problems and reviews how they can be or have been solved. In doing so, it reflects work that has been done at Racal-Tacticom in the development of the Jaguar series of ECCM radios.

Beginning a hopping design

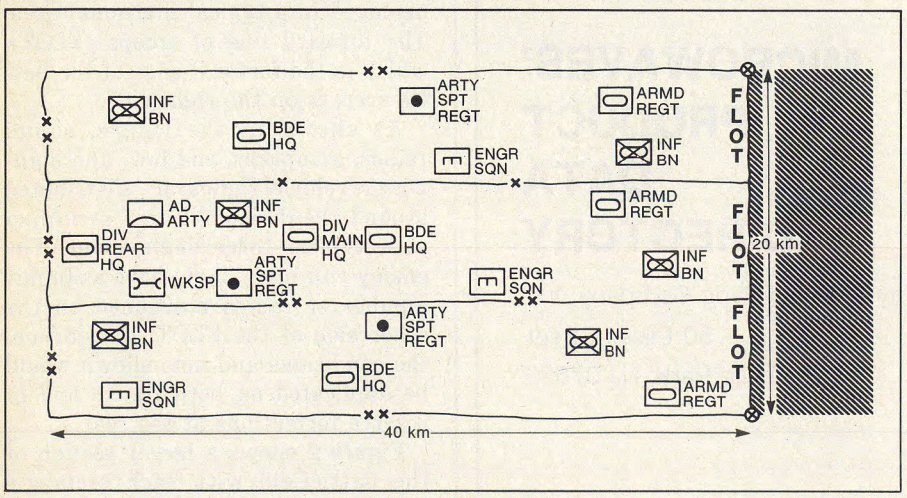
Before a frequency-hopping system can be designed, fundamental parameters such as the number of hop channels and the bandwidth over which they will be spread must be determined. Obviously, using the maximum number of channels makes the enemy's task of finding the signal more difficult, and may force him to jam all of the channels simultaneously. The additional jamming power that is required to counter the frequency-hopping equipment is referred to as the "processing gain" for the communications network.

The bandwidth over which the channels can be spread is subject to two constraints. To keep the programming of the radio as simple as possible, all of the channels within a specified hopping bandwidth must be used. A further constraint is that when two or more radios are used in proximity, their operating frequencies must not be closer than 10 percent of their center frequencies.

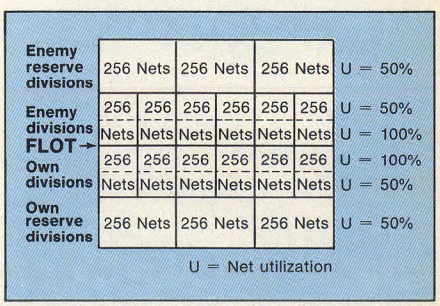
The hop sequence in a band must appear random to an enemy, must be determined by the operator, and must not repeat before it is changed. Since all radios in the same net must hop simultaneously to the same frequency, a synchronizing signal must be provided to all units. This synchronizing signal contains a digital data word that informs the units in the net of the position that has been reached in the frequency-hopping sequence. It can be radiated on all of the frequencies in use to defeat jamming.

The digital nature of the system also increases its effectiveness against ESM and ECM. To increase the jammer's confusion, the speech

(continued on next page)

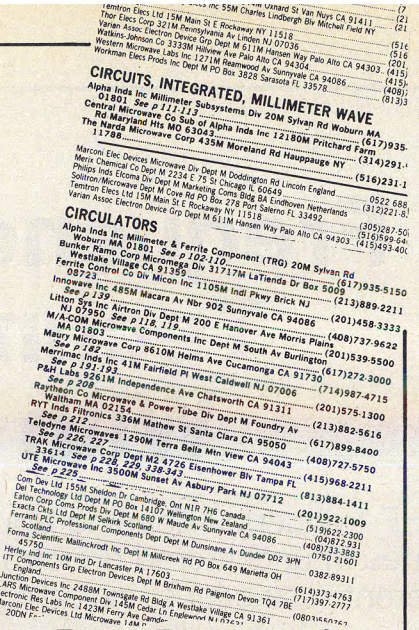


1. VHF frequency hopping can be studied *using this model of a conventional battlefield, which shows a divisional area.*



2. A larger view of the battlefield *shows the interrelationship between a friendly division and enemy forces.*

Looking for suppliers of circulators?



CIRCUITS, INTEGRATED, MILLIMETER WAVE

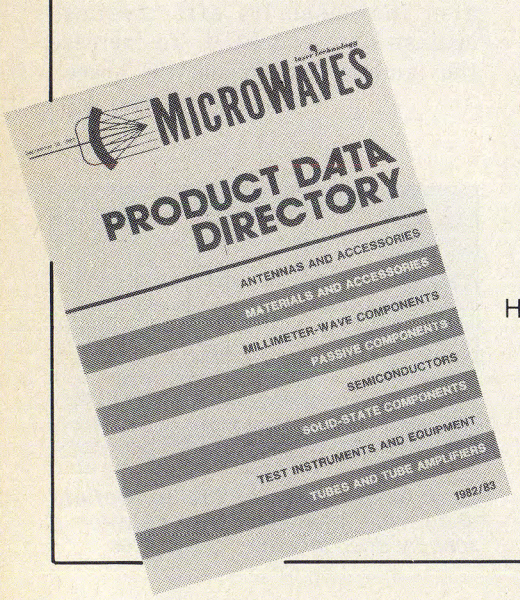
CIRCULATORS

Use **Microwaves' Product Data Directory**—the *only* guide to the RF/microwave industry. You'll find more than 55 manufacturers of circulators listed, complete with addresses and phone numbers so you can contact them *immediately*. Many companies even include data sheets to further simplify your search.

And Circulators is only one of more than 275 product categories detailed in 400 pages.

Keep **Microwaves' Product Data Directory** on your desk, and the solutions to your design needs will always be at hand.

Don't be at a disadvantage! If you don't have a copy of **Microwaves' Product Data Directory**, order one NOW. Send check, money order, or purchase order for $23 each (US, Canada, Mexico, Central America), or $32 each (all other countries) to:



MICROWAVES' PRODUCT DATA DIRECTORY

Hayden Publishing Company, Inc.
50 Essex Street
Rochelle Park, NJ 07662

FREQUENCY HOPPING

(continued from p. 97)

signals can be digitized and transmitted in discrete packets at a rate slightly higher than normal. The short gaps left between the packets allow the frequency to be switched and the synchronizing signal to be occasionally inserted without losing any speech or data. The digital signals can also be encrypted for added security.

Although a hop rate that is too slow will ease the enemy's task of finding a signal, too fast a rate poses severe spectral occupancy problems by limiting the available time between frequency changes for the transmission of useful information. As the data rate is increased to accommodate the narrow time period, the channel bandwidth must be increased to handle the rising data rate. Pollution of the entire spectrum becomes a serious risk. An intermediate rate between 50 and 500 hops per second is a reasonable compromise.

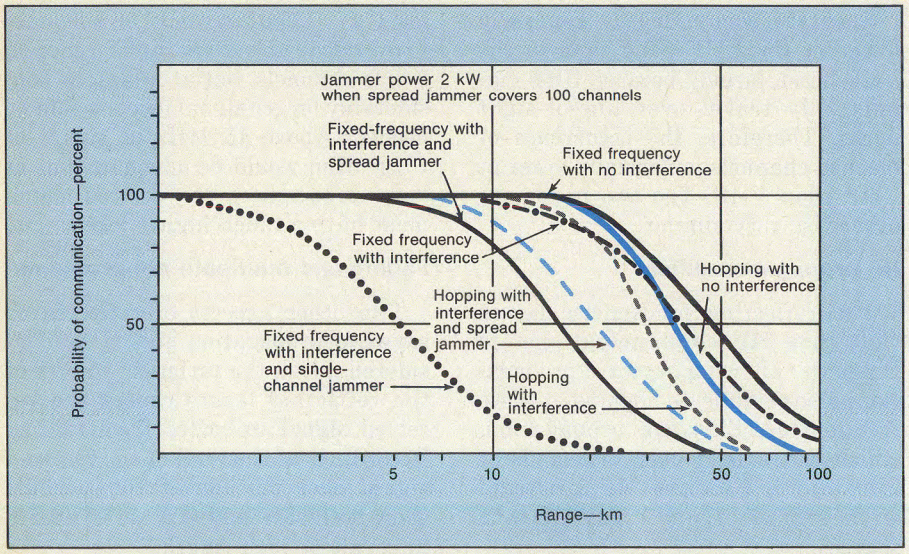
A problem arises when the system hops to a channel that is already occupied or otherwise blocked by other signals. Instead of receiving the transmitted digital signal, a string of zeros or ones is usually produced at the detector. As a result, the radio produces a large click or pop in the audio output. Fortunately, the magnitude of this effect can be reduced by a circuit that changes the string of zeros or ones into an alternating sequence of zeros and ones.

Hoppers on the battlefield

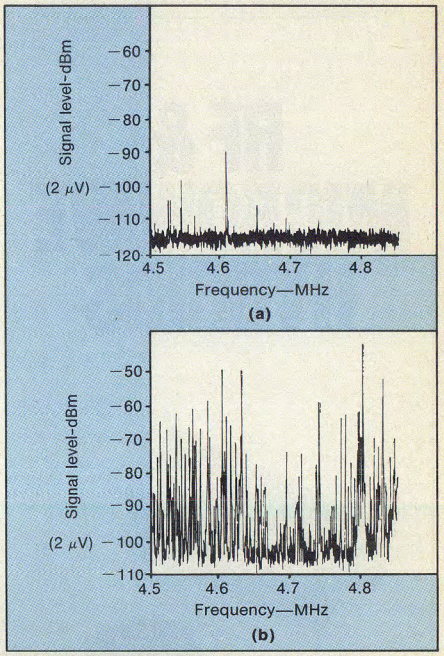
Figure 1, a model of the battlefield, helps illustrate the capabilities of frequency hopping in the VHF band. In this example, combat net radios are deployed in a typical divisional area. The forward line of troops (FLOT), which is the forward edge of the battle area, is on the right side.

As shown in the figure, squad radios, manpacks, and low- and high-power vehicle radios are distributed around the divisional area according to a typical force deployment. The enemy will most likely have a similar number of radios positioned on the other side of the FLOT. In addition, the conditions and nets shown would be duplicated on both flanks and in reserve formations at the rear.

Figure 2 shows a larger section of the battlefield with each rectangle representing a divisional area. A worst-case model has been devised



3. A computer simulation based on the model battlefield can predict *the probability with which fixed-frequency and frequency-hopping equipment will be able to communicate under different conditions.*



4. HF propagation at 3 pm (a) and at midnight (b) *shows its dependence on the time of day.*

for this battlefield communications system that includes a total of 256 nets in each divisional area. These nets are utilized 100 percent near the FLOT and 50 percent in the rear. (Recent experiments indicate that spectral occupancy will actually be much less than this at any particular time.)

The frequency-hopping design for the VHF band most familiar to the author is, of course, the Jaguar V. This radio uses all of the 256 channels available in each of the nine 6.4-MHz hopping bandwidths into which the band has been divided. It produces a processing gain of 256:1 (about 24 dB) and offers a choice of nine bands to avoid interference between co-sited radios.

Only 20 percent of the nets are assumed to be equipped with frequency hopping radios. The enemy has 2-kW jammers situated 3 km behind the FLOT and spaced 4 km apart.

A computer analysis based on this model can chart the probability that a 50-W transmitter will be able to communicate with a receiver placed 10 km behind the FLOT (Fig. 3). The simulation shows that in the ideal case (i.e., with no interference) fixed-frequency equipment has a 90-percent probability of communicating at a range of 17 km. The frequency-hopping equipment will have a range slightly greater than 19 km with the same probability.

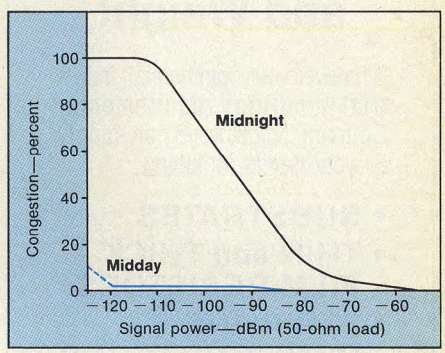
The situation changes radically when the nets are attacked by a 2-kW jammer on a single channel. In this case, the range of the fixed-frequency units plummets to 2 km. The jammer goes unnoticed to the frequency-hopping net, however, since it would block only one of the 256 channels in use. If the jamming power were spread over 100 channels, the range of the hopping net, as shown in Fig. 3, would be reduced to about 10 km. Forcing the jammers to spread their energy to counter the hopping nets stretches the enemy's resources and also benefits the fixed-frequency nets. Note that the shift to wideband jamming has increased the range of the latter networks from 2 km to 8 km.

UHF offers wider bandwidth

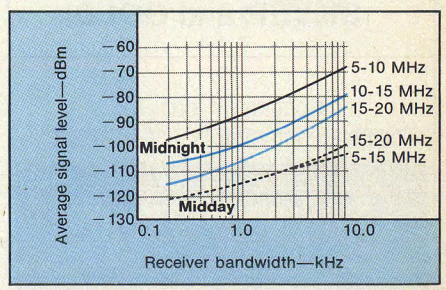
Unlike the 58-MHz VHF band, the UHF band covers 175 MHz. Consequently, the same design philosophy used in the VHF band can divide the UHF band into nine 19.2-MHz hop bandwidths.

By hopping over 19.2 MHz instead of 6.4 MHz, the processing gain of the UHF system against a wideband jammer increases by a factor of three to about 29 dB. The range of fixed or semi-fixed installations can be increased by using simple Yagi antenna arrays. Although the bandwidth of this type of antenna is limited to about 50 MHz, this permits the use of up to three 19.2-MHz hop bands and allows the use of adjacent or alternate

(continued on next page)



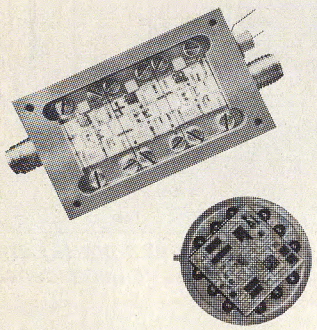
5. Spectral occupancy measurements *show that virtually all HF channels are blocked at midnight.*



6. The effect of receiver bandwidth *on average received signal level can be derived from the previous curves.*

Solitron/Microwave

RF & MICROWAVE HYBRIDS



Save on Cost...
Save on Space and Weight

Whatever your commercial, industrial or military requirements, Solitron/Microwave can supply all your needs including:

- SUBSTRATES
- THIN and THICK FILM RESISTORS
- STRIPLINE CONFIGURATIONS
- COAXIAL CONNECTORS
- CUSTOM DESIGNS
- CHIPS, PACKAGES and CONDUCTIVE PASTES (COPPER, SILVER and GOLD)

Contact us today for complete information and literature.

Solitron/Microwave
Cove Road, Port Salerno, Florida 33492
(305) 287-5000
TWX: (510) 953-7500

READER SERVICE NUMBER 58

 (continued from p. 99)

hop bands.

Spectral occupancy is generally lower in the UHF band than in the VHF band, largely because UHF signals only travel over line-of-sight paths. Therefore, the occurrence of blocked channels is normally lower at UHF than VHF. The two bands are otherwise very similar.

HF propagation differs

The reflecting ionospheric layers that give HF communications its range (by allowing skywave propagation) also complicate hopping at these frequencies. Skywave propagation, which can extend over thousands of kilometers, fills the HF spectrum with signals from many distant sources.

The effectiveness of the reflecting layers varies with the time of day, sunspot cycle, distance, and frequency. For example, Fig. 4a shows the signal levels (versus frequency) received at 3 pm by an antenna on an island in the Mediterranean. Roughly five signals that exceed 1 μV are present in this 300-kHz band. But by midnight (Fig. 4b), the levels have increased by as much as 40 to 50 dB.

Interpreting the results of spectral occupancy measurements like these is a challenge. In Fig. 5, the percentage occupancy or congestion is plotted against the signal level received at midnight and midday within a 0.5-MHz band centered at 3.2 MHz. At midnight, virtually all the channels were occupied at levels up to −110 dBm. Even at a level of −90 dBm, 40 percent of the channels were blocked.

According to the earlier discussion of VHF operations, communication should be possible at midnight with 40 percent of the channels blocked (even though −90 dBm is a large signal to generate). The situation improves at midday when the congestion at −110 dB is a mere 1 percent. Frequency hopping is thus entirely feasible for short-range (a few hundred km) ground-wave signals in the HF band at all hours of the day.

Although using a receiver with a 3-kHz bandwidth would have given a very different result than the 300-Hz bandwidth used in Fig. 5, it would obviously be harder to find an unoccupied 3-kHz channel.

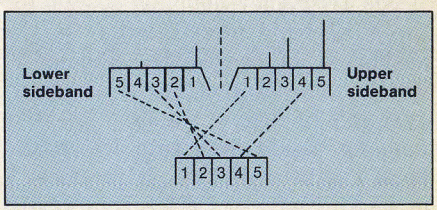
The previous figures can be used to derive another set of curves that show average received signal level versus receiver bandwidth (Fig. 6). These curves show that at midday, a signal level of −110 dBm would be adequate to overcome unwanted interference on 3-kHz channels, but at midnight considerably larger signal levels would be needed. Above 15 MHz, a signal of −100 dBm would be adequate, but at lower frequencies the desired signal must have a much higher level.

Fading and multipath are problems

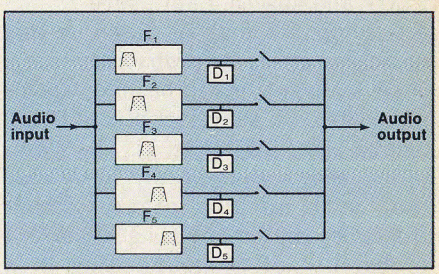
Two other aspects of reflected or skywave propagation should be considered. First, the turbulent nature of the reflecting layers causes the received signal to suffer from fading. Recordings of the level of the received signal over periods of 100 seconds show both slow and fast variations in intervals of such length.

The second consideration, multipath transmissions, are created when the transmitted signal is reflected by more than one ionospheric layer. The various reflected signals arrive at the receiver with different time delays and produce a complex fading pattern. Since the time difference between paths can be as long as a few milli-

(continued on p. 102)



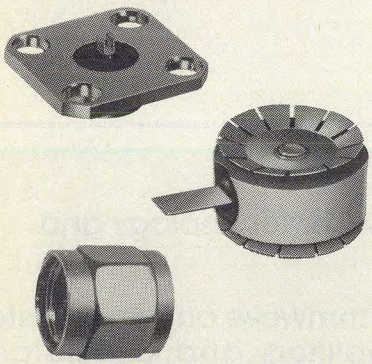
7. The audio from each of an HF signal's sidebands *can be divided into five sub-bands. Segments make up a composite signal.*



8. A more refined system could use detectors *to remove an undesired sub-band from the audio output. The loss of a sub-band has little effect on the final intelligibility of speech. Detectors to do this job have yet to be developed.*

Solitron/Microwave

FLANGE, STRIPLINE & COAXIAL TERMINATIONS



Solitron/Microwave offers Type N, TNC and SMA flange terminations with such low VSWR that up to 10 db isolation improvement for ferrite circulators can be achieved at 18 GHz.

High reliability stripline terminations are used in many military programs including HARM and STANDARD missiles. Our new 1/16" termination for 40 GHz applications is the first of its kind in the industry.

Hundreds of various coaxial terminations are available, including one no larger in size than a coupling nut and offering less than 1.05 VSWR up to 18 GHz. Identified as the 8018-6060, it meets or exceeds MIL-D-39030, as do all Solitron/Microwave terminations.

Contact us today for complete information and literature.

Solitron/Microwave

Cove Road, Port Salerno,
Florida 33492
(305) 287-5000
TWX: (510) 953-7500

READER SERVICE NUMBER 59

 (continued from p. 100)

seconds, the data rate of any digital transmission under these conditions would be limited to a few hundred hertz.

The requirements for a frequency-hopping system for HF can now be considered. The bandwidth for successful propagation, especially at night, must be as small as possible. This restriction precludes all but single sideband modulation. Because of the multipath, the synchronizing information sent in digital form must be kept to rates below a few hundred hertz. Large unwanted signals on some of the channels and the fading of the desired signal put demands on the design of the AGC circuitry. The AGC must be carefully arranged to ignore the presence of the occasional large signal, while being sufficiently fast to follow a fading signal.

Because of the limited bandwidth of simple HF antenna systems used on manpacks and land vehicles, a smaller hop bandwidth must be used at low frequencies than at high frequencies. This means that a smaller processing gain, or anti-jam margin, must be accepted at the low end of the band than can be obtained at the higher end. Since the bandwidth of the system must be kept low, and the data rate modest, it is necessary to limit the hop rate to a few tens of hops per second.

Heterodynes plague HF

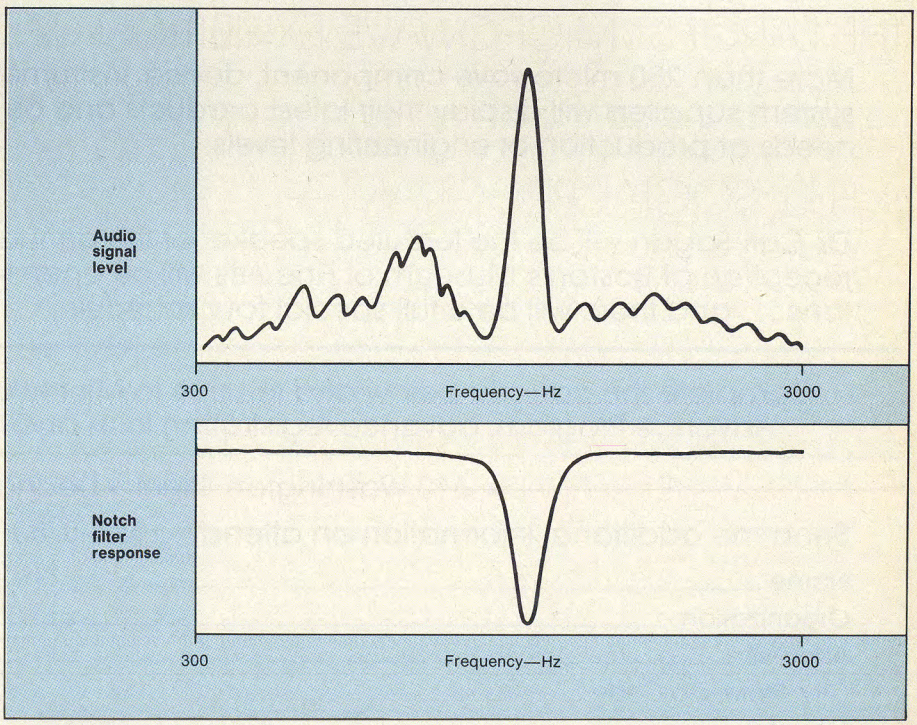
The low data rates also require the HF system to use analog rather than digital speech tranmission. As a consequence, unwanted HF carriers on the hop channels cause annoying audio tones (heterodynes) that must be minimized. Several techniques may be considered for this purpose.

One technique requires both sidebands to be transmitted and the sideband with the better audio selected at the receiver. Trials using this method have produced considerably improved audio.

Going a step further, the audio from each of the sidebands can be divided into five sub-bands, and a composite signal formed from the best of these sub-bands (Fig. 7). Simulations of this technique, however, have produced very little improvement over the single selection of the best sideband. This probably stems from not more than one unwanted signal being present in a channel.

Unfortunately, the above schemes have three disadvantages in common:

(concluded on p. 105)



***9. A steerable notch filter** can be used instead of detectors to block the unwanted audio segment. The design of a quick reacting steering circuit for the notch filter is a challenge that has been overcome.*

(continued from p. 102)

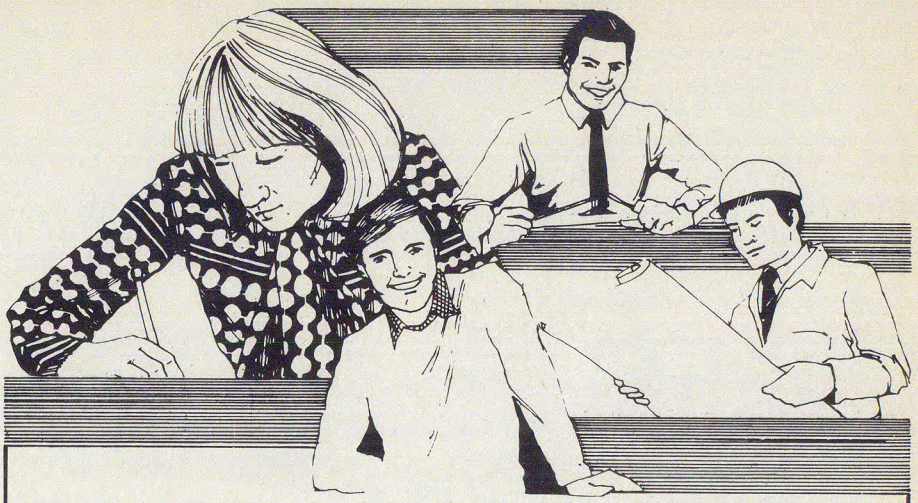
- First, they reduce the effective transmitter power. Although this loss of power is 3 dB in theory, current and voltage limitations in practical transmitters can increase the loss to 6 dB.
- Second, two separate IF amplifier chains must be provided in the receiver. This duplication increases cost.
- The third disadvantage of these two methods involves the actual selection of the best sideband or sub-band audio. In principle, the decision should be based on a look at the next intended hop channel. Circuitry for this purpose would be even more expensive.

A workable system might still be based on some of the ideas in the two earlier concepts, however. Let's suppose that only one unwanted tone exists in a particular hop channel, and that the audio band is divided as before into five sub-bands by the filters shown in Fig. 8. If suitable detectors D1 to D5 can be devised, a large, unwanted tone can be detected and the branch of the circuit that contains it switched out of the audio circuit. Consequently, the audio output would not contain the offending tone.

Fortunately, large parts of the audio spectrum can be removed without losing intelligibility in speech. The difficulty lies in designing the detectors.

One more approach could be used to reduce the unwanted tone. An audio notch filter might be adjusted in frequency very quickly to reduce the offending heterodyne.

The audio spectrum and the unwanted tone are shown in Fig. 9. Again, a portion of the audio band can be removed without affecting the intelligibility. Although the development of a circuit that can quickly steer the notch filter to the frequency of the unwanted tone is difficult, this technique appears to be the method of choice. A proprietary design has been selected for this function on the Jaguar H radio. ••



Engineers, join the Spirit of Emerson. We're part of the Spirit of St. Louis.

St. Louis, born of the spirit of adventure and progress, is now known as the "gateway to the west." It is a city combining the best of the north, south, east and west.

There are more than 4,000 Emerson people now living in St. Louis and take their word for it. . . St. Louis is a great place to live and raise a family.

Just consider a city with all the advantages of a large metropolis and yet only a short drive from Ozark country with its many rivers, lakes and recreational areas.

Then too, St. Louis is a great sports town. It's strictly big league baseball, football and hockey. And the weather makes it easy to participate in sports such as golf, boating, fishing, bicycling, skating, riding, tennis and much more. Our four-season climate is stimulating without the hardships of extreme heat or cold.

Yes, a great place to live but what about the cost of living? Well, we're below the national average in cost of food, utilities and transportation.

If you are interested in career accomplishment in a working atmosphere of constant challenge, you'll like our spirit.

Interested? We're interested in electronics and mechanical engineers at all levels in these areas:

ATE
- Software/Hardware Design & Development

ELECTRONIC WARFARE
- Airborne/GSE Electronics Packaging
- Product Development

RADAR
- Coherent/Non-Coherent Design & Development

ENGINEERING SUPPORT
- Electro/Mechanical Control Systems Analyst
- Maintenance Engineers

We have similar positions available at our Orlando, Florida facility.

Why not call Toll Free 1-800-325-0783 or send your resume and see what happens. We think you'll want to join the Spirit of Emerson.

Dept. M-1-83
Mail Station 4303

EMERSON ELECTRIC CO.
Government-Defense Group
8100 W. Florissant St. Louis, MO 63136
we are an equal opportunity employer in every respect.

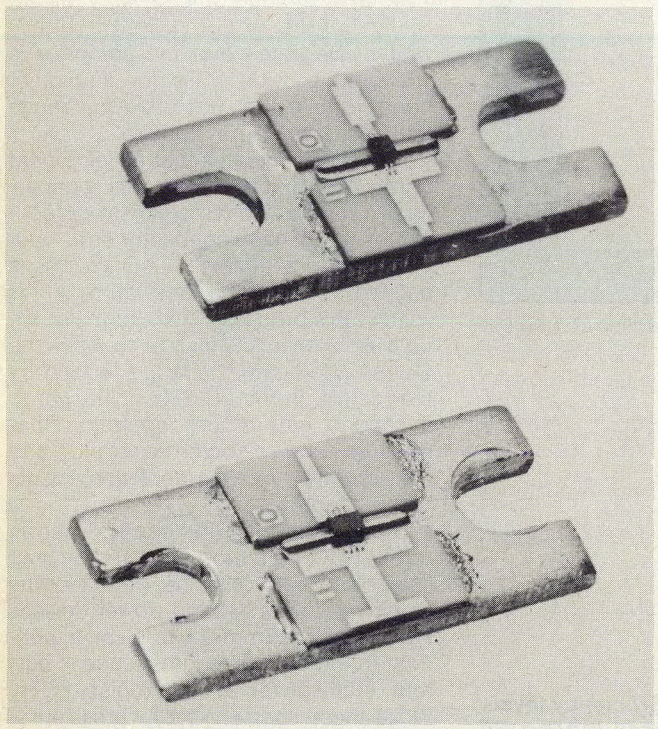
READER SERVICE NUMBER 62

Cover Feature

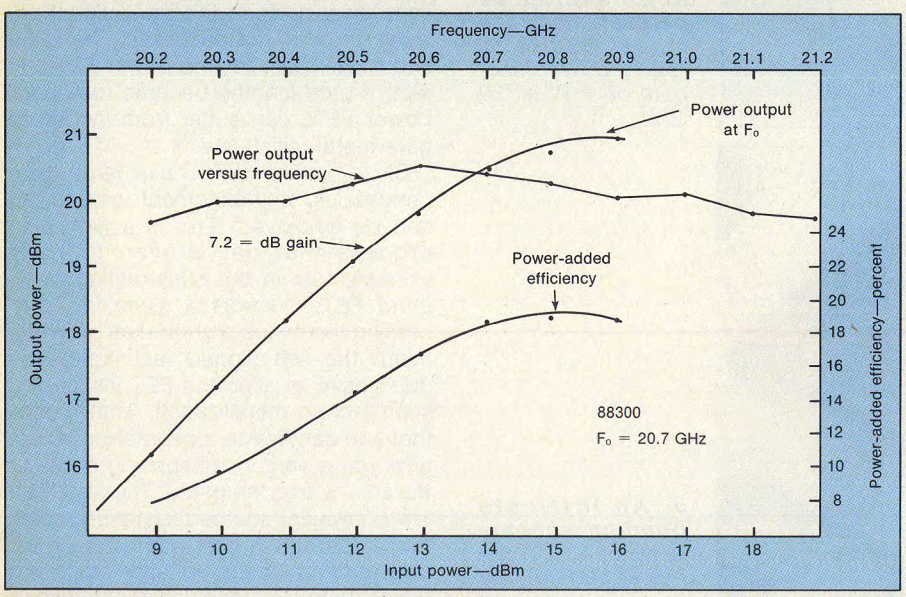
One company's quest for solid-state power

The introduction of devices capable of 1-W output power at 20 GHz and 6-W power at 6 GHz marks the steady improvement of power-FET technology. One reason for success is high-quality substrates.

Jack Browne, Associate Editor/Product Technology



1. These two members of the 88000 series of power GaAs FETs *are capable of typical outputs of 100 mW (top) and 500 mW (bottom) at frequencies from 20.2 to 21.2 GHz. The partially matched devices feature a size of only 0.20 × 0.41 in.*



2. Performance curves for the model 88300 *indicate power-added efficiency levels as high as 18 percent.*

True solid-state power is the elusive goal of many semiconductor researchers, but the heat and power levels that must be dissipated represent formidable barriers. A series of recent developments at Microwave Semiconductor Corp. (Somerset, NJ) should bring new hope to those seeking tube-like power with semiconductors.

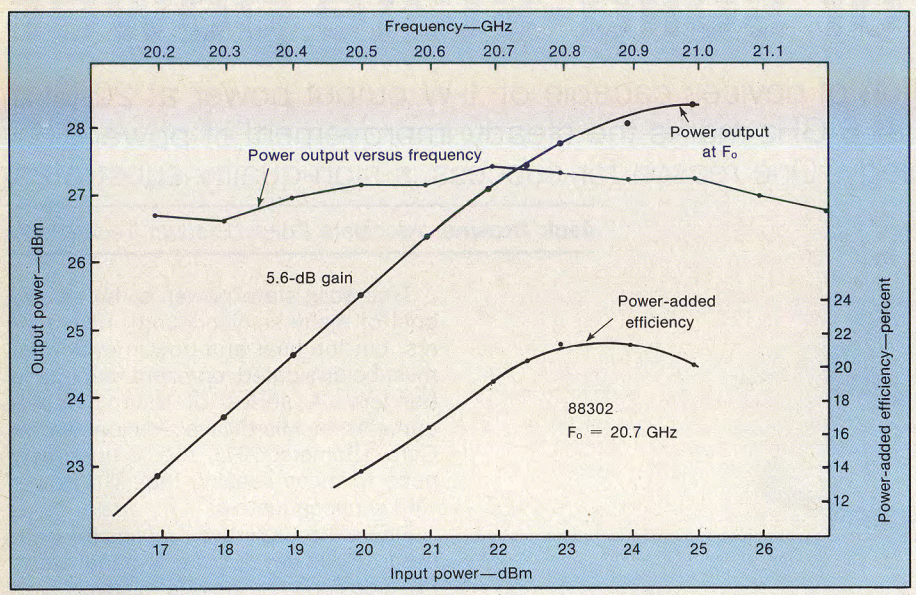
Figure 1 reveals two reasons for optimism. Both devices are K-band GaAs FETs designed to provide relatively high levels of linear power at frequencies from 20.2 to 21.2 GHz. Model 88300 (top) is rated for 80 mW minimum output power and 100-mW typical output (when supplied with a +14-dBm input) at 20 GHz. Its power-response and efficiency curves are shown in Fig. 2. The FET handles saturated drain currents (I_{DSS}) of at least 50 mA and typically 90 mA, and has a typical transconductance of 30 mS. The transistor can dissipate up to 0.64 W of power.

Model 88302 (bottom of Fig. 1) can produce at least 400 mW of output power, and typically 500 mW, at 20 GHz, when provided with a +22-dBm input (Fig. 3). The I_{DSS} is typically 300 mA, and the FET transconductance is 100 mS. This device can dissipate up to 3.2 W. The 88300 and 88302 power transistors are rated for a maximum drain-to-source voltage (V_{DS}) of 10 VDC and a maximum gate-to-source voltage (V_{GS}) of −8 VDC. Both devices have a typical pinchoff voltage of −4 VDC. They represent just two models of a line that will soon include different power levels, and already boasts a 1-W, 20-GHz FET, the model 88304 (Fig. 4). There is even a lower-power version of the K-band FETs, the model 88299, which offers a minimum power output of 50 mW and typical power of 65 mW, from 20.2 to 21.2 GHz. These 20-GHz GaAs FETS should find their way into numerous fixed-satellite and land-mobile communication systems.

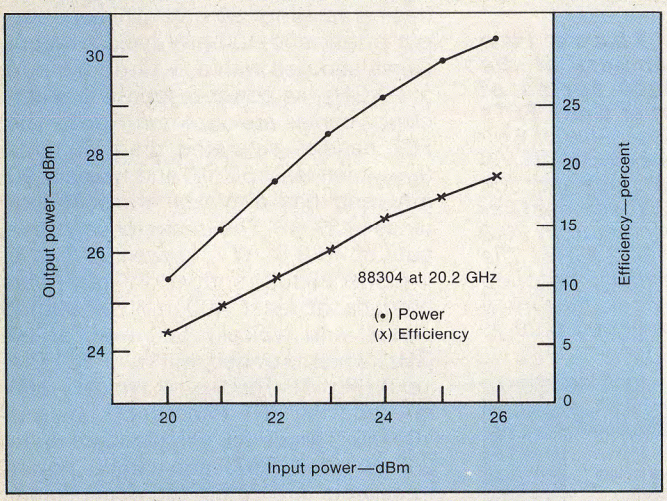
One of the keys to the high gain and power-added efficiency performance of the K-band FETs is the use of partially

(continued on next page)

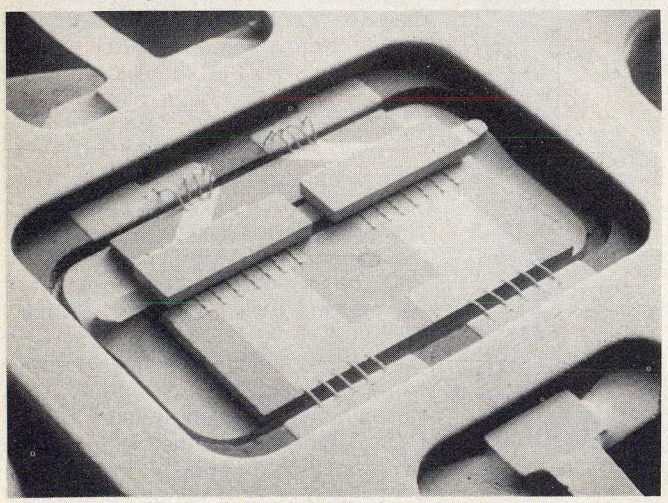
matched chip carriers. These new carriers permit the heat dissipation necessary for high-power operation, without the parasitics found in some older matched designs. Dr. Anthony A. Immorlica, Jr., manager of GaAs device development, comments that parasitic removal was a chief concern: "The main problem has been working with the chip-carrier package, because there are parasitics which are difficult to control. We had to go through a program to develop a matched carrier for the 20-GHz pellets [i.e., die] to take away these parasitics." What grew out of the development program was a carrier that is "partially matched," because its impedance is not quite 50 ohms. The technique of flip-chip mounting the K-band chips on these carriers has allowed the considerable gain and power-added efficiency evidenced by the performance curves of Figs. 2 and 3.



3. The power-added efficiency of this 0.5-W model 88302 *FET reaches 20 percent for inputs between +23 and +24 dBm.*



4. Efficiency levels approaching 20 percent *enable the model 88304 to reach power outputs of 1 W at 20 GHz.*



5. An intricate bonding scheme *is required by the model MPF-5964-6 in order to handle 6-W power levels.*

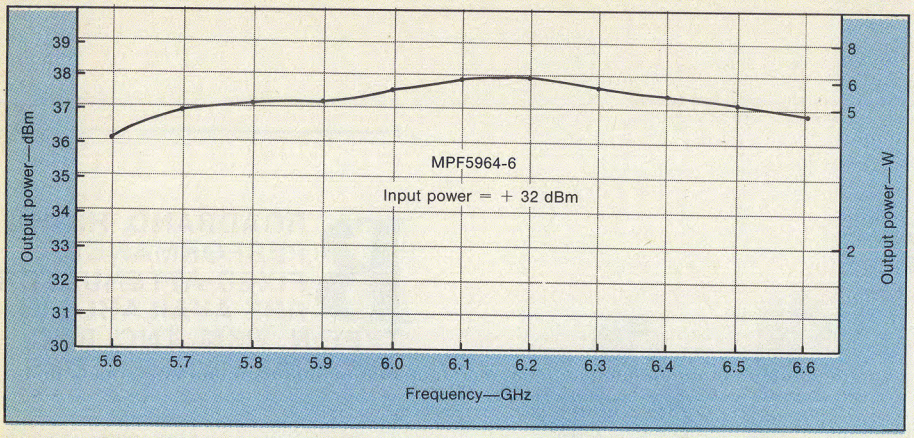
Of course, the use of partially matched carriers is not without some tradeoffs. Immorlica admits that the main concession is when limiting the inherently wide bandwidth of the FETs. "Once you've partially matched a FET, which is essentially a wideband device, you've specified a band," he says. "Right now, we've built FETs for 20.2 to 21.2 GHz, although the devices will actually handle about 1.5-GHz bandwidth." He notes that the company is willing to provide FETs for any other bandwidth in the 18-to-22-GHz range that a customer may require.

Immorlica indicates that development of the 20-GHz FET represents a departure from traditional processing techniques for the semiconductor firm: "Our FETs are all self-aligned. A 1-μm line is defined on the mesa, and ion milling is used in this process. Then, normally, we do a slight chemical etch to cut back the GaAs underneath the ledge formed by the metals. In the 20-GHz FETs, we do a second gate-recess operation that gives us a lower source resistance and more control over the depletion effects in the channel."

Greater gate lengths can be used in power FETs than those required by their low-noise brethren. The gate lengths employed in the K-band power devices typically range from 0.7 to 1 μm, in contrast to the 0.3-μm lengths found in current state-of-the-art low-noise FETs. While these shorter gate lengths represent lower noise in the small-signal devices, they do not necessarily translate into higher gain for the power FETs. In fact, if gate lengths become too short, power FETs can suffer from increased gate-metal resistance.

Since power FETs have large gate peripheries, self-alignment processing can be employed. This is a high-yield process that has proven to be a valuable tool in the construction of K-band FETs. Immorlica gives this processing technique a great deal of credit: "With the self-aligned technique, you don't have to align the FET inside of a source-drain metallization. That means that you can devise a geometry that will give you a very small spacing between the source and the gate." The result is a low equivalent source resistance, which translates into higher gain. The lower saturation of "knee" voltage, which is a consequence of self-alignment, allows the use of lower drain bias. This leads to

(continued on p. 115)



6. The MPF-5964-6 power FET, *although only specified for 5.9-to-6.4-GHz operation, will actually handle a much broader frequency range.*

higher efficiency and, generally, better reliability.

High-power advances for MSC have not been restricted to the 20-GHz band. Considerable activity in the 5.9-to-6.4-GHz band has led to the development of the model MPF-5964-6, a 6-W device (Fig. 5). It is the first member of a group of very high power transistors that feature internal input and output matching in a space-qualified hermetically sealed package. The FET will produce +38 dBm at the frequency band edges, with an associated gain of 6 dB (Fig. 6). The transistor's electrical properties include a typical I_{DSS} of 4800 mA and a transconductance of 1100 mS. Its pinchoff voltage is typically −4 VDC, with a −8 VDC maximum. External tuning is not required to meet rated specifications.

In-house epitaxy helps

An important factor in the development of the high-power semiconductors has been the availability of quality epitaxial material, thanks to in-house facilities (Fig. 7). The company has, at present, three gallium/hydrogen/arsenic trichloride epitaxial reactors, with provisions for a fourth if it's needed. The reactors utilize a microprocessor to carefully sequence gas flows and control temperature limits.

Recently, 1-in. square wafers were abandoned in favor of 2-in. round wafers. This move has helped in several ways, as Jim Thompson, MCS's operations manager for semiconductor materials, explains: "A processing run with an epitaxial wafer has fixed costs, whether it's a small or a large wafer. You will get four times more usable area with a 2-in. wafer than with a 1-in. wafer. We originally expected this four-times increase in yield, but we are actually seeing something like a ten-times increase."

The epitaxial facilities have even aided the company's R&D efforts. Thompson views the equipment as a research tool. "Having the facilities gives us the chance to explore material parameters such as thickness and doping concentration. Also, the materials section gets feedback from the device people," he says. This feedback comes

(continued on p. 118)

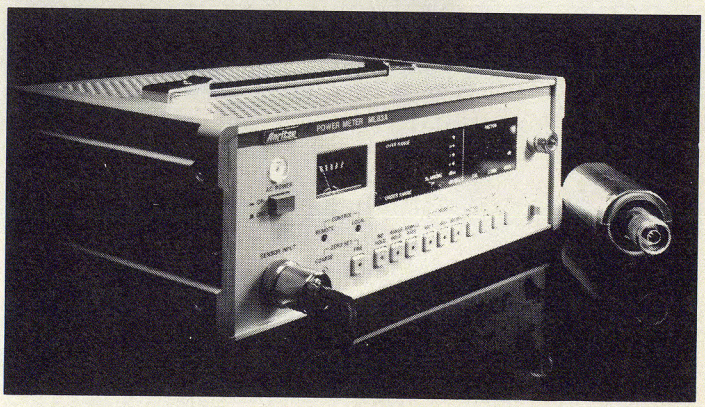
One Power Meter...No Peers

10MHz to 140GHz with a single instrument

The ML83A from Anritsu: It's the one instrument with no equal at measuring RF power over all frequency ranges from 10MHz to 140GHz. Simply by selecting from a variety of versatile sensors, you can use this single low-priced power meter to handle all your power measurement needs.

The ML83A Power Meter has the ample capabilities to make it the mainstay of your lab bench or production line. Each sensor has a thin-film thermocouple (or a diode) that provides a high degree of accuracy with excellent VSWR characteristics and temperature stability. And you'll appreciate such ML83A ease-of-use features as digital readout, self-calibration, and a handy analog meter for viewing output peaks. There's even a GPIB option for use in an automatic measurement system.

The ML83A. From the extensive Anritsu line of high-quality measuring instruments.



Anritsu

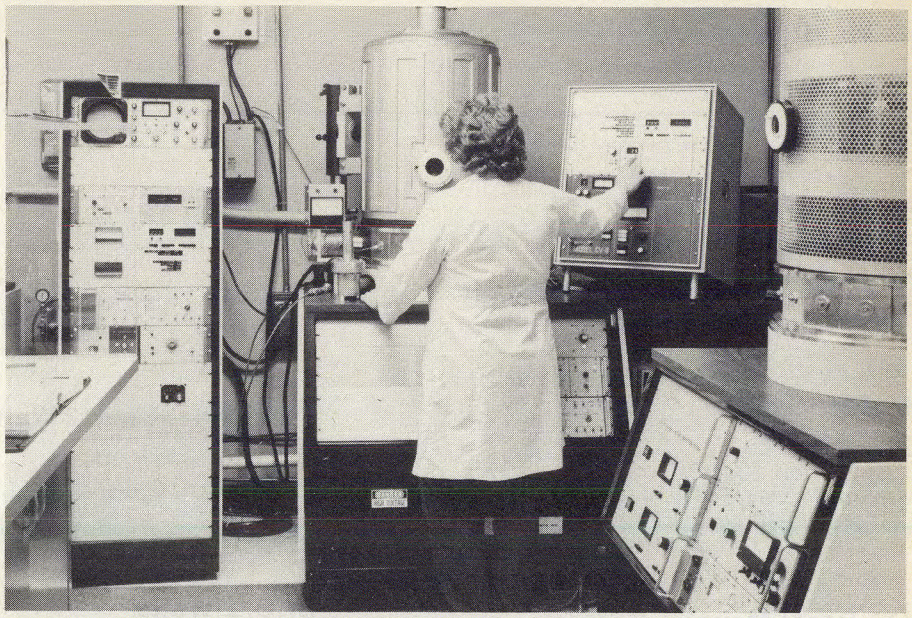
ANRITSU ELECTRIC CO., LTD.
OVERSEAS MARKETING DIVISION
10-27, Minamiazabu 5-chome, Minato-ku, Tokyo 106, Japan
Phone (03) 446-1111/Telex: 0-242-2353
Cable: ANRITDENKI TOKYO

Anritsu America, Inc.
128 Bauer Drive, Oakland, NJ 07436, U.S.A. Phone: 201-337-1111 Telex: 642-141 ANRITSU OKLD
Anritsu Europe Limited
Thistle Road, Windmill Trading Estate, Luton, Beds, LU1 3XJ, U.K. Phone: (STD0582) 418853 Telex: 826750 ANRSEU G
Anritsu Eletrônica Comércio Ltda.
Av. Passos, 91-8º Ander, 20.051-Rio de Janeiro-RJ, Brasil Phone: 221-6086, 224-9448 Telex: 2131704 ANBR

READER SERVICE NUMBER 69

from the analysis of a "key row" which is placed on *every* wafer. The row consists of sample devices, such as Schottky barriers, which are used to calibrate and check the electrical properties of the wafer. One of these special devices is the "fat FET." Thompson describes this as an important device for the evaluation of electron-drift mobility in the epitaxial wafers: "It's an oversized FET with a gate that might be 5 μm instead of 1 μm. This permits us to neglect the metal resistances in our FET calculations, so that it is easier to calculate the drift mobility."

The device parameters of these "fat FETs" help the materials group determine the characteristics of the material itself—for example, to discover whether a problem was caused by dirt on the substrate or by improper metallization. The key row has also helped form a large statistical base for future material and semiconductor development.



7. Three epitaxial systems are currently on-line *to handle in-house FET production needs and outside customer requirements for wafers.*

MOCVD to come

Although MSC's epitaxial processing is at a level where excess capacity is now available to outside customers, Immorlica outlined plans to add another processing technology: Metal-Organic Chemical Vapor Deposition (MOCVD). Said Immorlica, "We are putting together an MOCVD system to increase our wafer capacity. It will also provide a great deal more flexibility for research, since it will be possible to grow a number of different compound materials." Thompson acknowledges the need for MOCVD: "It allows us to run a multiwafer setup. Our design criteria will handle six 3-in. wafers or twelve 2-in. wafers."

The first evaluation run for the system is expected this fall. Of course, as with any emerging technology, there are some reservations, and Thompson is not without his. "It's a technique that will do the job, but not all of the questions have been answered yet," he said. "There are two basic problems—the purity of the starting chemicals and achieving the uniformity in doping required by microwave semiconductors." Successes using MOCVD by researchers at Bell Laboratories (Murray Hill, NJ) have been on the scale of one device at a time. If MSC can produce microwave-quality wafers with its MOCVD system, it will certainly add to an already considerable wafer capacity.

One of the materials that has fascinated MSC researchers is BeO. At a time when many semiconductor manufacturers point to MMICs as the future, Immorlica offers the alternative of miniature power FET amplifiers based on BeO substrates. "We considered many factors and concluded that we could not justify getting into the power MMIC field through the rest of this decade," Immorlica said. "So we made a decision to develop an alternative to power MMICs, one that has many of the advantages and none of the problems. The alternative we came up with was BeO technology."

Beryllium oxide has a very high thermal conductivity—about 70 percent that of OFHC copper—and provides a very close thermal match to GaAs. Immorlica noted that "You can even

PIN DIODES .0001-24 GHz
• 0.2 ohms • 1200 volts • 1KW CW • 150°C • 0.05 pF



High Performance PIN and NIP DIODES for attenuating and switching. They offer designers high power levels, high voltages, low loss, reproducibility, fast switching and MIL-S-19500 reliability. Available as chips. Exact replacements for HP 5082-3000 series. Call today.

FREQUENCY SOURCES, INC.
GHz / KSW Semiconductor Division
16 Maple Road, Chelmsford, Massachusetts 01824 (617) 256-8101 TWX: (710) 343-0404

READER SERVICE NUMBER 71

grow GaAs epitaxially on single-crystal GaAs. Presently, our miniature hybrid circuits are created by flip-chipping a GaAs FET on an amorphous BeO substrate on which the passive matching circuits are defined. In effect, we are flip-chipping a FET right onto the circuit-matching patterns."

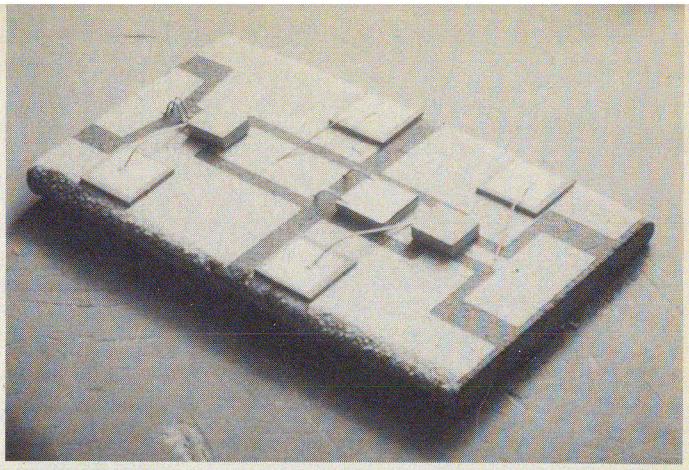
These designs promise several advantages over power MMICs. A beryllium oxide microwave integrated circuit (BOMIC) will be slightly larger than a comparable power MMIC, but it will suffer none of the thermal problems associated with high power levels in small packages (Fig. 8). Since MMICs are fabricated from a single material, such as GaAs, they must use matching devices which are compatible with that material. These devices may not always be the best, however, for a given frequency band. Better matching is possible with the BeO approach since optimized components, such as high dielectric capacitors, can be used. Also, the BeO can be reasonably thick (about 15 mil) so that there is no tradeoff in line losses in order to minimize the heat in the circuit. The MMICs must be much thinner to achieve adequate heat dissipation, a practice that invites excessive line loss.

Immorlica compared the yields possible with the two technologies: "If you were making a 1-W MMIC from a 2-in. wafer, you might get 10 working devices. We can get about 800 1-W pellets from that same 2-in. wafer. BeO technology offers all of the advantages of MMICs with the fast design turnaround and power capabilities of conventional hybrid MICs." BeO performance has already been demonstrated by one MSC program for 4-to-10-GHz devices, and plans continue to build devices for 8 to 18 GHz.

Immorlica stressed that the BOMIC technology is available *now* and is not merely a laboratory curiosity. In fact, MSC has recently completed delivery of over 200 X-band units to a customer for a phased-array antenna application and, in another program, has demonstrated 4-to-10-GHz wideband performance. BOMIC technology is available on a custom basis at frequencies in the 4-to-18-GHz spectrum.

All of the company's production FETs are provided in hermetically sealed packages. Hermeticity is checked by pumping each device with helium and then running a vacuum-chamber gas-leak analysis. P&A: 6 to 8 weeks (88000 series) and stock (MPF-5964-6). **Microwave Semiconductor Corp., 100 School House Rd., Somerset, NJ 08873. (201) 469-3311, TWX: (710) 480-4730.**

CIRCLE NO. 232



8. The BeO technology is responsible for this 400-mW, 9-to-10-GHz two-stage driver amplifier. *The interstage DC blocks and RF choke circuits are shown on the board.*



Picture Excellence.

No matter how you look at it, Sawtek offers you the highest performance in surface acoustic wave (SAW) filters and resonators. Sawtek's wideband 70 MHz IF filters for TVRO applications are available in bandwidths from 10 MHz to more than 36 MHz. The superior rejection and group-delay performance of these filters compliment even the finest receivers. Moreover, you can avoid costly assembly and tuning time and maintain signal quality in your IF for years under the most demanding field conditions without adjustment.

Sawtek's resonators provide that same reliability with quartz stability for your local oscillators at fundamental frequencies up to 1000 MHz. Many standard frequencies including 668, 674, and 680 MHz are in production at competitive prices.

Quality and performance have made Sawtek the leading manufacturer of VSB filters for the CATV industry and, if what you need is not among our hundreds of standard products, we can provide technical assistance and rapid response to new design and production requirements. You can rely on us for the engineering support you need.

When your system demands the advantages of SAW Technology . . . Demand SAWTEK.

SAWTEK INCORPORATED

P.O. BOX 18000, ORLANDO, FL 32860, (305) 886-8860

READER SERVICE NUMBER 72

Radiation monitors measure potential health hazards

Radiation monitors can tell a user when the strength of an EM field is outside the limits of accepted guidelines. To do this, the sensor probe must be carefully designed and calibrated.

Jack Browne, Associate Editor/Product Technology

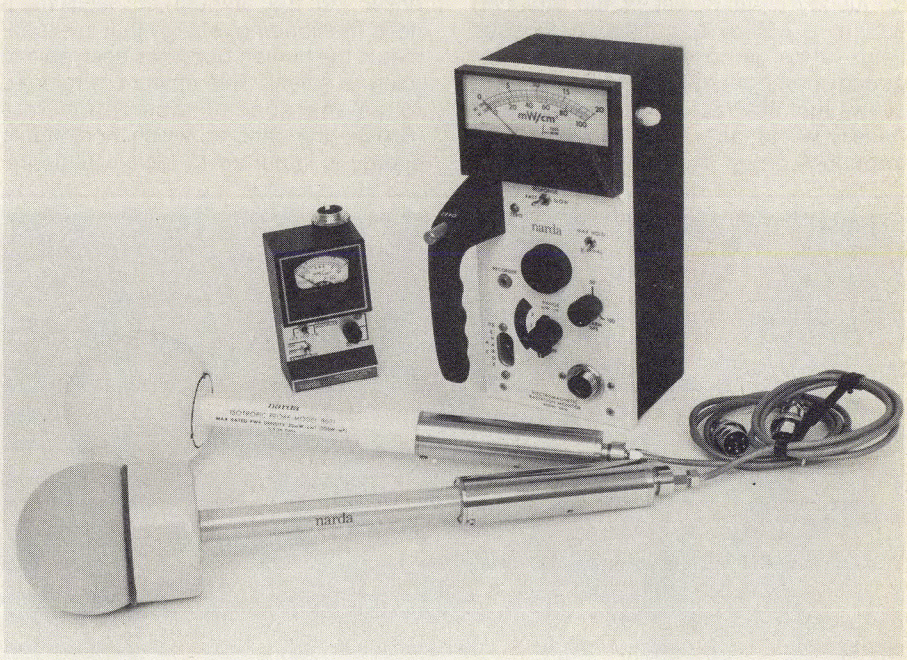
Like many other phenomena once dismissed as harmless, nonionizing radiation is now considered a potential health hazard at certain power levels. Ironically, one of the first devices to introduce the general public to the benefits of microwave radiation—the microwave oven—also presented the public with its potential hazards. Another microwave device, the radiation monitor, provided the measurement capability to detect which ovens were leaking excessive RF energy.

Radiation monitors, which were once extremely narrow-band devices intended expressly for leak detection in microwave ovens, have blossomed into extremely sensitive, broadband devices capable of measuring near- and far-field nonionizing radiation at frequencies as high as 40 GHz. Most modern radiation monitors are similar in appearance and consist of a diode-based detection probe connected directly or via coaxial cable to a measurement meter (Fig. 1).

Several companies manufacture these radiation monitors, including Narda Microwave (Hauppauge, NY), General Microwave (Farmingdale, NY), and Holaday Industries (Eden Prairie, MN). All three firms are dedicated to the task of providing industry and health officials with instrumentation capable of making accurate readings. Al Schwartz, Narda's instrument marketing manager, notes, "We are not in a position to say whether radiation is hazardous—and what levels are hazardous; we just want to be able to provide accurate measurement tools."

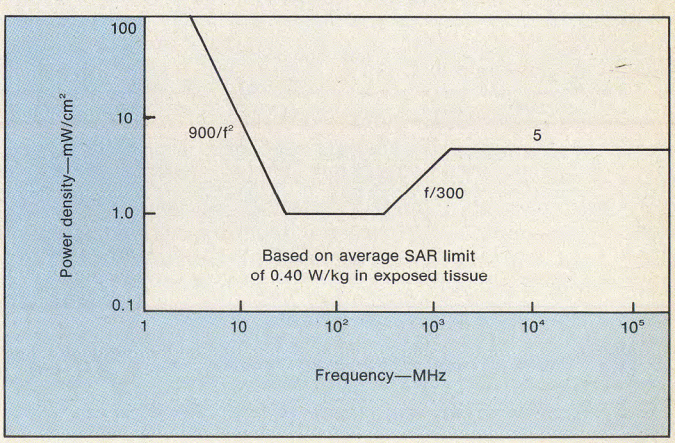
The growing interest in radiation monitors can be traced in part to increasing awareness that electronic devices act as emitters of radiation and the investigative work performed by such groups as the American National Standards Institute (ANSI), the Bureau of Radiological Health (BRH), and the Department of Labor's Occupational Safety and Health Administration (OSHA). Late last year, ANSI approved a new safety standard for exposure to RF and microwave energy fields covering frequencies from 300 kHz to 100 GHz (Fig. 2). ANSI's earlier standard had minimum levels of 10 mW/cm^2; the new standard goes down as far as 1 mW/cm^2 from 30 to 300 MHz. These levels are the mean squared electric (E^2) and magnetic (H^2) field strengths and are given in terms of the *equivalent*

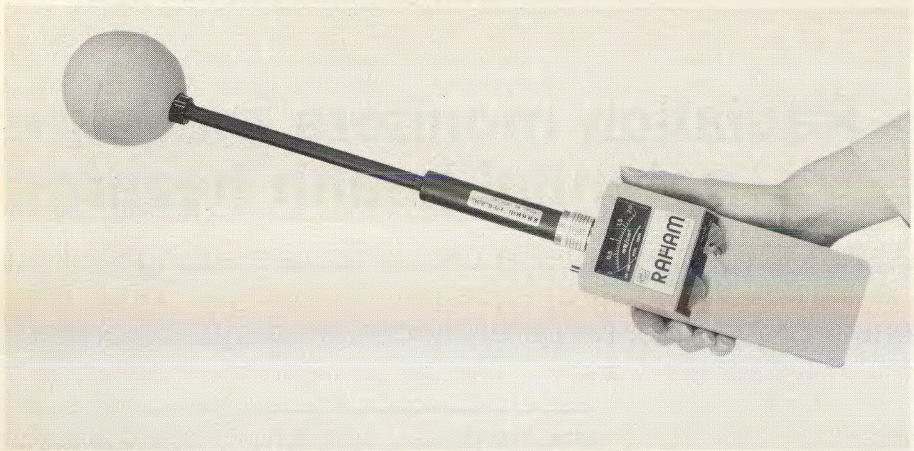
(continued on next page)



1. Narda Microwave's radiation monitoring systems *include broadband meters, models 8616 (left) and 8611 (right), with isotropic probes. Frequency coverage is from 10 MHz to 26 GHz, and calibration is available to 40 GHz.*

2. The recently updated ANSI standards *for RF and microwave radiation exposure call for monitoring systems capable of a wide dynamic range.*





***3. General Microwave's RAHAM series of hazard monitors** offer a measurement capability of 0 to 200 mW/cm^2 and frequency coverage to 18 GHz.*

plane-wave, free-space power density, measured at a distance of at least 5 cm from an emitter. The new ANSI standard (C95.1-1982) does allow one exception to the 1 mW/cm^2 level: when the radio frequency input power of the radiating emitter is 7 W or less. When hazardous fields are composed of different frequency components, the ANSI standard allows that the fraction of the equivalent density level that is incurred within each frequency group should be determined, and the sum of these fractions should not exceed unity.

The ANSI standard has resulted in the development of a "Radio Frequency Protection Guide" (RFPG) which is based on the amount of electromagnetic (nonionizing) energy that in experiments the human body has been able to tolerate safely. This amount is referred to as the specific absorption rate (SAR)—the rate at which nonionizing energy is imparted to biological tissue. The ANSI standard is based on a SAR of 0.4 W/kg as the upper limit, when averaged over the entire body. The spatial peak SAR is 8 W/kg when the average absorption is measured for one gram of tissue. The ANSI RFPG provides investigators with a safety guideline when checking a known or suspected hazardous source of RF.

The role of the radiation monitor manufacturer is to provide health inspectors with accurate instrumentation, and to respond to the needs of government health agencies. Burton Gran, vice-president of Holaday Industries, referring to the ANSI standards in much the same way a project engineer might talk about a system specification, says, "We've been looking at that standard since it's been discussed. In fact, our company president is on the standards subcommittee, so our instrumentation is designed with that standard in mind."

Broadband systems are fully calibrated

Six models make up the 8600 series of broadband isotropic radiation monitor systems. All models will measure power levels regardless of the polarization or direction of the incident power. Models 8606, 8607, and 8608 cover the frequency ranges of 300 MHz to 26 GHz, 10 to 300 MHz, and 10 MHz to 26 GHz, respectively, and will measure power levels from 0 to 100 mW/cm^2. All are based on the model 8616 metering instrument (see Fig. 1), so that full frequency coverage is always possible simply by adding the required probe. The 8616 meter has a response time that can be switched between slow (3 s) and fast (1 s). The meter also includes a maximum hold function, audible alarm, and automatic zeroing. Typical frequency accuracy is within ±0.5 dB.

Where more compact systems are required, models 8601, 8602, and 8603 also operate over the above three frequency ranges, respectively, but are based on the much smaller monitor meter, model 8611. It has a fixed 1-s response time but offers the same general electrical characteristics as the model 8616 meter.

All probes are fully calibrated across their entire range of operation and, in special cases, will be calibrated to 40 GHz. The calibration accuracy is ±0.5 dB. **The Narda Microwave Corp., 435 Moreland Rd., Hauppauge, NY 11786. (516) 231-1700, TWX: (510) 221-1867.**

CIRCLE NO. 231



READER SERVICE NUMBER 74

The revised ANSI standard has spurred new research at General Microwave. (For a current example of a General monitor, see Fig. 3.) Sam Hopfer, vice-president and director of engineering, relates this work to the standard. "There is a need for an instrument which can reflect the way the human body reacts to different frequencies," he says. "You need an instrument with a sensitivity profile that follows that of the ANSI standard. We are currently working on such a device. It will cover the ANSI range from 300 kHz to 40 GHz and will automatically weigh the contributions of the various frequency bands." Hopfer notes that the new meter will not show radiation levels in terms of the equivalent power density, but by the percent of allowable exposure. Hopfer adds that the instrument will be extremely easy to use. "If I am a person who is not technical and simply want to know if there is a hazard," he says, "this will tell me. In fact, the Navy has been pushing this development because of its need for such a general purpose instrument."

Recognizing the enemy

What are the sources of hazardous levels of RF radiation? Generally, any electronic component that can be described by the phrase "high-power." Potential sources include radar, point-to-point communication transmitters, and medical diathermy equipment. A potential industrial hazard is the RF dielectric plastic heat sealer (Fig. 4). It is a device using low-frequency RF energy at kilowatt levels to close plastic packaging. A recent report from the BRH studied the emission from various heat sealers having typical power-operating levels in the 7-to-40-kW range.[1] The heat sealers, which work at center frequencies of 13.56, 27.12, and 40.68

(continued on p. 126)

Radiation monitors operate to 18 GHz

The RAHAM series of radiation hazard monitors consists of five models. The most broadband of these, the model 4A, is more of an EMI meter than a hazard monitor, with a high end of only 20 mW/cm^2. All other models have a full-power range of 0.02 to 200 mW/cm^2. Models 1 and 2 are anisotropic devices employing single probes to cover frequencies from 0.3 to 18 GHz and 0.01 to 3 GHz, respectively. The combined bandwidth of these two models is also available in a single instrument, the model 12, which uses two probes for energy detection from 0.01 to 18 GHz.

The true flagship of this radiation monitor line is the model 3. It uses a single isotropic probe to operate from 0.3 to 18 GHz. The probe employs three thin-film thermocouple arrays to sense the strength of the field. Its frequency response is within ±1 dB across the full bandwidth, and its isotropic response is within ±0.5 dB in any direction or field polarization.

Each probe is calibrated at 2.45 GHz, as well as at a number of additional frequencies, depending on the bandwidth of the probe. The probes exhibit a calibration accuracy of ±0.5 dB. The radiation monitors are supplied with a 4-ft coaxial cable for remote probe use. The measurement meters show a typical response time of 1 s. **General Microwave Corp., 155 Marine St., Farmingdale, NY 11735. (516) 694-3600.**

CIRCLE NO. 229

Monitors move from ovens to broadbands

Radiation monitors in the HI-3000 series have been designed to measure hazardous field-strength levels at frequencies from 0.5 to 6 GHz. The series includes four battery-powered instruments with self-zeroing, even in the presence of a field, as well as a peak-hold memory and outputs for an audio tone or a chart recorder.

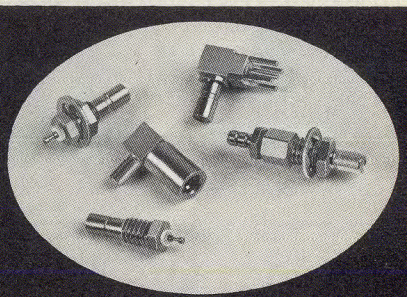
The most broadband of these meters is the model HI-3002, which operates from 0.5 to 6 GHz, although it measures the E-field and H-field in field strength units squared rather than in mW/cm^2. Perhaps more suitable for use as a general purpose hazard monitor is model HI-3003. It features a scale in mW/cm^2 and operates from 5 MHz to 1 GHz with a response of ±2 dB. Field strengths of 0 to 100 mW/cm^2 can be evaluated with this instrument. Its probe is calibrated at specific frequencies, rather than over the entire frequency range. At those frequencies, it has a calibration accuracy of ±0.5 dB. The isotropic response of the probe is within ±0.5 dB. Other monitors in the company's lines include models HI-1600 and HI-1800, intended to measure radiation leaks at 915 and 2450 MHz in microwave ovens. The typical response time for these probes is 3 s. **Holaday Industries, Inc.,14825 Martin Dr., Eden Prairie, MN 55344. (612) 934-4920.**

CIRCLE NO. 230

AEP SERIES 7000 MICROMINIATURE RF CONNECTORS

MATE WITH "NANOHEX®-TYPES"

NANOHEX® is a Registered Trademark of Sealectro Corp.



Here's the 'second source' for Nanohex® type connectors you've always wanted. This new, AEP group of microminiature connectors is available with nickel or gold plating for cables up to .110" dia. Frequency range is DC to 12.4GHz.

They're engineered in the most asked for models — straight plugs, right angle plugs, bulkhead jacks, front and rear mount bulkheads plus straight and right angle PC board mounts.

As with all AEP Subminiature and Miniature RF Connectors, the Series 7000 is backed by a strong quality control program. Produced in short and long runs, including "special purpose" types.

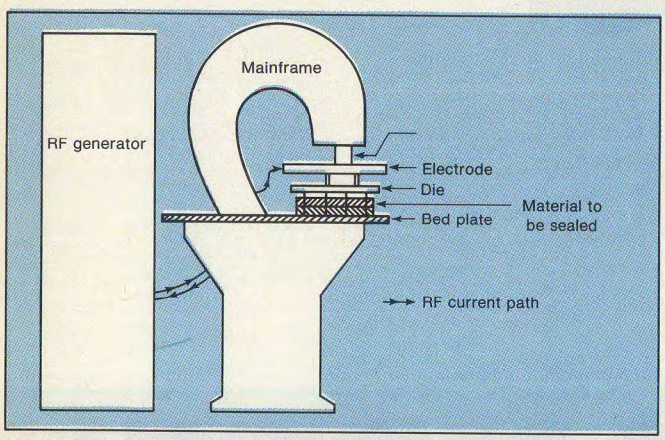
Drop us a note or call in your requirements.

AEP APPLIED ENGINEERING PRODUCTS

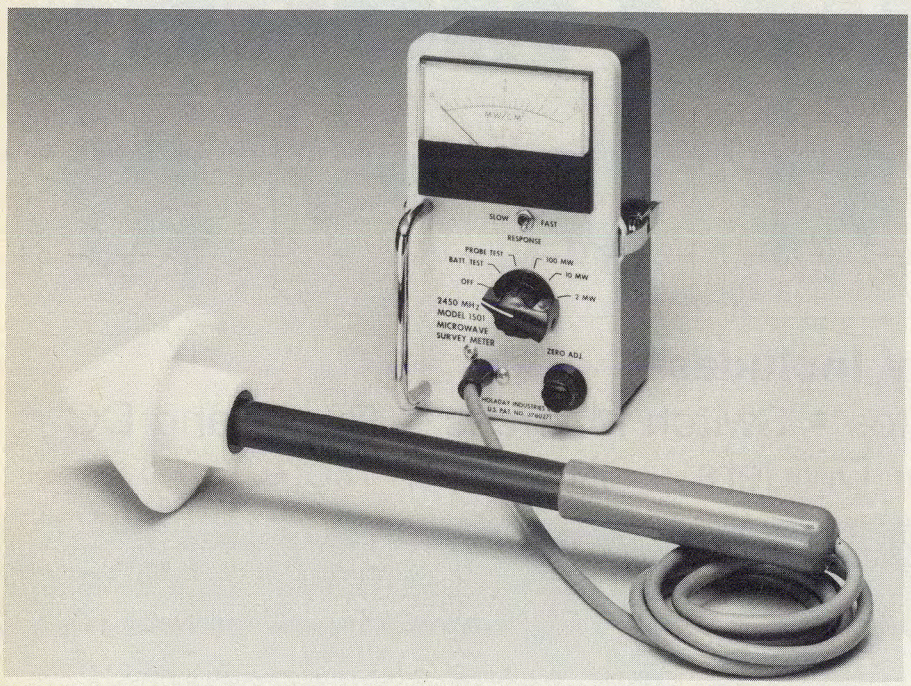
1475 Whalley Avenue, New Haven, CT 06525
(203) 387-5282 TWX 710 465 1173

READER SERVICE NUMBER 76

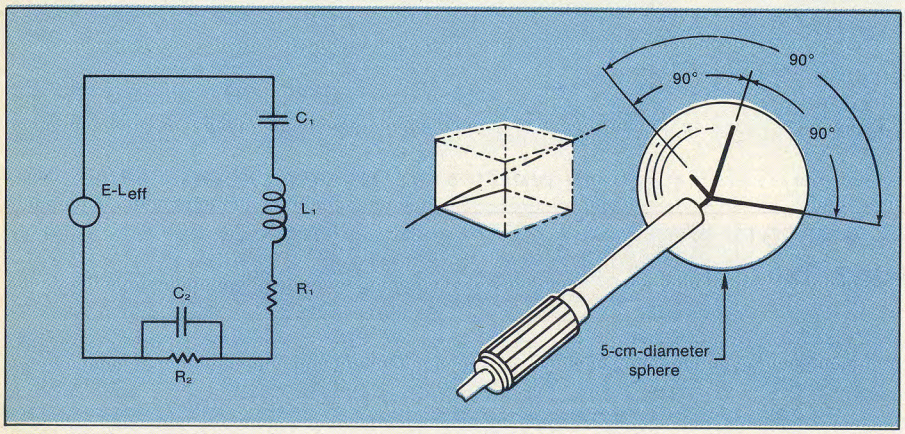
MHz, were capable of producing emission levels high enough to be perceived as heat or tingling in the nerve endings. The investigators recommended various emission remedies, including free-space attenuation (in effect, getting the operator away from the sealer), and RFI shielding. They also reported the importance of instrumentation in detecting these potentially hazardous levels, citing such manufacturers as Amplifier Research (Souderton, PA) and Instruments For Industry (Farmingdale, NY), in addition to Narda, General, and Holaday, as likely sources. (One of the monitors designed for heat sealer radiation detection is Holaday's device, see Fig. 5.)



***4. A dielectric RF heat sealer**, when improperly shielded, can be a source of hazardous-level nonionizing radiation.*



***5. Holaday Industries, once known primarily for anisotropic leak detectors**, now manufactures broadband isotropic equipment.*



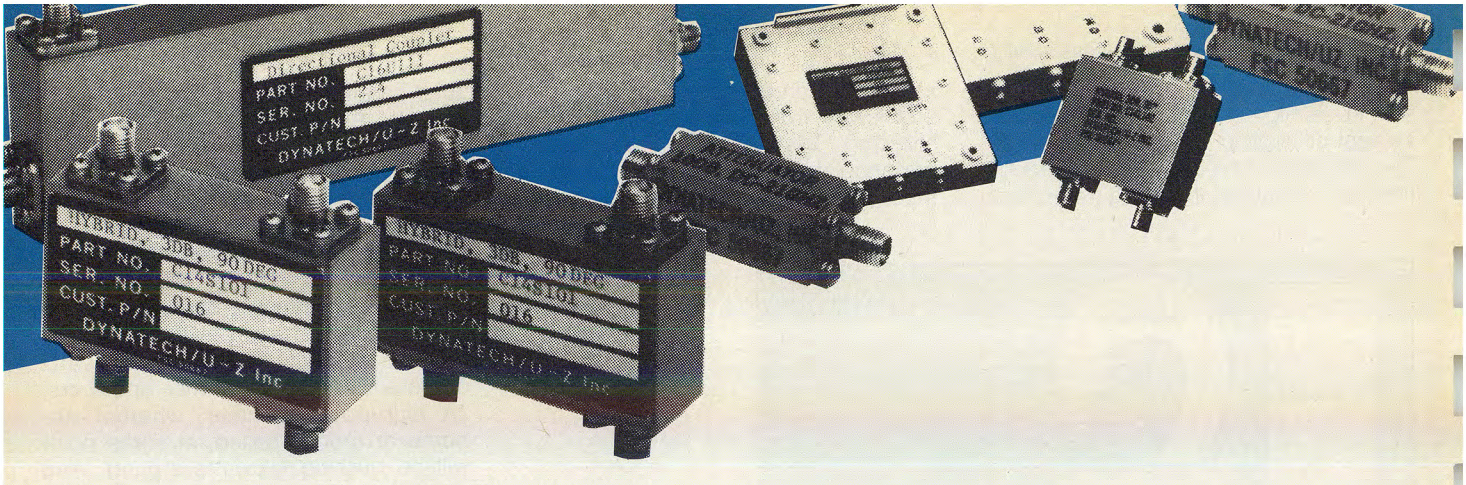
***6. In the design of Narda's isotropic probes**, three detector elements are located orthogonally within a 5-cm spherical volume. The equivalent circuit for a single element is shown at left.*

A great number of EW and ECM systems also operate at power levels in or near the danger zone. Narda's Schwartz offers a warning to jammer operators, "A high-power jammer, whether airborne or ground-based, at some point will be pushing kilowatts around. And when that happens, you have a potential hazard." Narda chief scientist Edward Aslin remarks that hazards can surface in unlikely places, "You can see high-power RF sources pop up in totally unexpected places. For example, there is a potential hazard from the high-power transmitters used in surveillance vehicles, such as unmarked police cars. You can find 'hot spots' in these cars, and they should be checked. An officer may have the transmitter on for some length of time, and if he's sitting near the steering wheel, he's got a nice directional mechanism for a high-energy field." The value of a radiation monitor is in its ability to locate these "hot spots" so that suitable shielding can be installed.

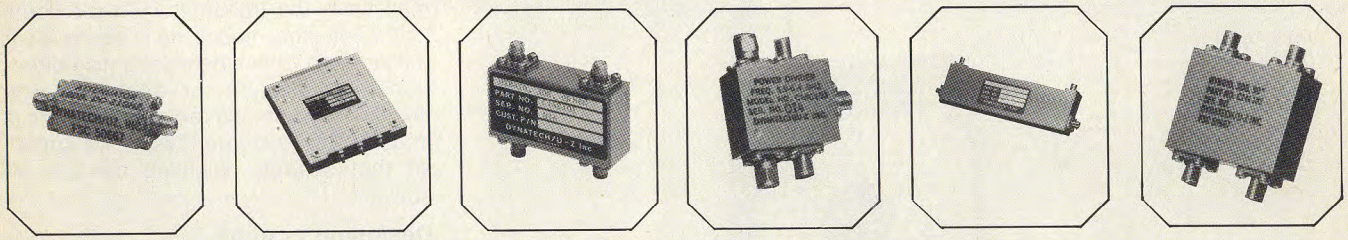
Designing a probe

The key component in any radiation monitor is the probe. It can be constructed to detect radiation anisotropically (in two dimensions) or isotropically (in three dimensions). Anisotropic probes, which have become associated with microwave-oven leak detection, play an important role in hazards testing, as Aslin at Narda explains: "The standard for microwave ovens says that the power density shall not be greater than 5 mW/cm^2 at 5 cm from the surface of the oven. Since the surface of the oven is a plane, you have to measure it in a plane, unless you want to shrink your measuring device down to an extremely small dimension, such that you can keep the entire device in the plane. Therefore, you must keep it in two dimensions." Anisotropic probes provide the near-field response required for leak detection.

Isotropic probes offer an equal response to energy fields, regardless of their direction or polarization. In addition, they exhibit true square-law response to far-field radiation, so that an equivalent measure of power density can be ascertained. Aslin stresses the significance of square-law response. "If you have a diode-type sensor that is not operating in the square-law region," he says, "measurements will not be valid. The response you see will be the result of squaring the sums of the voltages



AND MUCH MORE!



Component Diversity Includes:

- Integrated Assemblies • Switch Matrices — RF, IF and DC
- Attenuators • Power Dividers . . . And Much More.

POWER DIVIDER/COMBINERS

Frequency:	Octave bandwidth standard, 10:1 bandwidth available. Minimum frequency is 100 MHz, maximum frequency is 18 GHz.
Type:	2-way thru 16-way split is available, with 6-way and up limited to 4:1 bandwidth.
Isolation:	20-25 dB typical for units below 6 GHz; as frequency increases thru 18 GHz, the isolation decreases to 13-15 dB (at 18 GHz).
VSWR:	1.25:1 maximum
Power:	Limited primarily by isolation requirement and terminating VSWR: (Submit any requirement below 200 watts CW).

DIRECTIONAL COUPLERS

Frequency:	Octave bandwidth standard, 30:1 bandwidth available. Minimum frequency is 100 MHz, maximum frequency is 20 GHz.
Type:	Single or dual directional versions.
Coupling factor:	3 dB-50 dB, customer to specify.
Directivity:	22 dB typical for units below 4 GHz; 14 dB typical at 20 GHz. Levels in excess of 30 dB below 6 GHz are available in octave bandwidths
VSWR:	1.25:1 maximum
Power:	100 watts CW is standard using stripline techniques; 400 watts is achievable with barstock /airline methods.

CALL OR WRITE FOR "UZ" CATALOG

589 Venice Blvd. • Venice, CA 90291
(213) 392-9821 • TWX: 910-343-6907

Dynatech/UZ, INC

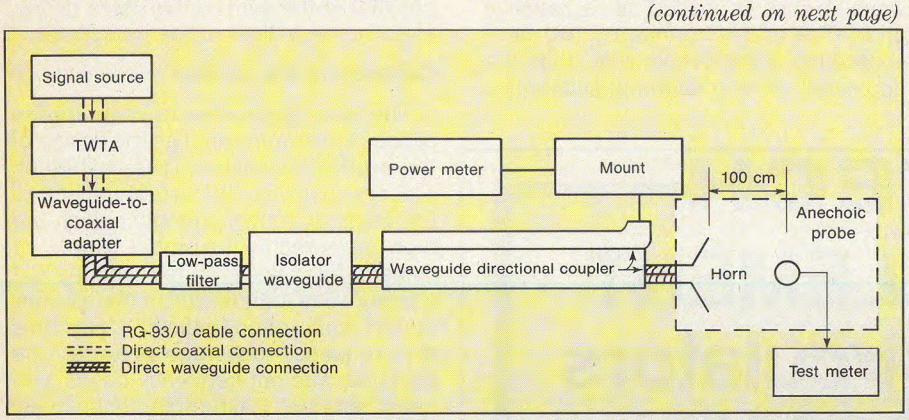
Dynatech/UZ, INC Dynatech/UZ, INC Dynatech/UZ, INC Dynatech/UZ, INC Dynatech/UZ, INC

READER SERVICE NUMBER 77

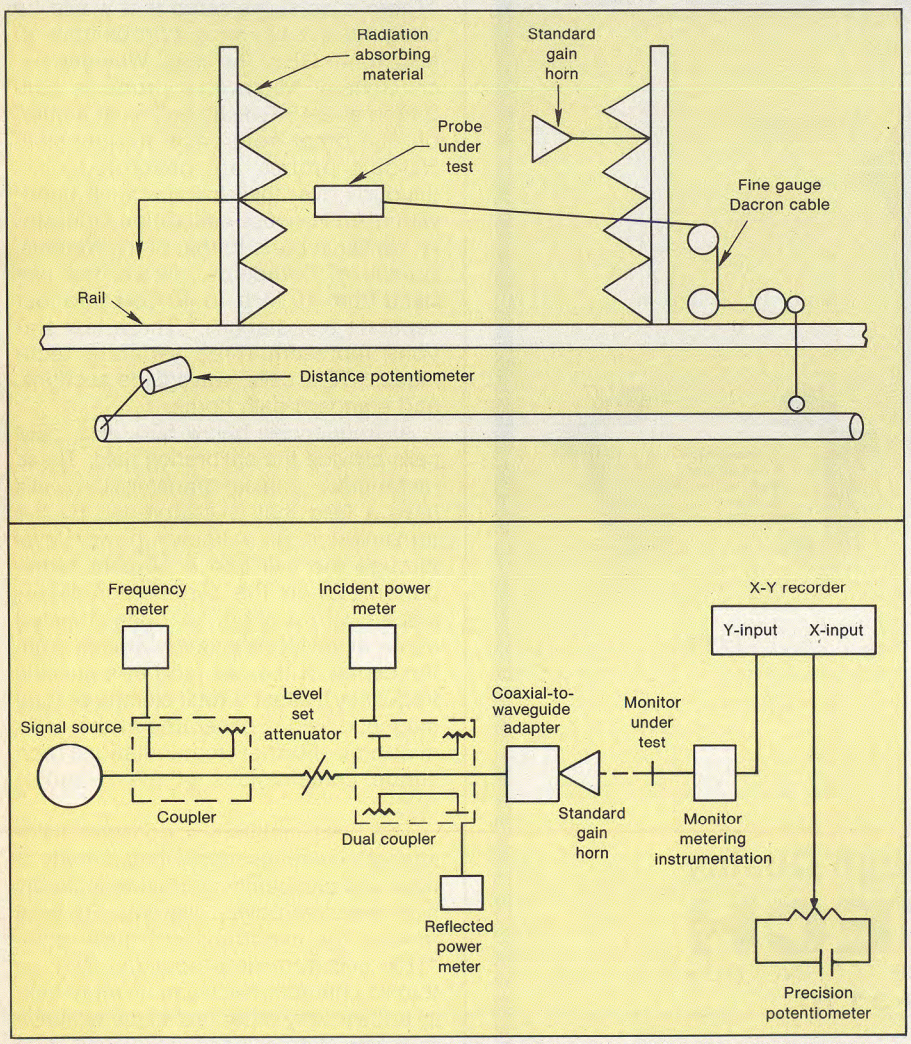
received, rather than summing the squares."

One approach designed to achieve this far-field probe response is that taken by Narda (Fig. 6). Each probe is constructed with three orthogonal lossy probe elements contained within a 5-cm spherical volume. The summation of the DC signals from the three elements provides a measure of the total energy or equivalent power density, independent of signal direction or polarization. The detectors used for the DC-signal generation are thermocouples of overlapping antimony and bismuth, deposited on a plastic thin-film substrate. The DC signal is proportional to the power dissipated in the thermocouple elements and the average power density in the volume in which the elements are contained.

(continued on next page)

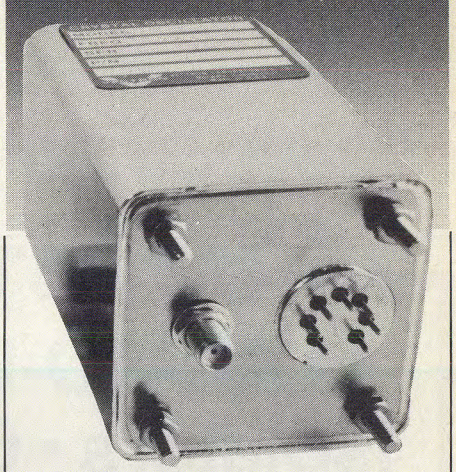


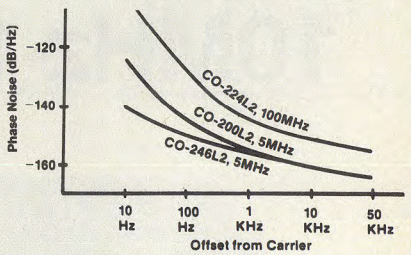
7. In the calibration of Narda probes *from 12.4 to 18 GHz, a setup is used in which coaxial and waveguide interconnections are combined.*



8. The anechoic sled used in Narda's high-frequency calibrations *(top) consists of a movable transmitter pedestal which holds the standard gain horn, and a fixed receiver pedestal for mounting the probe. The components required for the setup are shown below.*

Low Noise Crystal Oscillators





HF MODELS		
Series:	CO-200L2	CO-246L2
Frequency:	4-25 MHz	5 MHz (opt. to 100 MHz)
Aging:	$1x10^{-9}$/day $3x10^{-7}$/year	$1x10^{-10}$/day $3x10^{-8}$/year
Phase noise:	at 5-10 MHz	
@100 Hz:	−145 dB/Hz	−150 dB/Hz
@ 1 KHz:	−155 dB/Hz	−155 dB/Hz
@ 50 KHz:	−163 dB/Hz	−163 dB/Hz

VHF MODELS		
Series:	CO-224L2	CO-220L2
Frequency:	25-300 MHz	25-125 MHz
Aging:	$1x10^{-8}$/day $2x10^{-6}$/year	$1x10^{-9}$/day $3x10^{-7}$/year
Phase noise:	at 100 MHz	
@100 Hz:	−130 dB/Hz	−120 dB/Hz
@ 1 KHz:	−145 dB/Hz	−130 dB/Hz
@ 50 KHz:	−155 dB/Hz	−140 dB/Hz

Write, phone or TWX today for complete details...

From the world's largest and most respected full line manufacturer of crystal oscillators...

VECTRON

VECTRON LABORATORIES, INC
The Crystal Oscillator Company
166 Glover Avenue, Norwalk, Connecticut 06850
Telephone: 203/853-4433 TWX: 710/468-3796

READER SERVICE NUMBER 78

Broadband characteristics are obtained by distributing resistive thermocouple dipoles in series along the length of the elements, at spacings that will not create any resonant lengths over the frequency range of the probe. The sum of the outputs of these dipoles provides the energy reading of the measured field.

Very light coupling is used between the probe and the monitoring instrumentation, in order to minimize the amount of scattering in the EM field caused by the probe. For this purpose, high-resistance films are employed to connect the probe's DC outputs to the instrumentation—a technique that approximates floating the probe in the free space of the EM field to be measured. An additional feature of the Narda probes is the inclusion of an integral preamplifier to minimize noise and cable modulation.

The design of some General Microwave probes is based on a resistive grid.[2] The grid is formed by two noncontacting meandering lines that are deposited on two separate substrates. The lines are connected by appropriate through-holes in the substrates and form one continuous path that does not intersect itself. The resistive line is composed of alternating line segments of bismuth and nichrome. These segments overlap slightly to form thermocouple junctions. By creating one continuous path, all of the thermocouples are connected in series. They produce an output that is the sum of the EMFs generated by the individual thermocouples.

Calibrating the probes

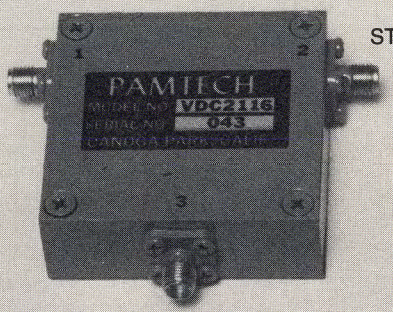
The techniques used to calibrate the probes are as important as the design of the probes themselves. The calibration process involves the establishment of EM fields of known strength, which are then measured by the probes. Hopfer at General Microwave states that the extremely wide bandwidth of the probes makes calibration difficult. "Because the frequency coverage is wide," he says, "at different frequency bands, you need different calibration techniques, with different radiating elements to form the fields." Narda's Aslin concurs. "There is no single setup that would be adequate in calibrating a probe from 10 MHz to 40 GHz," he says. Whereas each General Microwave probe is calibrated at 2.45 GHz as well as at a number of other reference frequencies, Narda's probes are calibrated continuously over their full operating bandwidth. An in-house calibration laboratory, similar in parts to that of the National Bureau of Standards, divides the test band from 10 MHz to 40 GHz into four separate test stations.[3] These test stations represent three separate techniques: TEM cells, waveguide sections, and standard gain horns.

At frequencies below 500 MHz, TEM cells provide the calibration field. These rectangular coaxial transmission cells have a field that is established by the transmission of a known power level through the cell into a 50-ohm termination. When the termination is replaced with a short- or open-circuited cable at an appropriate distance from the center of the cell (and at a specific frequency), either a total electric or total magnetic field is generated at the cell's midpoint. Further manipulations can create combinations of the E and H fields.

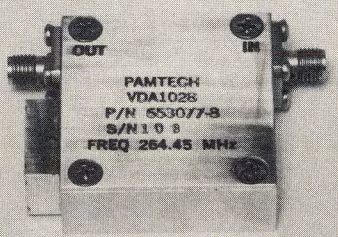
The cells maintain a constant field-strength over reasonably long periods of time and can safely contain reasonably high levels of power. Narda's Ed Aslin reviews the importance of these cells: "TEM cells provide a bounded field, so that its characteristics can be more easily known. Any other technique will have too many errors associated with it at these frequencies. You can get tremendous scattering at these low frequencies, but the TEM cell is a consis-

(concluded on p. 154)

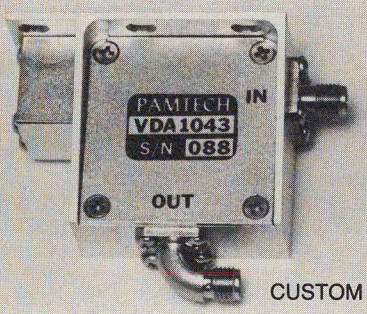
PAMTECH
LUMPED-ELEMENT
Isolators • Circulators
10MHz-1000MHz



STANDARD



HI-REL



CUSTOM

Reliability Through Quality
PAMTECH
PASSIVE MICROWAVE TECHNOLOGY
(213) 999-3110

8030 REMMET AVENUE #1, CANOGA PARK, CALIFORNIA 91304

READER SERVICE NUMBER 79

Band-reject filters suppress second harmonics

In the generation of high-frequency test signals, second-harmonic components often result as undesired by-products. Band-reject filters help keep the distortion to a minimum.

Kurt E. Zublin, Microwave Project Engineer, and **Behzad Moeen-Ziai,** Microwave Engineer, Wavetek San Diego, 9045 Balboa Ave., San Diego, CA 92123.

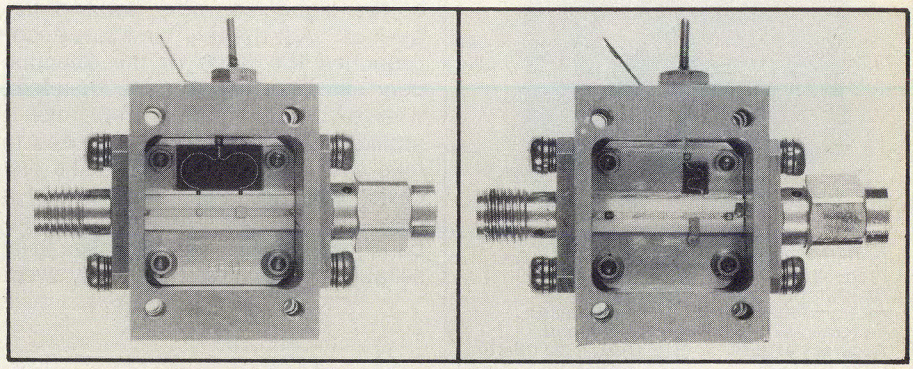
Excessive second-harmonic distortion is never desirable, especially in broadband signal sources. The harmonic signals usually act as "unwanted guests," disrupting the proper operation of a microwave test setup. For example, when a microwave signal source is used as a local oscillator, the second harmonic outputs can lead to intermodulation products in the mixer. If, in signal-locking applications using a broadband receiver or frequency counter, the level of the second-harmonic components is too high, false signals will be locked instead of the desired fundamental. In many cases, excessive second harmonics interact with a device under test and degrade the quality of most measurements.

There are three basic design strategies aimed at suppressing second harmonic distortion. All involve filtering techniques and rely on two families of filters: switchable low-pass and band-reject filters, and tunable band-reject tracking filters. Figure 1 shows a hardware comparison betwen a switchable band-reject filter and a tunable band-reject tracking device. Of course, it is also possible to limit second harmonic distortion with a bandpass filter that tracks the fundamental, although this configuration will not be discussed here.

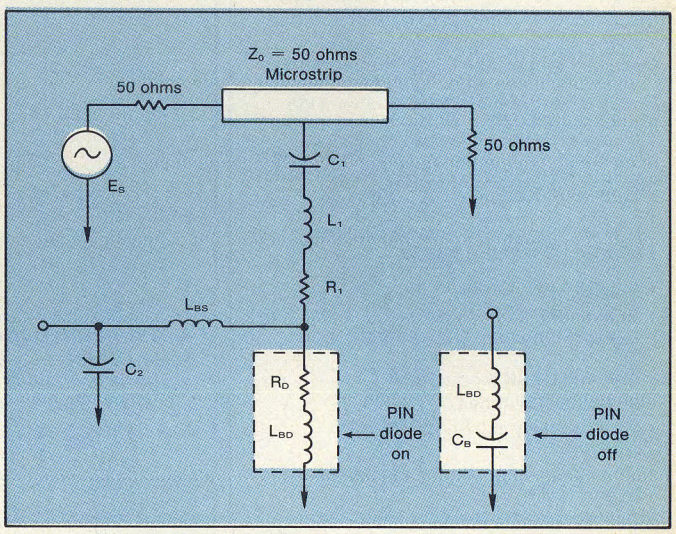
Choosing a switchable filter

When a switchable filter is to be used in a signal generation system, the choice is essentially between a low-pass or band-reject type. The low-pass filter operates by switching from one cutoff frequency to another. As a signal source is tuned from its low end to its upper frequency limit, the low-pass filter will switch from a cutoff at just under twice the value of the low-end frequency to a cutoff that is slightly less than twice the

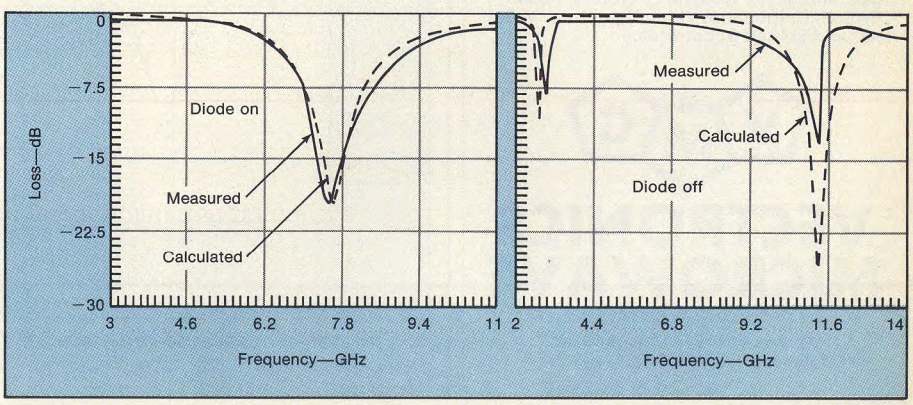
(continued on next page)



1. A switchable band-reject filter (left) and tunable band-reject filter (right) *can be implemented in similar fashion. In both cases, bias is brought in on transmission lines realized on soft Duroid substrates.*



2. The switchable band-reject filter *relies on the small RF resistance of a PIN-diode for its effective performance. The inset at right shows the diode in its off condition. The PIN-diode is in chip form.*

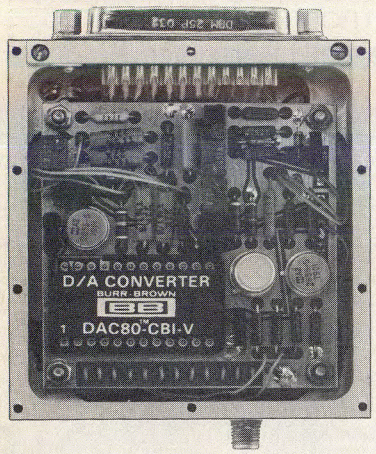


3. The performance of the PIN-diode switchable band-reject filter *is compared with theoretical expectations with the diode in its on (left) and off (right) conditions.*

STATE-OF-THE-ART-MICROWAVE

PRECISION DIGITAL ATTENUATORS

- **High Accuracy**
- **Microstrip Construction**
- **TTL Control**
- **High Reliability**



80 dB Attenuator, C-Band

Frequency	UHF to X-Band
Bandwidth	Up to 2:1
Attenuation Range	50, 80 and 100 dB
Increments	1 dB, Monotonic
Accuracy at 25 °C	± (0.5 dB + .03 dB/dB)
Incremental	± 0.25 dB, Non-Cumulative
Control	TTL, Binary or BCD
Insertion Loss	1.5 - 3.5 dB Depending on F
VSWR	1.5:1 any Attenuation
DC	+ 5V, + 15V, - 15V
RF Connectors	SMA

Designed for use in ATE or for Integration into systems, these units combine balanced P-I-N Diode Attenuators on alumina substrates with digital drive circuits in compact packages. Each unit is individually programmed for highest accuracy. Their rugged construction assures excellent repeatability and long-term stability.

Other MIC Signal Processing Circuits available from VMC include:

- Analog Attenuators
- Digital Phase Shifters
- Digital Frequency Translators/Doppler Simulators
- PSK and QPSK Modulators
- PIN Diode Switches
- Mixers, Balanced, Image-Reject, Quadrature IF
- Monopulse Converters and Feed Networks
- Integrated Front Ends
- Custom MIC Modules

Also: Microstrip Couplers, Hybrids, Power Dividers/Combiners, Video Detectors, Metalized and Etched Substrates.

VECTRONICS MICROWAVE CORPORATION
P.O. Box 70—276 Lincoln Blvd.
Middlesex, N.J. 08846 (201) 356-2377

READER SERVICE NUMBER 82

(continued from p. 131)

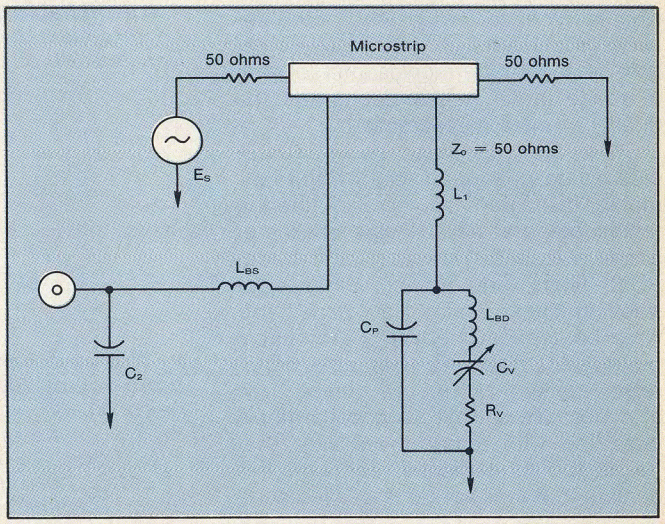
value of the signal generator's highest frequency. In some designs, this type of filter can be switched completely out of the circuit before the fundamental signal reaches the filter cutoff frequency. A switchable low-pass filter is only practical when the second-harmonic level is low enough at the switch point and when it has a natural rolloff with increasing frequency.

Switchable band-reject filters, on the other hand, offer a practical solution to the rejection of second harmonic outputs in a broadband signal source. These devices operate by providing at least 20-dB rejection at twice the value of the signal source's low-end frequency. As the signal source approaches the edge of the rejection band, the filter switches off. Therefore, when extremely broadband operation is required, another filter can be used to take over at the point where the first device switches off, in the form of a crossover network. The very low passband loss of these devices makes them suitable for use with electronically swept sources as well as manual instruments. In reflective-type filters, if PIN diodes are used as the switching elements, signal sources with outputs as high as 1 W can be safely employed.

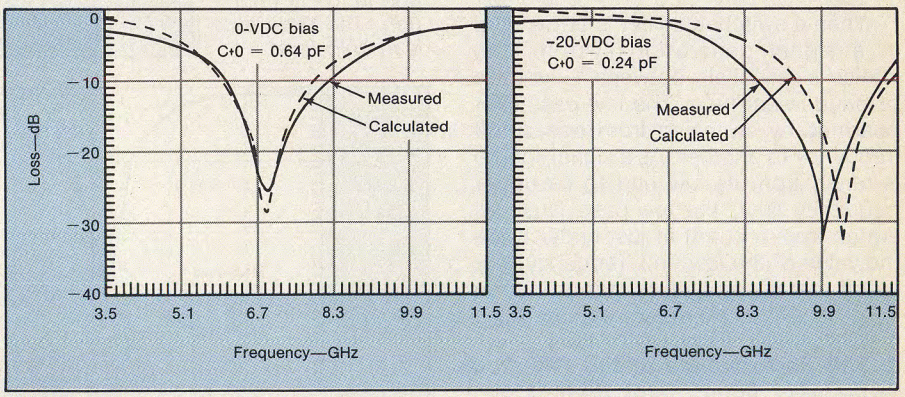
The equivalent circuit of a switchable band-reject filter is presented in Fig. 2. When the PIN diode is on, the series resonant circuit is connected in shunt to the transmission line. The circuit represents a low reactance and reflects energy at the filter's resonant frequency. The correlation between the theoretical and actual performances of these devices is shown in Fig. 3. Some of the off-band deviation from theory is due to mismatches occurring at the connector/filter-circuit interfaces.

When the PIN diode is off, the diode's parasitic elements can cause unwanted resonances in the filter. Perhaps the best design approach is to make sure that these resonances fall outside the frequency range of interest.

A switchable band-reject filter is constructed as a microwave circuit with a certain number of lumped elements.



4. A tunable band-reject filter *can be constructed with a varactor diode as the tuning element.*



5. The performance of the varactor filter *is fairly consistent with frequency. The device is swept from one frequency to another by adjusting the tuning bias to the diode.*

Looking at the equivalent circuit of Fig. 2, C_1 is a chip capacitor, L_1 is the bond wire, and R_1 is the resistive loss through L_1. The PIN diode is attached to the ground with epoxy, and bias is brought in through a high-impedance line etched on a Duroid substrate. The basic transmission line is nominally 50 ohms, on an alumina substrate, with input and output RF signals routed through miniature coaxial connectors. The number of resonant stages required is dictated by the depth and width of the desired notch for a particular filter.

Choosing a tracking filter

Band-reject filters can also be designed to tune across a frequency range. Either varactor diodes or YIG resonators are used as the tuning elements. These filters operate by creating a reflective notch at frequencies which are twice the value of the fundamental. As the fundamental is tuned, the notch is also tuned, tracking any second harmonic products. An advantage of making a band reject filter this way is its small varactor-tuned filter is about one-half the size of a switchable filter. Unfortunately, the passband insertion loss for the smaller design is higher. There are other negative features: a tuned band-reject filter has a limited tuning range of about one octave, and the power-handling capability of these devices is only about 10 mW.

A varactor-tuned filter's tuning range is proportional to the square root of the ratio of the maximum capacitance of the varactor junction to the value of the minimum capacitance. The tuned configuration provides a deeper rejection notch than the switchable band-reject filter, and provides more rejection. Also, since the notch can be tuned, bandwidth requirements are not as critical with a tunable filter.

An equivalent circuit of the varactor-tuned band-reject filter for a packaged varactor diode is drawn in Fig. 4. In this circuit, a reactance is placed across the transmission line by a circuit consisting of a varactor in series with an inductive wire and an additional inductance which is due to the bonding structure. As the varactor is tuned by its bias voltage, the capacitance of its junction changes, causing a change in the resonant frequency of the filter stage.

In building this type of filter, a 50-ohm transmission line is implemented on an alumina substrate. The varactor diode is connected to ground with epoxy, in a fashion similar to that of the switchable PIN-diode filter. An inductive ribbon is connected to the other end of the diode. Bias is injected through a conductive path on a Duroid substrate which is joined directly to the transmission line.

(concluded on next page)

Double Balanced MIXERS

Guaranteed (not typical)
4.5dB Tacan Band to 5.5dB X-Band
Conversion Loss

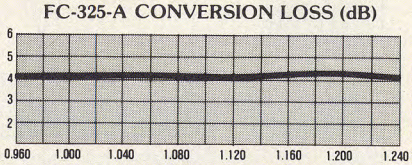


Lorch Electronics is proud to announce a new series of microwave mixers with extremely low conversion loss — at affordable prices. Single side band conversion losses range from 4.5 dB for the Tacan Band (0.960–1.215 GHz) to 5.5 dB for X-Band (7.125–7.750 GHz). The ultra-low conversion losses achieved with our mixers are guaranteed to be maximum (not typical) values, and result from a breakthrough in technology.

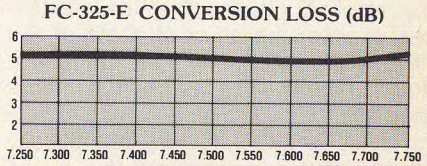
Frequency Range, RF (GHz)	Frequency Range, IF (GHz)	Conversion Loss (dB max)	Model Number
0.960-1.215	DC-.200	4.5	FC-325A
1.700-2.500	DC-.200	5.0	FC-325B
3.700-4.200	DC-.500	5.3	FC-325C
3.700-4.200	DC-1.100	5.3	FC-325CD
4.400-5.000	DC-.500	5.3	FC-325D
DC-1.100	5.900-6.400	5.5	FC-325U1*
5.900-6.400	DC-1.100	5.5	FC-325DE
7.250-7.750	DC-1.100	5.5	FC-325E
7.900-8.400	DC-1.100	5.5	FC-325F
9.000-9.500	DC-1.100	5.5	FC-325G
10.000-10.500	DC-1.100	5.5	FC-325H

*Up-Converter

FC-325-A CONVERSION LOSS (dB)



FC-325-E CONVERSION LOSS (dB)



Specific models of our Series FC-325 are designed for the most popular frequency ranges. Other bands can be covered, if your requirement demands it. For complete details write for Data Sheet FC-803. Better yet: call us!

LORCH ELECTRONICS CORP.
105 CEDAR LANE, ENGLEWOOD, NJ 07631 • (201) 569-8282 • TWX: 710-9718

READER SERVICE NUMBER 83

Miniature connectors are used at the input and output ports.

The performance of the varactor filter is demonstrated in Fig. 5. By using a varactor diode, it's possible to more closely approach the theoretical performance than it is by using a switchable filter.

Evaluating real conditions

A good example of the switchable band-reject filter approach to second-harmonic suppression can be found in the model 904 signal generator. (For a review, see *MicroWaves*, April, 1982, p. 106.) This signal source operates both in manual and swept-frequency modes, from 3.7 to 7.6 GHz. The filter is positioned in the RF chain at the output of an isolated YIG-tuned oscillator (Fig. 6). After passing through the filter, the signal is leveled and channeled through a modulator and a programmable PIN-diode attenuator. The signal is then routed through an isolator and on to the output connector.

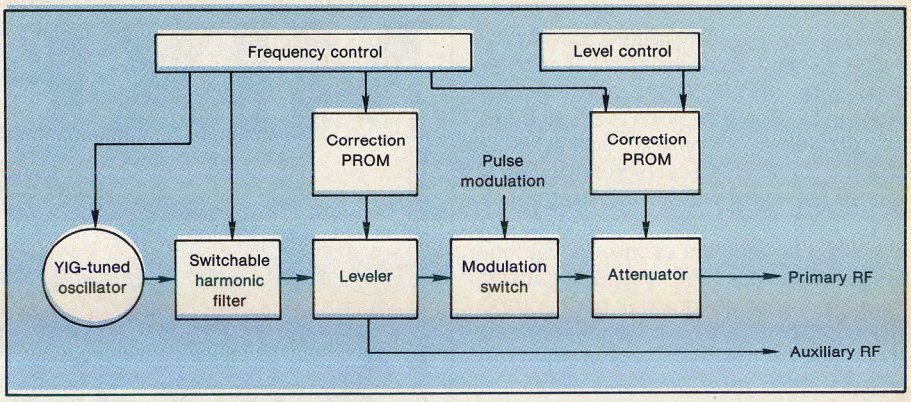
The filter in the 904 is centered at 7.8 GHz, and has rejection of 20 dB at 7.4 GHz. With the particular source used in the 904, there is high second-harmonic output for fundamental frequencies from 3.70 to 4.15 GHz.

As a result, the 20-dB bandwidth of the rejection notch must lie between 7.4 and 8.3 GHz. In order to achieve the proper bandwidth and rejection, a two-stage filter is required. The second stage increases the bandwidth by a factor of two over a single-stage design. The rejection at the center of the notch increases from about 15 dB to more than 30 dB. Above 4.15 GHz, the second harmonic from the source tapers off and the additional components of the RF chain further reduce the harmonic levels.

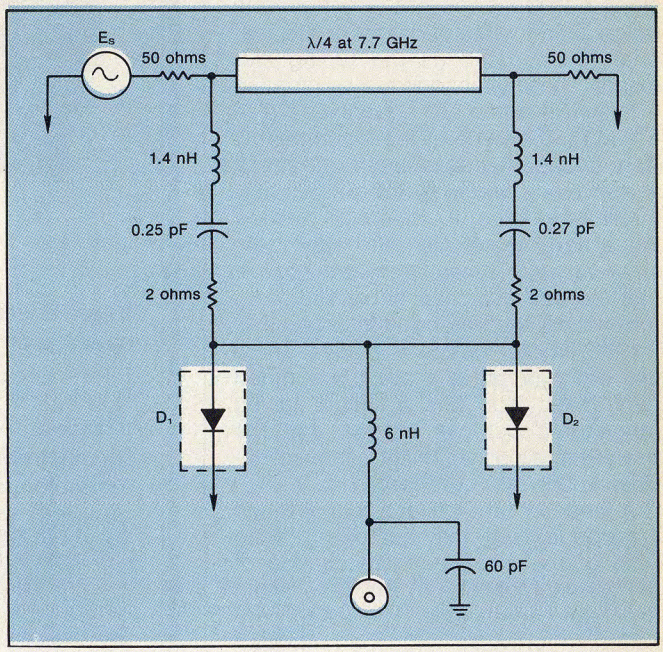
As the fundamental frequency is increased past 4.15 GHz, the filter starts to switch off at 4.80 GHz. By the time it reaches 5 GHz, it is totally off. The switching operation is controlled by the frequency control voltage in the signal generator. At no time does the insertion loss in either the on or off state of this filter exceed 0.7 dB. The equivalent circuit for the filter used in the 904 is shown in Fig. 7. In Fig. 8, its actual performance is compared to theoretically possible levels.

As a result of the insertion of this switchable band-reject filter, the second-harmonic level of the 904 signal generator is only −25 dBc, at frequencies from 3.7 to 7.6 GHz and power levels from 0 to −127 dBm. This is one noise-filtering approach that has proven its effectiveness.

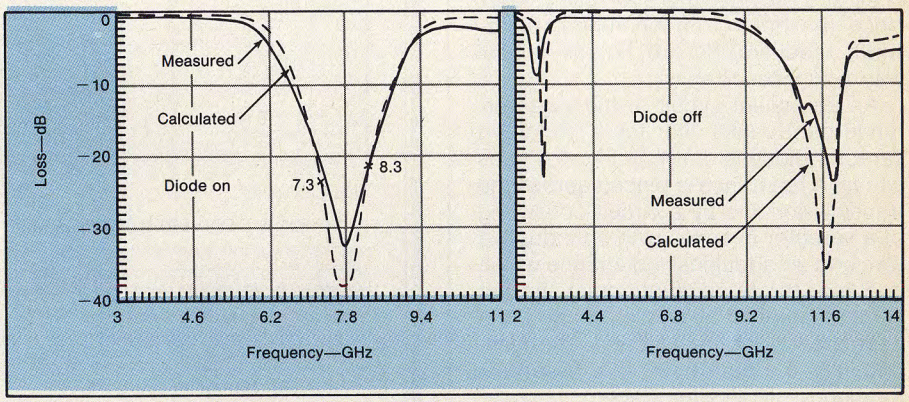
It should be noted that the equivalent circuits shown in Figs. 2, 4, and 7 were generated by three separate Micro-COMPACT programs. To obtain a copy of each of these programs, send a self-addressed envelope with $0.20 postage to Cathy Fedele, *Microwaves & RF*, Hayden Publishing Co., 50 Essex St., Rochelle Park, NJ 07662. ●●



6. In the design of the 904 signal generator, *a switchable band-reject filter was selected for harmonic rejection.*



7. This diagram shows how to construct the switchable harmonic band-reject filter *used in the 904 signal generator.*



8. The switchable filter suppresses harmonics *to generally below −30 dBc, although the signal generator is only rated at −25 dBc.*

Acknowledgment

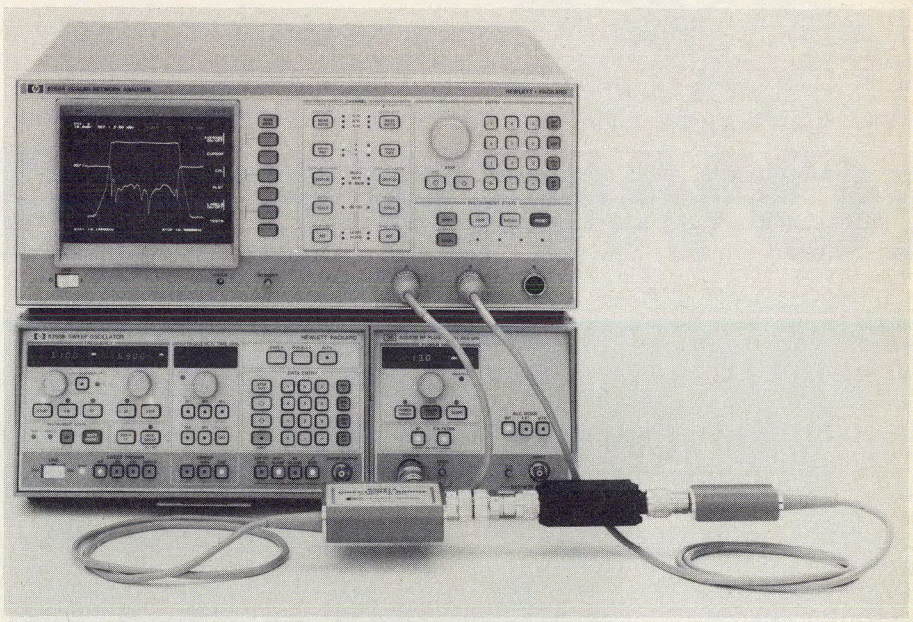
The authors would like to thank Guy Lyons for his patience and diligent efforts in the assembly of the various components described in this article.

SNA simplifies loss measurements from 10 MHz to 40 GHz

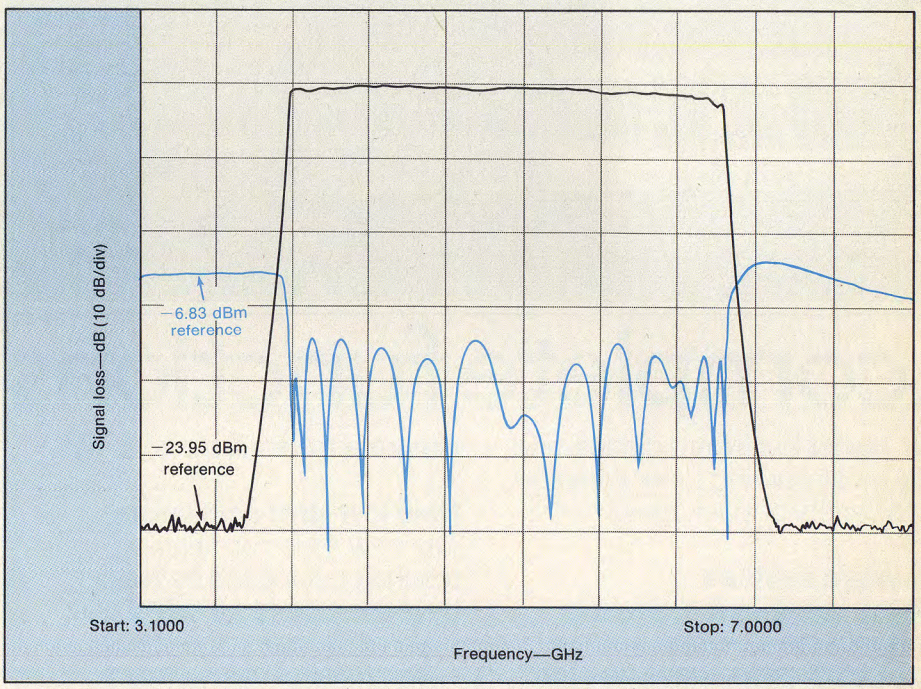
Transmission and return-loss measurements have been greatly simplified by the introduction of an easy-to-use, microprocessor-controlled scalar network analyzer (SNA) from Hewlett-Packard. The instrument, model 8756A (Fig. 1), has been designed to perform these once-difficult tests over frequencies from 10 MHz to 26.5 GHz in coaxial setups, and to 40 GHz in waveguide.

The scalar network analyzer has a dynamic range of +10 to −50 dBm in all three of its input ports. Two completely independent measurement channels are provided for simultaneous displays of such parameters as transmission and reflection. The instrument's dynamic accuracy is ±0.1 dB (+0.01 dB/dB) from +10 to −40 dBm and ±0.2 dB (+0.02 dB/dB) from −40 to −50 dBm. The display resolution of the front-panel CRT can be selected from a choice of 0.1, 0.2, 0.5, 1, 2, 5, 10, or 20 dB/division, and is independently controlled for each measurement channel. Offset power levels can be adjusted from −70 to +20 dBm for absolute measurements or from −90 to +90 dB for ratio analyses. The scalar network analyzer requires that test input signals be modulated with square-wave AM at 27.8 kHz. This modulating signal can be obtained from the 8756A and is also built into the HP8350B sweeper and 8340A synthesizer.

The 8756A SNA will execute microwave measurements when connected to a suitable signal source, directional bridge and diode detector. Measurement traces are displayed on the front-panel CRT, which also gives the status of input selections and reference levels. In addition, when the frequency source is an 8340A synthesizer (see *Microwaves*, October, 1982, p. 114) or an 8350B sweep oscillator (see "Sweep oscillator gains five more modules," p. 142), frequency data will also be displayed on the screen. With these particular signal sources, two different frequency or power ranges can be swept and displayed simultaneously.



1. The 8756A scalar network analyzer *makes transmission loss and gain measurements from 10 MHz to 40 GHz with 40-dB directivity.*



2. This graph of a filter's transmission and return loss *was generated with an HP7470A digital plotter connected directly to the SNA.*

Every bit helps

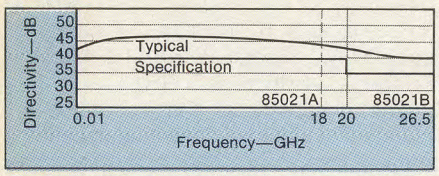
Digital circuitry (based on a Motorola 68000 microprocessor) accounts for the SNA's simplicity of operation. Basic measurements can be made using as few as five keys. Another group of keys adds functions such as "open/short calibration," "plotting," "cursors," and "averaging." The active function of each of these "soft" keys is always available for monitoring on the CRT. The digital memory of the SNA is such that the instrument can perform many of the functions of a system controller. For example, sweep limits and marker frequencies from a suitable sweeper or synthesizer can be stored in the SNA's memory for access at a later time. The SNA can also be used to command a digital plotter to precisely reproduce the information appearing on the CRT. Figure 2 is an actual SNA plot from an HP7470A plotter.

(continued on p. 141)

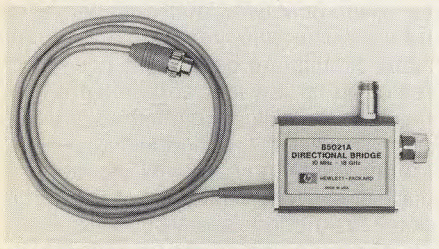
Cursors on the CRT can be moved along a transmission loss, gain trace, or return-loss response in order to discern both magnitude and frequency readings at a given point. Minimum and maximum points can also be determined automatically, through the use of "cursor min" and "cursor max" functions. When a "cursor Δ" function is selected, the magnitude and frequency difference between any two points on a measurement trace is calculated automatically and displayed. To minimize the effects of noise than can occur when testing at low signal levels, the 8756A SNA includes averaging circuitry, which divides data acquisition into a series of successive sweeps: from as little as 2 to as many as 256. In operation, successive sweeps of 1/n of a loss or gain reading are taken and stored in memory until the sum of these 1/n parts converges on the actual value of the measurement. Traces are stored and normalized to a resolution of 0.006 dB, regardless of the scale selected or the level offset chosen.

Since the use of an SNA involves accurate directional bridges, several models have been developed in conjunction with the model 8756A (Figs. 3 and 4). Model 85021B covers the full coaxial band from 10 MHz to 26.5 GHz, with 40-dB directivity to 20 GHz and 34 dB directivity to 26.5 GHz. Its test port is an

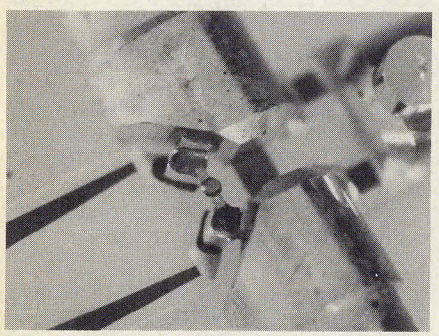
(concluded on next page)



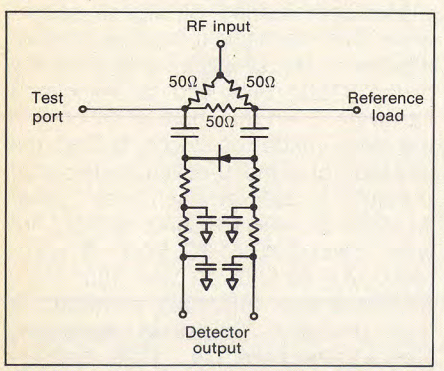
***3. Typical directivity** for the SNA's bridges generally exceeds the rated specification of 40 dB.*



***4. A series of directional bridges** was developed to meet the high-directivity needs of the 8756A SNA. One model is shown here.*



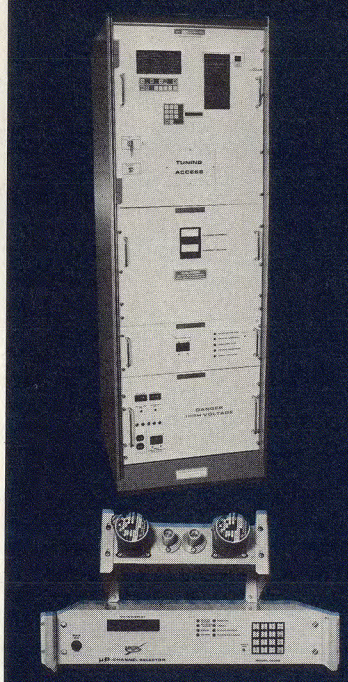
***5. Precision machining was required to produce bridge transmission section.** The arm trailing off to the right is the transmission line from the test-signal input port. The arm at the top left runs to the test port, while the arm at the lower right leads to the reference load.*



***6. This circuit defines the elements** needed by the directional bridges.*

SELECT MCL

KLYSTRON HIGH POWER AMPLIFIERS



Setting the pace with innovative design and engineering MCL offers the finest and most "Energy Efficient" satellite communication amplifiers for high power microwave transmission. Unsurpassed for reliability, unequalled for quality, earth station operators are selecting MCL with unequivocal confidence.

The versatile Klystron Amplifier line Series 10000 is field-proven, constructed for long life, easy access, with solid state power supplies and a host of other needed, tested, exclusive features. The Klystron Amplifier shown is M/N 10667-3.35KW C-Band high gain with microprocessor interface, the latest in the continuously evolving line of MCL's State-of-the-Art Satcom transmitters. Options include the M/N 13049 microprocessor controlled Channel Selector unit.

Used throughout the world, the desirability of MCL microwave transmission equipment constantly grows. This includes Satcom C-and Ku-Band TWTA's (75W-3KW), instrumentation TWTA's, Satcom and instrumentation KPA's, and coaxial low frequency transmitters.

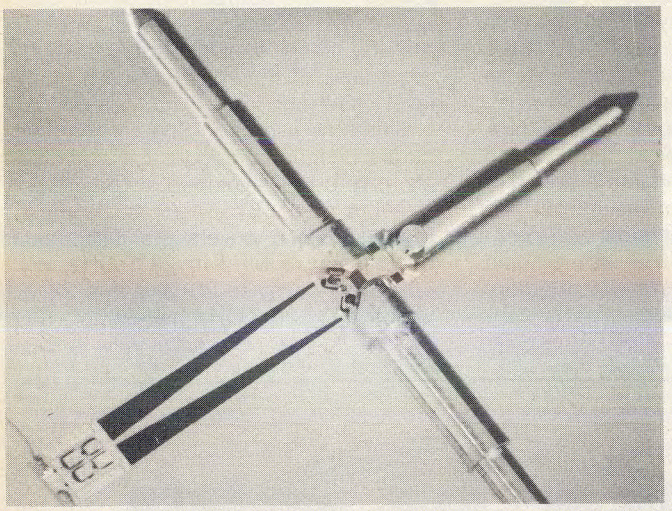
MCL assures you of 24 hour maximum parts replacement; provides 24 hour-7 day access to MCL personnel for assistance in installation or servicing.

WRITE for complete illustrated, technical reference brochure. SELECT "MCL", you'll be glad you did.

MCL, INC. Ten North Beach,
La Grange, Illinois 60525
(312) 354-4350 TWX 910-683-1899

MCL

READER SERVICE NUMBER 89



7. Contoured balanced resistors *(bottom, left) were used in the bridge circuit to help isolate the detection system from the microwave circuitry.*

APC3.5 connector. Model 85021A handles frequencies from 10 MHz to 18 GHz with 40-dB directivity, using an APC7 connector as its test port. Because it has a type-N connector, model 85021C has lower directivity (36 dB from 10 MHz to 12 GHz, 34 dB to 18 GHz). For RF work, models 85020A (50-ohm) and 85020B (75-ohm version) with type-N connectors have 40-dB directivity for the ranges from 10 MHz to 3.0 GHz and 10 MHz to 2.4 GHz, respectively. (Directivity of the 50-ohm bridge is 34 dB to 4.3 GHz.)

The directivity of these bridges includes the inherent contributions of the connectors, so much attention was given to the bridge circuitry to minimize its effects on the overall directivity. Since large mechanical geometries offer excellent directivity at the expense of transmission line moding, and small scale circuits are capable of good port matching for low loss and detector flatness but are difficult to machine, a compromise was reached in the final design. Moding was placed well above the upper frequency limit and, at the same time, the design is reproducible. Even so, the precision of the machining required should be apparent from the bridge circuit in Fig. 5; a simplified schematic diagram of the equivalent circuit is shown in Fig. 6. Any deviation between elements in the two arms which serve as transmission lines to the reference and test ports (see Fig. 7) will degrade directivity. The mechanical tolerances of these arms are 3.5 ± 0.005 mm o.d. (outside diameter) and 1.20 ± 0.0025 mm i.d. (inside diameter).

In order to meet these machining needs, parts matched to better than 1.2 μm are produced. Laser microscopes are used to measure these tight tolerances and a variety of machining techniques are employed to cut the parts, including turning, milling, and wire electro-deposit machining (wire EDM). Wire EDM is a numerically controlled process by which a current-charged cutting wire is used to shape metal parts with very fine tolerances.

The combination of digital, microwave, and mechanical engineering contributes to the simplicity and accuracy of the 8756A SNA and its associated hardware. Even the chore of calibration has been made fool-proof through the inclusion of a menu-driven routine that prompts a user at each step. P&A: $11,000, 8 wks. (8756A); $2,800, 12 wks. (85021B); $2,500, 8 wks. (85021A); $2,650, 12 wks. (85021C); $1,050, 8 wks. (85020B); and $950, 8 wks. (85020A). **Inquiries Manager, Hewlett-Packard Co., 1820 Embarcadero Rd., Palo Alto, CA 94303. (415) 857-1501.** **CIRCLE NO. 233**

Sweep oscillator gains five more modules



A logical choice for signal source with Hewlett-Packard's model 8756A SNA will be the HP8350B sweep oscillator. Besides offering one RF plug-in with the same 10-MHz-to-26.5-GHz bandwidth as the 8340A synthesizer, the sweep oscillator's RF modules provide a certain amount of flexibility. The recent addition of five more plug-ins (bringing the total to 32) improves frequency coverage even further.

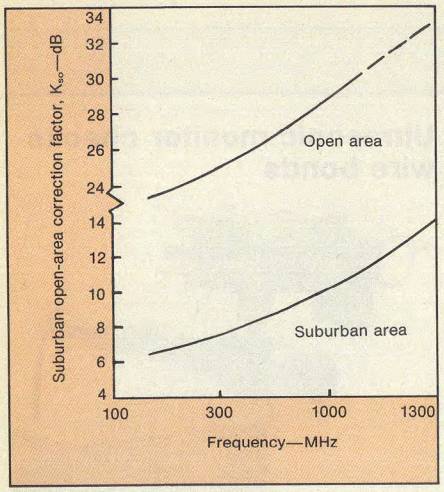
Millimeter-wave frequencies are generated by model 83572A, which operates from 26.5 to 40 GHz with at least +3 dBm unleveled output power. When regulated power is required, a minimum of +2 dBm leveled power is available. The frequency accuracy is ± 100 MHz in the CW mode, and frequency is stable with temperature from 20 to 30°C within ±8 MHz/°C.

The most wideband of the five new modules is model 83592B, with a span from 0.01 to 20 GHz. It can provide at least 20 mW of leveled power up to 18.6 GHz and 10 mW up to the frequency band edge. Its frequency accuracy is ±5 MHz in the CW mode, and is stable with temperature by ±600 kHz/°C up to 20 GHz and ±200 kHz/°C below 7 GHz.

The remaining RF modules are models 83525B, 83540B, and 86251A, which cover the frequency ranges from 0.01 to 8.4 GHz, 2 to 8.4 GHz, and 7.5 to 18.6 GHz, respectively. The first two offer harmonic levels of less than −45 dBc from 2 to 8.4 GHz and (in the 83525B) less than −25 dBc from 0.01 to 2 GHz. The remaining plug-in, expressly intended for ECM and EW testing, provides at least 10 mW leveled output power across the full band. It is stable with temperature by ±1.5 MHz/°C.

P&A: $14,540, 16 wks. (83572A); $26,580, 12 wks. (83592B); $15,540, 4 wks. (83525B); $10,280, 4 wks. (83540B); $10,780, 12 wks. (86251A); and $4,565, 2 wks. (8350B mainframe). **Inquiries Manager, Hewlett-Packard Co., 1820 Embarcadero Rd., Palo Alto, CA 94303. (415) 857-1501.**

CIRCLE NO. 234



8. These correlation factors can be used with the curves of Fig. 7 to calculate free-space losses *at various distances from the transmitter and at different frequencies.*

signing a total system. Table 1 offers a comparison among various 30.4-m sections of coaxial line. At 800 MHz, dielectric losses in coaxial cable are more severe than at longer wavelengths. For example, RG-58C coaxial line shows a loss of 4.9 dB/30.4 m. Typical 4-m mobile-communication runs call for losses of only about 0.65 dB. If the RG-58C line were to be used at 800 MHz, a 4-m section would lose about 2.5 dB of signal. Thus, lower loss cables should always go into the design of an 800-MHz system.

Power radiation characteristics change with the type of braiding found in coaxial line. Single-braid shielded cable will radiate 10,000 times (40 dB) more power at 800-MHz than a double-braided line, precluding its use in land-mobile communications. A cable such as RG-142B should be a minimum standard for 800-MHz land-mobile radio. For multiple radio installations or situations where transmission-line leakage must be controlled, 0.2-in. Heliax is a good choice. At fixed station locations, runs in excess of 10 m and less than 30 m should employ 0.875-in. foam solid sheath cable. If a run is more than 30 m and less than 60 m, go with 1.625-in.-diameter foam solid sheath cable. Beyond 60 m, 1.625-in. air solid-sheath coaxial line is a good choice. In general, when considering cable, its additional signal loss (in dB) due to VSWR can be determined by the following equation:

$$L_{VSWR} = 10 \log_{10} \frac{(VSWR+1)^2}{4(VSWR)} \quad (6)$$

Analyzing free-space loss

In a mobile-communication system, some signal strength will be lost via free-space attenuation. When first Fresnel-Kirchhoff clearances are obtained in the system, the free-space loss can be computed by the following relation:

$$L_{FS} = 34.2 + 20 \log_{10} \times f(MHz) + 20 \log_{10} d(km) \quad (7)$$

Of course, many land-mobile systems do not achieve this clearance over various portions of their coverage. To improve the validity of calculations in this case, a model must integrate geometric diffraction and refraction in addition to considering energy absorption.

Some free-space losses that commonly occur are listed in Table 2. These theoretical levels offer basic guidelines, but should not be taken as accurate representations of what is actually taking place. A pioneer 1977 study by Watson in Illinois found that the mean-wave propagation loss at 800 MHz was 14 dB greater than that predicted by the free-space/Bullington model.[5] Rural areas showed an increase (over theory) of 19.5 dB in mean propagation loss. Areas that were semi-urban, that is, with a fair amount of large, densely packed buildings, were 25.4 dB above calculated levels. Figure 6 shows a comparison of attenuation values with free-space Bullington model calculations at a rural test site for a single radial measured at distances of 13 to 50 km from the transmitter. Correlation between theory and fact does occur, but only up to distances of 16 km. In fact, at 800 MHz, variations from free-space predictions of as much as 25 dB are not uncommon. There is a general trend for signal levels to increase in variation from free-space values the farther a mobile unit is from the transmitter site, which is in contradiction to the 6-dB/octave slope that free-space theory predicts. The rate of signal decrease does not appear to change significantly with increasing aerial height, although the added height does tend to decrease path attenuation. The gain with height follows a 6-dB/octave slope for heights up to about 200 m.[6,7] Above this, and at radial distances of greater than 30 km, the gain looks more like a 9-dB/octave slope. Figure 7 presents Okumura curves for the basic median attenuation relative to free-space predictions in an urban area.[8] The base-station height is set at 200 m, and by applying a 6- or 9-dB/octave gain slope, losses can be calculated for other heights. Figure 8 presents correction factors for open and suburban areas.

A form of loss not considered in basic theory is foliage attenuation, which should be treated as an additional diffraction loss. Studies have shown that attenuation variations as great as 10 dB can occur between summer and winter months.[9] Therefore, in compiling system parameters, the most accurate evaluation should rely on a minimum correction factor of 10 dB for foliage attenuation.

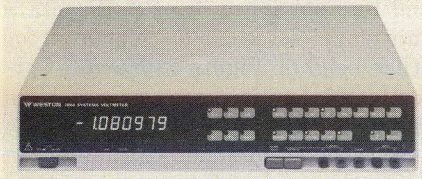
Thus, the construction of a land-mobile communication system involves the evaluation of a great many variables. One of the best approaches to system design is to put together a worksheet listing such things as foliage attenuation, variation from free-space theory, etc., and then to total the losses and variations. To receive a sample copy of such a land-mobile worksheet, simply send a self-addressed envelope with $0.20 postage to Cathy Fedele, *Microwaves & RF*, 50 Essex St., Rochelle Park, NJ 07662.●●

References

1. H. Jasick, ed., *Antenna Engineering Handbook*, First Edition, McGraw-Hill, NY (1961).
2. ITT, *Reference Data for Radio Engineers*, Sixth Edition, Howard W. Sa & Co., pp. 29-1, 29-2 (1975).
3. Cy Lee, *Mobile Communications Engineering*, McGraw-Hill, NY, pp. 38-40 (1982).
4. N.H. Shepard, *UHF Radio Wave Propagation in Dallas, Texas*, General Electric, R-75MRO-1 (March 5, 1975).
5. Jack T. Watson, *800 MHz and 900 MHz Land Mobile Developmental Tests*, Illinois State Toll Highway Authority (January 10, 1978).
6. W.C. Jakes, Jr., ed., *Microwaves Mobile Communications*, Ch. 2, Wiley, NY (1974).
7. Ibid.
8. Y. Okumura, E. Ohmori, T. Kawano, and K. Fukuda, "Field Strength and Its Variability in VHF and UHF Land Mobile Service," *Review of The Electrical Communications Laboratories*, Vol. 16, pp. 825-873 (September-October, 1968).
9. Jakes, *Microwave Mobile Communications*, Ch. 2.

TEST EQUIPMENT

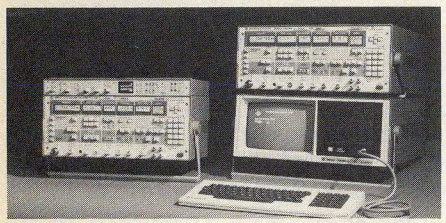
DMA serves as fast-response ATE voltmeter



Model 7060A is a low-cost programmable digital-multimeter (DMM) that makes voltage measurements from 200 mV to 1000 V with 5-1/2 digit resolution for a basic accuracy of 0.002 percent of the reading. The measurement speed of the device is typically 48 readings/s. By using the integrated GPIB bus, readings can be made at speeds of up to 320 readings/s. P&A: $2,995; stock. **Weston Instruments, 614 Frelinghuysen Ave., Newark, NJ 07114. (201) 242-2100.**

CIRCLE NO. 218

Mobile testers examine transceiver equipment



Models SMFP-2 and SMFS-2 are mobile test sets that are designed to make precision measurements of AM, FM, and phase modulation transceivers operating from 0.4 MHz to 1 GHz. The SMFP-2 is a programmable unit while the SMFS-2 is a semi-automatic set. The transceiver test units, which contain built-in oscilloscopes, feature RF voltmeters capable of measuring values from 1 mV to 100 V up to 1 GHz. **Rohde & Schwarz GmbH and Co., Muhldorfstrasse 15, D-8000 Munich 80, West Germany. (089) 4129-1.**

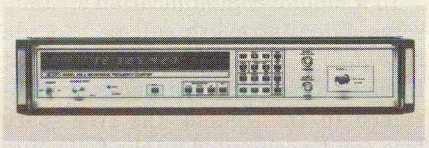
CIRCLE NO. 225

Low-cost DMM capable of eight functions

Model 8026B is a 3.5 digital multimeter with a basic DC accuracy of 0.1 percent. It can measure resistance from 0.1 ohms to 20 Mohms with resolution as good as 0.1 ohms. The unit also is capable of measuring AC voltage from 100 μV to 750 V. P&A: $219; stock. **John Fluke Manufacturing Co., Inc., P.O. Box C9090, Everett, WA 98206. (206) 356-5400.**

CIRCLE NO. 226

Frequency counter undergoes modifications



The model 545 frequency counter has gone through some changes lately. The 10-Hz-to-18-GHz counter is now available in a configuration that features an input YIG filter for frequency selective power measurements. This allows output power to be measured at the feedhorn test point for fast and simple adjustments of transmitter power levels on multiple carrier systems. Also, final power can be measured without having to switch off the modulation mode. The new configuration, designated model 545-W29, also includes a built-in power meter for direct power readings, and a burn-out protection circuit for 5-W overload insurance. P&A: $7,400. **EIP Microwave, Inc., 2731 North First St., San Jose, CA 95134. (408) 946-5700.**

CIRCLE NO. 223

Signal generator allows low-noise RF coverage

Model 9087 is a 10-kHz-to-1.3-GHz signal generator with outstanding spectral purity. Its single sideband noise is only -148 dBc/Hz at a 3-kHz offset from a 320-MHz carrier signal. The unit's broadband noise is only -150 dBc/Hz and harmonics are less than -35 dBc. Spurious signals range from -90 to -102 dBc, depending upon the carrier frequency. Power levels as high as $+19$ dBm at 1300 MHz are available; the signal generator features a 159-dB dynamic range with 0.1-dB resolution. Frequency resolution is 1 Hz across the full operating bandwidth. The device can operate with either external or internal AM and FM and external phase, pulse, and FSK modulation, with various simultaneous combinations possible. Frequency switching is less than 400 μs, with switching rates available up to 1 kHz. The output level accuracy is maintained throughout any switching operations. The digital sweep function permits sweeping and frequency stepping in increments as small as 1 Hz. A nonvolatile memory allows the storage of up to 100 complete front-panel settings. **Racal-Dana Instruments, Inc., 4 Goodyear St., P.O. Box C 19541, Irvine, CA 92714. (714) 859-8999, TWX: (910) 595-1136.**

CIRCLE NO. 222

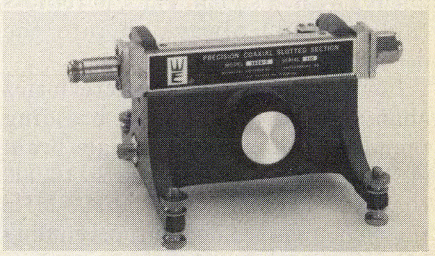
Ultrasonic monitor checks wire bonds



A laser ultrasonic monitor has been developed to measure the ultrasonic energy used in ultrasonic wire bonding. The system employs a He-Ne laser to measure the mechanical excitation of the bonding tool; it has the capability of focusing to a spot 0.001 in. in diameter. P&A: $10,000; 120 days. **Hughes Aircraft Co., Industrial Products Div., 6155 El Camino Real, Carlsbad, CA 92008. (619) 438-9191.**

CIRCLE NO. 224

Slotted line permits VSWR measurements to 18 GHz



Model 1024 is a precision coaxial slotted line designed for fixed and swept frequency VSWR measurements from 2 to 18 GHz. It has a characteristic impedance of 50 $\pm$ 0.1 ohms and a maximum residual VSWR of less than 1.01:1. The slotted line uses 7-mm coaxial connectors that comply with IEEE-STD-287. Interchangeable slotted sections are available with male or female type-N, SMA, or TNC connectors. The residual VSWRs for these sections are 1.02:1, 1.04:1, and 1.09:1, respectively. P&A: $1,125 (main assembly) and $875 (each slotted section); 90 days. **Weinschel Engineering, One Weinschel Lane, Gaithersburg, MD 20877. (301) 948-3434, TWX: (710) 828-9705.**

CIRCLE NO. 219

tent way to calibrate probes at these low frequencies." A TEM cell is also more realistic at these frequencies than a standard gain horn, which would have to be at a size that Aslin refers to as "overhead crane territory." A further point in their favor is their ability to restrict the enormous amounts of communications energy below 500 MHz from the calibration field.

Waveguide techniques are used from 500 MHz to about 1500 MHz. Aslin indicates that the waveguide must be customized for calibration purposes, explaining Narda "built a slide into the sidewall of the waveguide so that we can then probe the fields. By tuning the termination of the load, we can get a situation where there are almost no standing waves. And, by knowing the energy that we are propagating down the waveguide, we can establish the field strength."

At frequencies from 1500 MHz to 18 GHz, the calibration procedure is turned over to standard gain horns and a specially designed anechoic sled (Figs. 7 and 8). The anechoic sled makes it possible to average errors due to multipath interference and scattering from lossy materials. The probe calibration using the anechoic sled is very elaborate, and must be corrected for scattering errors. As Aslin describes it, "First we move the probe and the transmitting antenna together so that the spacing between them remains constant. The output of the received energy will follow a sinusoid on a horizontal line. Then we position the probe at a zero-energy crossover point and move the transmitter towards and away from the fixed probe. This gives us a sinusoid which is exponentially decaying as the horn moves away." The two curves of received power are then compared to derive a standard calibration field.

The last frequency calibration range is from 18 to 40 GHz. The Narda probes are generally calibrated only to 26 GHz, although special requests are honored to 40 GHz. The test setup includes a modified optical bench with millimeter-wave components that supply a field just large enough to accommodate one probe element at a time. Aslin explains that the optical bench is necessary to position each element accurately in the limited-size field. "We don't have adequate power to illuminate the entire probe with a uniform field," he says, "so we position each element into a known part of the field." The other elements are positioned so that they remain normal to the field, in order to minimize their detected contributions. Each element's output is measured, the mean is taken, and a calibration field is determined.

Radiation monitors will have a large role to play as more is learned about the long-term effects of exposure to nonionizing radiation. Accurate probes, created by careful designs and precision calibration practices, will work hand in hand with safety standards, such as those approved by ANSI, to familiarize engineers, the military, and the general public with the potential hazards of high-energy EM fields. Said Burton Gran, of Holaday Industries: "There's getting to be more of a concern on the part of everyone, simply because there is more microwave and RF in the general environment." Radiation monitors will help everyone coexist with that radiation in the years to come. ●●

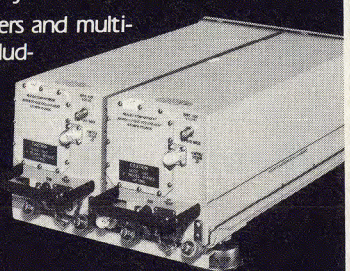
References

1. Paul S. Ruggera and Daniel H. Schaubert, "Concepts and Approaches for Minimizing Excessive Exposure to Electromagnetic Radiation from RF Sealers," US Department of Health and Human Services, Publication FDA 82-8192, pp. 1-4 (July 1982).
2. Samuel Hopfer, "The Design of Broad-Band Resistive Radiation Probes," *IEEE Transactions on Instrumentation and Measurement*, Vol. IM-21, No. 4, p. 416 (November 1972).
3. Edward Aslan, "Narda Radiation Monitor Calibration Technique," The Narda Microwave Corp., Hauppauge, NY.



Performance counts, and E-3A AWACS aircraft have counted on our UHF antenna multicouplers and filters to eliminate co-location interference, reduce spares costs, and improve system reliability.

AWACS is only one of our many programs. RF filters and multicouplers are used in programs around the world including the U.S. Army Guardrail, U.S. Air Force Rivet Switch, Royal Air Force Nimrod AEW and many other airborne, shipboard, mobile and stationary communications systems.



Meeting the test of time under the most severe operating conditions has provided us with the experience to meet your toughest RF communications requirements. If you'd like to know how we can help with your next program, please call or write today.

RF PRODUCTS, INC.
Davis & Copewood Sts.
Camden, NJ 08103
(609) 365-5500 • TWX 710-891-7087

READER SERVICE NUMBER 98

NEW PRODUCTS

PASSIVE COMPONENTS

Terminations touch 1-kW peak power levels

A series of terminations has been designed to handle frequencies from DC to 4.2 GHz with an average VSWR of 1.1:1. The terminations are constructed with either BNC or SMA coaxial connectors and will operate at temperatures from −25 to +85°C. Power dissipation is 0.5 W CW and 1-kW peak power. P&A: $5 and up; 30 days. **Elcom Systems, Inc., 4032 Clint Moore Rd., Boca Raton, FL 33431. (305) 994-1774.**

CIRCLE NO. 209

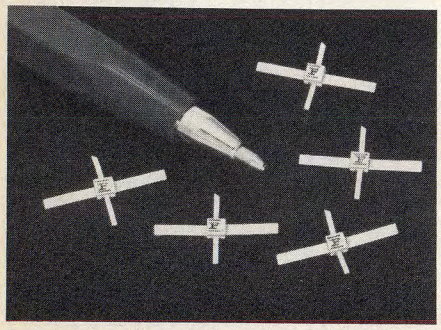
Power dividers are eight-way splitters

A series of eight-way power dividers offers in-phase operation from 0.5 to 18 GHz. Standard models are shipped with SMA female connectors. A typical model, YE-41, works from 4 to 8 GHz with an insertion loss of 1.2 dB, isolation across the band of 16 dB, phase balance of ±5 degrees, and input/output VSWR of 1.55:1. **Triangle Microwave, Inc., 60 Okner Pky., Livingston, NJ 07039. (201) 740-0100, TWX: (710) 986-8202.**

CIRCLE NO. 204

TRANSISTORS

High-gain FETs serve X-band applications



Two high-gain FETs have been developed for amplification chores at 12 GHz. Model FSX100X is a chip transistor, while model FSX100FA is a packaged version of the FET. The chip transistors feature small-signal gain of 8.5 dB and power output at the 1-dB compression point of +12 dBm output at 1-dB compression. Both transistors have storage temperatures from −65 to +175°C. **Fujitsu Microelectronics, Inc., Microwave and Optoelectronics Div., 3080 Oakmead Village Dr., Santa Clara, CA 95051. (408) 980-8585, TWX: (910) 338-2324.**

CIRCLE NO. 228

ECM

Here at NORTHROP DSD, our energies are focused on the continued development of the most sophisticated electronic countermeasures systems in the world. Perhaps that is the reason "ECM" and "NORTHROP" are synonymous.

We offer exciting challenges to talented engineers with expertise in any of the following specialties:

Electrical Design/Development Engineers

BSEE, or equivalent; background in design/development and proposal preparation in one of the following areas:

Microwaves: Active/passive microwave integrated circuit design (2-26GHz), YIG oscillators, filter detectors, wave guides, high frequency solid state amplifiers and S-parameters.

Receivers: Receiver components/subsystems; RF design to 26 GHz (I-J bands), system architecture, receiver signal processing, oscillator design/specification.

Send resume with salary requirements to: **Manager, Professional Employment.**

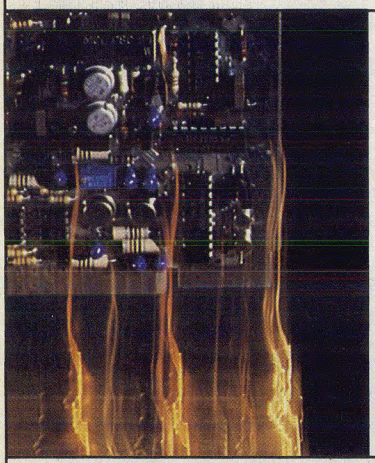
NORTHROP CORPORATION
DEFENSE SYSTEMS DIVISION
500 Hicks Road, Rolling Meadows, IL 60008

We are an equal opportunity employer, and encourage minorities, females, veterans and the handicapped to apply.

NORTHROP
MAKING ADVANCED TECHNOLOGY WORK

Microwaves & RF

APRIL 1983 • VOL. 22, NO. 4



cover feature

101 Comstron lures OEMs with modular synthesizer. Comstron Corp. introduces its 1200 series of compact, reliable, low-noise frequency synthesizers. The new design makes extensive use of digital techniques and modular circuits. (Photo courtesy of Douglas Samuel Advertising, Inc., West Caldwell, NJ)

departments

13 Feedback
17 Editorial
55 R&D Roundup
62 For Your Personal Interest
100 Bookmark
150 Infocenter
152 Looking Back
152 Looking Ahead

news

28 Police enhance radar systems in response to public outcry. The new standards are bringing speeders down to the courthouse again.

35 High-resolution wideband radar adds new dimension to imaging
45 MMICs fare well at the 1983 ISSCC

19 The Front End • **43** Financial News • **58** On the Agenda • **60** People

design features

64 Exotic Geometries Yield High-Fidelity Chaff. Richard M. Berg, from the US Army Mobility Equipment R&D Command, zeroes in on the polydeltatrihedron.

73 Numerically Modeling Sea Backscatter Coefficients. David Abraham, of Tracor, Inc., calculates SBCs for grazing angles up to 60-degrees and sea states up to 7.

75 Harmonic Gunn Oscillators Allow Frequency Growth. K. Solbach and colleagues, from AEG-Telefunken, demonstrate how second-harmonic generation overcomes frequency barriers as well as cost.

83 PIN-Diode Driver Allows Linear RF Attenuation. Gary M. Homer, of E-Systems, Inc., develops a circuit that provides a linear curve of attenuation versus control voltage input.

87 Two-Cavity Klystron Uses Single-Cavity Tuning. Antonio Muratore and colleagues, from Italy's Microwave Tubes and Components Lab, uses a new approach to eliminate two-cavity tuning.

93 Digital Modulation Techniques Compared. Bernhard E. Keiser, a consulting engineer, shows how hardware and transmission medium influence your choice of methods.

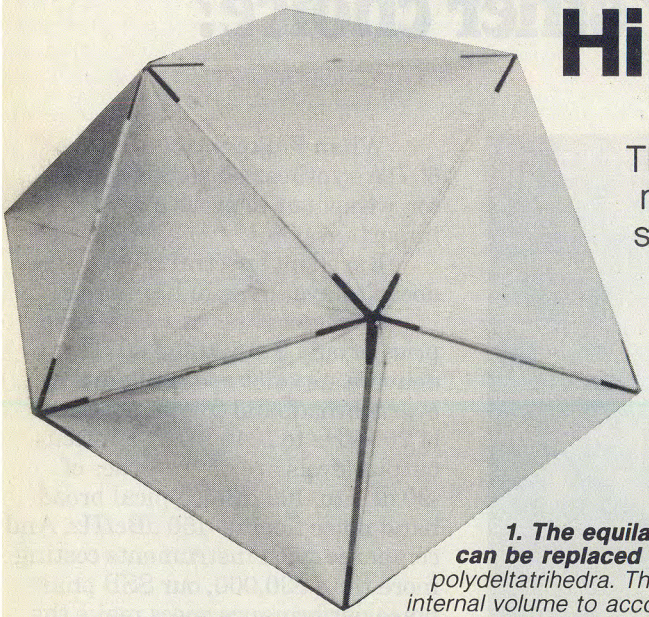
product technology

107 Closed-loop YIG filters stay on frequency. Allen E. Rosenzweig, of Ferretec, Inc., explains how closed-loop locking can increase YIG-filter stability.

121 Blind-mating connectors cure modular system woes. John Morelli and William Pitcher of Automatic Connector, Inc., describe the miniaturization of spring-loaded, blind-mating coaxial connectors . . . **Features—105** Computer-science techniques hatch new circuit-analysis library . . . **116** Economical group-delay analysis . . . **118** Quick-time pulse inversion . . . **119** Liquid crystals aid microwave analyses

130 New Products • **146** Application Notes • **148** New Literature

Exotic Geometries Yield High-Fidelity Chaff



The author is working to bring passive countermeasures down to earth. Although the answer seems to be the polydeltatrihedron, the search continues for the most efficient structure.

Richard M. Berg, US Army Mobility Equipment R&D Command, DRDME-ND, Fort Belvoir, VA 22060.

1. The equilateral triangles of a deltahedron can be replaced by deltatrihedral cavities *to produce polydeltatrihedra. The original deltahedron must have enough internal volume to accommodate the cavities.*

CHAFF has been used as an airborne countermeasure since the inception of radar. Passive EW devices are now being developed to give ground forces a similar capability for camouflage and deception (Fig. 1). These devices can be used against surveillance radars to enhance clutter or against "fire and forget" missiles and munitions to shift the centroid of a target's radar cross section. Structures for "clutter clusters," as these devices are called, must be small enough to transport, assemble easily in the field, and produce radar returns that are indistinguishable from those of real targets. In short, they must provide the largest broadband radar cross section from the smallest possible surface area.

The principal uses of these clutter clusters require them to act as omnidirectional radar targets that bounce a large amount of incident energy back in the direction from which it came. In the past, clutter enhancement devices have taken the form of one of the classical eight-cornered octaheda or corner reflectors (see table).[1] Although they have been used for decades as navigation aids, calibrating targets and, in some cases, decoys, all of these reflectors have deep directionally dependent nulls in their returns.* However, corner reflectors can be combined into larger structures to overcome this deficiency.

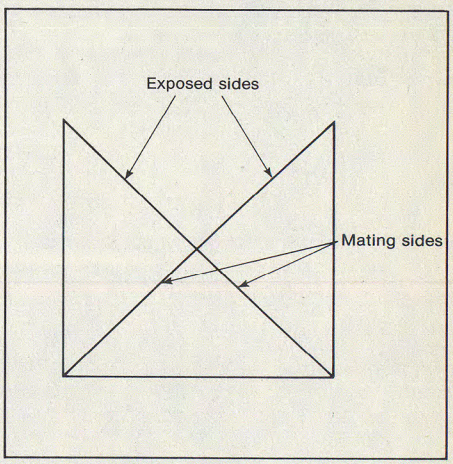
The basic corner reflector consists of three mutually perpendicular planes known collectively as a trihedron. The trihedron having equilateral triangles as its frontal face projections (the "triangular corner reflector" in the table) has particular advantages as a building block for clutter clusters. This trihedron is known as a deltatrihedron and is formed by the assembly of three right isosceles triangles (Fig. 2). The edges along which the sides of two triangles meet is assumed to be hinged (or otherwise able to bend or fold) so that the exposed edges of the left and right triangle can be joined and fastened.

Creating a multicavity structure

The triangular face projection of the deltatrihedron coincides with the principal features of a unique class of polyhedral solids, the deltahedra family. The deltahedra have their face-plane polygons in the form of equilateral triangles. If convex deltahedra or antiprisms** can be found with enough internal volume, their triangular faces can be replaced by trihedral cavities that will efficiently reflect incident radar signals. Figure 1 shows a 20-cornered polydeltahedron produced in this way. Note that the projected face planes of this cluster remain equilateral triangles.

*The table assumes, as does the remainder of this article, that the wavelength of the incident energy is considerably smaller than the dimensions of the devices and, therefore, can be analyzed according to optical theory.

**Antiprisms are polyhedra that have two congruent and parallel faces joined by a set of triangles that form the sides of the solids. Of principal interest in this discussion are the equilateral triangles of the antiprism. For this reason, they are grouped with the deltahedra family here.[2]



2. Deltatrihedra are made up of three right isosceles triangles. *The mating edges at the sides of the triangles are assumed to be hinged so that the exposed edges can be joined.*

With the exception of the 10- and 12-surfaced deltahedra, all of the polyhedra in the deltahedra family can be internally packed to form polydeltatrihedra. Furthermore, a very compact array can be derived from a 12-sided antiprism. Since the equatorial belt of this antiprism consists of 12 equilateral triangles, and its open ends are hexagons, each hexagon being divisible into six additional equilateral triangles, a continuous disk-shaped, 24-cornered polydeltatrihedron is formed (Fig. 3). This configuration, which has earned the tongue-twisting name of tetraicosadeltatrihedron, can easily be expanded by adding alternating triangles to the equatorial belt. The shapes can also be stacked. In this way, cylindrical polydeltatrihedral arrays of any size can be created, such as the 36-cornered cylinder shown in Fig. 4.

Multifaceted, omnidirectional corner reflectors need not be limited to equilateral triangles. In certain bistatic radar applications, polyhedra not having equilateral triangles as face planes may be advantageous for space filling. For example, facets in the form of isosceles triangles can also be used; however, such arrays are not as convenient to fabricate and assemble.

Simplified techniques needed

As the desired, multifaceted clutter clusters are created, their geometries soon become unwieldy. To make these devices practical, simpler methods must be used to derive and construct them.

Properties of corner reflectors

Type	Peak echo area	Principal coverage region	Average echo area (all aspects)
Square corner reflector 	$\frac{2\pi d^4}{\lambda^2}$	Cone of 23 degrees total included angle about axis of symmetry (3-dB-down points).	$\frac{0.7l^4}{\lambda^2}$
Circular corner reflector 	$\frac{15.6l^4}{\lambda^2}$	Cone of 32 degrees total included angle about axis of symmetry (3-dB-down points).	$\frac{0.47l^4}{\lambda^2}$
Triangular corner reflector 	$\frac{4\pi l^4}{3\lambda^2}$	Cone of 40 degrees total included angle about axis of symmetry (3-dB-down points).	$\frac{0.17l^4}{\lambda^2}$
Spherical Luneberg lens reflector  Conductor	$\frac{2\pi d^4}{\lambda^2}$	Cone of approximately 150 degrees total included angle about axis of symmetry (3-dB-down points). Appreciable return over 180-degree cone.	$\frac{2d^4}{\lambda^2}$

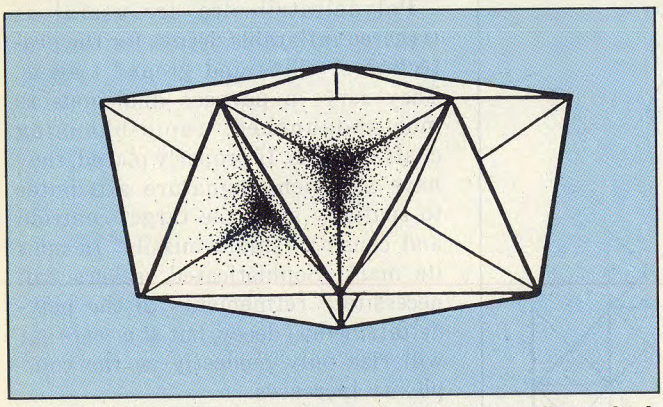
Figure 5 illustrates one such method. All of the complex polydeltahedral clusters can be separated at any edge and, when laid flat, formed into a two-dimensional pattern of alternating triangles. These two-dimensional patterns are the "planar networks" for the three-dimensional solids.

The process, of course, works just as well in reverse. By replacing each equilateral triangle in the planar network of a deltahedra or antiprism with the deltatrihedral network of Fig. 2, a polydeltatrihedral network results. (An example for the icosadeltatrihedron is shown in Fig. 6.) This method of developing more complex solids can be applied to any valid convex deltahedra and to the entire family of semiregular antiprisms.

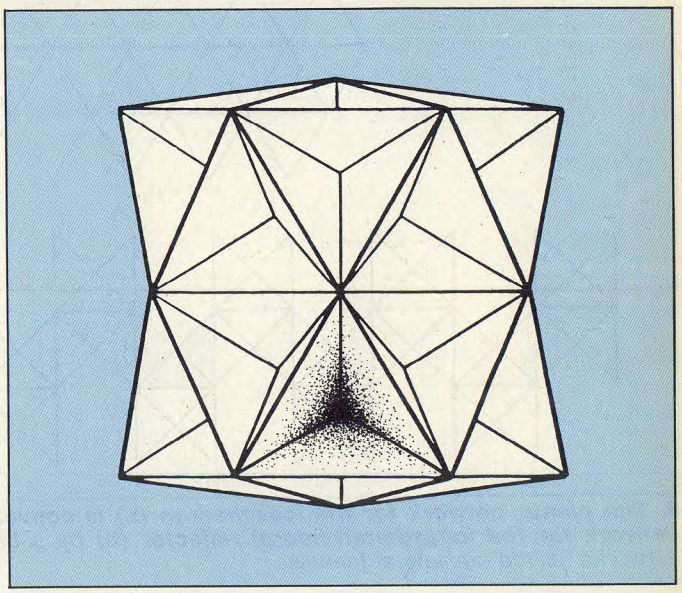
In general, the polydeltatrihedral arrays are formed from these networks by lifting forward (up) on the diagonal edges and by pushing back (down) on vertical and horizontal edges. In practical devices, edges can be affixed by hinges and pins for rigid structures, and heat sealed if the material is a metallized or reflective plastic laminate. In the latter instance, air-tight inflatable devices can be made that possess blackbody radiator properties and serve as microwave/millimeter-wave/IR decoys. Polarization scattering similar to that produced by actual targets can also be accomplished by etching a grid network into the surface of the conducting/reflecting layer.

Nonrigid structures can exhibit inherent deficiencies. If the three mutu-

(continued on next page)



3. Antiprisms with face planes formed by equilateral triangles *can also be the basis of polydeltatrihedra. The tetraicosadeltatrihedron is shown here.*

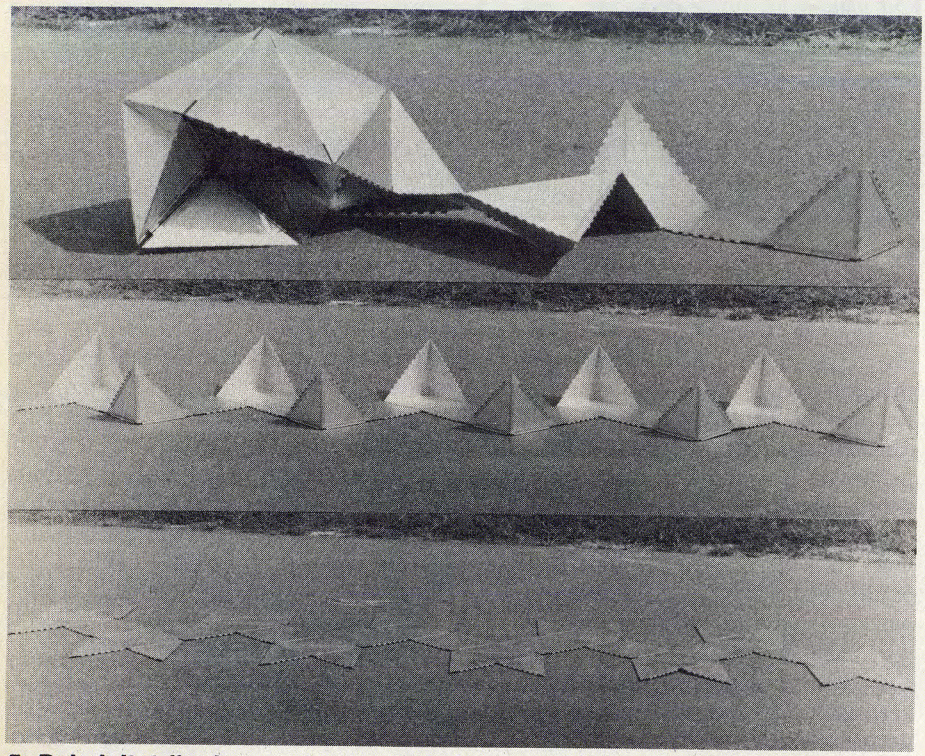


4. Polydeltatrihedra based on antiprisms *are often amenable to stacking.*

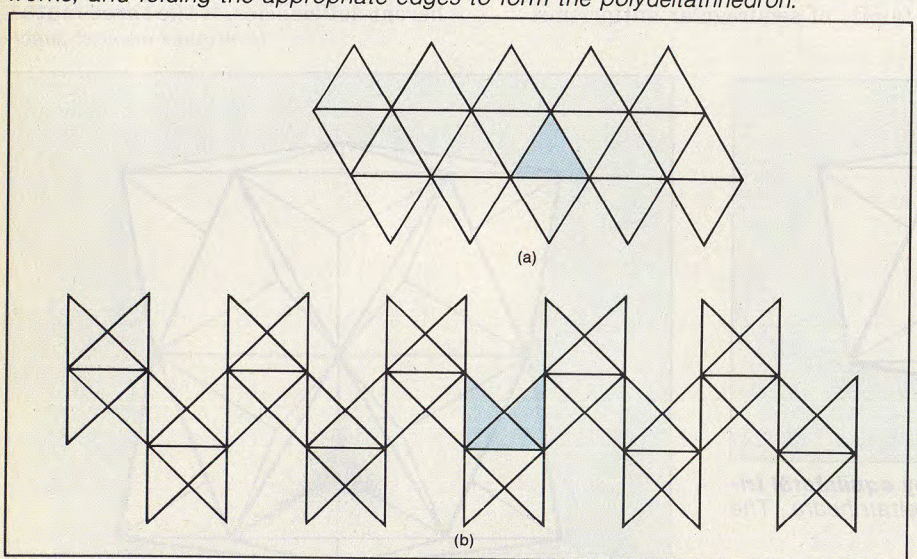
 (continued from p. 65)

ally perpendicular trihedral planes are not orthogonal, the internal reflections of the trihedral can be significantly degraded and the effective echoing area per cavity greatly reduced. This problem may occur in inflatables constructed with nonrigid planes, but the random nature of the effect distributed over several cavities may compensate for the losses it causes.

Tessellation, the repetition of a pattern of similar or dissimilar polygons, is another tool that aids in the development of clutter clusters. (Tessellation can also be called "tiling," and should be familiar to anyone who has ever laid down a kitchen floor.) Tessellation can be applied to the planar networks of the deltahedra and the antiprisms previously described to increase the number of cavities in a cluster. Of special interest is the internal tessellating properties of the equilateral triangle itself. By repeated edge bisecting and trisecting, the equilateral triangle can be subdivided into an infinite number of smaller equilateral triangles. A second order tessellation of a planar equilateral triangle is shown in Fig. 7 along with its associated tessellated deltatrihedral network. It is relatively simple to construct the N-ordered polydeltatrihedral networks and form a complex array having any number of corner reflectors and distributions. Examples of the tessellated icosadeltatrihedron are shown in Fig. 8.



5. Polydeltatrihedra can be separated at any edge and unfolded into a two-dimensional planar network. *The process can be used in reverse by starting with the planar network for a deltahedron, replacing its triangles with deltatrihedral networks, and folding the appropriate edges to form the polydeltatrihedron.*



6. The planar network for the icosohedron (a) is converted into the planar network for the icosadeltatrihedral reflector (b) *by substituting deltatrihedral networks for the equilateral triangles.*

Tessellation increases the number of scattering centers on the surface of the cluster and makes its return more closely resemble a real target. Interference is created among the returns from the reflecting corners. The cancellations and additions produce a return with a very fine structure. The final effect can be referred to as "high-fidelity" chaff.

The most desirable shapes for the clutter clusters leave no voids between their mating surfaces when they are combined into larger arrays. Some shapes don't have enough room for the internal corners and cause the exterior of the cluster to bulge. Metal models of a proposed configuration will often uncover this problem. One particular polyhedron, the truncated tetrahedron (four hexagons, four equilateral triangles), initially offered 28 deltatrihedral corners and, when it abutted a tetrahedron, completely filled space. Unfortunately, this ideal shape has insufficient internal volume and was abandoned.

Reflectors have many uses

Polydeltatrihedra are useful as tethered inflatable decoys for the protection of ships and ground targets. They serve a purpose analogous to mortar-launched, rapid-blooming chaff systems. If properly placed, they have sufficient signature attributes to spatially shift the target centroid and cause a "smart missile" to miss its mark. Sophisticated seekers will necessitate refinements to the polydeltatrihedral decoy, but at a cost that will rise only modestly as the complexity increases.

To counter high-resolution synthetic-aperture radar, numerous arrays can be connected to produce different shapes and simulate the return of a true target. Multiple scattering centers at different locations

(concluded on p. 70)

on the decoy can be accommodated by selectively placed second or greater ordered tessellations.

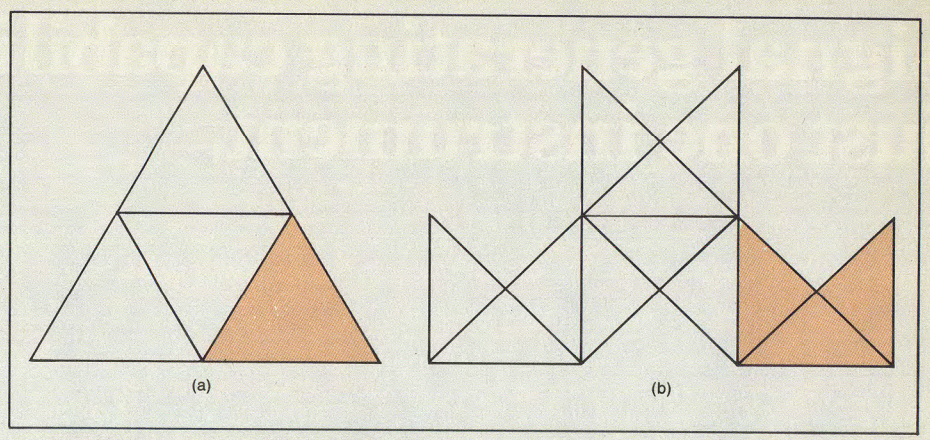
Polydeltatrihedra can also be employed as clutter enhancement devices to raise the CFAR (continuous false-alarm rate) threshold of area clutter-averaging radars.[3] Each polydeltatrihedra possesses a backscatter coefficient, σ^0, that can be obtained by the ratio of its tumble average radar cross section and its projected area. One might expect a tessellated icosadeltatrihedron to exhibit the highest backscatter coefficient but to date, none of these solids have been examined for this property except the octatrihedra.[4]

If practical, an area on the battlefield can be seeded to any desired density and the clutter level surrounding a target array can be increased. The quantity of discrete point clutter targets needed to raise the background level enough to degrade the MTI (moving target indicator) performance of a threat radar remains to be determined.

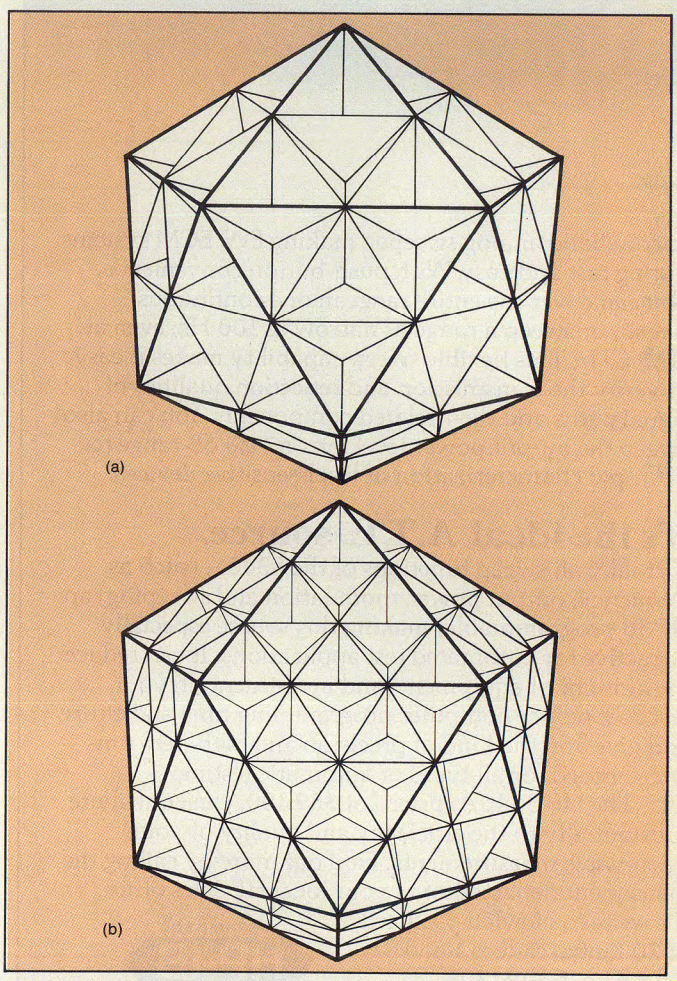
Certain of the polydeltatrihedra can be used as radar calibration targets and can even serve as models to specify radar performance. Traditionally, a radar is designed against a specific statistical target that any number of target shapes can satisfy. Since a polydeltatrihedron is a well-defined shape, a more deterministic approach can be taken and consistent comparisons between measured data and analysis made.

As a warning device that determines the direction of an active energy source, such as a laser target designator, each deltatrihedron can have a detector on one of its planes. When a target is illuminated by a laser, the energy in one particular cell will be greater than the adjacent ones, and the source of the laser can be determined by the spatial orientation of that cell on the polydeltatrihedron.

Finally, polydeltatrihedra can serve as navigation aids and hazard-warning devices for ground, sea, and space environs. It should also be noted that reflectors optimized for C-band radars are effective as sonar targets.●●



7. Tessellation provides a method of increasing the surface complexity *of a structure and, thereby, refining its radar return. Equilateral triangles lend themselves very well to tessellation. A second-order tessellation of an equilateral triangle (a) is shown with its companion deltatrihedral network (b).*



8. A second-order (a) and third-order (b) tessellation of an icosadeltatrihedron *show the effect of this technique. As the number of deltatrihedra on the surface increases, interference effects produce returns that more closely mimic real targets.*

References

1. L. Peters, "Passive Bistatic Radar Enhancement Devices," *Proceedings of the IEEE*, Vol. PTC-109, No. 15, (March 1962), also published as Monograph No. 455E (July 1961).
2. P. Pearce and S. Pearce, *Polyhedra Primer*, Van Nostrand Reinhold Co., New York (1978).
3. L.M. Novak, "Optimal Target Designation Techniques," *IEEE Transactions*, Vol. AES-17, No. 5, pp. 681-684 (September 1981).
4. D. Levine and W.H. Welch, "Spatial Coverage of Radar Reflectors," *IEEE Transactions*, Vol. AES-2, No. 2, pp. 160-165 (April 1964).

Numerically Modeling Sea Backscatter Coefficients

A numerical model has been developed to calculate X-band sea backscatter for grazing angles up to 60 degrees and sea states up to 7.

David Abraham, Principal Scientist, Tracor, Inc., 1601 Research Blvd., Rockville, MD 20850.

ESTIMATING sea backscatter coefficients (SBCs) is important in the design of radars for detection of sea targets because the SBC will determine how much RF energy the sea reflects and, thus, how much of a problem clutter will be. Since backscatter varies with grazing angle, or angle of incidence, a meaningful estimate of radar performance—attained by solving the radar equation—requires accurate SBCs for the range of grazing angles that can be expected in a specific application.

This article presents a numerical model for calculating SBCs at X-band for any grazing angle from 0.1 to 60 degrees and for sea states from 0 to 7. The model, which uses simple formulas, is based on previously published data that have been evaluated, edited, and updated.[1] These data, however, only include values for sea states up to 5 and for grazing angles of 0.1, 0.3, 1, 3, 30, and 60 degrees. In addition, the published tables (shown on page 136 as Tables 1 and 2) are incomplete, and some of the values are marked with a warning that "5-dB errors are not unlikely." Since the data show that backscattering is not a linear function of grazing angle, linear interpolation between and extrapolation of the tabulated values (see tables) are not considered acceptable.

Building the model

The numerical model was developed because a computationally adequate physical model was not available and the cost of developing one would have exceeded available resources. The method used to develop the model is presented because readers may be interested in trying to model other bands in the microwave spectrum.

Separate matrices of X-band SBCs for horizontally and vertically polarized waves were assembled in the tables and the differences between adjacent entries were determined. The differences between horizontally adjacent elements come close to having a regular pattern that could be expressed as a simple function of sea states:

$$\Delta = 7 - n \qquad (1)$$

where Δ is the difference in dB between the value for sea state (n) and the next higher sea state.

A reference value for an SBC at sea state 7 was selected for each grazing angle in the published tables. Equation 1 was then used to produce matrices of SBCs that were compared with the published matrices. Next, the reference values were adjusted to allow the new matrix elements to better fit the published data subject to two constraints:

- corresponding matrix elements for data without the published accuracy warning (shown by an asterisk in the tables) should differ by no more than 3 dB, and
- all other things being equal, the model should not underestimate the backscatter.

The resulting values are the ones used to make up the tables.

A comparison of the previously published data and the values derived from the model shows that all non-asterisked data are within 3 dB of the corresponding model values. Data marked with an asterisk are within 5 dB except for horizontal polarization at angles of 0.1 and 0.3 degrees and sea states of 1 and 2. For these exceptions, the model's SBCs predict greater backscatter than the admittedly questionable published values and thus would not lead to an overoptimistic estimate of radar performance. As a practical matter, the backscatter under those conditions is so small that it is negligible in the computation of the total signal-to-noise ratio used in target detection.

The last step in constructing the model was to fit the reference values of SBC (those selected for sea state 7) with continuous functions. Since three regions of grazing angles for X-band backscatter have been identified,[2] these three regions were used to cover the range from 0.1 to 60 degrees, with transition angles chosen to provide continuity in the three functions. All reference values fit to within 0.33 dB.

Final product

After the manipulation was complete, the following set of equations was developed, where GA equals grazing angle in degrees, SS equals sea state, SSN equals 7 − SS, and SUM equals SSN (1+SSN)2.

- For horizontal polarization:
  If GA $\leq$ 1.24:
  SBC = 30 + SUM − 12log GA
  If 1.24 < GA *$\leq$ 24.33:
  SBC = 29 + SUM − GA/10
  If 24.33 < GA $\leq$ 60:
  SBC = SUM + 32cos^2 GA

(concluded on p. 136)

Harmonic Gunn Oscillators Allow Frequency Growth

The authors describe the theory behind the operation of Gunn oscillators at the second harmonic as well as results obtained from a practical system.

K. Solbach, F. Sickling, and **H. Barth,** Radar Systems, AEG-Telefunken, Ulm, Federal Republic of Germany.

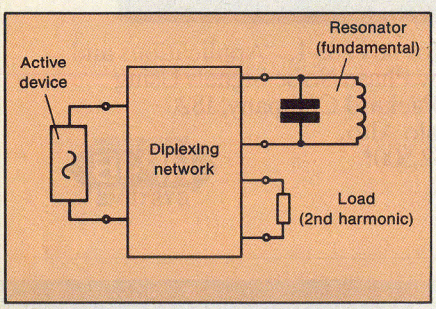
THE history of oscillator design has shown that whenever a technological barrier is reached in the struggle for higher frequencies one reasonable alternative to fundamental-mode oscillation always exists: harmonic generation. Such a barrier has been reached in the millimeter-wave spectrum. Because of their inherent material properties, GaAs Gunn elements will not allow operation above about 80 GHz. Although Indium-phosphide (InP) Gunn elements will go far beyond that no InP Gunn elements are commercially available.[1] Harmonic Gunn oscillators appear to be the solution.

Harmonic oscillation can be accomplished either in a separate stage (e.g., a varactor-multiplier) or in the oscillator itself. At millimeter waves, a second-harmonic oscillator typically is more efficient and cost-effective for second-harmonic generation. At higher harmonic orders, a varactor-multiplier often is more efficient, depending on the cut-off frequencies of the varactors available.

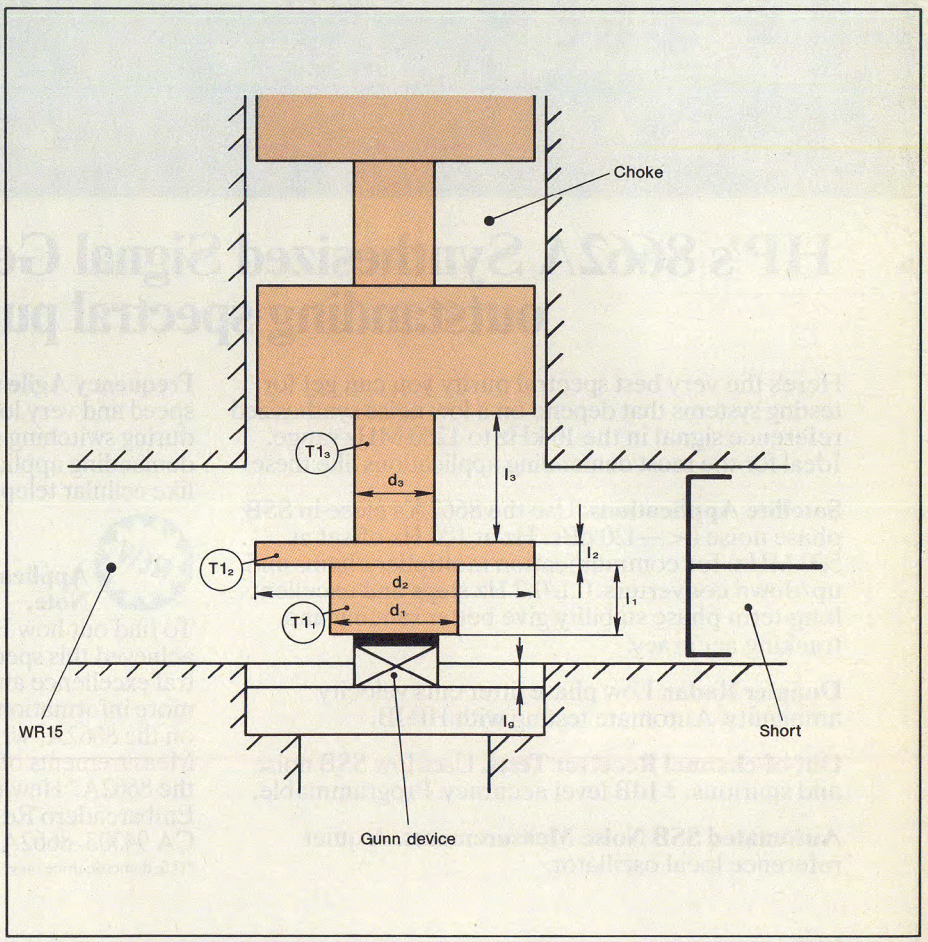
To provide low-noise power for such applications as local oscillators and master oscillators in power amplifier chains, second-harmonic oscillators for 75 to 110 GHz [2,3,4] and a harmonic oscillator up-convertor for 140 GHz[5] have been designed using conventional GaAs Gunn elements. These oscillators exhibit some interesting features: they are relatively low-noise, and they have much higher load-pulling stability than most fundamental-mode oscillators. In fact, these advantages have led to the development of a 60-GHz second-harmonic Gunn oscillator even though fundamental GaAs Gunn oscillators are feasible at 60 GHz.

Another advantage of second-harmonic oscillators is cost. For example, it is less expensive to generate 25 mW power at 60 GHz by using a 30-GHz Gunn element producing 100 mW nominal (fundamental) power than it is to use a currently available 50-mW fundamental-mode Gunn element at

(continued on p. 77)



1. The diplexing network of a second-harmonic oscillator *can be a conventional filter.*



2. In this cross-section of a typical second-harmonic oscillator for 60 GHz, the Gunn device is mounted in the broad wall of the waveguide. *The three-section transformer structure is designed to act as a resonator at the fundamental and as a matching transformer at the second harmonic. The moveable short is used to tune the imaginary part of the load impedance.*

60 GHz. Furthermore, since the technology of Gunn element preparation at 30 GHz is more mature, greater reliability and a longer life can be expected from 30-GHz devices than from 60-GHz devices.

Principle of operation

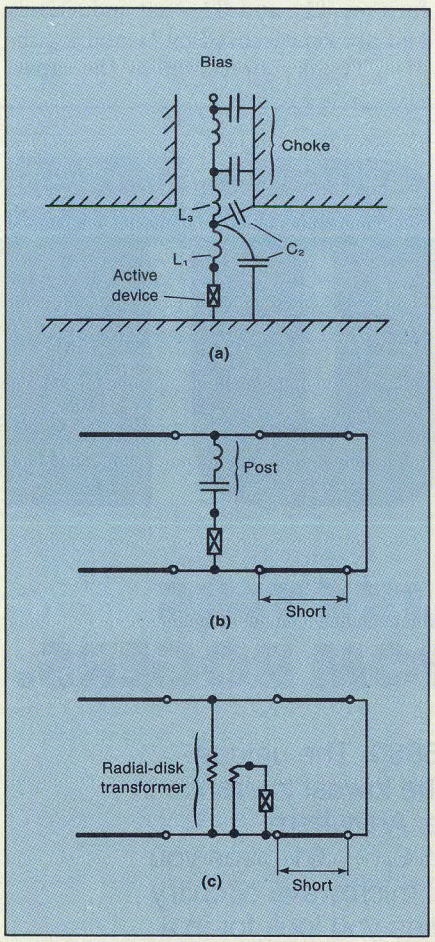
Recently, the basic principle of operation of a negative resistance element in a second-harmonic oscillator has been investigated.[6] The equivalent circuit for such an oscillator is shown in Fig. 1. The active device works into a resonator at the fundamental, and power is delivered to a load only at the second harmonic. The network performing the diplexing may be a conventional filter.

The desirable high Q of this circuit results from the fact that the fundamental-frequency resonator is greatly decoupled from the second-harmonic load. The oscillator thus has higher Q (less noise) and is less sensitive to load pulling (higher pulling Q).

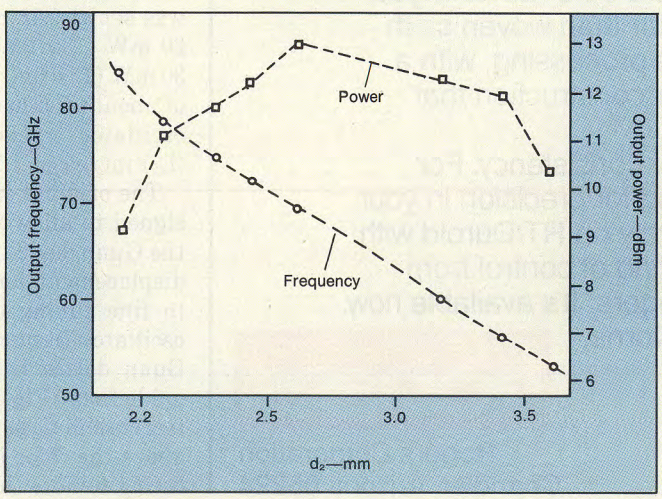
The investigation also revealed that the increase in the pulling Q is inversely proportional to the harmonic efficiency, which is the ratio of output power from the harmonic oscillator to the output power of a fundamental-mode oscillator employing the same active element. This relationship implies that a harmonic oscillator generally will not produce the same amount of power as a fundamental-mode oscillator. Harmonic efficiencies of about 10 to 20 percent are common in millimeter-wave oscillators yielding a Q-factor gain of from 7 to 10.

It was also determined that the source impedance of the harmonic oscillator circuit will be reduced by a factor of about two (depending on the voltage-current characteristic of the active device) compared to the fundamental-mode circuit. Thus, it will be more difficult to match the oscillator's second-harmonic port to the relatively high-impedance waveguide, since impedance must be transformed from 20 ohms to 400 ohms.

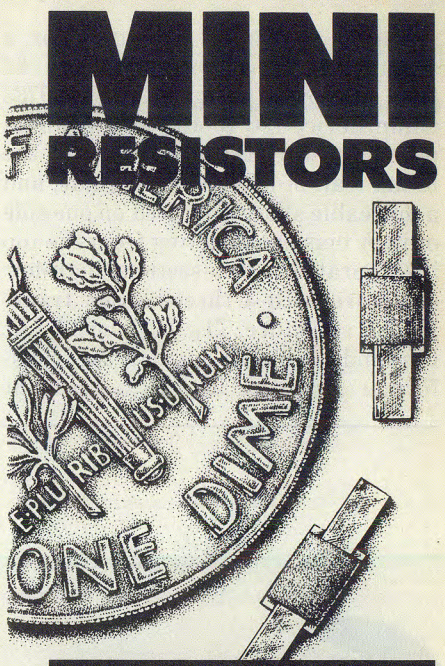
(continued on next page)



***3. These equivalent circuits are valid** at the fundamental (a), the second harmonic with $l_1 \geq 0.25$ mm (b), and the second harmonic with $l_1 \leq 0.25$ mm(c).*



***4. The oscillation frequency of the experimental module** was nearly inversely proportional to the diameter of the radial disk, d_2.*



They're Overachievers

At 100 x 200 mils, our new 30-Watt rated RV30-50 and RV30-100 are among the smallest high-power resistors on the RF microwave market. And they pack all the performance, durability and high reliability you expect in ACRIAN products.

They're On Target

We designed and constructed them for the best possible combination of electrical and thermal performance. Thin film NiCr metallization on gold-backed BeO ceramic substrates, high-temperature brazed packages, and 100% testing of the finished products guarantee it.

And Under-priced

Actually, there is one area where our new resistors aren't overachievers: the price. In quantities of one hundred, they're $5.25 each, and can be shipped immediately.

For more information or samples, contact us today.

ACRIAN INC
10060 Bubb Road
Cupertino, CA 95014
(408) 996-8522

READER SERVICE NUMBER 54

The cross-section structure for a second-harmonic oscillator for 60 GHz is shown in Fig. 2. An MA49733 Gunn device (50 to 100 mW nominal power at 35 GHz) is mounted in the broad wall of a WR15 waveguide, and a moveable short is located on one side of it. A bias choke acting from the top incorporates a two-section, high-low structure with a three-section transformer structure, $T1_1$, $T1_2$, and $T1_3$. At the fundamental frequency, the transformer structure acts as a resonant circuit, while at the second harmonic the structure matches the characteristic impedance of the waveguide to the low source impedance of the Gunn device, with the imaginary part of the load impedance being tuned by the short.

Figure 3a shows an equivalent circuit valid at the fundamental frequency. The post sections of the transformer, $T1_1$ and $T1_3$, act inductively and are represented by L_1 and L_3; the disk, $T1_2$, is represented by the capacitances, C_2. The parallel-resonance frequency of the circuit with respect to the terminals of the active device is determined by all three of these values plus the input impedance of the choke and the parasitic elements of the Gunn device.

At the second harmonic, the equivalent circuit is that shown in Fig. 3b, for a relatively long first post section ($l_1 \geq 0.25$ mm), or in Fig. 3c if the disk is practically flush with the Gunn device ($l_1 \leq 0.25$ mm). In the latter case, the impedance transformation structure is that of the radial-disk transformer,[7] while in the former case the structure resembles the post-coupled circuit.[8]

Since an exact theoretical treatment of this oscillator circuit (including the Gunn device) would be a formidable problem, the oscillator was investigated experimentally, and an optimized circuit for an industrial Doppler-sensor application was derived empirically.

First, post section 1 was omitted, and the output power and frequency were monitored as a function of the diameter of the radial disk, d_2. Figure 4 shows that the frequency of oscillation is almost inversely proportional to d_2 (i.e., to capacitance C_2). A d_2 above 3.7 mm was not possible, since the disk would have touched the walls of the waveguide. The upper frequency limit was about 80 GHz, where d_2 equals 2.2 mm. Below 2.2 mm, the pure second-harmonic operation of the circuit breaks down due to propagation of the fundamental frequency in the waveguide, whose cutoff is at 39.9 GHz.

The output power of the experimental circuit was increased by adding post section 1 between the Gunn element and the disk, whose diameter was set at 2.75 mm. Power rose from 20 mW (13 dBm) without the post to 30 mW (15 dBm) with a post length, l_1, of about 0.7 mm (Fig. 5). However, the oscillator frequency decreases as l_1 (L_1) increases from 0.

The original oscillator had been designed to allow vertical movement of the Gunn device and the choke. Such a displacement lends itself very nicely to fine tuning of the oscillator; the oscillator frequency is reduced as the Gunn device is sunk into the waveguide floor (Fig. 6a). This is due to the increase in C_2 as the height of the disk above the floor is reduced. It is interesting to note that the oscillator with

(continued on p. 80)

$\epsilon_r \pm .01$

CONTROL LIKE THIS COMES ONLY FROM ROGERS.

Rogers RT/Duroid® 5870, 5880. The unique microwave laminates with the lowest tolerance in dielectric constant available. Anywhere.

Rogers RT/Duroid with $\epsilon_r \pm .01$ gives you the edge in the most critical microwave circuitry design. It delivers the qualities you look for in a microwave laminate. Closer control. Consistency. Precision. It far exceeds the strict standards of the military, stands up to your toughest demands.

Rogers RT/Duroid offers other advantages, too. A lower dissipation factor than woven cloth structures. And trouble-free processing, with a non-woven glass microfiber construction that prevents wicking.

For closest control. For consistency. For trouble-free processing. And for precision in your most demanding designs, rely on RT/Duroid with $\epsilon_r \pm .01$ You can get this kind of control from precisely one company. Rogers. It's available now. Ask us about it. Call Mike Norris, at (602) 961-1382.

ROGERS

Rogers Corporation
Chandler, Arizona 85224

READER SERVICE NUMBER 55

a large post length (Fig. 6b) yields a wider tuning range than the circuit with the Gunn device flush with the disk. (Fig. 6a). This characteristic could be important if parameter variations of active devices must be compensated for in production.

Figure 7 shows the oscillator module developed using the experimental results discussed above. The module operates at 61 to 61.5 GHz (IMS-band), and the 10 units built as of this writing produce an average of 15 mW. Typical operating voltage is 6 V at 400 mA.

The noise spectrum of the module has not been measured, but the load-pulling Q was found to be about 1500. Consequently, the oscillator can be used in a circuit without a ferrite uniline for load-pulling protection, which is extremely attractive with respect to the price of the complete sensor.

Bias pushing was typically found to be 150 MHz/V, while frequency drift was about 300 MHz from 0 to 70°C. In its present application, the oscillator's frequency drift is not a major concern, but if it were, temperature compensation is feasible using bias voltage control.

Scale model investigated

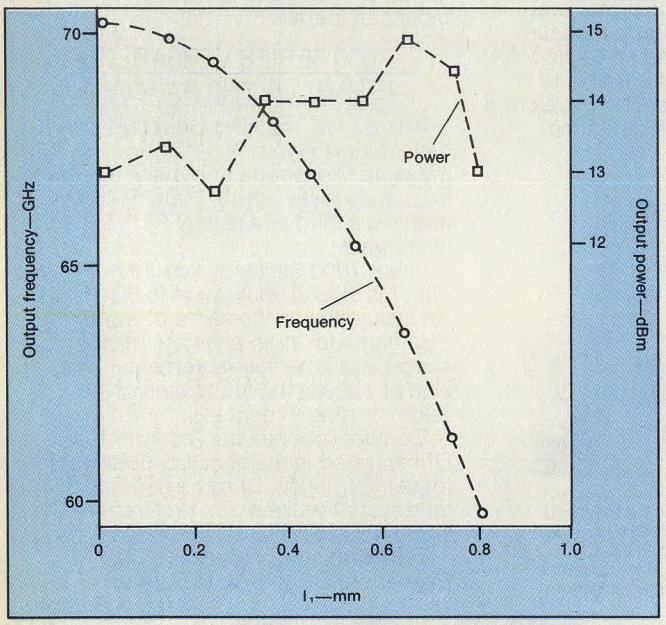
To confirm the circuit's principle of operation and to gain more insight into the impedance levels present in the 60-GHz second-harmonic oscillator, a scale model of the complete circuit of Fig. 2 was investigated using a microwave network analyzer. The metal waveguide used in the model was WR 284, which produced a scale factor of approximately 18.5.

In order to measure the impedances at the terminals of the active element, the Gunn device also was scaled. The package of the device was modeled by a ring of high permittivity plastic ($\epsilon_r = 9$) and a brass cap on top. The package bond wires used in millimeter-wave Gunn devices were modeled by two wire ribbons soldered to the cap. The intrinsic chip capacitance of the Gunn device was modeled by a disk capacitor that used an Epsilam-10 substrate. The center conductor of the SMA-connector was connected to both the wire ribbons and the disk capacitor, providing the terminals for the modeled Gunn device.

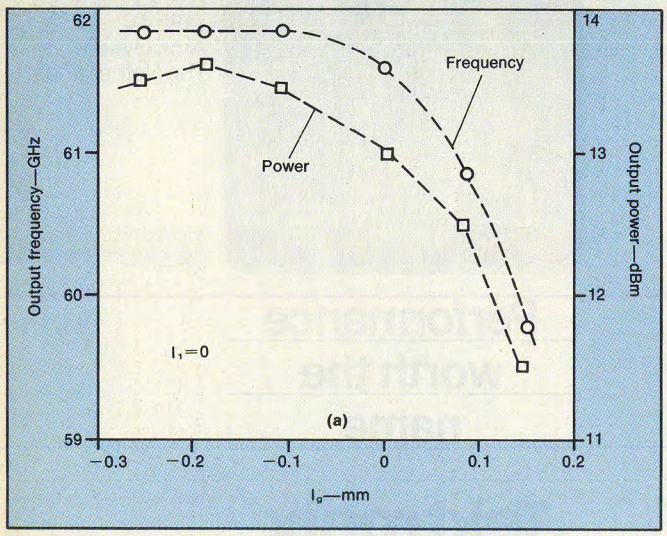
The choke structure chosen for the model corresponded to an operating frequency of about 57 GHz in the original oscillator. The two waveguide ports of the model were matched and the input coefficient, S_{11}, at the modeled terminals of the active device was measured (Fig. 8). Parallel resonance ($S_{11} = +1$) occurred at 1.35 GHz, which was 15 percent below the original oscillator's frequency. The unloaded Q of the parallel resonance was roughly 1000. This was reduced by a factor of about five at the original frequency due to an increase in the skin effect and the smaller dimensions of the conductors involved. Thus, the effective circuit Q at the fundamental frequency of the original oscillator may be assumed to be about 200, which is much greater than that of conventional, unstabilized, fundamental-mode oscillators (about 30 to 50).

Tests were then made to determine the impedance at the terminals of the

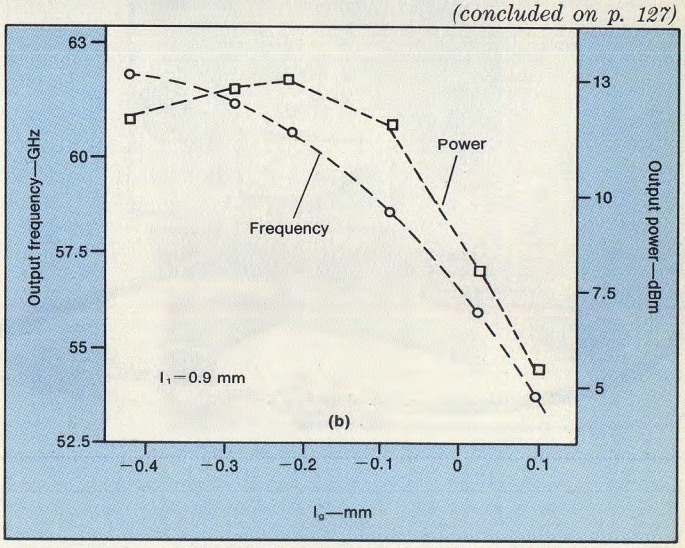
(concluded on p. 127)



5. Adding post section 1 (l_1) to the circuit increased output power, *but the oscillation frequency decreased as the section's length increased.*



6a. The oscillator can be fine-tuned *by adjusting l_g, the height of the Gunn device relative to the waveguide.*

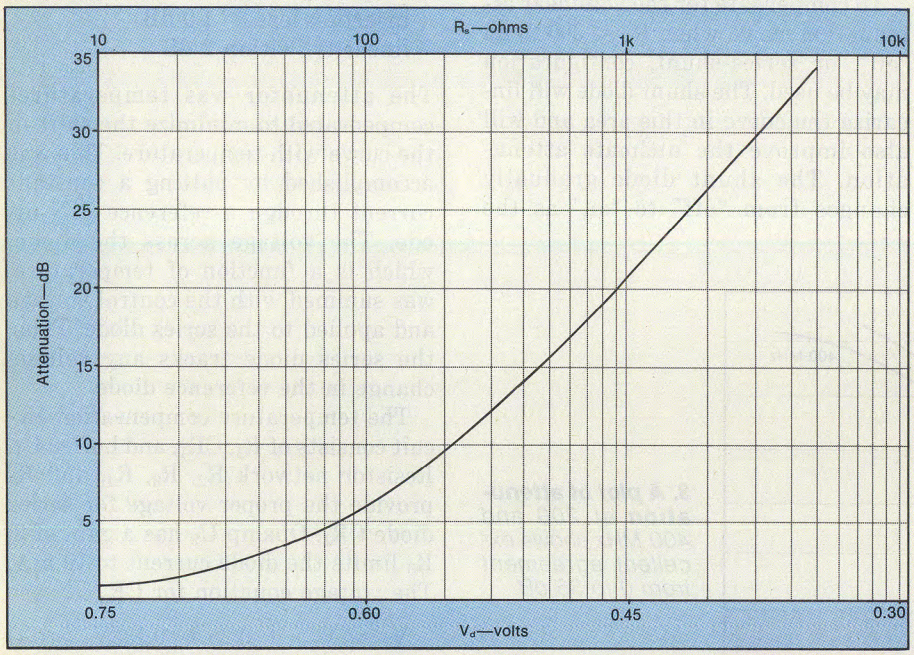


6b. The tuning range that is available *by adjusting l_g increases as the length of post section 1 (l_1) increases.*

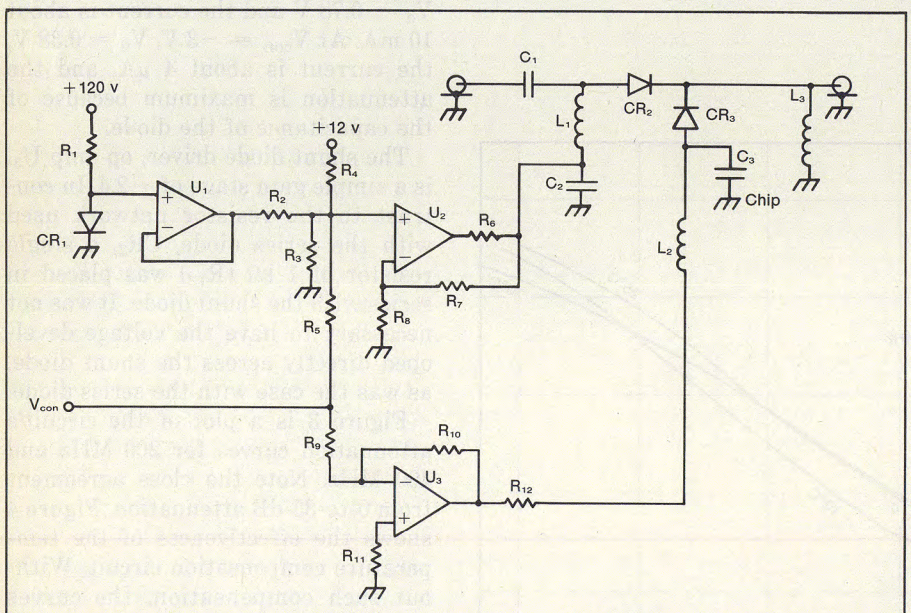
PIN-Diode Driver Allows Linear RF Attenuation

A new type of driver circuit provides the linear response needed in the design of PIN-diode variable RF attenuators

Gary M. Homer, Engineer, E-Systems, Inc., ECI Div., Transceiver Section, 1501 72nd St., St. Petersburg, FL 33733.



1. A plot of attenuation versus series resistance and voltage *across the diode shows the linearity that can be obtained with PIN diodes.*



2. The PIN diode ell attenuator that was designed included *temperature compensation to minimize the temperature shift in the attenuation curve.*

ONE of the major problems encountered in designing a PIN-diode variable RF attenuator is coming up with a driver circuit that provides a linear curve of attenuation (in dB) versus control voltage input. Linear attenuation is required by a well-behaved AGC loop.

Looking at a simple series PIN diode in a 50-Ω system, the attenuation (in dB) is:

$$20 \log (1 + R_s/100) \qquad (1)$$

where R_s is the series diode's series resistance. If the control voltage is varied linearly from 10 to 0 V and is applied through a 1-kΩ limiting resistor, the diode current would change from 10 to 0 mA. From 10 mA to 0.1 mA, R_s will typically vary from a few ohms to 300 Ω, providing an attenuation change of 12 dB, while from 0.1 mA to zero current, the attenuation change could be 20 dB or more. Thus, this type of driver would produce a very nonlinear curve.

A solution was found by applying a voltage directly across the diode. If this voltage, V_d, is varied from about 0.3 to 0.8 V, the current will increase exponentially from nearly zero to about 10 mA. In turn, R_s will decrease exponentially. An empirical re-

(concluded on next page)

lationship between R_s and V_d for a few popular diodes was developed:

$$R_s = K(10)^{-6.6V_d} \quad (2)$$

where K is a function of the diode and the temperature. This equation states that a 0.15-V increase in V_d would cause R_s to decrease by a factor of 10.

For $R_s > 300\ \Omega$, the attenuation can be approximated by:

$$\text{atten. (dB)} \approx 20 \log (R_s/100)$$
$$\approx 20 \log \left(\frac{K \times 10^{-6.6V_d}}{100}\right)$$
$$\approx K - 132\ V_d \quad (3)$$

Thus, the slope of the attenuation curve will be 132 dB/V for $R_s > 300\ \Omega$. At room temperature, a value of 83 for K is a good approximation. This equation, however, does not take into account the limitations that diode capacitance places on maximum attenuation. Figure 1 is a plot of attenuation versus log R_s and versus linear V_d for a series PIN diode.

To compensate for the nonlinear attenuation curve when $R_s < 300\ \Omega$, an "ell", or series-shunt, configuration may be used. The shunt diode will linearize the curve in this area and will also improve the ultimate attenuation. The shunt diode gradually changes from "off" to "on" as the series diode's resistance is increased to 300 Ω.

An ell attenuator (Fig. 2) was designed with the following characteristics:

attenuation range = 45 dB
control voltage = 0 to −3 V
slope = 16 dB/V
frequency range = 100 to 400 MHz
insertion loss = 1.0 dB
linearity: within 2 dB

The attenuator was temperature-compensated to minimize the shift in the curve with temperature. This was accomplished by putting a constant current through a reference PIN diode. The voltage across the diode, which is a function of temperature, was summed with the control voltage and applied to the series diode. Thus, the series diode tracks any voltage change in the reference diode.

The temperature compensation circuit consists of R_1, CR_1, and buffer U_1. Resistor network R_2, R_3, R_4, and R_5 provide the proper voltage for series diode CR_2. Opamp U_2 has a gain of 2; R_6 limits the diode current to 10 mA. The voltage equation for CR_2 is:

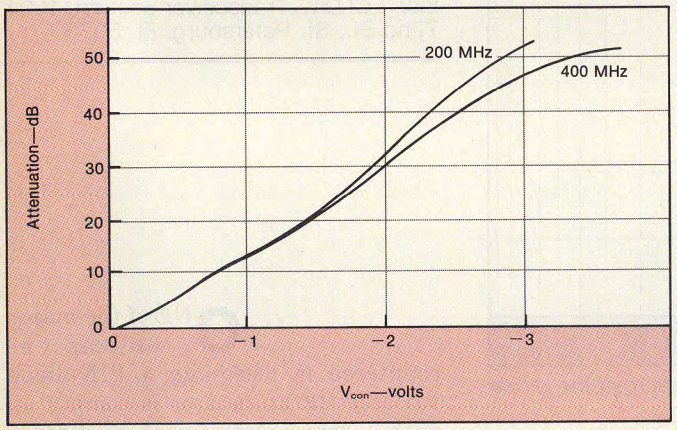
$$V_d = V_{ref} + 0.25 + 0.133V_{con} \quad (4)$$

where reference voltage V_{ref} is 0.53 V at room temperature. At $V_{con} = 0$, $V_d = 0.78$ V and the current is about 10 mA. At $V_{con} = -3$ V, $V_d = 0.38$ V, the current is about 4 μA, and the attenuation is maximum because of the capacitance of the diode.

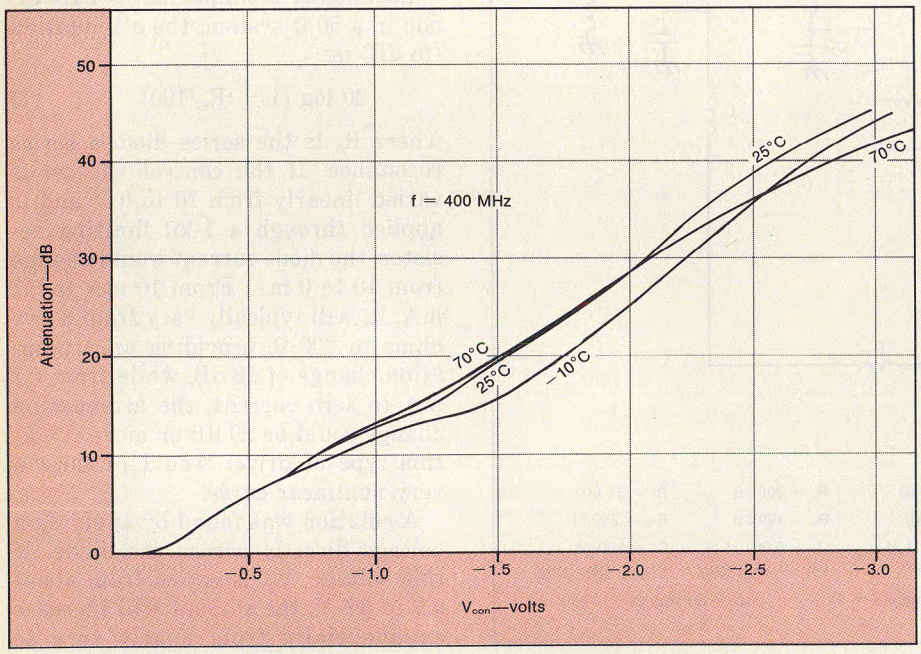
The shunt diode driver, op amp U_3, is a simple gain stage of −2.4. In contrast to the resistor network used with the series diode, CR_2, a single resistor of 1 kΩ (R_{12}) was placed in series with the shunt diode. It was not necessary to have the voltage developed directly across the shunt diode, as was the case with the series diode.

Figure 3 is a plot of the circuit's attenuation curves for 200 MHz and 400 MHz. Note the close agreement from 0-to-35-dB attenuation. Figure 4 shows the effectiveness of the temperature compensation circuit. Without such compensation, the curves would be widely divergent.

The circuit described in this article shows that a linear gain-control circuit can be constructed inexpensively and with readily available parts. With the proper level shifting, this design can be modified to fit any desired attenuation curve. ●●



***3. A plot of attenuation** at 200 and 400 MHz shows excellent agreement from 0 to 35 dB.*



***4. The temperature compensation circuit proved to be quite effective.** Compensation was accomplished by putting a constant current through a reference diode.*

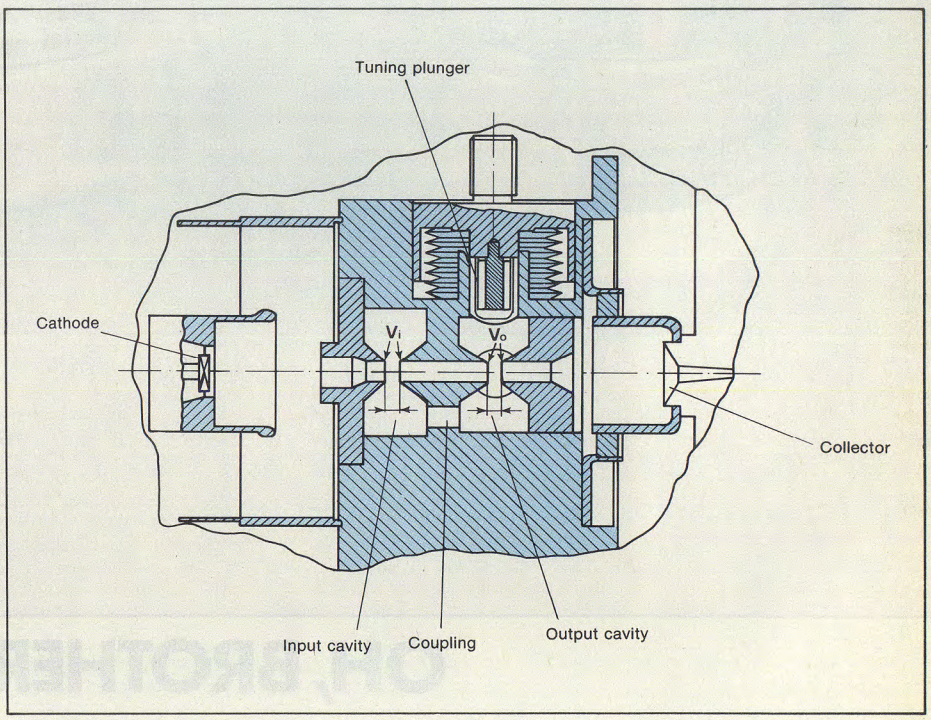
Two-Cavity Klystron Uses Single-Cavity Tuning

Most klystrons require tuning of both cavities, a complex procedure. This newly developed device is tuned only at the output cavity.

Antonio Muratore, Senior Engineer; **Guido Busacca,** Director, Microwave Tubes Plant; and **Vincenzo Meli,** Manager, Microwave Tubes and Components Laboratory, Italtel, Via Villagrazia 79, 90100 Palermo, Italy.

IN the past, two techniques have been used to construct a tunable, two-cavity klystron. The first is complex and involves the use of a movable plunger in each cavity. The second method uses a single diaphragm to tune both cavities. The output power of such a unit varies with tuning because the changing size of the coupling between the two cavities changes the ratio of the input and output gap voltages (V_i and V_o in Fig. 1). Maintaining a constant ratio is important to insure a flat output-power characteristic over the tuning range of the tube. This article describes a klystron designed to be tuned only at the output cavity, eliminating the problems inherent in the two earlier techniques.

The klystron was designed for a CW output of about 200 W at X band. The resonant frequency of the structure without perturbation, f_o, is 10 GHz, and the tuning range is 100 MHz. The required voltage ratio is maintained by use of considerable detuning (about 10 percent) between the input and output cavities, accomplished by using different dimensions for each cavity.



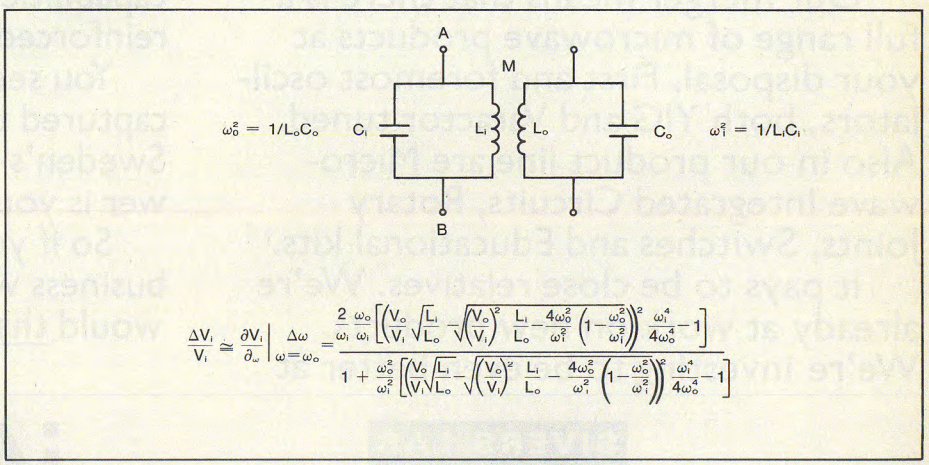
***1. The new klystron is tuned** only at the output cavity, eliminating the requirement for complex simultaneous tuning of both cavities.*

Voltage-frequency relation

The mutually coupled circuits in Fig. 2 can be used to represent the two cavities of the klystron. The voltage at terminals A-B is a function of the input resonant frequency, f_i ($\omega_i/2\pi$), and the ratio of f_o/f_i, as shown in the equation of Fig. 2.

Figure 3a shows how $\Delta V_i/V_i$ varies with f_o/f_i, while Fig. 3b indicates how $\Delta V_i/V_i$ varies with f_o. The small variation of V_i with frequency allows the correct drift length for obtaining the

(continued on p. 89)



***2. The klystron's two cavities can be represented** by two coupled, tuned circuits, with input voltage V_i related to frequency as shown.*

desired output over the tuning range of the tube to be determined.

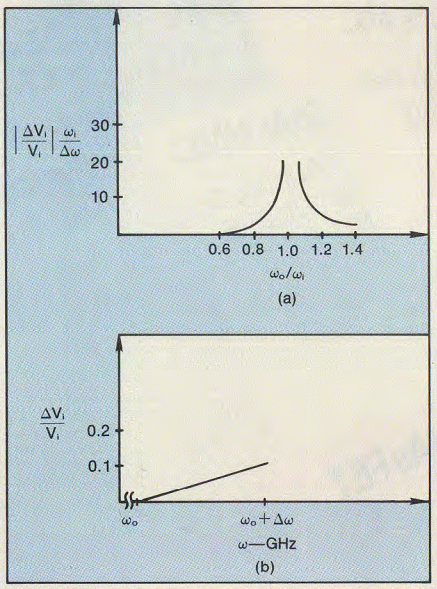
A very simple method has been developed to measure the output-to-input voltage ratio and relate it to the input and output gap lengths. The technique is valid only when the input or output cavity has been perturbated and the input voltage, V_i, remains constant. This can be accomplished by the insertion of a small Teflon rod into the drift tunnel. The voltage ratio can be stated as:

$$\left|\frac{V_o}{V_1}\right| = \sqrt{\left|\frac{(f''-f_r)d''}{(f'-f_r)d'}\right|}$$

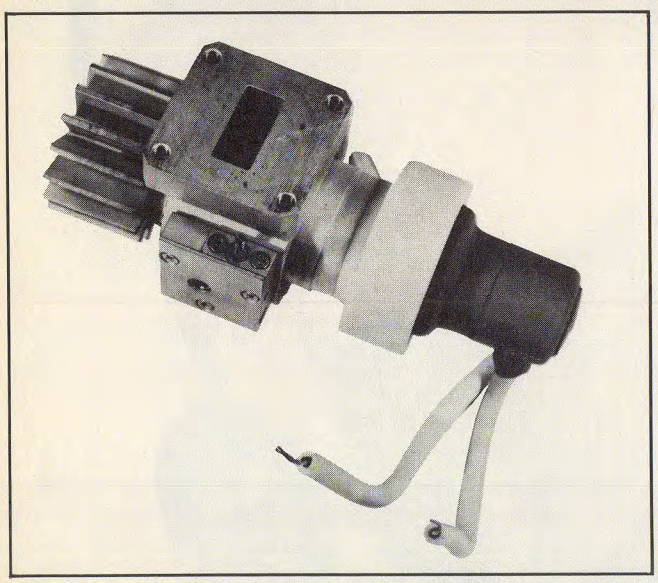
where:
f_r = resonant frequency of the structure without perturbation, f' = resonant frequency of the structure with perturbation of the input cavity only, f'' = resonant frequency of the structure with perturbation of the output cavity only, d' = input gap length, and d'' = output gap length.

A prototype of this tube has been built and successfully

(concluded on p. 91)



3. The relationship between $\Delta V_i/V_i$ and frequency *can be used to determine proper drift length.*



4. The prototype *single-cavity-tuned klystron.*

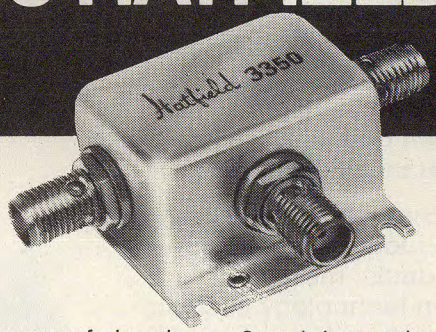
Call them what you like–



Power Dividers
Hybrid Couplers
Signal Dividers
Passive Couplers
Signal Combiners

But get the name right.

It's 'HATFIELD'!

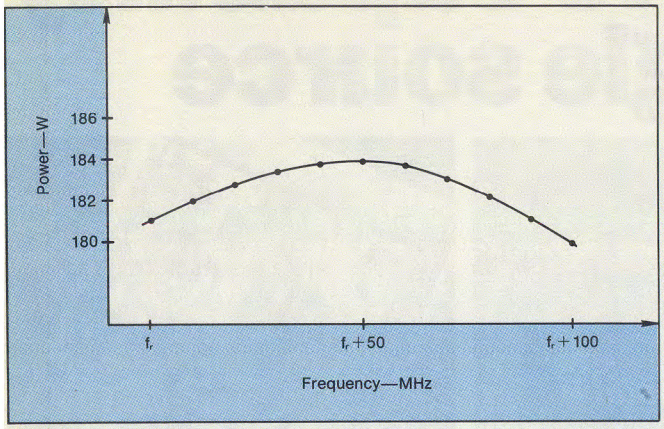


This range of signal processing components consists of passive, constant impedance devices for passing r.f. signals from one to a number of output ports with minimum of loss and high isolation between output ports.

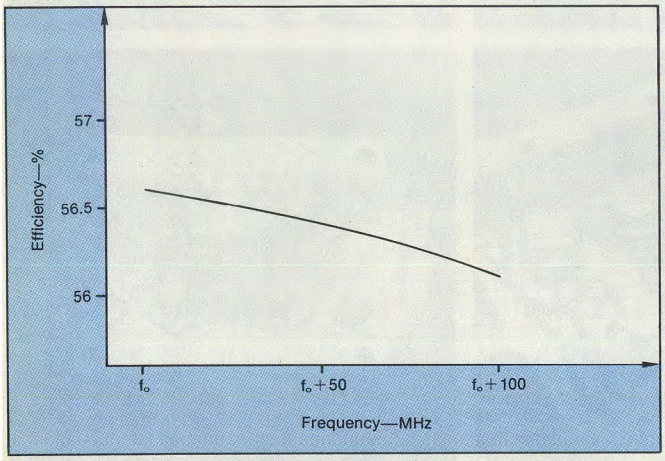
2 and 4-way devices are manufactured in a wide variety of enclosures covering the broad frequency range from 1 kHz to 600 MHz. Send for details of our 3100 Series or our complete signal processing components catalogue.

W&G
W & G Instruments Ltd.
Burrington Way, Plymouth,
Devon, PL5 3LZ
Telephone: 772773
Telex: 45592

READER SERVICE NUMBER 62



***5. Power output varied by 4 W** over the 100-MHz tuning range of the device.*



***6. Efficiency varied only slightly** over the tuning range.*

tested (Fig. 4). The device's power output versus frequency over the 100-MHz tuning range of the device is shown in Fig. 5. The klystron's efficiency also was plotted (Fig. 6). The slight variation in efficiency over the tuning range can be attributed to the choke used in the device. The experimental unit was tested to insure that its unloaded Q is not reduced because of the modified distribution of the surface currents caused by the large coupling holes between the cavities.

The low-noise characteristics and flat output power of the tube should lead to its use in applications that require ruggedness. Presently, the tube is used in an illuminator for an Italian missile system.●●

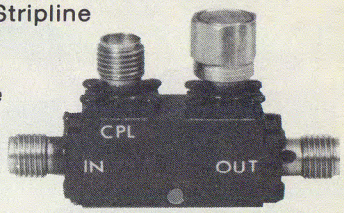
Smallest Available

Subminiature Directional Couplers

Octave and Multi-Octave Bands

■ Low Cost ■ Available from Stock ■ Subminiature Size
■ Excellent Electrical Performance ■ 0.5 GHz to 18 GHz
■ Meets Mil-E-5400 ■ Superior Connector Mounting
■ Low Insertion Loss ■ High Directivity

Triangle Microwave's new subminiature couplers are the smallest Stripline Couplers available.
The selection is extensive, they're in stock and the price is right.
To answer any questions, or to place an order call our sales department at (201) 740-0100.



Actual Size
Model CA-716

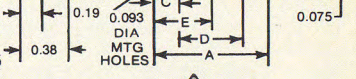
ELECTRICAL PERFORMANCE

Model No.	Freq. Range GHz	Nominal* Coupling dB	Deviation from Nominal Coupling vs. Frequency dB	Min. Directivity dB	Max. Input/ Output VSWR	Max. Ins. Loss Above Coupling Loss dB	Max. Peak Power kW	Max Avg. Power Watts	Outline
CA-516	.5-1.0	6	±0.7	25	1.10	0.1	10	50	1
CA-511	.5-1.0	10	±0.8	25	1.10	0.1	10	50	1
CA-512	.5-1.0	20	±0.8	25	1.10	0.1	10	50	1
CA-513	.5-1.0	30	±1.0	25	1.10	0.1	10	50	1▲
CA-521	.5-2.0	10	±0.75	23	1.20	0.2	10	50	2
CA-522	.5-2.0	20	±1.0	23	1.20	0.2	10	50	2
CA-556	.75-1.5	6	±0.7	24	1.15	0.2	8	50	3
CA-551	.75-1.5	10	±0.8	24	1.15	0.2	8	50	3
CA-552	.75-1.5	20	±0.8	24	1.15	0.2	8	50	3
CA-553	.75-1.5	30	±1.0	24	1.15	0.2	8	50	3▲
CA-596	1.0-2.0	6	±0.7	24	1.15	0.2	8	50	4
CA-591	1.0-2.0	10	±0.8	24	1.15	0.2	8	50	4
CA-592	1.0-2.0	20	±0.8	24	1.15	0.2	8	50	4
CA-593	1.0-2.0	30	±1.0	24	1.15	0.2	8	50	4▲
CA-636	1.5-3.0	6	±0.7	22	1.20	0.2	7	50	5
CA-631	1.5-3.0	10	±0.8	22	1.20	0.2	7	50	5
CA-632	1.5-3.0	20	±0.8	22	1.20	0.2	7	50	5
CA-633	1.5-3.0	30	±1.0	20	1.20	0.2	7	50	5▲
CA-676	2.0-4.0	6	±0.7	22	1.20	0.2	5	40	6
CA-671	2.0-4.0	10	±0.8	22	1.20	0.2	5	40	6
CA-672	2.0-4.0	20	±0.8	22	1.20	0.2	5	40	6
CA-673	2.0-4.0	30	±1.0	20	1.20	0.2	5	40	6▲
CA-691	2.0-8.0	10	±0.75	17	1.30	0.3	2	20	7
CA-692	2.0-8.0	20	±1.0	17	1.30	0.3	2	20	7
CA-716	2.6-5.2	6	±0.7	22	1.25	0.25	4	40	8
CA-711	2.6-5.2	10	±0.8	22	1.25	0.25	4	40	8
CA-712	2.6-5.2	20	±0.8	22	1.25	0.25	4	40	8
CA-713	2.6-5.2	30	±1.0	20	1.25	0.25	4	40	8▲
CA-771	6.0-18.0	10	±.75	14	1.45	0.50	2	20	8
CA-772	6.0-18.0	20	±1.0	14	1.45	0.50	2	20	8
CA-756	4.0-8.0	6	±0.7	18	1.25	0.3	4	40	8
CA-751	4.0-8.0	10	±0.8	18	1.25	0.3	4	40	8
CA-752	4.0-8.0	20	±0.8	18	1.25	0.3	4	40	8
CA-753	4.0-8.0	30	±1.0	17	1.25	0.3	4	40	8▲
CA-796	7.0-12.4	6	±0.7	17	1.30	0.4	2	30	8
CA-791	7.0-12.4	10	±0.8	17	1.30	0.4	2	30	8
CA-792	7.0-12.4	20	±0.8	17	1.30	0.3	2	30	8
CA-793	7.0-12.4	30	±1.0	17	1.30	0.3	2	30	8▲
CA-836	8.0-16.0	6	±0.7	15	1.40	0.5	2	30	8
CA-831	8.0-16.0	10	±0.8	15	1.40	0.5	2	30	8
CA-832	8.0-16.0	20	±0.8	15	1.40	0.4	2	30	8
CA-833	8.0-16.0	30	±1.0	15	1.40	0.4	2	30	8▲
CA-876	8.0-18.0	6	±0.8	14	1.45	0.5	2	20	8
CA-871	8.0-18.0	10	±1.0	14	1.45	0.5	2	20	8
CA-872	8.0-18.0	20	±1.0	14	1.45	0.5	2	20	8
CA-873	8.0-18.0	30	±1.2	14	1.45	0.5	2	20	8▲
CA-916	12.4-18.0	6	±0.7	15	1.40	0.5	2	30	8
CA-911	12.4-18.0	10	±0.8	15	1.40	0.5	2	30	8
CA-912	12.4-18.0	20	±0.8	15	1.40	0.4	2	30	8
CA-913	12.4-18.0	30	±1.0	15	1.40	0.4	2	30	8▲

*Nominal Coupling: ±0.25 dB

Outline	A in	B in	C in	D in	E in
1	3.10	0.50	0.80	1.50	—
2	3.40	0.50	0.95	1.50	—
3	2.50	0.50	0.60	1.30	—
4	1.80	0.50	0.43	0.94	—
5	1.40	0.50	0.50	0.40	—
6	1.00	0.50	—	—	0.50
7	1.30	0.50	—	—	0.65
8	0.90	0.50	—	—	0.45

INCHES XX±.03 XXX±.010
▲For all 30dB couplers "B" dimensions 0.55



triangle microwave
incorporated

60 OKNER PARKWAY, LIVINGSTON, N.J. 07039
(201) 740-0100 • TWX: 710-986-8202

READER SERVICE NUMBER 65

Digital Modulation Techniques Compared

Digital modulation can be performed in a number of ways. The hardware and transmission medium used will influence the choice of methods.

Bernhard E. Keiser, Consulting Engineer, Keiser Engineering, Inc., 2046 Carrhill Rd., Vienna, VA 22180.

THE transmission of digital data and digitized voice or video from one point to another may be accomplished by a number of techniques. This article examines the techniques currently in use and discusses their advantages and disadvantages.

Modulation is the variation of some parameter of a carrier signal in accordance with the characteristics of a wave to be transmitted. If the carrier is sinusoidal, as is usually the case, it can be expressed as: $A \sin(2\pi ft + \phi)$, which indicates that there are three parameters that can be varied: the amplitude, A; the frequency, f; and the phase, ϕ. If a continuum of values of the modulated parameter is allowed, the modulation is said to be analog, but if only specific values are allowed, the modulation is said to be digital.

Thus, digital modulation refers to techniques in which amplitude, frequency, or phase assumes specific values. Accordingly, these techniques bear the names *amplitude-shift keying* (ASK), *frequency-shift keying* (FSK), and *phase-shift keying* (PSK).

Although determining specific values of amplitude and frequency presents no problems to a receiver, how is the receiver to measure phase without a phase reference? To handle this problem, two types of PSK techniques have been devised: differential PSK and coherent PSK. With differential PSK the *change* in carrier phase is in accordance with the modulation; with coherent PSK the receiver derives its phase reference by filtering the incoming data stream and using the result to phase-lock a reference oscillator. Coherent PSK, therefore, requires somewhat more complex receiver circuitry, but it provides a lower bit-error rate at a given input carrier-to-noise ratio to the receiver.

The term modulation is sometimes used to describe processes that really are not modulation but coding techniques. For example, pulse-code modulation (PCM) and delta modulation (DM) are techniques used to convert analog voice or analog video signals to digital bit streams. Versions of each exist. The resulting bit streams then can amplitude-, frequency-, or phase-shift key a carrier, and thus modulate it. For example, the designation PCM/FM means that an analog input has been digitized by a PCM technique, and the resulting digital stream used to frequency modulate a carrier.

Bandwidth vs. speed

Two theorems central to the understanding of digital modulation are those of Nyquist and Shannon, both of which relate bandwidth to transmission rates.

Nyquist's theorem relates bandwidth to keying rate, which is synonymous with symbol rate, with a symbol being one or more bits. The theorem says that a maximum of 2W symbols/s can be sent in a bandwidth of W hertz. The symbol/second rate also is known as the baud rate.

Using a telephone circuit with a 3-kHz bandwidth, the maximum symbol rate is 6 kilobaud. However, that maximum can be achieved only with single-sideband (SSB) modulation. In other words, since the modulation process produces sideband frequencies above and below the carrier, with both sidebands containing the same information, one of the sidebands must be eliminated in order to transmit the maximum amount of information in the given bandwidth.

Normally, however, SSB modulation is not used in digital transmission. While the removal of one sideband of an amplitude-modulated signal is a commonly used analog voice-transmission technique, such a removal in frequency or phase modulation would result in a signal with varying amplitude. These amplitude variations, which would be seen by the receiver as distortion and consequently cause a higher bit-error rate, result from the way in which power is distributed between the carrier and the sidebands in an angle-modulated (frequency- or phase-modulated) signal. As a result, the symbol rate usually is limited to W baud.

Thus, on a telephone circuit the theoretical maximum symbol rate is 3000 baud, although better performance can be achieved in most cases by limiting the rate to 2400 baud or less. Double-sideband transmission at 1 baud/Hz can be done, but it requires filters with very sharp roll-off characteristics at their band edges. This is the result of the sin x/x type of spectrum produced by digital transmission and the consequent need to confine the power to the stated bandwidth. A rate of 0.8 to 0.9 baud/Hz is easier to achieve.

At this point, you might be puzzled by claims that someone is using a "9600-baud modem" on a telephone circuit. The problem is one of terminology. That 9600-baud modem should be called a 9600-bit/second (b/s) modem. Very likely it operates by using 4-bit symbols, which means that

(continued on p. 95)

its symbol rate is 2400 baud.

Recently, some 16,000-b/s modems have become available for use over voice-bandwidth circuits such as conditioned telephone lines. These modems use 6-bit symbols and a 2667-baud rate. They represent the current limit on data-rate transmission over a long-distance telephone circuit.

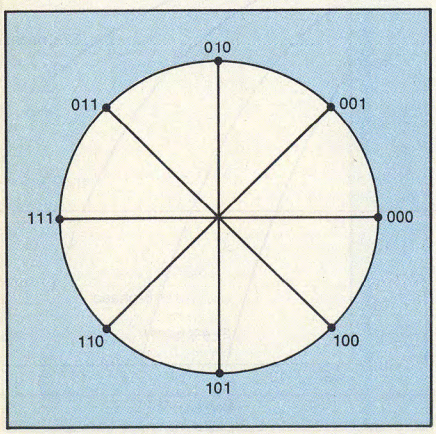
While Nyquist's theorem relates channel bandwidth to the symbol rate, Shannon's theorem relates channel bandwidth to bit rate, or information rate, and to channel carrier-to-noise ratio (C/N). Shannon states that in random noise the maximum information rate, or channel capacity (C), is:

$$C = W \log_2 [1 + (C/N)] \text{ b/s} \quad (1)$$

Thus, a telephone channel with a 3000-Hz bandwidth and a 40-dB carrier-to-noise ratio has a channel capacity of 39,864 b/s. Moreover, Shannon states that it is possible to achieve this rate error free. Obviously, the Shannon rate has not been reached in practical systems. The closer one gets to it, the more complex the equipment becomes.

Medium limits choices

Microwave relay systems, as well as satellite circuits, use repeaters with somewhat restricted amplitude linearity. Various amplitude levels can be used, but amplitude compression tends to become a problem, with intermodulation resulting if attempts are made to operate the repeaters too close to their power limits. FSK and PSK, which maintain constant amplitudes, are much more satisfactory under these circumstances, but PSK tends to be favored because it uses less spectrum than FSK.

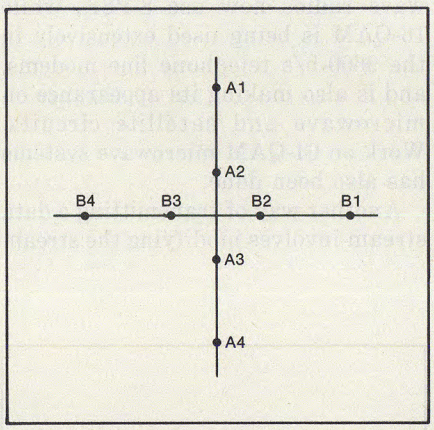


***1. The eight states of** a 3-bit/symbol phase-shift keying modulation system can be diagramed as shown.*

New developments in solid-state amplifiers, which are more linear than traveling-wave tubes, allow more use of multiple amplitude levels at microwave frequencies. Above 20 GHz, however, phase-jitter problems tend to outweigh spectrum economy, so at these higher frequencies FSK is preferred.

On circuits that depend upon radio-wave reflection from the ionosphere—for example, high-frequency (HF) circuits—phase distortions and rapid amplitude changes may occur because of ionospheric changes. Consequently, FKS tends to be popular for HF digital circuits.

Often, FSK is used on cable circuits at data rates that are low enough (about 1200 b/s and below), so that the occupied bandwidth does not press the limits of the voice channel. However, at higher data rates, PSK (often combined with ASK) can achieve the desired spectrum economy by using the good phase stability and amplitude linearity of such circuits.



***2. Amplitude-phase keying** incorporates multiple amplitude levels at various phases.*

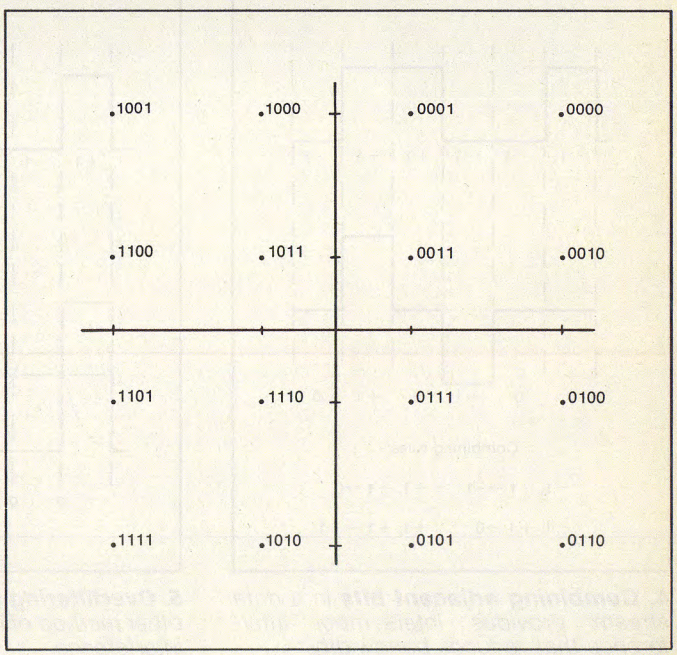
On fiber-optic circuits, the linearity of the light sources presents some unique problems. While these sources can be analog modulated or modulated at various amplitude levels (and this is being done in some operational systems), the most satisfactory mode appears to use only two amplitude levels—low and high. The result is only one bit per symbol.

The large bandwidths available to fiber-optic system users help to compensate for this limitation. However, a fiber-optic system capable of a 400-Mb/s transmission rate can handle only five video channels, each at 80 Mb/s. Such limitations have slowed the application of fiber optics in cable television systems. However, good digital video at 30 Mb/s, combined with monomode fibers capable of 600 to 900 Mb/s between repeaters, are improving the prospects for widespread use of fiber-optic trunks to carry digitized video for cable TV.

Multilevel modulation

In order to transmit more than one bit per symbol, a modulation technique must incorporate a number of digital states. In general, for n bits/symbol, 2^n states are needed.

(continued on next page)



***3. The four amplitude levels** of the APK signal in Fig. 2 can produce 16 states.*

In PSK systems, the digital states consist of the equally spaced phases shown in Fig. 1, which illustrates an 8-PSK system providing 3 bits/symbol. Sometimes this type of diagram is called a "signal-state space diagram" or a "constellation." Bit combinations can be assigned in various ways to the different phases, but adjacent phases usually are made to differ by only one bit to minimize the effects of possible phase errors.

A technique that is less susceptible to noise is amplitude-phase keying (APK). Since it generally involves multiple amplitude levels at various phases, APK may be produced by a technique called quadrature amplitude modulation (QAM). In fact, APK is often called QAM.

Figure 2 illustrates the QAM concept. Two carriers at the same frequency but differing in phase by 90 degrees are amplitude modulated on a multilevel basis. When this modulation is performed simultaneously in various combinations, a total of L^2 states results, where L is the number of amplitude levels on each of the two quadrature carriers. Thus, the APK levels shown in Fig. 3 can be obtained from the QAM levels shown in Fig. 2. The result is called 16-APK or 16-QAM. Bit assignments are shown.

If the modulation of the two quadrature carriers is not done simultaneously, but is offset to result in a 50-percent overlap of the signal intervals, the result is called offset keying. With offset keying, synchronization of the reference recovery circuits to the incoming carrier can be achieved at a 3-dB lower C/N ratio than is possible with the aligned systems.

Four-phase PSK, also called quaternary PSK (QPSK), frequently is used on digital satellite circuits, and higher-order systems also are making their entrance. Many digital microwave radios now use 8-PSK, while 16-QAM is being used extensively in the 9600-b/s telephone line modems, and is also making its appearance on microwave and satellite circuits. Work on 64-QAM microwave systems has also been done.

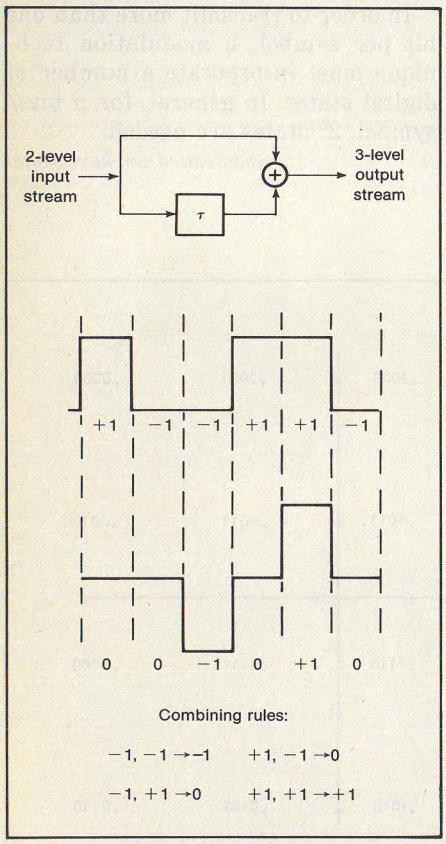
Another way of transmitting a data stream involves modifying the stream before it is placed on a carrier. Accordingly, the name "baseband techniques" may be given to such methods. Correlative-level encoding is a baseband technique in which a predetermined amount of intersymbol interference is intentionally introduced at the transmitter and then removed at the receiver. The result is more carrier power required from the transmitter, but less bandwidth occupied at a given bit rate.

The intersymbol interference can be added either by performing digital operations on the data stream, as is illustrated in Fig. 4 (combining adjacent bits in a two-level stream to produce a three-level stream) or by overfiltering the data stream as in Fig. 5. This correlative technique sometimes is called partial response signaling (PRS). If only adjacent bits or symbols are used, the technique is called duobinary; if bits or symbols separated by one keying interval are combined, the technique is called modified duobinary. A polybinary technique involves the combination of symbols separated by two or more keying intervals.

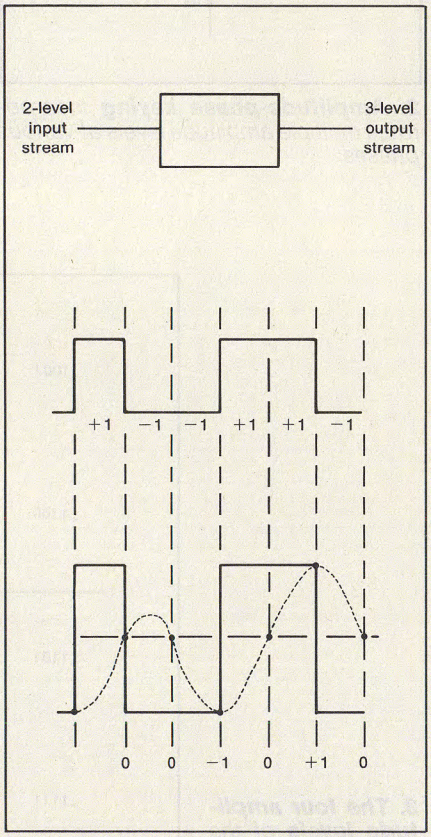
Longer correlation spans result in more energy being concentrated at lower frequencies in the baseband, and thus less spectrum occupancy. Longer spans also require longer memories and more transmitter power.

Applications for PRS are found in

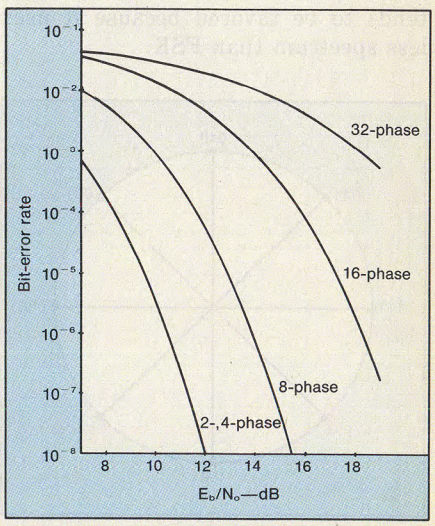
(concluded on p. 99)



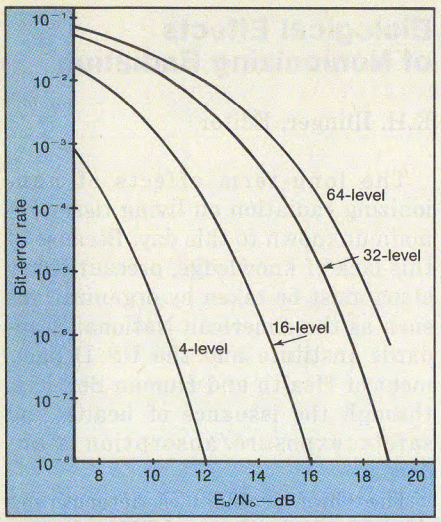
***4. Combining adjacent bits** in a data stream provides intersymbol interference that reduces bandwidth.*



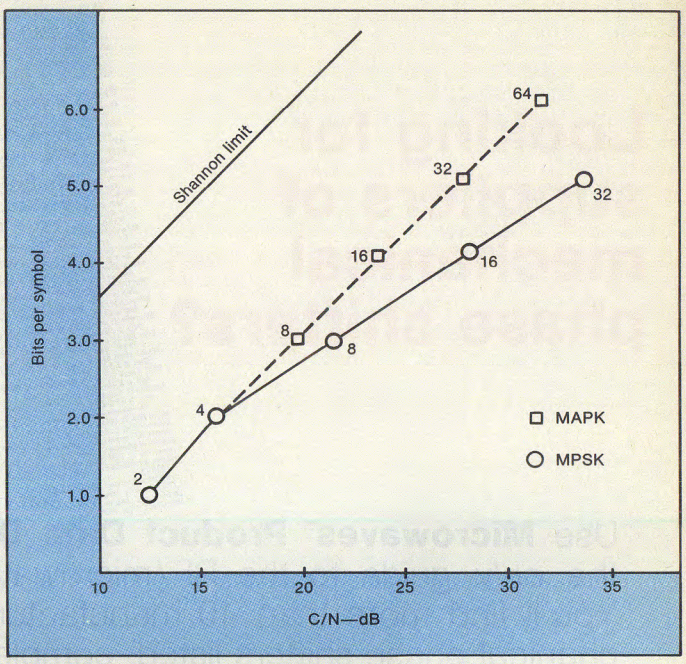
***5. Overfiltering the data stream** is another method of introducing intersymbol interference.*



***6. The more phases in an MPSK system,** the more susceptible it is to bit errors caused by noise.*



***7. An MAPK system is less susceptible** to noise errors than is an MPSK system at higher levels.*



***8. At similar carrier-to-noise ratios,** C/N, an MAPK system allows more bits/symbol than an MPSK system.*

the GTE systems for T1C and T2 transmission (at 3.152 and 6.312 Mb/s, respectively) in the company's 2-GHz radios, and in the Western Electric 1A-RDS data-under-voice system for adding digital transmission at 1.544 Mb/s to an analog microwave radio relay system.

Noise effects

In multilevel PSK (MPSK) systems, the detector must be able to distinguish among differing phases in the presence of channel noise. Otherwise, a symbol error will occur. For example, in Fig. 1 a noise vector resulting in a phase shift of more than ±22.5 degrees could cause the symbol 000 to be read as 001 or 100. Thus, the more phases used in a system, the more susceptible the system is to channel noise. In fact, for a system using n phases equally spaced, the distance between the points is related to the peak amplitude by the expression:

$$\frac{\text{dist. between pts.}}{\text{peak amplitude}} = 2 \sin (\pi/n) \quad (2)$$

The bit-error rate (ber) is:

$$\text{ber} = (\log_2 n)^{-1} \text{erf } z \quad (3)$$

where:

$$z = \sin (\pi/n) \sqrt{(\log_2 n)\,(E_b/N_o)} \quad (4)$$

and:

$$\text{erf } z = 2/\sqrt{\pi} \int \exp (-t^2) dt \quad (5)$$

The expression of E_b/N_o is the ratio of the energy per bit to the noise power spectral density. Since both E_b and N_o have the dimensions of W/Hz, the ratio is dimensionless, and expressed in dB. It is a form of normalized signal-to-noise ratio. Figure 6 is a plot of the ber equation for various numbers of phases.

In multilevel APK (MAPK) systems, the detector must be able to distinguish among the various phase-amplitude points in the presence of channel noise. The more points (symbols) to be distinguished from one another, the more susceptible the system is to channel noise. However, since amplitude differences as well as phase differences are used, the system is somewhat less susceptible to overall channel noise for a given number of points or "levels."

For an MAPK system using L levels along each axis, the distance between the points is related to the peak amplitude by the expression:

$$\frac{\text{dist. between pts.}}{\text{peak amplitude}} = \frac{\sqrt{2}}{L-1} \quad (6)$$

Figure 7 is a plot of the bit-error rate of μ MAPK system as a function of E_b/N_o.

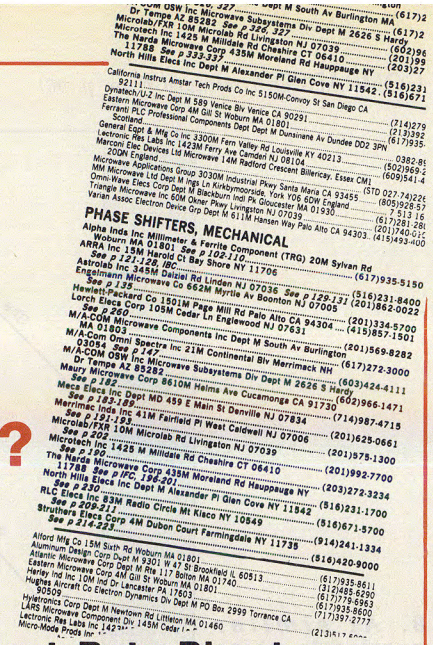
A technique known as forward error correction can be used to improve the error rates in Figs. 6 and 7. The technique involves the use of redundant bits to detect and correct errors in real time at the receiver without retransmission. A general discussion of forward error correction techniques is beyond the scope of this article. It should be noted, however, that the added redundancies result in a slower bit rate and require more complex circuits. These are the prices paid for the reduced error rate.

Figure 8 compares two of the techniques discussed, MPSK and MAPK. the numerals on the plots are the number of signaling states. For comparison, the Shannon limit is shown. Such techniques as offset keying and correlative coding are not plotted, but they generally provide somewhat lower bandwidth efficiency (b/s/Hz) than the techniques shown. Their relative advantages have already been discussed. The curves in Fig. 8 are based on a 10^{-8} bit-error rate. Equipment complexity is not displayed, but of course, becomes greater as the number of signaling states increases.

In fact, equipment complexity can be a limiting factor in system design. But the availability of large-scale integration technology is allowing increasingly complex circuits to be built economically and reliably. The result is an increase in the number of signaling states and thus the ability to transmit more bits per second in a given bandwidth or at lower error rates, or both. The upper limit on the number of signaling states now becomes channel noise rather than circuit complexity.

Forward error correction techniques also will be used to an increasing extent, especially on radio channels subject to propagation variations, such as in land-mobile radio telephony. ●●

Looking for suppliers of mechanical phase shifters?

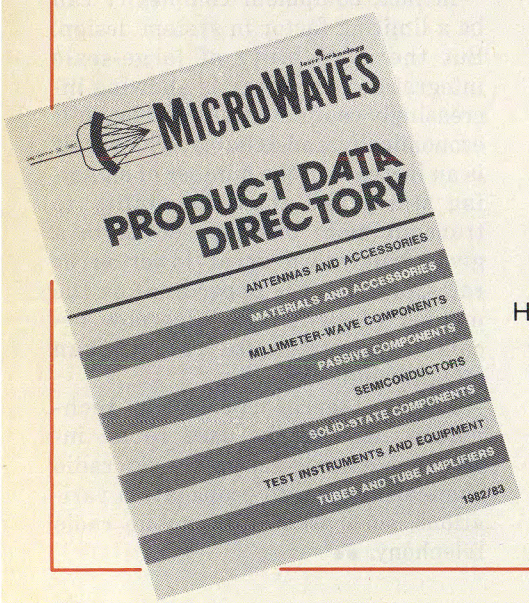


Use **Microwaves' Product Data Directory**—the *only* guide to the RF/microwave industry. You'll find more than 40 manufacturers of mechanical phase shifters listed, complete with addresses and phone numbers so you can contact them *immediately*. Many companies even include data sheets to further simplify your search.

And Mechanical Phase Shifters is only one of more than 275 product categories detailed in 400 pages.

Keep **Microwaves' Product Data Directory** on your desk, and the solutions to your design needs will always be at hand.

Don't be at a disadvantage! If you don't have a copy of **Microwaves' Product Data Directory**, order one NOW. Send check, money order, or purchase order for $23 each (US, Canada, Mexico, Central America), or $32 each (all other countries) to:



MICROWAVES' PRODUCT DATA DIRECTORY

Hayden Publishing Company, Inc.
50 Essex Street
Rochelle Park, NJ 07662

BOOKMARK

Biological Effects of Nonionizing Radiation

K.H. Illinger, Editor

The long-term effects of nonionizing radiation on living tissue remain unknown to this day. Because of this lack of knowledge, precautionary steps must be taken by organizations such as the American National Standards Institute and the US Department of Health and Human Services, through the issuance of health and safety exposure/absorption standards.

The chief problem in determining the biological effects of EM radiation is the difficulty of measuring the interaction between the EM fields and biological test systems. This matter is confronted by a number of groups in *Biological Effects of Nonionizing Radiation.* In the book, editor Illinger has assembled 18 technical papers that examine the problem, at frequencies ranging from low RF to millimeter wavelengths.

The information is divided into four sections: dielectric absorption phenomena at the molecular level, dielectric absorption phenomena at the membrane levels, nonequilibrium phenomena, and the microwave auditory effect. The studies on nonequilibrium phenomena tend to be speculative, due to the nature of the research, but they represent a valuable genesis of research in this area.

The book is, for the most part, representative of the current research on the biological effects of EM radiation. One of its added charms is the bounty of additional information contained in the reference sections of each of the 18 works. It is an excellent starting point for anyone interested in this line of research. (ISBN: 0-8412-0634-1, 1982, 342 pp., $28.50). **American Chemical Society, 1155 16th St., NW, Washington, DC 20036.**

Advertisers . . .
Products . . .
Literature . . .

Find them fast in **infocenter**

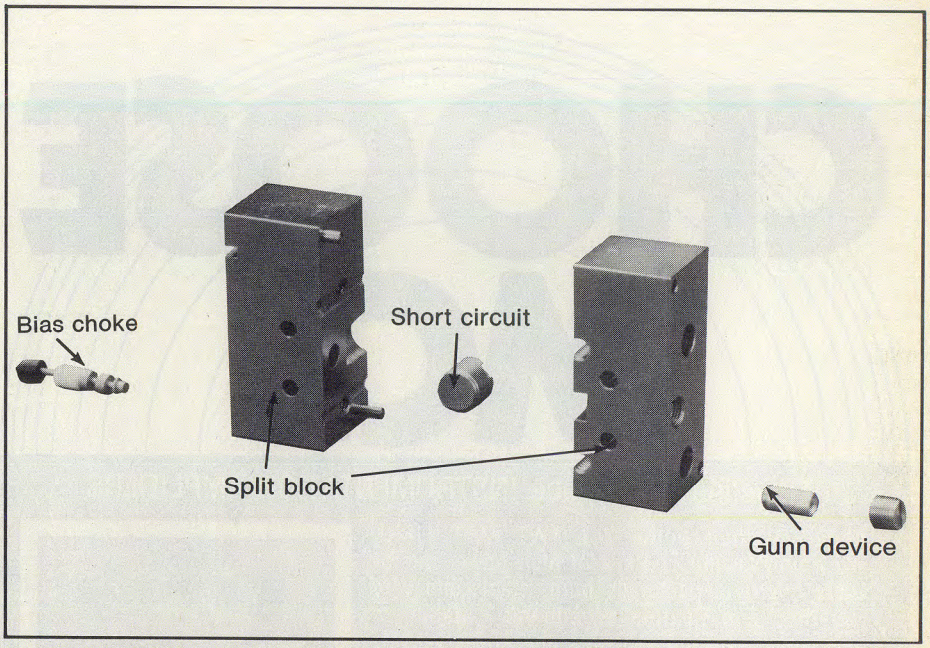
active device with the moveable short circuit incorporated in the model. The S_{11} curves in Fig. 9 show the effect of moving the short in the model waveguide while the other waveguide port remained matched. At the parallel-resonance frequency, the waveguide is below cutoff, and the short has no influence unless it penetrates the concentrated fields of the choke structure to within a few millimeters of the edge of the disk $T1_2$. In that case, a down-shift in the parallel-resonant frequency of as much as 150 MHz was observed, corresponding to 6 GHz at the original oscillator's output frequency (60 GHz).

At the second harmonic the waveguide is above cutoff, and the short circuit has a considerable effect. At 2.8 GHz, near the second harmonic of the parallel-resonant frequency, the widest transformation can be realized by moving the short. As shown in Fig. 9, the impedance can be adjusted to very low levels on the order of 10 to 50 ohms, which corresponds to the source impedance level predicted by theory.[6] Interestingly, such a transformation of high waveguide impedance to a rather low value of some tens of ohms also occurs at about 8 GHz, which means that the sixth harmonic of the oscillator should also be well matched, while all others in between are not.

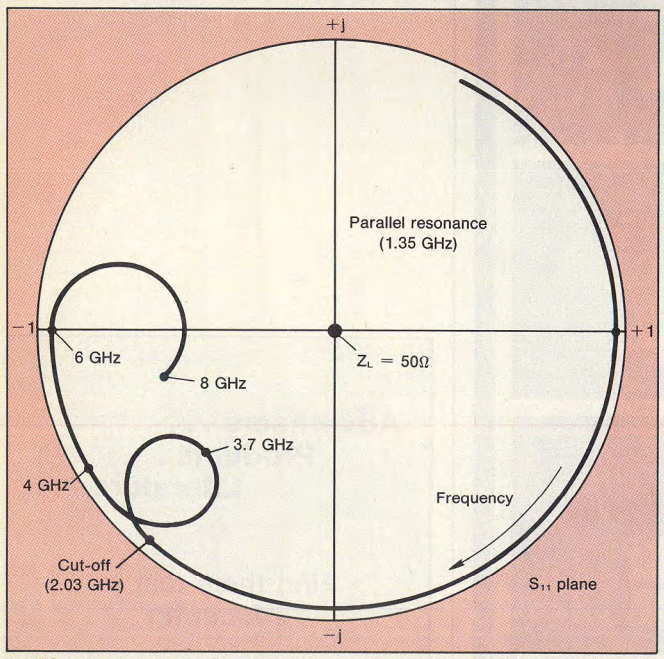
In a third measurement of the scale model, the attenuation of the choke's low-pass filter was determined. For the design frequency of the filter (60 GHz actual, 3.25 GHz at scale), the attenuation exceeded the limits of the network analyzer's dynamic range (> 40 dB). At the fundamental frequency (30 GHz actual, 1.6 GHz at scale), there still was 30-dB attenuation left. This indicates that a two-section, low-pass filter is easily sufficient to separate the millimeter-wave generation from the bias current.

References

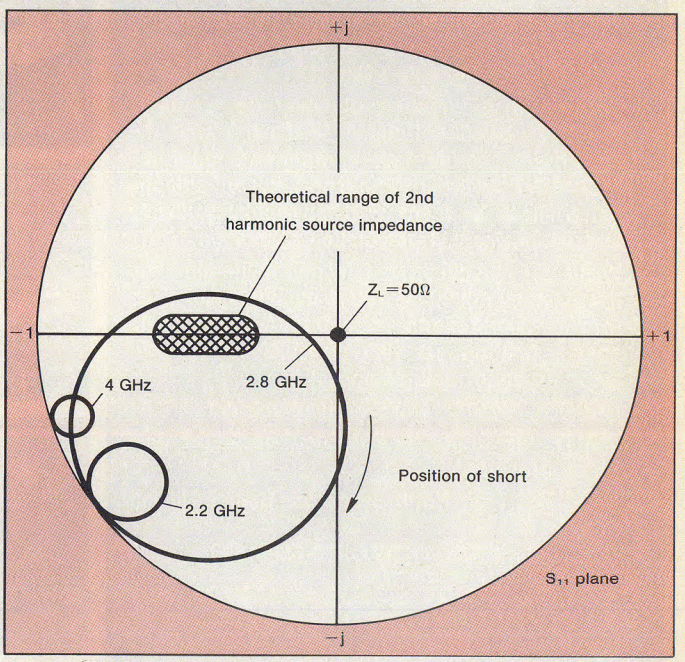
1. J. Gallagher, "InP: A promising material for EHF Semiconductors," *Microwaves* (February 1982), pp. 77-84.
2. J. Ondria, "Wide-band mechanically tunable W-band (75-110 GHz) CW Gunn-diode oscillator," AGARD-Conf. Millimeter and Submillimeter Wave Propagation and Circuits, Munchen, FRG, (September 1978), Conf. Reprint No. 245, pp. 12-1 to 12-16.
3. H. Barth, "A wideband backshort-tunable second harmonic W-band Gunn-oscillator," *IEEE-MTT-S Inter. Microwave Symp. Dig.*, (1981), pp. 334-337.
4. M.J. Lazarus, F.R. Pantoja, S. Novak and M.G. Somekh, "Wide-band tunable mm-wave Gunn-oscillator design," *Electron. Lett.*, Vol. 17, No. 20, (October 1981), pp. 739-741.
5. H. Barth, "141-GHz generation by a GaAs Gunn-oscillator up-converter chain," IEEE International Microwave Symposium, Digest, (1981), pp. 364-366.
6. K. Solbach, "Simulation study of harmonic oscillators," *IEEE Trans. MTT*, Vol. MTT-30, No. 8, (1982), pp. 1233-1237.
7. J. Ondria, "Partially integrated electronically tuned millimeter-wave (33-75 GHz) Gunn-oscillators," 11th EuMC Proceedings, Amsterdam, (1981), pp. 887-893.
8. R. Eisenhart, P. Khan, "Theoretical and experimental analysis of a waveguide mounting structure," *IEEE Trans. MTT*, Vol. MTT-19, No. 8, (1971), pp. 706-719.



7. The oscillator module that was developed *produces about 15 mW at 61 to 61.5 GHz with a typical operating voltage of 6 V at 400 mA.*



8. The input impedance, S_{11}, at the terminals of the modeled Gunn device *was measured with both ports of the waveguide matched.*



9. The input impedance of the modeled Gunn device *also was measured with one waveguide port matched and the moveable short in place.*

electrical length throughout the test procedure. By comparing the loss measurements within the two subgroups—subtracting the insertion loss of the original assembly from the loss of the modified assemblies—a final specification of 0.06(f) dB (with f in GHz) was reached for the insertion loss of the straight-type PMMAs.

An important point in using blind-mating connectors is to establish the number of coaxial interfaces required by a modular system early in the design procedure. For one thing, this will help to simplify the equipment layout. For another, it aids in determining the viability of the final design. Remember: mating forces accumulate. Too many interfaces can create an unrealistic slide-in pressure when the system must finally be aligned.

The PMMA series of push-on coaxial connectors require from 2 to 8 ounces of force to engage and disengage. They are designed to withstand at least 500 mating cycles and, for the sake of ruggedness, have been machined from type-303 stainless steel. The center contacts, outer conductor, and wedge are constructed from beryllium-copper, and the center and outer contacts are gold plated. The axial and longitudinal float are provided by very exacting tolerances, and these are shown in Fig. 6.

Right-angle connectors are included in the PMMA series. The design is somewhat unusual (Fig. 7), in that one-piece center contacts are used rather than the customary soldered two-piece construction. The contacts are contained within a one-piece body that is suitable for passivation. PMMA cable connectors undergo electrical testing in order to insure VSWR of less than 1.30:1 per mated pair. In addition, the components are built to meet the environmental requirements of MIL-STD-202 and MIL-C-39029 for temperature, shock, vibration, industrial gas, and humidity. Additional production tests, as well as approval tests, have been conducted by several major OEMs. The tests, which were system-oriented, included shock, vibration, and phase noise. All tests were passed. **Automatic Connector, Inc., 400 Moreland Road, Commack, NY 11725. (516) 543-5000, TWX: (510) 226-3744. CIRCLE NO. 218**

Acknowledgment

The PMMA design is the subminiaturization of a larger, spring-loaded, float-mounting RF coaxial connector design. The authors wish to acknowledge the contribution and guidance provided by O.A. Lin Ciniero of Westinghouse (Baltimore) during the development of this concept.

CHOOSE MCL

Traveling Wave Tube INSTRUMENTATION AMPLIFIERS

Ahead of their time, MCL TWT AMPLIFIERS are highly useful sources of high power microwave energy, specturally pure, stable and very reliable. The flexible broadband capabilities plus solid state components and conservatively rated circuitry make the illustrated 20 watt series and the 100/200 watt series consistently dependable for any laboratory application. A number of options provide versatility and standard units cover 1-20 GHz.

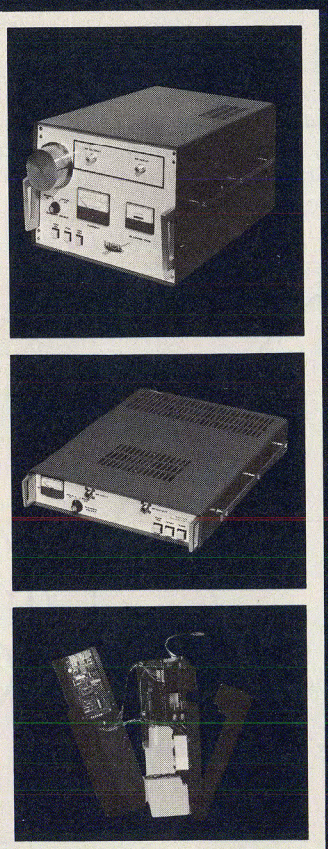
Combining a vacuum tube voltage regulator (for suppression of ripple sidebands) with the amplifiers' solid state components qualifies MCL TWT AMPLIFIERS especially for antenna pattern measurement, EMI susceptibility testing and RF power instrumentation calibration.

Write for the illustrated technical literature on these standard 20 to 200 watt amplifiers. Custom designed units, including Airborne, with special features are also available to meet your most exacting requirement.

CHOOSE "MCL": you'll be glad you did.

WRITE for complete illustrated, technical reference brochure.

MCL, INC. Ten North Beach, La Grange, Illinois 60525
(312) 354-4350 TWX 910-683-1899



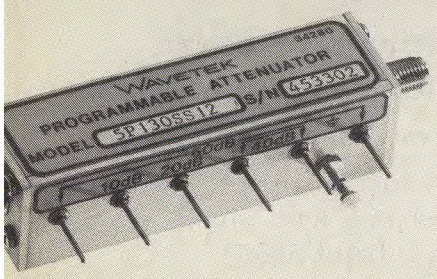
READER SERVICE NUMBER 83

Advertisers . . .
Products . . .
Literature . . .

Find them fast in
infocenter

ttenuators

- Programmable
- Bench Mount Rotary
- OEM Rotary
- Panel Mount
- Fixed Pad



- Matching Pads
- RF Bridges
- Detectors
- Filters
- DC Blocks

*Phone toll-free
800-428-4424

WAVETEK

Wavetek Indiana Inc.
5808 Churchman, P.O. Box 190,
Beech Grove, IN 46107

READER SERVICE NUMBER 111

SEA BACKSCATTER COEFFICIENTS *(continued from p. 73)*

- For vertical polarization:
  If GA $\leq$ 1.00:
  SBC = 29 + SUM − 13log GA
  If 1.00 < GA $\leq$ 7.74:
  SBC = 30 + SUM − GA
  If 7.74 < GA $\leq$ 60:
  SBC = SUM + 68/3cos^2 GA

●●

References

1. Fred D. Nathanson, Airborne Radar Short Course Notes, Technology Service Corp. (1982).
2. Merril I. Skolnik, *Radar Handbook*, McGraw-Hill, New York, pp. 26-5, 26-6 (1970).

Acknowledgment

The author wishes to thank Fred E. Nathanson of Technology Service Corp. for providing updated tables of sea backscatter coefficients and for granting permission to use the data.

Table 1: X-band sea backscatter coefficients in dB below 1 M^2/M^2 (Horizontal polarization)

Grazing angle (degrees)	Sea state 0	1	2	3	4	5	6	7
0.1		**71***	**61***	**53***	**48**	**42***		
	70	63	57	52	48	45	43	42
0.3	**74***	**66***	**56***	**46**	**42**	**39**		
	64	57	51	46	42	39	37	36
1.0		**51**	**46**	**40**	**36**	**33**	**30***	
	58	51	45	40	36	33	31	30
3.0	**58***	**48**	**42**	**39**	**35**	**33**	**28**	
	57	50	44	39	35	32	30	29
10	**56***	**51**	**43**	**37**	**34**	**30**	**27***	
	56	49	43	38	34	31	29	28
30			**44***	**34**	**29**	**26**	**21***	
	52	45	39	34	30	27	25	24
60	**34***	**26**	**23**	**21**		**14**	**12***	
	36	29	23	18	14	11	9	8

*5-dB errors are not unlikely
Bold face values are previously published data.[1]

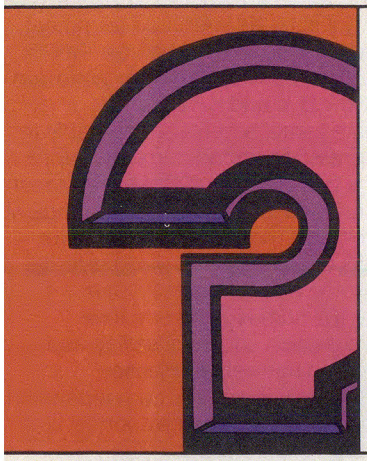
Table 2: X-band sea backscatter coefficients in dB below 1 M^2/M^2 (Vertical polarization)

Grazing angle (degrees)	Sea state 0	1	2	3	4	5	6	7
0.1		**65***	**65***	**51***	**48**	**44***		
	70	63	57	52	48	45	43	42
0.3		**58**	**52**	**45**	**43**	**39**		
	64	57	51	46	42	39	37	36
1.0	**60***	**50**	**44**	**39**	**37**	**33**	**29***	
	57	50	44	39	35	32	30	29
3.0	**56***	**45**	**41**	**33**	**35**	**33**	**28**	
	55	48	42	37	33	30	28	27
10	**49***	**42**	**36**	**32**	**29**	**25**	**22**	
	50	43	37	32	28	25	23	22
30		**36**	**32**	**28**	**24**	**22**	**17**	
	45	38	32	27	23	20	18	17
60	**36***	**24**	**18**	**16**	**14***	**13***	**11***	
	34	27	21	16	12	9	7	6

*5-dB errors are not unlikely
Bold face values are previously published data.[1]

Microwaves & RF

MAY 1983 • VOL. 22, NO. 5



technology assessment

Microwaves & RF addresses the questions that will affect the future of our industry with 20 *Personal views* from top experts in various segments of the high-frequency field. Also featured are a discussion of the importance of subjective values in setting RF radiation standards and insights from a major manufacturer that has penetrated the Japanese market.

departments

13 Feedback
17 Editorial
51 R&D Roundup
58 For Your Personal Interest
190 Infocenter
192 Looking Back
192 Looking Ahead

news

28 **A conversation with Motorola's man in Japan.** Stephen H. Levy, senior vice-president, Japanese Operations, discusses Motorola's experiences in the Japanese market.

35 Spectrum scarcity drives land-mobile technology

42 American HF firms are welcomed in Third World

19 The Front End • 47 Financial News • 54 People • 56 On the Agenda

special section

60 **The 1983 International Microwave Symposium.** Abstracts of all scheduled papers, *Personal views* from experts in the field, and highlights of products to be shown round out our MTT-S coverage.

design features

137 **Subjectivity In Standards: The Case of ANSI C95. 1-1982.** Nicholas H. Steneck of the University of Michigan explains the role values play in setting controversial safety standards.

145 **Hyperabrupt Diodes Make Simple VCOs.** Jon Grosjean, a consultant with Frequency Sources, Inc., shows how hyperabrupt tuning diodes can be used to design voltage-controlled oscillators.

153 **Transform Noise Figure To Noise Temperature.** William E. Pastori of Eaton Corp. uses several simple equations to transform the noise figure of a low-noise amplifier to a noise temperature.

product technology

155 **Rubidium oscillator emerges as time and frequency standard.** AQtron, Inc. used rubidium isotope Rb87 to develop an extremely stable 10-MHz reference signal.

159 VHF/UHF MMIC arrives as general-purpose IF amp . . . 163 New Si MMICs join a growing family

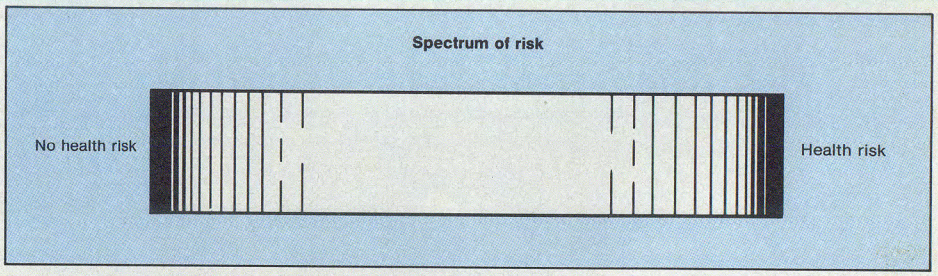
170 New Products • 186 New Literature • 189 Application Notes

Science may be value-free, but applied science—and, thus, ANSI's new radiation standard—is not.

Subjectivity In Standards: The Case of ANSI C95.1-1982

Nicholas H. Steneck, Professor, Dept. of History, University of Michigan, Ann Arbor, MI 48109.

THE American National Standards Institute's involvement in the RF* field began in the late 1950s. By 1958, the military had reached tentative conclusions on the RF standards needed to protect its personnel from the potential hazards of new, larger radar facilities being planned. Since RF exposure was at the time becoming a civilian problem as well, ANSI, one of the largest independent standard organizations, was asked to develop broader guidelines. After close to a decade of deliberation and bureaucratic shuffling, ANSI issued its first Radio Frequency Protection Guide (RFPG) in 1966. Since then, its RFPG has been revised twice, in 1974 and 1982. The latter revision, ANSI C95.1-1982, "Safety Levels with Respect to Human Exposure to Radio Frequency Electromagnetic Fields, 300 kHz to 100 GHz," is used here to analyze the role that values play in setting standards.**



***1. Scientists on ANSI's Subcommittee C95.IV** decided where radiation standards should be set on the safety-risk spectrum.*

Values in standards

Standards are simply reference points used to measure relative safety or risk, with the conditions stipulated in a standard representing the presumed point at which risks begin to outweigh safety or the reverse. In the case of potentially hazardous air pollutants, for example, exceeding standards implies adverse health effects from toxic particles or physical damage to buildings from acid rain; staying within standards implies safety.

As reference points, standards reflect compromises between absolute safety and known risk. Our society has generally agreed that anything that presents a very high probability of health risk ought to be prevented. We have also agreed that life is inevitably hazardous, making it impossible and undesirable to achieve zero risk. The task policymakers face in setting standards is judging where on the safety-risk spectrum a particular standard ought to be set (Fig. 1).

When setting standards, judgments must be made on how much risk is acceptable, on how much uncertainty can be permitted and on whose or what interests ought to be protected. None of these judgments is absolute. There is no single acceptable level of risk, no single amount of permissible uncertainty, no proper balance of interests to protect. There are many opinions on each of these issues, each of which reflects values. Setting standards of necessity begins with values.

Biased toward science

The preeminent value that is built into most standards is a bias toward science. Since the need for RF standards first arose, science has been championed as the key to standard setting. The need for more science is the principal recommendation that emerged from two military conferences sponsored in 1953, which in turn led to the 1956-to-1960 tri-service research program. Similar recommendations were made during an influential symposium held in Richmond, VA, in 1969, the deliberations of the Electromagnetic Radiation Management Advisory Council in the early 1970s, the ANSI review in 1972-74, and Senate hearings in 1973 and 1977. Policymakers in this field, predominantly scientists, have always assumed that the best standard is the one that rests on the most complete and up-to-date research.

The newest ANSI RFPG is no exception to this rule. It is "based on the best available interpretations of the literature" (5). By literature the report's authors mean exclusively "scientific literature." ANSI C95.1-1982 was drawn up by scientists using and interpreting the science they produced. It is not a policy document drawn up by persons expert in making policy decisions; it is not a social

(continued on p. 139)

*Understood to include radio frequency and microwave electromagnetic radiation.

**All citations of this standard (indicated in parentheses) are numbered by section and, when appropriate, paragraph. The terms "RF standard" and "RFPG" are used interchangeably, it being understood that ANSI standards, called "American National Standards," are concensus documents and have no binding legal or legislative authority.

document drawn up by social scientists nor a political document drawn up by politicians. It is, to repeat, first and foremost a scientific document drawn up by scientists.

The principal reason science is relied on so heavily in setting standards such as ANSI's RFPG is the belief that science can eliminate the arbitrariness that would creep in if factual information was not used. Science is stressed as the most effective method of getting rid of other values and the best way of imparting *objectivity* to the standard-setting process. But science does not and can not eliminate all values from decisions on standards. The decision to stress science is, after all, a subjective decision itself. Standards do not have to rest on scientific facts. In a democracy, they could rest on the will of the majority, however that will was informed. Or standards could be mandated by strict economic determinism (i.e., protection equals maximizing economic good). Science has no absolute hold on standard setting. To give it such a hold represents a value

Once the decision is made to use science in standards, further choices have to be made on what type of science to use. Extrapolation from animal experiments can be stressed, or inference from epidemiological studies. Replication can be made the rationale for accepting the existence of hazards or safety. A knowledge of mechanisms can be deemed essential for demonstrating effects. Many decisions are made about the science that goes into setting a standard, and each decision brings its own values.

In the past, ANSI's RFPGs have reflected a narrow, rigorous interpretation of science. Quantification, replicability, and mechanism have been stressed, with the goal being an exactness akin to the physical sciences. Any work that fell short of this goal was stamped unscientific and excluded from decisions about standards. In the 1960s and early 1970s, when scientists almost universally agreed that the only thing RF radiation could do to living tissue was heat it, any reported effects that occurred without heating were dismissed as unreplicable, not quantifiable, and of unknown mechanism. This left thermal evidence as the only acceptable evidence for setting standards and made the old 10-mW/cm^2 ANSI standard a thermal standard.

The new RFPG backs away slightly from this rigorous interpretation of science. Knowledge of cause is not made an essential prerequisite for accepting effects. The subcommittee charged with setting the standard, Subcommittee C95.IV, reviewed the scientific literature "without prejudgment of mechanisms of effects" (6.4). As a result, some effects that were not taken into account in setting the old 10-mW/cm^2 standard are included in the new one. The "emerging data that indicate the existence of athermal effects" (6) have now been judged sufficiently scientific to be used in setting standards. Thus the new standard is not, in this sense at least, a thermal standard.

Very few such concessions are granted in the new RFPG. "Demonstrability . . . relevance, reproducibility, and dosimetric quantifiability" (6.3) are still regarded as criteria for science. Failure to meet any of these criteria can eliminate a study from consideration. This means that the new RFPG continues in the tradition of older ones and excludes "some effects reported in the Eastern European literature . . . because of questionable control procedures and lack of information on environmental parameters and physical measurements" (6.5).

The question whether "modulation frequency and peak intensity may pose a risk to health" (6.8) is not answered, again because no evidence of such a risk exists. The demand for rigor also continues to exclude epidemiological studies. Under the heading "Human Studies" in the selected list of scientific reports used to draw up the RFPG, one finds a brief notation: "none" (A.8).

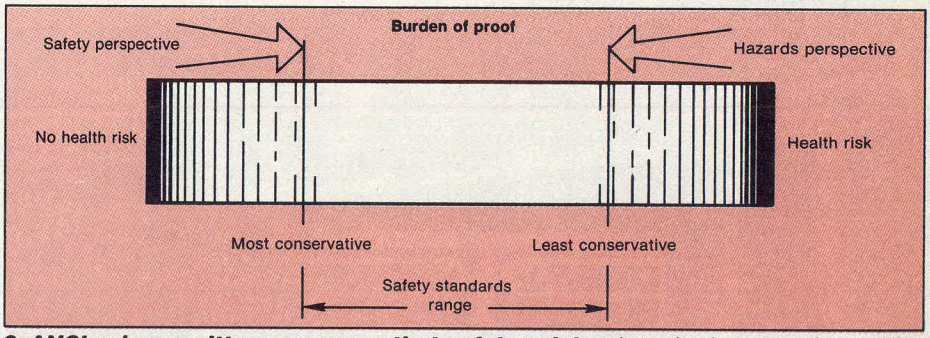
The demand for such rigor is not the necessary product of science—it is the result of embracing a *philosophy* of science. Soviet and Eastern European scientists have for years believed in using science to set standards without demanding complete and absolute verification on every point. They have even argued that to hope for such rigor may be deceptive. Commenting on the utility of epidemiological studies, Baranski and Czerski note: "It is far better to present approximative evaluations than to create an impression of accuracy where none can be had."[1] This too is a philosophical position, one that involves value judgment.

To understand the Eastern European standards, one needs to understand the Eastern European philosophy of science. No less is true of the new ANSI RFPG.

"Innocent until proven guilty" has been the unmistakable approach used in regulating RF technology. Radar and, later, microwave ovens, RF sealers, communication satellites, and video-display terminals were all developed and deployed before being demonstrated safe. The reason for this acceptance is obvious. During World War II, few persons were interested in investigating whether a device that was saving thousands of lives might inadvertently be endangering a few on the side. Once radar was successfully deployed without the appearance of any major hazards, its safety seemed manifest, and RF technological development continued. Anyone who doubted safety had to prove that hazards existed.

Making the demonstration of hazards a major burden in setting standards effectively focused the debate over standards at the upper portions of the safety spectrum (Fig. 2). ANSI's subcommittees approached standard setting from this hazards perspective. They presumed that safe-

(continued on p. 141)



2. ANSI subcommittees presume that safety exists *when the burden of proof for demonstrating hazards cannot be met. This guarantees that the least conservative standard will always be adopted.*

ty exists when the burden of proof for demonstrating hazards cannot be met. They did not approach standard setting from a safety perspective and assume that hazards exist when safety cannot or has not been demonstrated. This in turn dictated that ANSI's RFPGs reflected the least and not the most conservative standards that could be set.† ANSI C95.1-1982 is no exception to this rule.

The consequences of the selective placement of the burden of proof are aggravated by the required degree of scientific rigor (Fig. 2). Rigor is a sieve used to screen bad science from good. The finer the mesh in the sieve, the less scientific evidence will ultimately qualify as good science and be used in setting standards. If the sieve is applied to the process of demonstrating hazards, it inevitably will have the effect of limiting available evidence and therefore stand in the way of making standards more conservative.

Scientific rigor applied in the traditional context of burden of proof is an obstacle to conservatism. Scientific rigor applied in the context of requiring *proof of safety* could have just the opposite effect; it could hamper liberalization and hence favor more conservative standards.

Despite values that mitigate against greater conservatism, the new RFPG is more conservative than its predecessor, C95.1-1974, over some portions of the RF spectrum. Between 30 and 300 MHz, maximum permissible exposure levels are reduced to 1 mW/cm^2 from the old 10 mW/cm^2. The primary reason for this change is the fact that the new RFPG is based on absorbed energy (the amount that actually is absorbed or the "specific absorption rate"—SAR), rather than incident energy (the amount arriving at the skin surface, measured in mW/cm^2). When they started looking closely, scientists discovered that at some frequencies more incident energy was getting into the body than they previously suspected, requiring a lowering of the incident level over this range.

The use of more precision in this case is not a fundamental move toward greater conservatism. On the contrary, the basing of the new RFPG on absorbed energy further illustrates that its primary goal is to map out as precisely as possible the highest possible dividing line between known hazards and assumed safety. The assumption that is being made is that when one is walking along the edge of a potentially dangerous cliff, the best way to keep from falling is to know exactly where the edge is. Theoretically, if all of the twists and turns were properly plotted, one would not fall. (It is difficult not to point out in this regard that one could also avoid falling by not walking so close to the edge.)

A more precise standard, therefore, is not necessarily a more conservative one. This is, in fact, one major consequence of the new RFPG: It does raise permitted exposure levels over some portions of the RF spectrum.

The consequences of the use of precision are further complicated in the

(continued on next page)

†Conservative is used to refer to the goal of maximizing public protection. A "conservative" standard is one that offers the most protection, a "liberal" standard is one that offers the least protection.

Dexcel GaAs FET Express Service!

Order now and get our express service on all Gould Dexcel GaAs FET chips for EW/ECM.

- *Immediate delivery*
- *Competitive pricing*
- *DC test data available*
- *Unmatched quality*

GaAs FET Chips *(packages available)*

1503A—ultra low noise, high associated gain

2502A—10 dB gain at 10 GHz, space qualified

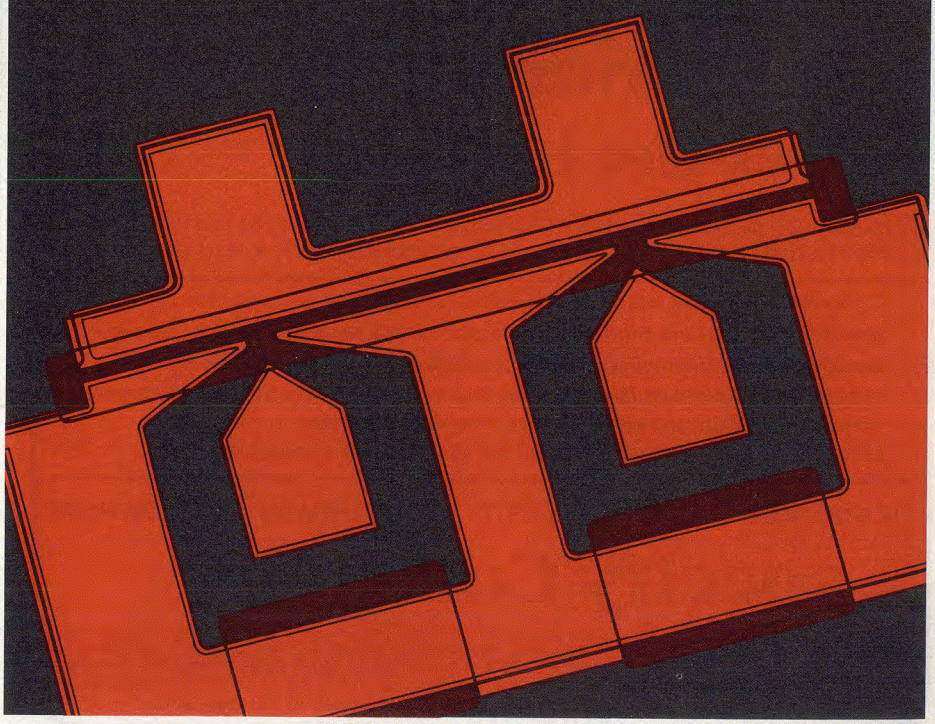
2503A—8 dB gain at 18 GHz, space qualified

2608A—excellent gain, wide dynamic range, high transconductance

3504A—90 mW at 18 GHz

Call now! Gould Inc., Dexcel Division, 2285C Martin Ave., Santa Clara, CA 95050. TWX 910-338-0180. **Phone 408/727-9833, ext. 45.**

GOULD Electronics



READER SERVICE NUMBER 97

case of C95.1-1982 by the fact that precision is not consistently applied to all problems raised in the standard-setting process. For example, while C95-IV subcommittee members were willing to use the precision of the specific absorption concept to reshape the RFPG, making it more conservative at some frequencies and less at others, they were not willing to employ SAR precision when they came to grips with the problem of hot spots—i.e., places in the body where more than average amounts of energy are absorbed. Because "1) the availability of data on distributive SARs is limited and 2) SAR distributions are highly variable" (6.2), the new RFPG does not determine safety on the basis of the peak absorption in the body (i.e., the hottest places), but rather chooses to stick with average whole-body absorption.

The reasoning used in the RFPG to assure the public that peak SARs can safely be ignored employs duplicitous logic. Essentially the public is told that since whole-body SAR is the average of all part-body SARs—hot and cold—both will increase and decrease together. Thus the hot spots will get hotter as the whole body gets hotter: "These localized SARs range from mean to peak and when integrated with localized SARs of less than the mean value, equal the whole-body average." (6.2)

But this is not the issue, and the explanation is essentially like telling the reader not to worry about sitting on an oventop because the temperature of the surface will be an average of the high temperature of individual burners combined with the lower temperature of the stove itself. Clearly, what one is worried about is not the average temperature of the stove, but that of the particular burner on which he or she happens to be sitting. The SAR data provide a great deal of *precise* information on just how hot the burners might be. This raises the following question: If we now have the precision, why not apply it? Why not contemplate setting RF standards on the basis of peak rather than average SARs?

For the past 20 years, Eastern European and Western scientists have disagreed over the term "hazard." Eastern European scientists have used the term "hazard" loosely, choosing to include everything from vague asthenic effects such as headaches, dizziness, and loss of memory to behavior modification and physiological damage. Western scientists have chosen to be more rigorous, usually demanding evidence of permanent physiological damage before deeming an effect hazardous.

This difference of opinion obviously affects the levels that are chosen for safety standards. As the definition of hazard is broadened to include more and more subtle effects, more effects are likely to be found and the standard lowered accordingly. A broad definition of hazard reflects a conservative philosophy of standards. A narrow definition of hazard reflects a less conservative philosophy of standards.

ANSI's new RFPG is in some ways more liberal than its predecessors in its definition of the term hazard. The explicit addition of behavioral modifications to the scientific base includes effects that were previously ignored. Moreover, the new RFPG broadens its definition of hazard even more by accepting reversible behavioral effects as significant. In the past, any effect that disappeared once the exposure ceased was seen as reversible and ignored. The new RFPG reasons that since exposure does not always come to an end, "reversible disruption during an acute (i.e., short-term) exposure is tantamount to irreversible injury during chronic (i.e., long-term) exposure" (6.4). There is, therefore, some added conservatism built into the new RFPG.

Permanence, however, is still required for accepting effects other than behavioral modification. C95.IV subcommittee members did not consider one controversial group of effects, calcium efflux effects, as hazardous—in part because of their belief that this "phenomenon is reversible" (6.5). The literature on "modulated frequency" and "peak intensity" effects did "not provide the evidence of adversity" (6.8) for which the subcommittee was looking. Similarly, "the absence of evidence that toxic agents are potentiated by weak RFEM fields" (6.8) kept these effects from being considered as hazards. As already mentioned, the lack of precise evidence on hot spots precluded "the explicit use of peak SARs" (6.2) in the standard.

(continued on p. 164)



Hyperabrupt Diodes Make Simple VCO's

Voltage-controlled oscillators can be designed quickly and economically by designing circuits around HF, VHF, and UHF hyperabrupt tuning diodes. Several examples show how.

Jon Grosjean, Engineering Consultant, Frequency Sources, Inc., Semiconductor Div., 16 Maple Rd., Chelmsford, MA 01824.

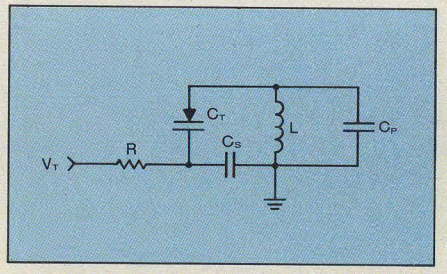
HYPERABRUPT tuning diodes can be used to construct HF, VHF, and UHF voltage-controlled oscillators (VCOs), especially when design requirements call for strictly defined frequency-range and linearity limits. Ion-implanted diodes, with their high Q's and linear frequency-versus-voltage specifications in LC circuits, require only simple circuits to form effective VCOs.

Diodes with capacitances that vary with voltage are conventionally described by the relationship:

$$C(V) = C_0/(1 + V/\phi)^{\gamma} \quad (1)$$
$$= C/(1 + V/\phi)^{\gamma}$$

For a theoretically ideal abrupt-junction diode, γ equals 1, although more realistic values lie between 0.4 and 0.48. A diode is considered "hyperabrupt" when γ is greater than 0.5. Unfortunately, Eq. 1 has its flaws as a design guide since, under hyperabrupt-junction conditions, the value of γ varies with the applied voltage. Fortunately, diodes manufactured with carefully controlled ion-implantation techniques produce such reproducible capacitance/voltage curves that simple, normalized curves can be used to predict the performance of entire families of devices at any chosen voltage.

In addition to this reproducibility, ion-implanted hyperabrupt tuning diodes can exhibit high Q's and linear frequency performance when tuned via voltage in an LC circuit. The circuit will exhibit low distortion at a constant frequency slope (df/dv) over the tuning range. Consequently, phase-lock-loop circuits are relatively easy to design, since the oscillator constant, K_o, is fixed, rather than variable as with diffused, abrupt-tuning diodes.



***1. This circuit was used to generate typical VCO capacitance** values in the HF, VHF, and UHF ranges.*

Choosing a diode

The task of narrowing the field of available diodes to a handful of devices that are suitable for a specific design begins by considering:

$$R = F_{max}/F_{min} \quad (2)$$

where F_{max} is the maximum VCO frequency required for a particular application and F_{min} is the corresponding minimum VCO frequency. If the final value of R is less than or equal to 1.4, the circuit can use a straight-line-frequency diode, and possibly a fixed capacitance in series or parallel with it. Linearity can be traded off for Q by tuning the diode at high voltages. When R is greater than 1.4, a wideband diode should be selected with a tuning range that exceeds both ends of the linear frequency region.

The next step in the diode selection process is to determine whether the VCO will be part of a loop. If the answer is yes, then fixed or trimmer capacitors are not needed in the circuit, unless the acquisition-time specification calls for accurate free-running frequency outputs. When the circuit is not part of a loop, a trimmer capacitor will be needed for the F_{max} adjustment, and a fixed capacitor will be required to add temperature compensation to the VCO.

Table 1: Frequency-dependent circuit capacitances

Freq.	Approx. active element and stray capacitance (pF)	Nominal trimmer capacit. (pF)
0.1-0.5 MHz	15	10
0.5-30 MHz	10	5
30-100 MHz	5	5
100-200 MHz	4	3
200-1000 MHz	1-3	1–2

Following the diode selection, the value of the VCO's parallel capacitance (C_P) can be derived. This capacitance represents the sum of the fixed, stray, and trimmer capacitances, along with the capacitance of the active element. Table 1 offers typical values for nominal trimmer capacitances, and approximations for stray and active-element capacitances, in

(continued on p. 147)

five commonly used RF frequency ranges. The basic circuit used for approximations is shown in Fig. 1.

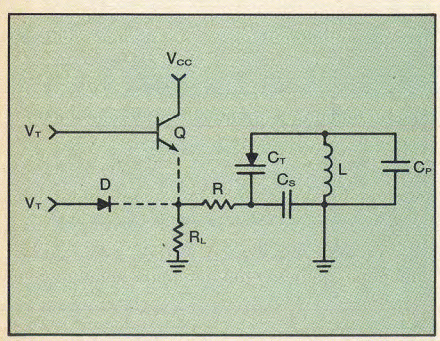
When designing with the circuit of Fig. 1, several considerations should be kept in mind. The tuning diode capacitance (C_T) will vary from a high value (C_{max}) at the minimum tuning-voltage and frequency values (V_{min} and F_{min}) to a low value (C_{min}) at the maximum tuning voltage and frequency (V_{max} and F_{max}). If the VCO must have a fast response time, the series capacitance cannot be too large. Since this capacitance is in series with the tuning diode, it can be used as a "padder" to reduce the tuning range of the VCO and, thus, the residual FM arising from noise or other tuning voltage variations. Some additional benefits from this padder capacitance are a reduction in the AC voltage across the diode (especially at the critical low frequency end of the tuning range), higher tank Q, and a lower overall temperature coefficient.

Resistor R in Fig. 1 combines with the series capacitance to decouple the tuning circuit from the RF circuit. If R is too small, the decoupling will be inadequate. If it is too large, the VCO will be noise-modulated by AC components from the diode leakage current. In critical applications where decoupling is important, an RF choke can be used in place of R.

The basic VCO design depends on knowing the maximum tuning diode capacitance, C_{max}. It can be found by:

$$C_{max} = R_v^2\, C_{min} + C_P\,(R_v^2 - 1) \quad (3)$$

The value of C_{min} should come from a diode's published data. The value of R is from Eq. 2, while C_P is the parallel capacitance as discussed earlier. The value of C_S should be assumed to be infinitely large. A diode's published maximum capacitance specification should slightly exceed the result gained from Eq. 3, in order to provide for a finite C_S, and to allow for a tendency to underestimate the stray capacitance.



***2. Temperature compensation can be added** to a VCO circuit via a transistor (Q) in series with the tuning voltage (V_T).*

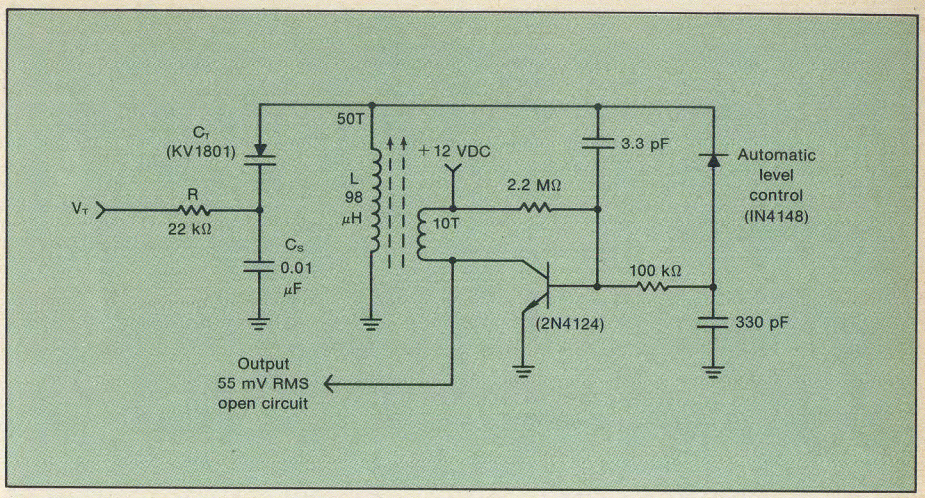
Another parameter that must be calculated is the required tank inductance, L. It can be found from the following equation (where L is in μH, C is in pF, and F_{max} is in MHz):

$$L = \frac{25{,}330}{(C_P + C_{min})\, F_{max}} \quad (4)$$

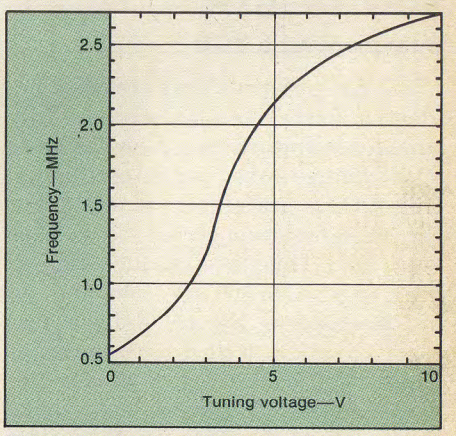
If the calculated value of L is not practical, it can be changed by simply switching to another diode. Choose a diode with a smaller C_{min} in order to increase the value of L; select a component with a larger C_{min} to decrease L. Table 2 should also be of help. In addition, a hand-held calculator program that takes C_S into account is available to help with the diode selection process. Details are presented in the closing paragraph.

Compensating for temperature

When a VCO is not locked to a stable reference source, it may be necessary to provide temperature compensation for the tuning diode's capacitance. One design approach is shown in Fig. 2, in which a silicon diode or silicon transistor "follower" is added in series with the tuning voltage. This compensates for the temperature dependence of the tuning diode's built-in junction voltage, ϕ. Resistor R_L should typically be a low-temperature-coefficient metal-film component in the 22-to-150-kΩ range.



***3. An automatic level control (ALC) helps to maintain** the proper AC level across a diode in a wideband VCO circuit.*

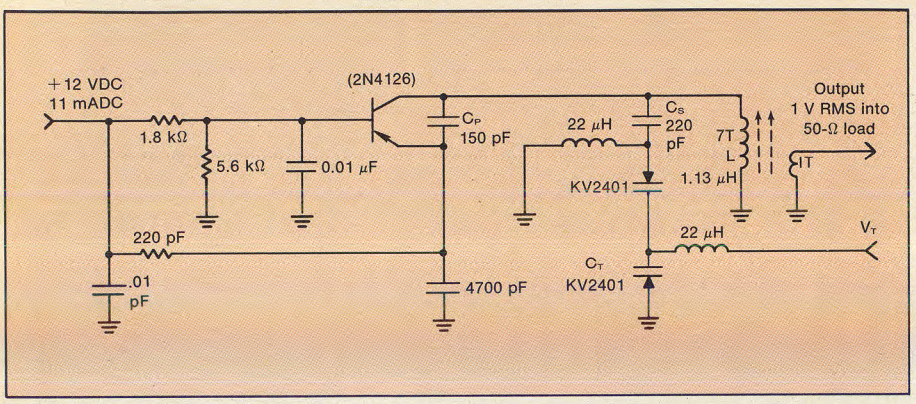


***4. The relationship of frequency to tuning voltage** is shown here for the 0.6-to-2.5-MHz oscillator.*

Low-cost silicon devices can be used for diode D or transistor Q. Since there will about a 0.5-to-0.7-V drop across D or Q, the tuning voltage must be adjusted accordingly. This type of compensation will reduce the tuning-diode temperature coefficients to less than 100 PPM/°C for VHF and UHF devices. Of course, this compensation can't reduce the temperature coefficient to zero, but it can make the coefficient value reasonably constant over a desired tuning range.

The residual tuning-diode capacitance temperature coefficient arises from slight variations with temperature in the dielectric constant of silicon, and can be corrected to within approximately 30 PPM/°C by selecting a temperature-compensating capacitor for C_P or C_S. This technique can also compensate for coil-

(continued on next page)



5. This high-output VCO is capable *of producing + 10 dBm outputs at frequencies from 10.2 to 11.2 MHz.*

Table 2: Tank inductances according to frequency

Frequency (MHz)	L (μH)
0.2 to 1.0	10 to 1500
0.5 to 2.0	10 to 1000
2 to 15	0.1 to 1000
10 to 100	0.08 to 25
50 to 200	0.04 to 0.4
200 to1000	0.008 to 0.04 and tuned lines

inductance or active-element temperature variations, as well as stray contributions to C_P.

Safeguarding a VCO

Certain practices that are often neglected with fixed or mechanically tuned oscillators must be followed with voltage-tuned diode oscillators. One of these precautions requires that the AC signal level across the diode be kept low. This level should be less than or equal to 300 mV RMS, and can be increased to 500 mV RMS (across each diode) when two series-connected, back-to-back diodes are used as a pair. These low levels make it possible to generate a reproducible tuning curve with low-distortion-output operation. Diode tuning characteristics can be negatively altered by excessive AC levels, causing mistracking between receiver LO and RF stages. In cases of serious mistracking errors, an oscillator automatic level control (ALC) may be necessary. This occurs, for example, when the resonant circuit impedance of wideband (large tuning range) oscillators varies greatly. Hyperabrupt tuning diodes have a certain advantage over their abrupt-diode counterparts, in that they provide both linearity and low distortion when combined in a back-to-back circuit layout. Abrupt diodes are capable of low-distortion performance in a back-to-back configuration, but their tuning characteristics tend to be nonlinear.

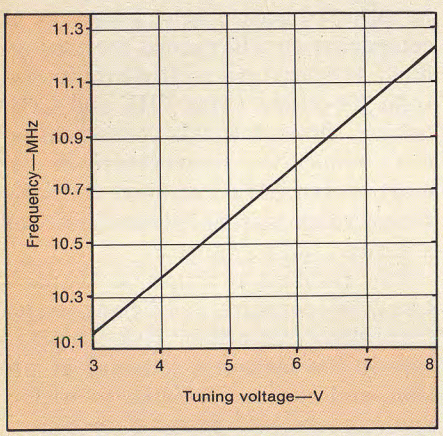
Designing in practice

Several design examples follow. They are meant to fill various typical operational requirements for HF, VHF, and UHF voltage-tuned oscillator circuits. Suppose a 0.6-to-2.5-MHz wideband VCO is needed. Plugging these frequency end points into Eq. 2 yields R = 4.17. Since this value is greater than 1.4, a diode should be selected that exceeds the nominal frequency range limits. In order to guarantee the wideband coverage dictated by the design premise, the highest possible capacitance diode should be chosen, with C_{min} = 26.5 pF. Assuming a reasonable value of 15 pF for C_P, Eqs. 3 and 4 yield:

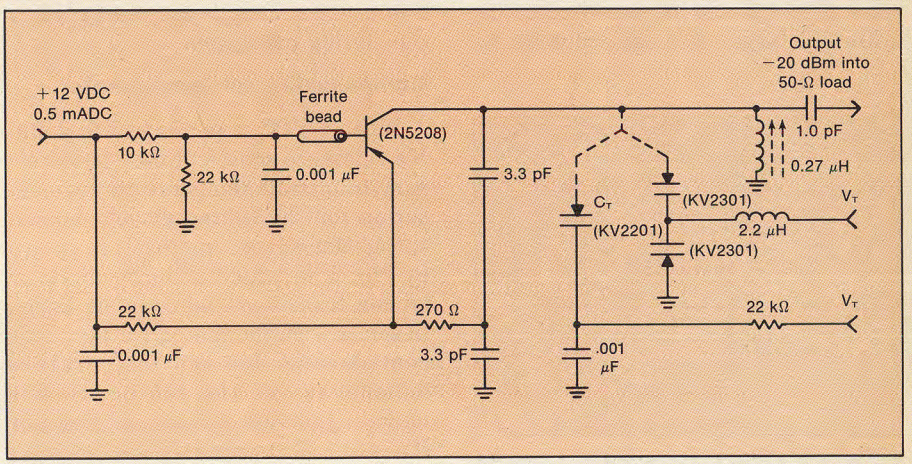
$$C_{max} = 705.5 \text{ pF} \qquad (5)$$
$$L_{max} = 97.7\ \mu\text{H}$$

This inductor value is fine for the design intended. Analysis of capacitance/voltage data for HF diodes will give a C_{max} of about 911.3 pF—far greater than the required C_{max} of 705.5 pF. From these data, the tuning range should come to about 0.5 to 10 V.

Since the frequency range of this VCO is relatively wide, there will be large swings of impedance in the tuned circuit. For example, a circuit with a loaded Q of 80 will have a resonant impedance of 29,000 Ω at 0.6 MHz and 123,000 Ω at 2.5 MHz. In order to maintain the proper AC level across



6. The tuning-voltage/frequency response relationship *for the high-output VCO circuit of Fig. 5 is nearly an exact linear function.*



7. Back-to-back tuning diodes were used *to implement this 40.7-to-60.7-MHz VCO circuit.*

the diode, an ALC should be added to the circuit. This has been implemented in Fig. 3. The pertinent tuning voltages and resulting frequencies are listed in Table 3, accompanied by a graph of the voltage/frequency function in Fig. 4.

Suppose a system requires a VCO capable of producing +10 dBm output power from 10.2 to 11.2 MHz (which translates into 1 V RMS into a 50-ohm load). Since this calls for a large AC voltage across the tank, two tuning diodes must be connected back-to-back in order to reduce the AC level that each diode sees. This individual diode AC can be further reduced by chosing C_S carefully. This last step also serves to linearize the frequency/voltage curve for the circuit. The circuit parameters can be generated by using the calculator program offered at the end of the article.

The diode chosen to construct this particular high-output VCO circuit was a model KV2401 (Frequency Sources, Inc.). When tuned over its recommended 3-to-8-VDC range, the following minimum and maximum capacitances result:

$$C_{min} = C(8\ VDC)/2 = 32.5\ pF \quad (6)$$
$$C_{max} = C(3\ VDC)/2 = 92.38\ pF$$

Trial and error experiments with this diode in this particular circuit have shown that the most linear frequency response is provided when C_S equals 220 pF. This value results in a C_P of 150.32 pF and an L of 1.13 μH. At the center frequency, X_L equals 76 Ω, and the loaded Q will be 30, giving a product, $Q_L X_L$ = 2280 Ω. This indicates that the transistor current need not be high to achieve the required output power. If a 12-VDC supply is assumed, the maximum swing at the transistor collector will be about 10 VPP or about 7 V RMS. For a 1-V RMS output, the tuned circuit transformer should have a turns ratio of 7:1. A circuit that satisfies all these design criteria is presented in Fig. 5, with its voltage/frequency relationship shown in Fig. 6.

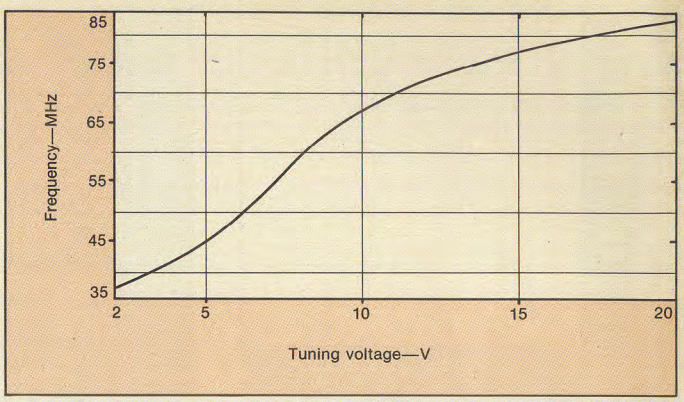
Synthesizing a receiver LO

When the design requirements for a synthesized receiver LO call for frequency coverage from 40.7 to 60.7 MHz, a simple VCO circuit can be developed to fulfill this need. By using these frequency band edges in the calculation of R with Eq. 2, the value obtained will be 1.491. This is an example of a value near enough to the 1.4 cutoff to use straightline tuning. This results in a fixed oscillator constant and a simple loop design. Since no trimmer capacitor is required, a relatively low value of C_P (6 pF) can be assumed. A diode for this circuit design should be a VHF type which tunes over the 4-to-8-VDC region. In creating an actual circuit, the diode chosen was a model KV2201 (Frequency Sources, Inc.). Its voltage tuning range yielded the following values for C_{min}, C_{max}, and L:

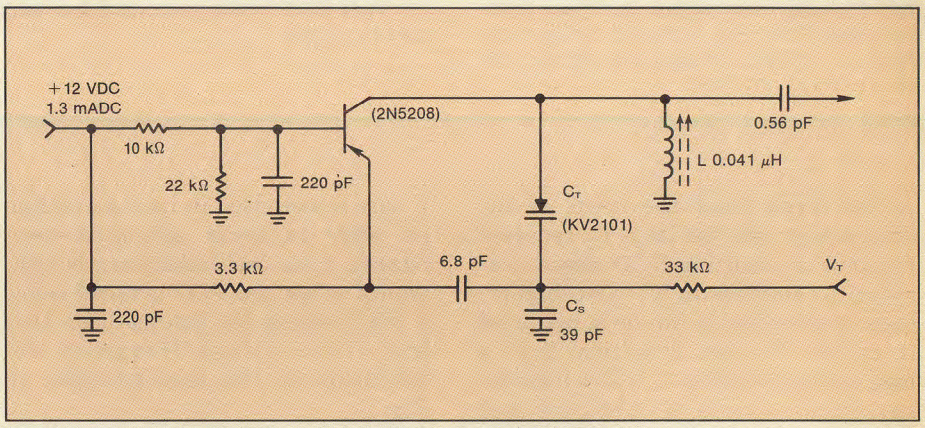
$$C_{min} = C(8VDC) = 19.5\ pF$$
$$C_{max} = 50.7\ pF$$
$$L = 0.27\ \mu H$$

Since this particular diode achieves its C_{max} near a voltage of V_T = 4 VDC, its C_{max} and L values are quite acceptable. The high Q and impedance

(concluded on next page)



***8. Straight-line voltage tuning can be used** with the circuit of Fig. 7, yielding this performance curve. The tuning range is slightly lower than expected because of excessive padder capacitance.*



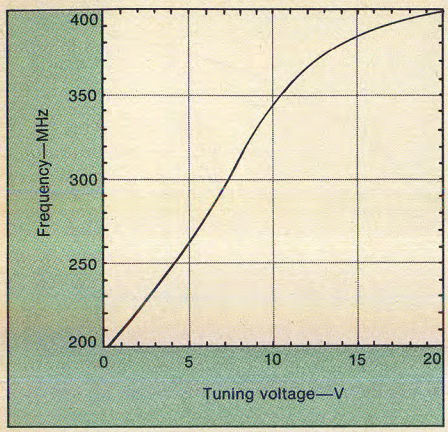
***9. Full-octave frequency coverage** (from 200 to 400 MHz) is offered by this particular VCO design.*

Table 3: A comparison of theoretical and actual tuned frequencies

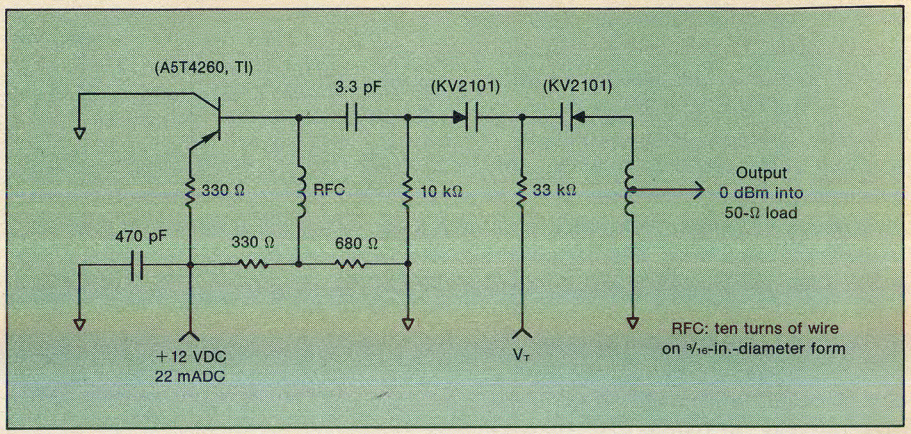
V_T (Vdc)	Freq. (MHz)	
	Actual	Calculated
0	0.5501	0.547
1	0.6923	0.693
2	0.8630	0.865
3	1.2106	1.17
4	1.7984	1.70
5	2.1193	2.04
6	2.3033	2.23
7	2.4327	2.37
8	2.5312	2.47
9	2.6116	2.56
10	2.6781	2.63

Table 4: Tuning voltages for the 10-MHz oscillator

V_T (Vdc)	Freq. (MHz)	
	Actual	Calculated
3.0	10.16	10.20
3.5	10.26	10.29
4.0	10.37	10.39
4.5	10.48	10.49
5.0	10.59	10.60
5.5	10.70	10.72
6.0	10.82	10.84
6.5	10.93	10.97
7.0	11.04	11.08
7.5	11.15	11.18
8.0	11.24	11.26



10. Tuning voltages for the full-octave VCO *of Fig. 9 should be kept low when a linear voltage/frequency relationship is required.*



11. This UHF voltage-controlled oscillator *tunes over the 750-to-950-MHz frequency range.*

of the diode meet the needs of the design plan, but the large C_S required makes the resulting VCO slow to respond to changes in V_T. Two higher-capacitance-diodes can be substituted to correct for this condition. Such a case is shown in Fig. 7, where back-to-back diodes (model KV2301) are used to generate low-harmonic-content outputs. This circuit, as indicated by the measured performance curve of Fig. 8, shows the tendency in C_P to be higher than expected; the actual voltage tuning range is from 3.7 to 8.3 VDC.

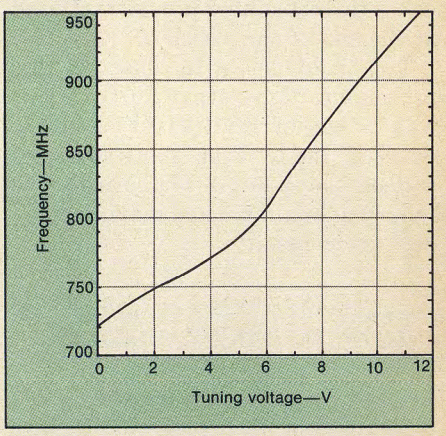
Two more VCO design examples remain. The first of these is a 200-to-400-MHz VCO. To achieve full-octave coverage, the stray capacitances must be relatively low. The optimum diode for this type of circuit should be a high-Q UHF type, used at its minimum and maximum tuning capacitance values.

When employing a typical UHF diode, a tuning range of 0 to 20 VDC can be used, provided that the tuning diode is made part of the capactive divider. A series capacitance of 59 pF has been chosen after trial and error experimentation. This is also the lowest possible capacitance that can be utilized for the required frequency range. From the diode's capacitance/voltage curves, the worst-case C_{max} value is 21.03 pF. Equations 4 and 5 and the hand-held calculator program will yield values of 1.66 pF and 0.4133 μH for C_P and L, respectively. This low value of C_P is possible if stray capacitance is minimized and a low-output-capacitance transistor is selected. The circuit in Fig. 9 can be used if care is exercised in its construction in order to avoid unwanted resonances. Also, oscillations can be controlled when the VCO is tuned below 1 VDC, where the tuning-diode Q is low. The voltage/frequency relationship for this circuit is given in Fig. 10.

The last VCO design example is a 750-to-950-MHz oscillator. Designing at UHF with lumped elements requires some experimentation (as well as patience) in circuit construction, since the external dimensions of the packaged tuning diode tend to approach the length of the tuning inductor, which is normally a short piece of printed-circuit board foil. The design for this UHF VCO is actually a simple one, and is shown in Fig. 11, with its voltage/frequency relationship offered in Fig. 12.

Such UHF circuits are quite sensitive to the physical layout, and problems may be encountered with spurious oscillations or "dead spots" (cessation of oscillation) in the tuning range. This problem is usually exaggerated at low tuning voltages where the Q is the lowest. There are several solutions, including the use of high-f_T transistors, increased inductor Q, or the avoidance of low tuning voltages.

The various systematic designs presented demonstrate the reproducible linear frequency response and low-distortion performance that is possible with ion-implanted, hyperabrupt tuning diodes. The calculator program and additional capacitance/voltage curves mentioned in the text can assist in the design of these fundamental circuits. For copies, simply send a self-addressed envelope containing $0.20 postage to Cathy Fedele, *Microwaves & RF*, 50 Essex St., Rochelle Park, NJ 07662. ●●



12. The voltage/frequency relationship *for the UHF oscillator of Fig. 11 shows a slight dip from true linear response at 6 VDC.*

Advertisers . . .
Products . . .
Literature . . .

Find them fast in
Infocenter
Page 190

Transform Noise Figure To Noise Temperature

The noise figure of a low-noise amplifier can be converted into a value for the effective input noise temperature with several simple equations. The calculations also serve to check instrument uncertainties.

William E. Pastori, Director of Marketing, Eaton Corp., Electronic Instrumentation Div., 5340 Alla Rd., Los Angeles, CA 90066.

THE noise characteristics of most low-noise amplifiers are given by a manufacturer in terms of noise figure. One of the reasons is that the majority of available RF and microwave instrumentation is calibrated to measure this parameter in decibels. Occasionally, the need arises for an amplifier's noise characteristics in terms of the effective input noise temperature, a quantity measured in degrees Kelvin. The necessary calculations are straightforward.

Unfortunately, the evaluation of the uncertainty in the effective input noise temperature from the noise figure uncertainty (as derived from the related accuracy of the test equipment) is not always a simple task. Often an engineer will convert the noise figure uncertainty to a fractional uncertainty. Then, noting the simple linear relationship between the effective input noise temperature and the noise figure, when expressed as the ratio F, he will assume that the fractional uncertainty that applies to the noise figure measurement also applies directly to effective input noise temperature. The results can be misleading.

The calculations that follow avoid this misconception. For simplicity, all quantities given in decibels are marked with the prime symbol. For example, the noise figure uncertainty (in dB) can be expressed by the following equations:

$$\Delta F' = F'_H - F_0' \quad (1)$$

$$\Delta F' = 10 \log_{10} \frac{F_H}{F_0} \quad (2)$$

where F is the noise figure, F_0 is the nominal value of F, F_H is the upper limit of F, and ΔF is the uncertainty of F (and is equal to the difference between F_H and F_0).

The ratio of the upper limit of the noise figure to its nominal value can be given as:

$$\frac{F_H}{F_0} = 10^{\Delta F'/10} \quad (3)$$

Bringing in the uncertainty quantity, ΔF, expressed as a ratio, we have

$$\frac{\Delta F}{F_0} = \frac{F_{h\,-.1}}{F_0} \quad (4)$$

which, by combining with Eqs. 3 and 4, can be written as:

$$\frac{\Delta F}{F_0} = 10^{\Delta F'/10} - 1 \quad (5)$$

This last equation relates the fractional uncertainty in the noise figure ratio $\Delta F/F_0$ to the decibel uncertainty.

The effective input noise temperature, T_E, is related to the noise figure by the expression:

$$T_E = (F - 1)\, 290 \quad (6)$$

It should be mentioned that noise figure measurements sometimes include an image, such as the measurement of a broadband RF amplifier followed by a downconverter. Equation 6 is also valid if F is what is commonly referred to as the "double-sideband noise figure."

The uncertainty in T_E as a function of the noise figure uncertainty can be expressed as

$$\Delta T_E = \frac{\partial T_E}{\partial F} \Delta F \quad (7)$$

By taking the derivative of this, a value for ΔT_E of 290F results. The simple matter of replacing ΔF with Eq. 5, and combining Eq. 6 with 290F gives:

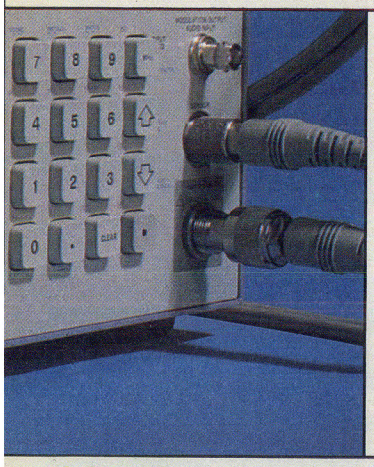
$$\frac{\Delta T_E}{T_{E_0}} = \frac{(10^{\Delta F'/10} - 1)}{(1 - \frac{1}{F})} \quad (8)$$

where T_{E_0} is the nominal value of T_E.

This last equation relates the fractional uncertainty in the effective input noise temperature to the decibel uncertainty in the noise figure. Due to the quantity in the denominator of Eq. 8, the T_E uncertainty is always larger than the fractional noise figure uncertainty. As an example, if an amplifier noise figure of 3 dB was measured with instrumentation having a ±0.3-dB uncertainty, the fractional uncertainty in the noise figure will be about ±7.2 percent. However, when using Eq. 8, the fractional uncertainty in the effective input noise temperature is found to be ±14.3 percent. This amounts to about ±41°K out of a T_E of 289°K. Written either way, the discrepancy is obvious and demonstrates the value of checking these noise uncertainties with Eq. 8. ●●

Microwaves & RF

JUNE 1983 • VOL. 22, NO. 6



cover feature

102 **Integration arms receiver with low noise floor.** Hewlett-Packard's model 8902A Measuring Receiver combines several measurement functions in an instrument that handles 150-kHz-to-1300-MHz signals down to −127 dBm. (Photo courtesy of Hewlett-Packard Co.)

departments

13 Feedback
17 Editorial
67 R&D Roundup
74 For Your Personal Interest
142 Infocenter
144 Looking Back
144 Looking Ahead

news

28 **US seeking to launch DBS at RARC '83.** A major goal of the US delegation to the Region 2 Administrative Radio Conference is a practical plan for implementation of direct-broadcast satellite services.

39 The world (and selling in it) according to Polarad's Joe Schindler
51 An industry insider looks at police radar
54 Emerging technologies call on Capitol Hill

19 The Front End • **59** Financial News • **70** People • **72** Agenda

design features

76 **Standardized Modules Speed Hybrid Layout and Testing.** Randall K. Kirschman of Eaton Corp. explains how interchangeable modules can ease construction of prototypes of hybrid circuits.

83 **Automatic Testing Revisited—Lessons From An RF Test Site.** Robert Rheinlander and Kevin Komorowski of Motorola Semiconductor Products provide an update on an automatic test setup.

89 **Design ATE Systems For Complex Circuits.** Richard S. Napier, George H. Flammer, and Scott A. Moser of Watkins-Johnson Co. describe the use of automatic test systems for complex circuits.

95 **Snap Varactors Prove Useful In High-Factor Multipliers.** Banmali Rawat of the University of North Dakota shows how snap varactors can be useful in frequency multipliers.

99 **TI-59 Program Simplifies Complex-Number Arithmetic.** Darko Kajfez of the University of Mississippi describes a program that performs complex arithmetic without the need for an EE module.

product technology

116 **EEs and MEs combine forces for packaging "can" do.** A staff-written report discusses some of the inter-disciplinary problems involved in designing semiconductor packages.

***126** **Build a miniature directional coupler.** Tomany Szilagyi of EIP Microwave describes the design of a miniature coupler for a microwave frequency source . . . **109** Service monitor serves land-mobile equipment . . . **110** PIN diode switches shrink in size . . . **112** "Intelligent" SNA provides versatile CRT display . . . **114** Miniature noise generator serves measurements from 10 MHz to 26 GHz . . . **119** SAW oscillators feature low phase noise . . . **121** Innovative configuration simplifies EM switch use

122 New Products • **134** New Literature • **138** Application Notes

*Domestic editions only

Standardized Modules Speed Hybrid Layout and Testing

A system employing interchangeable modules frees the designer from construction headaches encountered in getting a new hybrid design into prototype form.

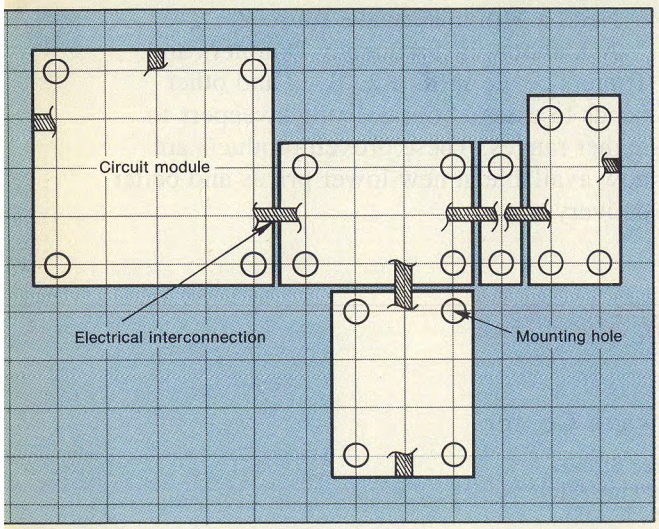
Randall K. Kirschman, Manager, Processing Lab, Research and Development Center, Electronic Instrumentation Div., Eaton Corp., Sunnyvale, CA 94086.

FEW things are more exasperating to the designer than that seemingly enormous gap between the conception of a design and seeing a piece of hardware before him on the test bench. This delay is often exacerbated by a futile search for hardware that will accommodate his requirements for circuit layout, testing, and packaging. These mundane tasks can be performed with far fewer headaches if one adopts a system that uses standardized hardware and parts geometry.

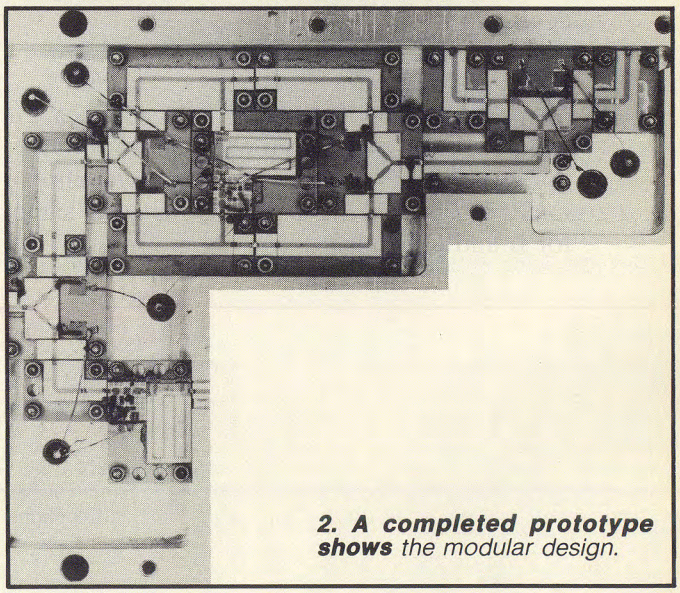
Such a system allows the use of a building-block approach and will ultimately lead to creation of a library of modules that, although designed for one project, can be transferred to others. The system is also readily usable with computer-aided design techniques. Breadboarding and testing have been aided substantially, and hardware lead time has dropped from several weeks to several days.

The essence of the system is a geometric configuration that uses standardized and inter-related mechanical mounting and electrical interconnections (Fig. 1). Modules have various standard lengths and widths, and all mounting-screw holes and interconnections lie on the equidistant lines of a grid. Module edges lie between the grid lines. This technique insures that modules can always be butted and interconnecting terminals can always be easily aligned on all four edges, which allows signal paths to make right-angle turns as well as to follow straight lines. The two orthogonal directions of the grid have the same spacing, and thus modules can be rotated 90 degrees without affecting their compatibility with the system. Spacing of 120 mils was chosen to provide comfortable clearance for standard socket-head #0-80 mounting screws. This grid spacing is really the only dimension the designer needs to remember.

The module bases, or carriers, have lengths and widths that are multiples of the grid spacing, less a small amount to allow for mechanical clearance and machining tolerance. A complete array of carrier geometries provides all possible pairs of length and width (Fig. 3). Because carrier length and width are interchangeable, fewer sizes must be stocked. Although this system is based on the use of metal carrier plates, the concept is equally well suited to other assembly techniques.



1. The standardization concept *employs evenly spaced orthogonal grid lines. Interconnections are made on the grid lines, mounting holes lie on the intersection of grid lines, and module edges lie between grid lines.*



2. A completed prototype shows *the modular design.*

Of course, standardization of any kind inhibits the random placement of parts. The sizes of carriers and the interconnection locations can no longer be chosen arbitrarily, and a centered interconnection cannot always be made. For example, a length or width of 600 mils allows a centered interconnection, but 480 mils does not. There will remain situations whose special requirements cannot be met by one of the standard carriers, but these requirements can often be met by simple carrier modifications.

Layout of the modules or subsystems can be performed by standard methods, with paper layout guides and scaled-up representations of each carrier geometry marked with mounting-hole and interconnection locations. The interconnection locations are the same as the grid lines and serve as the primary references for parts placement. The carriers are flat on top and bottom for economy in machining and flexibility in substrate size and in parts layout. If mounting or grounding surfaces are needed above the carrier surface, small metal ribs can be attached. Figure 4 illustrates that all sections of the carrier are available for circuit parts except for an area in each corner reserved for mounting screws.

Simplified assembly

This system requires no major changes from standard assembly procedures. Parts placement is referenced to the grid lines and is accomplished by temporarily placing precision alignment frame bearing marks at grid locations around the carrier (Fig. 5). Thus, the interconnection points are positioned directly rather than through secondary features such as the edge of the substrates. Other parts are positioned with respect to the substrate or metallization pattern in the usual manner.

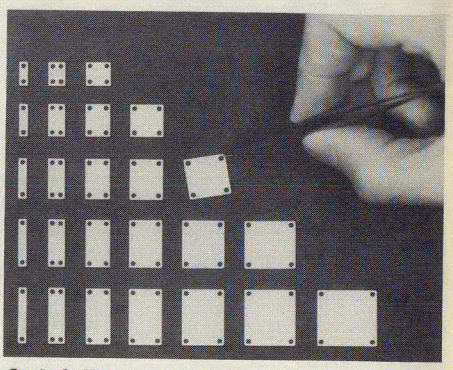
One of the system's major benefits is the ease with which it allows a breadboard circuit to be constructed. The breadboarding scheme is based on substrates with metallization in various general patterns, such as those shown in Fig. 6. The substrates are kept in stock already etched with the basic pattern, and can easily be modified by chemical and mechanical methods to meet particular circuit requirements. Although this breadboarding technique has inherent limitations, it has proven quite useful (Fig. 7).

Putting it to test

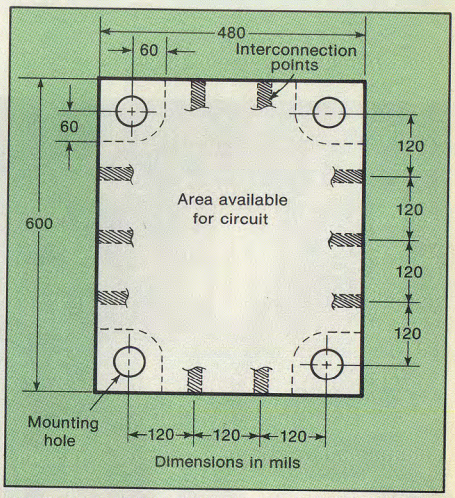
Modules to be tested are mounted individually or in their subsystem configuration onto test plates in the manner shown in Fig. 8. The test plate is simply a flat surface with threaded holes at the grid points. The plates in Fig. 8 are approximately 2 in. square. If a larger area is needed, the dimensions of the plates allow them to be butted. The module to be tested is connected to the test equipment with transition modules. These consist of a small carrier and microstrip substrate connected to a semirigid coaxial cable with a suitable connector on its free end. The connector shown in Fig. 8 is a female SMA.

Two means are presently used to connect the transition module to the module to be tested: a spring contact finger attached to the transition substrate or a ribbon welded between the two substrates. Modules with closely spaced interconnection locations are accommodated with a dual-transition module or intermediate module that spreads the interconnections. Coaxial connectors can be supported with a bracket screwed to the underside of the test plate; DC or low-frequency connections from the module are brought to feedthroughs mounted in support walls secured to the plate. The test plate and transition modules

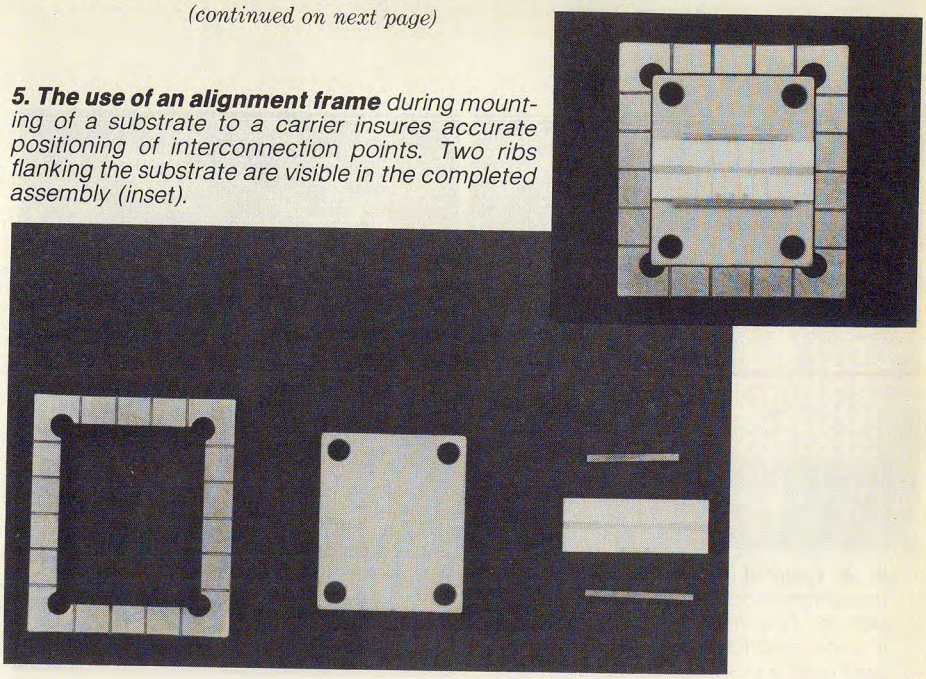
(continued on next page)



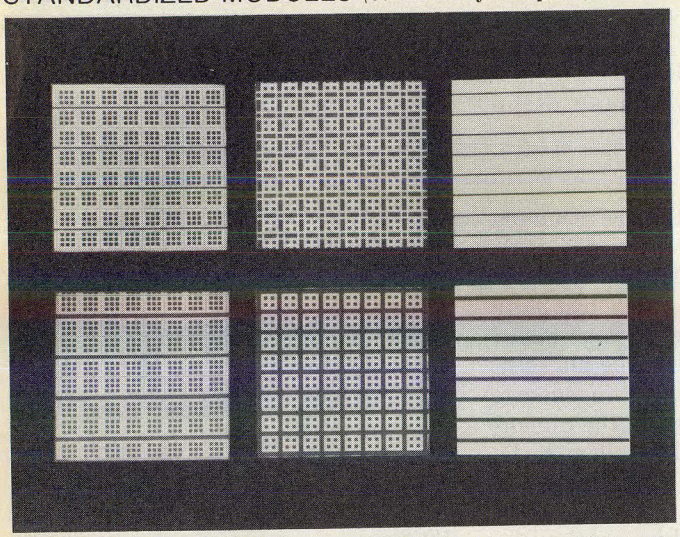
3. A full set of carriers is required *for standardization. Carriers are absent in the upper right as they are equivalent to those in the lower left rotated 90 degrees.*



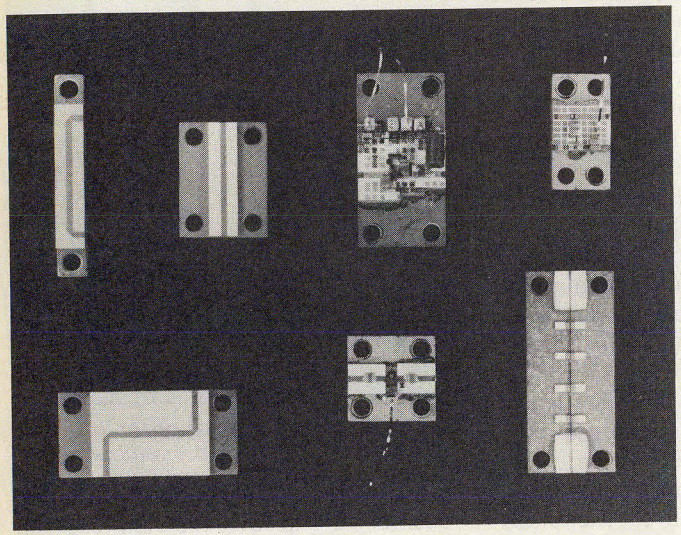
4. The layout of a typical module shows *that a centered interconnection is possible on the 600-mil edge but not on the 480-mil edge. The broken line at each corner indicates the area reserved for mounting screws.*



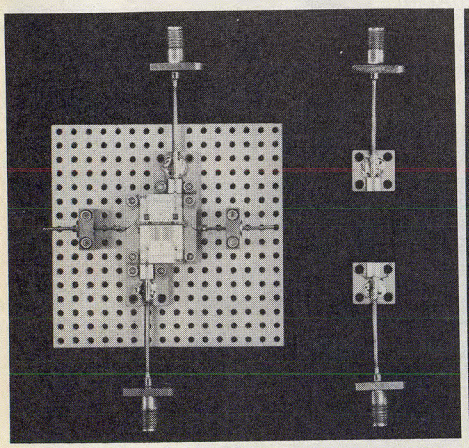
5. The use of an alignment frame *during mounting of a substrate to a carrier insures accurate positioning of interconnection points. Two ribs flanking the substrate are visible in the completed assembly (inset).*

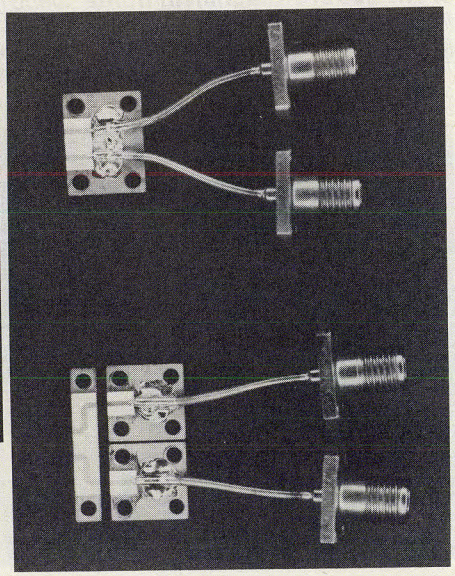


6. Substrates in various microstrip *and pad patterns are used for breadboarding.*



7. Breadboard modules show their origin from the substrates in Fig. 5. *On the left are 50-ohm lines for signal routing; the two modules in the upper right use both microstrip and pads.*





8. A typical test set-up *uses the transition modules shown separately above. Two methods of adapting to interconnections spaced closer than 360 mils are shown at right.*

allow connections to be made to any position on any size module on all four sides simultaneously. Accomplishing this with traditional test fixtures would be much more complex.

The system is invaluable for testing subsystems, as they may be built up and tested one module at a time. Sections of an assembled subsystem may also be measured by removing a module and installing a transition module in its place to extract or inject a signal, or a 50-ohm microstrip line can be substituted.

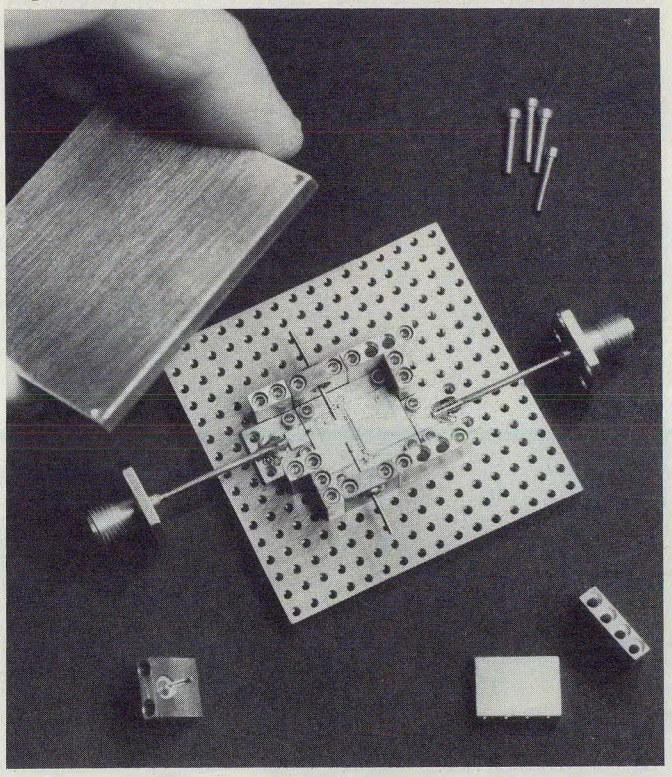
To normalize a test setup, a 50-ohm microstrip-line reference module can be substituted for the module to be tested. The importance of repeatable connections cannot be overemphasized, as they are the key to successful de-embedding with test fixtures of any kind. Obviously, the performance of this testing technique depends on many other factors as well, primarily the quality of the connector-to-coax and coax-to-microstrip transition, and the geometry of the gaps. This makes it somewhat misleading to provide rigid performance specifications for such a test system. However, VSWRs of 1.2:1 up to 12 GHz and 1.4:1 to 18 GHz have been obtained with a pair of transition modules connected to the ends of a 50-ohm microstrip line of 0.025-in.-thick alumina. The interconnections were widened to provide some compensation for the gap, but no additional tuning was performed.

Several types of housings have been used with the system during the various phases of component and subsystem development. The type shown in Fig. 9 allows a preliminary check to be made of the effect of walls, covers, and partitions, and uses hardware attached to the test plate. The hardware is standardized to system guidelines and is comprised of covers and three types of walls: those which allow microstrip intermodule connections, those which have feedthrough connections, and solid walls. All are fabricated in a range of sizes to accommodate any design. Flexible packaging at this stage is particularly important because it allows easy reconfiguration.

The standardized machined housings shown in Fig. 10 are sturdier but less versatile. The floor of the cavity is tapped with rows of holes to mount standard carriers. Separate walls and partitions can be installed in these

(concluded on p. 80)

housings as on the test plate, rather than having them machined in place. Holes in the ends accept coax connectors and feedthroughs. Internal connections can be rerouted with 50-ohm microstrip modules. The large number of possible layouts and sizes for complex components and subsystems makes it difficult to stock housings for all situations. However, this system can simplify the design and machining of such housings, as all the components conform to the standard grid pattern.

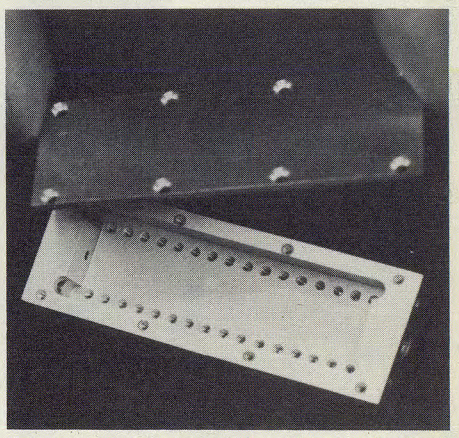


***9. Hardware attached to the test plate allows** the effects of enclosures to be checked.*

The finished product

The system has accomplished the following goals in its use in development and prototype assembly and testing:

- Time needed for layout and drafting of recurring basic features in module and package configurations has been reduced.
- Breadboarding is more quickly accomplished.
- Individual and interconnected modules can be evaluated with standard test fixtures, eliminating the need to manufacture new test fixtures for each design.
- Modules can be conveniently interconnected to form subsystems, and modules can be substituted for others allowing rapid reconfiguration of the system. Larger quantities of standard parts can be acquired, reducing their cost.



***10. A standard housing for prototype designs** has rows of tapped holes along both sides for mounting various combinations of modules. Ends accept coaxial fittings and feedthroughs.*

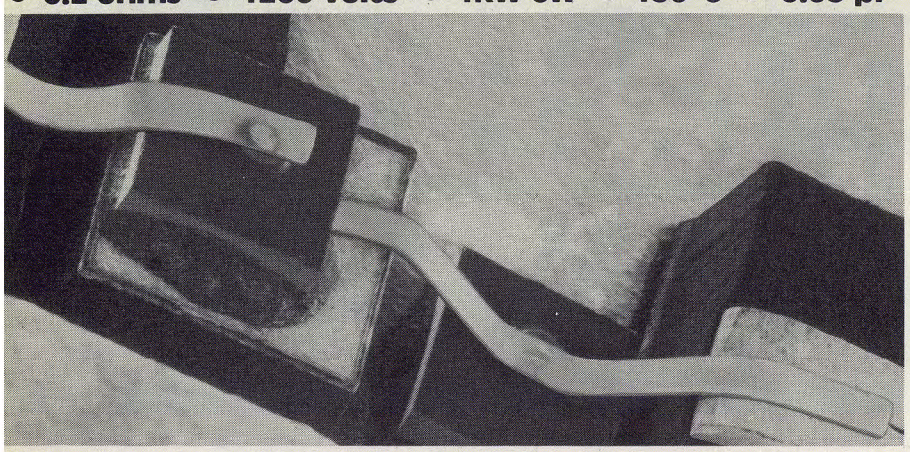
Although this system has been used only for development purposes, there is no reason why it could not also be extended to production operations, with a resulting gain in efficiency and reduction in cost. ●●

Acknowledgments

Angela Hu, Judy See, Al Sweet, Steve Van Fleteren, and Eric Wheelock made valuable contributions to this work.

PIN DIODES .0001-24 GHz

● 0.2 ohms ● 1200 volts ● 1KW CW ● 150°C ● 0.05 pF



High Performance PIN and NIP DIODES for attenuating and switching. They offer designers high power levels, high voltages, low loss, reproducibility, fast switching and MIL-S-19500 reliability. Available as chips. Exact replacements for HP 5082-3000 series. Call today.

FREQUENCY SOURCES, INC.
CHZ / KSW Semiconductor Division
16 Maple Road, Chelmsford, Massachusetts 01824 (617) 256-8101 TWX: (710) 343-0404

READER SERVICE NUMBER 54

Automatic Testing Revisited—Lessons From An RF Test Site

The surest way to establish useful guidelines for designing and operating an automatic test system is to take some tips from an experienced source.

Robert H. Rheinlander, Principal Staff Engineer, and **Keven Lomorowski,** Staff Engineer, High-Frequency and Optical Products Group, Motorola Semiconductor Products, 5005 E. McDowell Rd., Phoenix, AZ 85008.

AUTOMATIC test systems for RF components such as transistors and functional modules are virtually mandatory in today's market in order to insure high-quality, high-yield products. Such testers supplant error-prone manual methods and give manufacturers the means to obtain greater accuracy, faster throughput and statistical databases. The development of an automated test system called SIFT (single-insertion final test) was described earlier in these pages (*Microwaves*, January, 1982, p. 59 and February, 1982, p. 49).

Motorola's SIFT system has been in operation since October, 1980, sufficient time to determine whether automated testing concepts fulfill their promise of accuracy, economy and other benefits. As with any new techique, a learning period is involved. And the lessons learned from SIFT can be beneficial to designers contemplating their own automatic test system installations. By tracing the path of SIFT development, it is possible to establish a set of ground rules that can prove instructive for implementing a variety of automatic test systems.

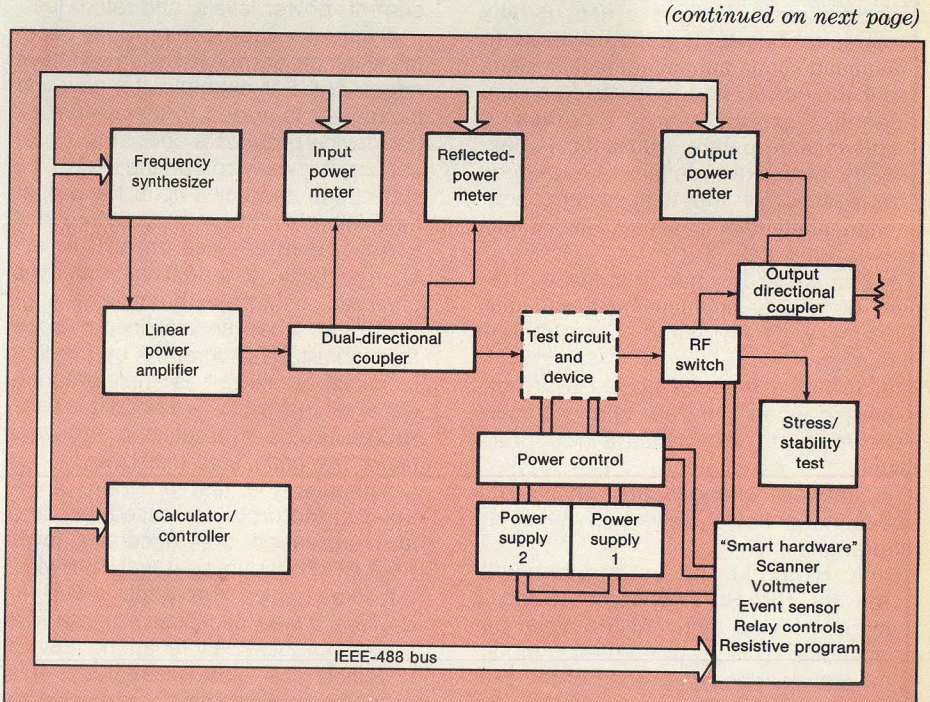
Sifting through SIFT

Four different types of SIFT systems are being used at Motorola. SIFT I tests discrete RF power transistors for parameters such as gain or output power, input return loss, collector efficiency, input versus output phase, and other characteristics, including ruggedness. The system sorts devices into predetermined categories according to the values of the parameters being tested.

SIFT I's frequency range varies from 100 to 1000 MHz at input powers from 1 to 30 W. The collector power supply is adjustable up to ±60 V, with measured setting resolution of 0.1 V and accuracy of ±0.1 V, at currents up to 25 A. A bias supply goes up to 20 V at current levels to 5 A. Programmable constant-current bias can be provided up to 5 A. To drive the transistor under test, a highly linear source covering two frequency ranges—100 to 512 MHz and 450 to 1000 MHz—is used.

All of these test sources are fully programmable. Also fully programmable are measurements of the input and output power, reflected power, and collector current. Only phase measurement is programmed manually, but it is read under com-

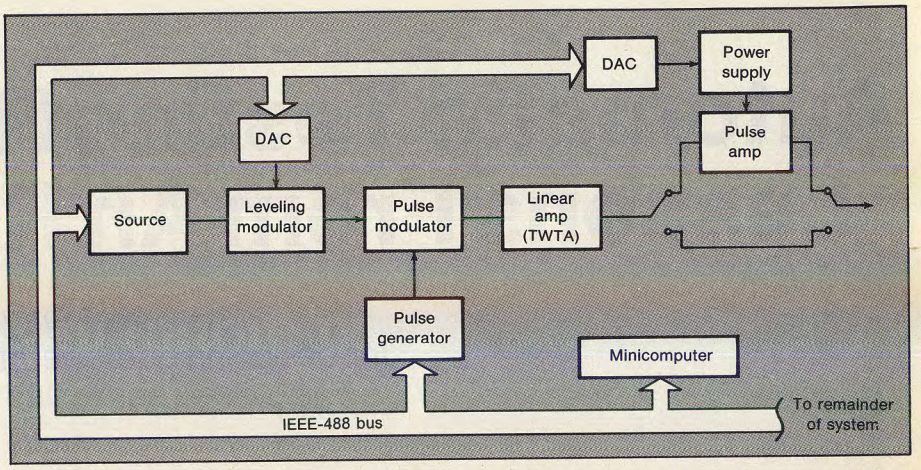
(continued on next page)



1. The generalized single-insertion final test (SIFT) automatic test system *shown here can test either individual RF power transistors or RF gain-block modules. Signal generators and measuring instruments communicate over the IEEE-488 bus.*

puter control. Any 50-ohm test circuit can be used with the system, provided it falls within the input and measurement limits of SIFT I.

SIFT II tests 50-ohm RF gain-blocks having gain-control ports and up to 40 dB of gain. SIFT II has all the capabilities of SIFT I in addition to a highly agile bias supply capable of 20-mV resolution. The system delivers linear input power over a 1-mW-to-10-W range, and can measure from 10 to 1000 MHz without any component changes. Although phase measurement is not currently incorporated, the capability is available. Figure 1 illustrates the basic block diagram form of SIFT I and II.



***2. This portion of SIFT III is designed** specifically for testing microwave pulse-power transistors. The circuitry handles the detection of synchronous peak power levels better than conventional systems.*

Follow some ground rules

Based on experience with the four systems, four basic ground rules for this and similar types of automatic test systems can be established:

- Don't build items that can be purchased. Semiconductor manufacturers are not in the test equipment business. They have neither the development resources nor the capital to provide unique design and documentation. In addition, they require warranty coverage and technical support.
- Use a single, commonly available interconnection system. This permits a wide selection of test instruments having common bus accessibility. SIFT uses the IEEE-488 or GPIB system. Other bus systems offer greater capabilities, but are not as readily available for test instruments.
- Choose a controller with considerable computational power. Make sure it interfaces simply to the bus, has at least 48 kbytes of random-access memory (RAM), and can communicate easily with a host computer. The software language should simplify problems, particularly those relating to the bus interface. We recommend a ROM-based language.
- If additional capital will reduce software problems, spend it. Software turns out to be the biggest cost pitfall

Software tops firmware i

Hardware designers are usually comfortable selecting the hardware to be used in an automatic test system, but they often find themselves on unfamiliar ground when it comes to software/firmware tradeoffs. If flexibility and expandability are primary objectives for the test system, software offers the following advantages over firmware:

- It is easier to change software than to burn-in a new firmware read only memory (ROM), much less change hardware.
- Software requires no hardware expertise when program changes must be made to accomodate new products.
- Software changes are usually less expensive than firmware or hardware changes.

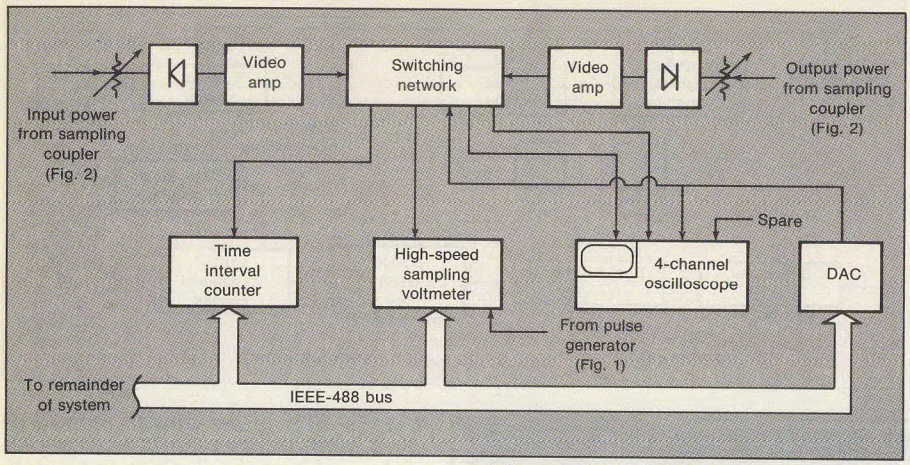
At Motorola, the first program written for the SIFT systems tested a single device type at multiple frequencies. This program used a modular design. The main body of the program called in subroutines that set power supply voltages, frequencies, and RF power levels, and measured current, power levels, and return loss.

A modular approach provides benefits when program expansion becomes necessary. For example, if a new test instrument is added to the system, or if a device requires a special test procedure, it is easy to add the necessary subroutine and call it up at the proper time. What's more, this structured program permits equipment interchangeability. If a test instrument is changed, only the subroutine is modified rather than several lines of code throughout the program. A by-product of modular design is that program debugging is simplified since it is easy to identify the subroutine in error and make the necessary changes.

Although the first program developed at Motorola decreased test time and increased test accuracy (over manual procedures), it was not without drawbacks. For each group of devices, it was necessary to answer a series of questions regarding device specifications and parameters. This required an engineer or technician to set up a test procedure. Another drawback was that only one type of device could be tested at a given time.

These difficulties pointed to the need for greater flexibility, faster execution time and less operator/computer interaction. Faster execution time requires placing the most used subroutines at the top of the program and the least used at the bottom. This is a simple procedure in a modular program. Flexibility requires the ability to test for more than one set of device parameters at a time. If a device fails the highest specifications, it should be tested automatically for less stringent requirements. It is also necessary to maintain statistical data on tested devices.

From these early problems, a dual program technique emerged. One program contains questions on device parameters and specifications. These specifications are recorded as a data file. The second program is an executive that uses the data file. With this technique, questions must be answered just once. A new product requires opening a new data file. But any changes can be handled completely in the data file; no program changes are



***3. Pulse-power measurements are made** by a high-speed sampling voltmeter in SIFT III. The time-interval counter provides time domain information.*

in automated systems (see "Software tops firmware in RF automated test systems," below).

These rules have stood the test of time since the inception of the SIFT systems, and have been the subject of intense prior study. While the performance of the systems is not flawless, steady, cost-effective improvements have occurred over time. Expandability to new requirements has been most successful and economical.

The primary cause of system failures is the failure of electromechanical components (relays). Relays offer simple isolation and low cost. But when parameter settings must be changed from device to device, relays do not hold up. Despite some early component problems, optically-isolated switching devices perform much better than relays.

The second highest failure rate can be attributed to integrated circuits having inadequate source inspection and no assembly pretest. As a rule, choose established vendors of test equipment and make sure that the ICs used have at least gone through current cycling tests.

Linear broadband RF amplifiers are another potential cause of system failures. Manufacturers of such amplifiers (greater than 10-W output and frequency response greater than a decade) sometimes use large-scale output transistors. These devices perform capably above 10 MHz in class-C service. But when they are biased for class-A or high-bias class-AB service, the output power rating must be reduced substantially (to less than 25 percent of the class-C rated output power). Even if the transistors are properly derated, they experience current-distribution faults under DC conditions that can promote early failure.

One solution is to substitute transistors designed for linear service and having gold rather than aluminum metallization structures. Although gold devices may use less active die area, they have proved effective in eliminating transistor failures in two types of amplifier assemblies. Gold is expensive, but it is a lot less expensive than test system failures.

Consider hybrid combinations for smaller-scale amplifiers. For example, a quad combination of four 3-W amplifiers can produce a linear output of 10 MHz to 1 GHz. One of the most reliable amplifiers in SIFT is one that combines 32 push-pull pairs for a 35-W linear output (IMD of −20 dBc) from 10 to 300 MHz.

Watch passive components

While most designers consider a 100-W termination or attenuator simply a passive component, such components must be checked and calibrated throughout their usable ranges. This also includes directional couplers. For example, a new −20 dBDC, 4-GHz attenuator met all its specifications up to a 1-W input. Above 2 W, attenuation rose to 21 dB and continued to degrade nonlinearly up to 10 W of input. This deviation was noted on two of seven units from a single manufactuer.

In another case, a −30-dB, DC-to-2-

(continued on next page)

RF automated test systems

necessary. Moreover, users with little technical background can use the data files for setting up device tests.

In addition to device-testing programs, a method of system calibration is needed. This is accomplished by comparing RF power measurements from a standard meter-pad combination to those of the system meter readings. Measurements are performed at equal frequency intervals and differences between these and the readings from the standard meter are stored in a data file.

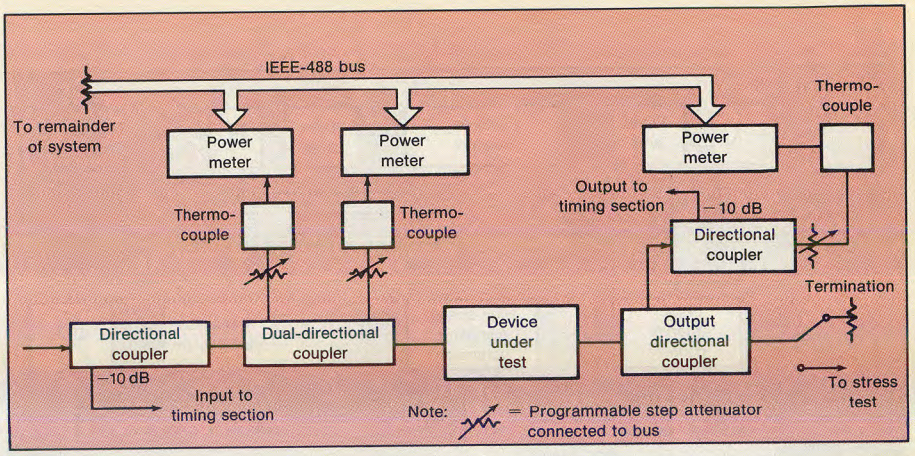
Each test station has its unique calibration file stored on magnetic tape. During device testing, the file is transferred to the computer memory and accessed as necessary. On a power measurement, the meter reading is added to the standard meter correction factor to obtain a corrected power value. If a correction factor for a particular frequency is not in the data file, a linear interpolation is performed to obtain the correct value. This insures repeatability, and the accuracy is traceable to the standards laboratory.

A complete calibration procedure takes just a few minutes and is performed regularly to ensure system accuracy. The calibration program was assembled primarily from subroutines used for device testing.

On the matter of system diagnostics, some basic procedures are included in the executive program. These procedures aid in identifying problems and, if necessary, can shut down the entire test system. The diagnosis of the problem is printed out.

Diagnostic routines were developed in the same manner as the basic program. Small subroutines were used to build a program to test a specific portion of the system. The programs are transferred to magnetic tape, and when needed, are run consecutively. This permits the entire system to be checked quickly and problems to be located. Although the test sequence runs as one large program, it is actually many small modules. Thus, the entire system can be checked using all the programs, or parts of the system can be checked using the appropriate program. ●●

GHz attenuator rated for 150 W input met all of its specifications up to 10 W. But two of ten units demonstrated erratic VSWR and attenuation performance above 10 W. One out of three new directional couplers showed erratic attenuation with deviations up to 2 dB above a 0.5-W average throughput within the TACAN band. These failures underscore the importance of testing and calibrating equipment—particularly new components—before installing them in an automatic test system. A component rated at a high power level may not have test-proven characteristics throughout its dissipation range. Temperature coefficient specifications may not be related to conditions imposed by high-power operations.



***4. SIFT III's pulse-power measurement section** uses the thermocouples to determine power dissipation by measuring temperature rise.*

In general, most automatic network-analysis equipment cannot handle input power levels much above 10 mW. But devices designed to operate at high input power levels can be tested at much lower power levels. Thus, if the system contains a directional coupler designed for a 50-W throughput, calibrate it at that level for reference. Prove component capabilities under actual conditions.

A principal advantage of a computerized system for automatic testing is its ability to "remember." This feature gives rise to one of the most important characteristics of such a system: It permits all testing to be repeatable. That is, the exact same conditions can be imposed on a component time after time. Repeatability leads to a second key attribute of automated systems, traceability. Together, these characteristics permit operation well within the limits of probable accuracy. No other aspects of automated testing are as important as these; in fact, added throughput efficiencies are minor by comparison.

By a simple extension, SIFT III (used for testing microwave pulse power transistors) evolved from SIFT I and II. Conventional methods of synchronous peak-power detection involve a host of variables, and most methods leave much to be desired. The approach chosen is an extension of the SIFT I and II systems (Fig. 2). The four steps are: Measure the average

(continued on p. 101)

Dexcel's Best-Kept Secret: TVRO GaAs FETs

Now you can order superior packaged GaAs FETs from Dexcel for 4-GHz applications with

- *competitive prices*
- *excellent performance*
- *best available service and quality*

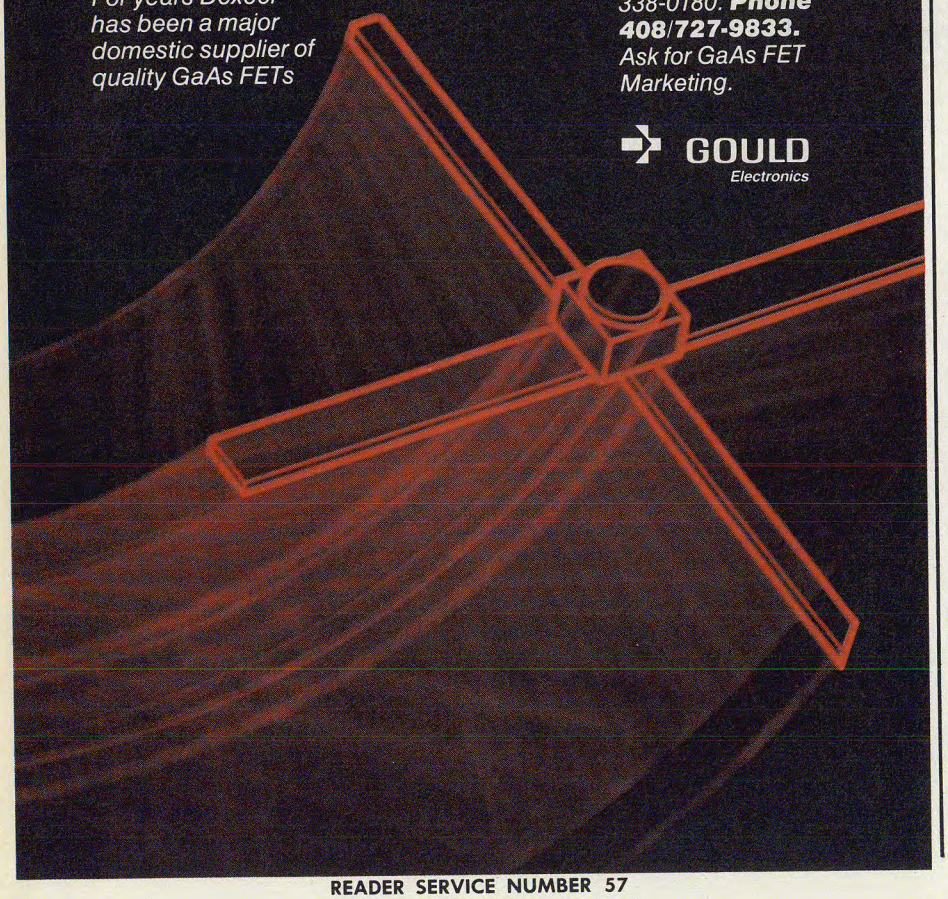
For years Dexcel has been a major domestic supplier of quality GaAs FETs to manufacturers of high-performance amplifiers for EW applications.

And for years Dexcel has manufactured superior FETs for its own proprietary line of TVRO low-noise amplifiers.

So check out our great specifications. Such as the noise figure on our front-end FET: less than 0.8 dB typical!

***Call now!** Gould Inc., Dexcel Division, 2285C Martin Ave., Santa Clara, CA 95050. TWX 910-338-0180. **Phone 408/727-9833.** Ask for GaAs FET Marketing.*

GOULD Electronics



READER SERVICE NUMBER 57

Design ATE Systems For Complex Assemblies

ATE systems have grown in sophistication to where they are able to perform specification testing on entire radios. Menu-driven software allows even nonskilled personnel to operate these systems.

Richard S. Napier, Head, Synthesizer Equipment Section, **G. H. Flammer,** Head, Analog ATE Section, and **S. A. Moser,** Applications Engineer, SSE Div., Watkins-Johnson Company, 3333 Hillview Ave., Palo Alto, CA 94304.

AUTOMATIC test equipment (ATE) systems have come to be associated with printed-circuit board troubleshooting or specification testing of individual devices, such as transistors or diodes. The sophistication of some of these ATE sytems, however, allows them to evaluate complex assemblies such as receivers, which can include RF, analog, and digital subsections. Simply put, the more sophisticated the test hardware, the higher the level of testing that is possible.

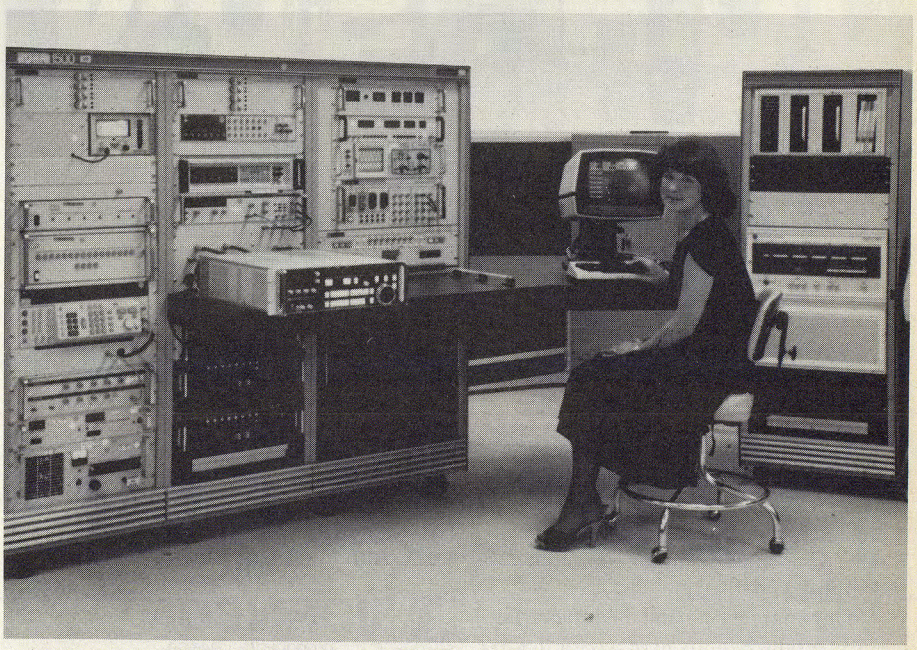
The use of ATE systems for receiver specification testing is a logical progression from the device stage. Specification testing lends itself to automation because of its highly repetitive nature. The need for increased productivity is by no means an insignificant motivating force. Automatic test systems can perform specification testing efficiently, accurately, and quickly. When the increased complexity of complex modules is combined with the shortage of skilled technical manpower, it would seem that the complex-assembly ATE setup is more of a necessity than a production-line luxury. And with time, it has become easier to put together an effective ATE system. The almost univeral acceptance of the GPIB interface has made it possible to quickly mate and adapt component instruments for automatic operation. Since nontechnical personnel can operate these systems (Fig. 1), engineers no longer have to be tied up with specification testing.

Radio specification testing is basically a five-part process which includes connection of the appropriate instrumentation, installation of the stimulus instruments, hookup of the unit under test (UUT), placement and reading of the measurement instruments, and interpretation of the acquired data. In a manual system, such as the one diagrammed in Fig. 2, each of these five steps is performed by a technician. The technician must set up the system with a receiver in place and read the instrumentation, then record the reading and/or use it to calculate the desired data. For consistently accurate measurements, it is often necessary to employ a skilled operator, although this can mean sacrificing an engineer's time and energy.

When the basic system is automated, the five basic steps do not change. As shown in Fig. 3, however, once the controller has access to the instrumentation and receiver, the steps are performed automatically.

The use of ATE systems for radio specification testing can result in an

(continued on next page)

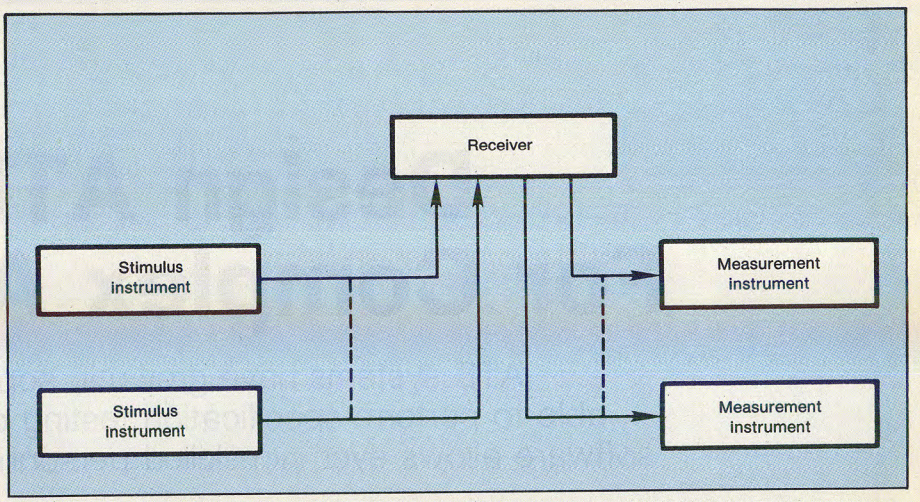


***1. Menu-driven automated test stations** have evolved to the point where a nonskilled operator can perform production specification testing on systems as complex as an entire radio assembly.*

approximate reduction of 90 to 95 percent in test time. The increase in speed is, of course, linked to a reduction in labor costs. With the increased throughput, the need for test personnel declines, along with the amount of test equipment required. An automatic test station can be operated by personnel with far less skill than might be required by a manual test setup.

An ATE system insures accuracy and repeatability in the test process. The system controller has full power over all measurements; as a result, human errors are not introduced into the readings. The system controller doesn't feel any need to increase output by allowing marginal units to pass through the system. In addition, the software compensates for predictable, repeatable system errors, such as cabling losses, which are an inherent part of the test setup. There are no variations in test procedures from unit to unit, so there is a constant repeatability factor.

Of course, there have been some problems in the past when automating a test system for receiver specification testing. For one thing, there is the cost: Considerable expense is usually involved in preparing the software. The real problem is every user is producing the same type of general receiver tests to accommodate their test hardware and a particular receiver. Often, the same user will duplicate his own efforts to adapt new software to another receiver, even if that receiver is to be tested on the same test system. The long programming time can be costly, and can leave an interim period when manual testing must be performed before the system can be operated automatically. Another problem has been that programming on the system would preclude testing on the system, since the system was being used for software development.



2. Before automation, *the basic production measurement setup included this configuration, which had to be set up by a technician.*

Many of these problems have been solved by recent advances in hardware and software. A number of new stimuli and measurement instruments have been designed for remote-control operation, permitting data transcription tasks to be automated efficiently. All instrumentation is routed through the various switching and signal processing assemblies to the UUT. The instruments themselves are controlled via the GPIB bus. Because of the ease of adaptability afforded by GPIB remote control, instrumentation can be added at any later date without any significant engineering effort aside from installation of the system software driver. Since many, if not all, modern ATE instruments are microprocessor-controlled, the instruments themselves serve to establish a system of distributed processing functions. Some of the system controller's workload can be shared by the individual instruments.

An area of significant change in receiver ATE systems is the receiver interface unit. In first-generation systems, these units were designed to



Johnson delivers variable capacitors when you want them.

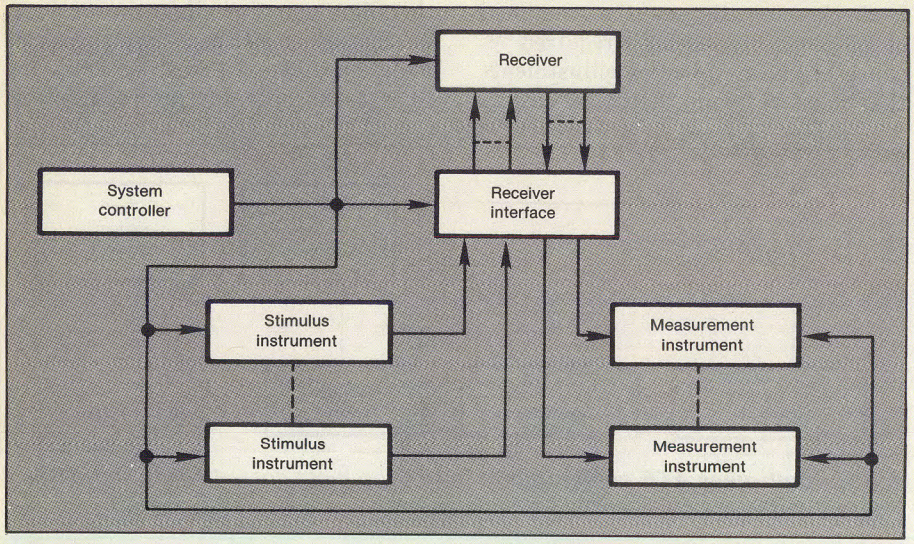
Air variable, tubular, ceramic or teflon dielectric, no matter what variable capacitor type you need, Johnson can meet your specifications—for both design and delivery.

Our engineering and manufacturing staffs produce innovative, cost-effective products. Our national network of 200 distributors helps with your prototypes.

Write for your free catalog or call 1-507-835-6307. Telex: 290470. TWX: 910-565-2161.

JOHNSON® Components Division
E. F. JOHNSON COMPANY, WASECA, MINN. 56093

READER SERVICE NUMBER 60



3. Following automation, the system controller (computer) *has taken over many of the repetitious tasks once performed by skilled operators such as engineers.*

form a unique interface with the receiver under test. But in second-generation systems, the interface has evolved into a general-purpose unit capable of functioning with most receivers. This is due to the fact that the I/O interface on most receivers has become essentially standard. In general, the only time that a new interface might be required is when an interconnection must go from a receiver to a different type of complex assembly.

Computer-intensive concept

Many of the problems associated with ATE system software can be avoided with the use of a software-intensive, or computer-intensive, system organization. Its goal is to minimize a user's need for software development and, in so doing, save time and expense. Menu-driven software is capable of guiding a user through the entire programming and operation phases of receiver testing. As a result, a user is freed from having to perform any actual receiver test programming. The operator is only required to fill in the blanks, via the menus, to give the necessary inputs to the already existing software. The system software then inserts the user's inputs into the resident receiver test software, which then automatically assembles the necessary test programs.

Another boon to users of receiver ATE systems has been the development of the UNIX operating system. The multi-user operating system allows the system hardware to be set in the configuration of Fig. 4. A single terminal is used to control the test execution, while other terminals can be connected to the CPU to function as programming stations. In this manner, several programmers can independently proceed with software development or with test execution.

The first step in the development of proper ATE software is the generation of driver subroutines for each instrument in the test setup. This priority facilitates ease of instrument handling by the actual test programs and eliminates the repetitious use of instrument programming statements. The test programs can then access the instruments by passing parameters back and forth among the subroutines. The use of GPIB instrumentation can help a great deal. For example, a GPIB digital voltmeter with peak storage capability can take many readings, and always keep in memory the highest and lowest values. These peak readings are then passed along to the controller. The controller is freed from the individual voltage measurements, and is only required to recall the final readings.

Once the driver subroutines have been produced, the actual receiver test programs should be generated. Since this is the most costly aspect of the software development, it is an area in which the computer-intensive philosophy attempts to simplify a user's efforts. General-purpose menu soft-

(continued on next page)

NOW...CADEC II for MICROWAVE applications

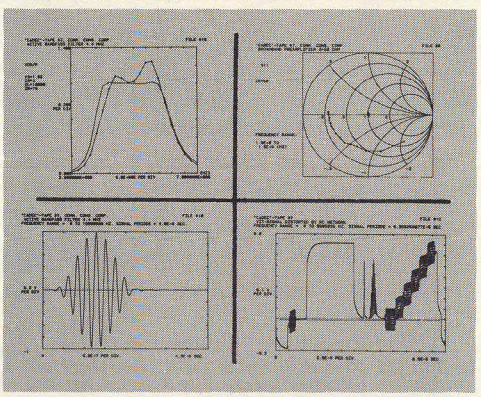
RF Design Engineers Call It AMAZING...

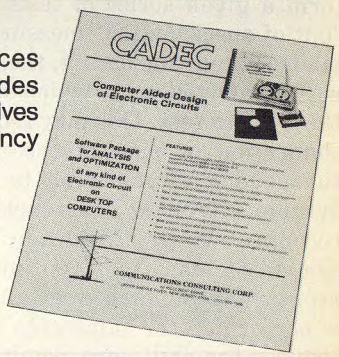
We Call It... CADEC

• CADEC Save's Time, Trouble and Money in the development and design of RF circuits.

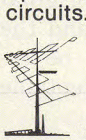
• CADEC...a complete software package compatible with all Tektronix and most HP desk computers.

• Only CADEC reduces design efforts, provides circuit optimization...gives results in both frequency and time domain.





Write for detailed 8 page CADEC Brochure. It describes the software package available for computerized analysis and optimization of any type of electronic circuits.



COMMUNICATIONS CONSULTING CORP.
52 HILLCREST DRIVE
UPPER SADDLE RIVER, N.J. 07458
(201) 825-7966

READER SERVICE NUMBER 61

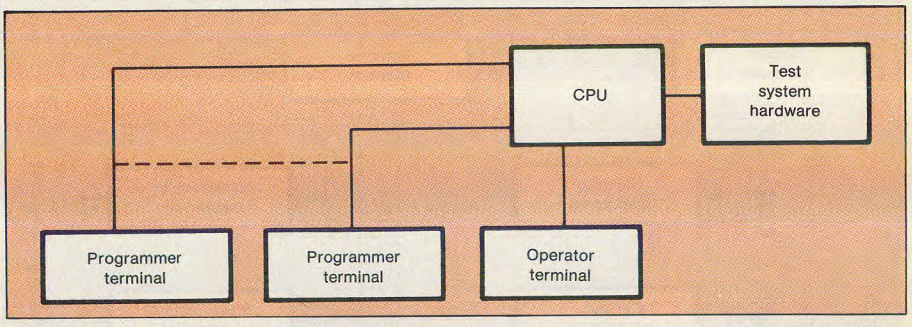
ware is generated which, when operated, prompts the user to call up the menus for the desired tests and to enter the necessary test parameters into the controller. The internal software then generates the necessary test programs automatically, a practice that eliminates a very time-consuming part of the software development.

An operator's interaction with a test system should be designed to minimize any chance of error. Another consideration is that the operator's capabilities should be used to best advantage. In some cases, it may be possible for an operator to sit at a table with the ATE display/controller and the UUT, while for larger systems this may not be practical, and remote control might be necessary.

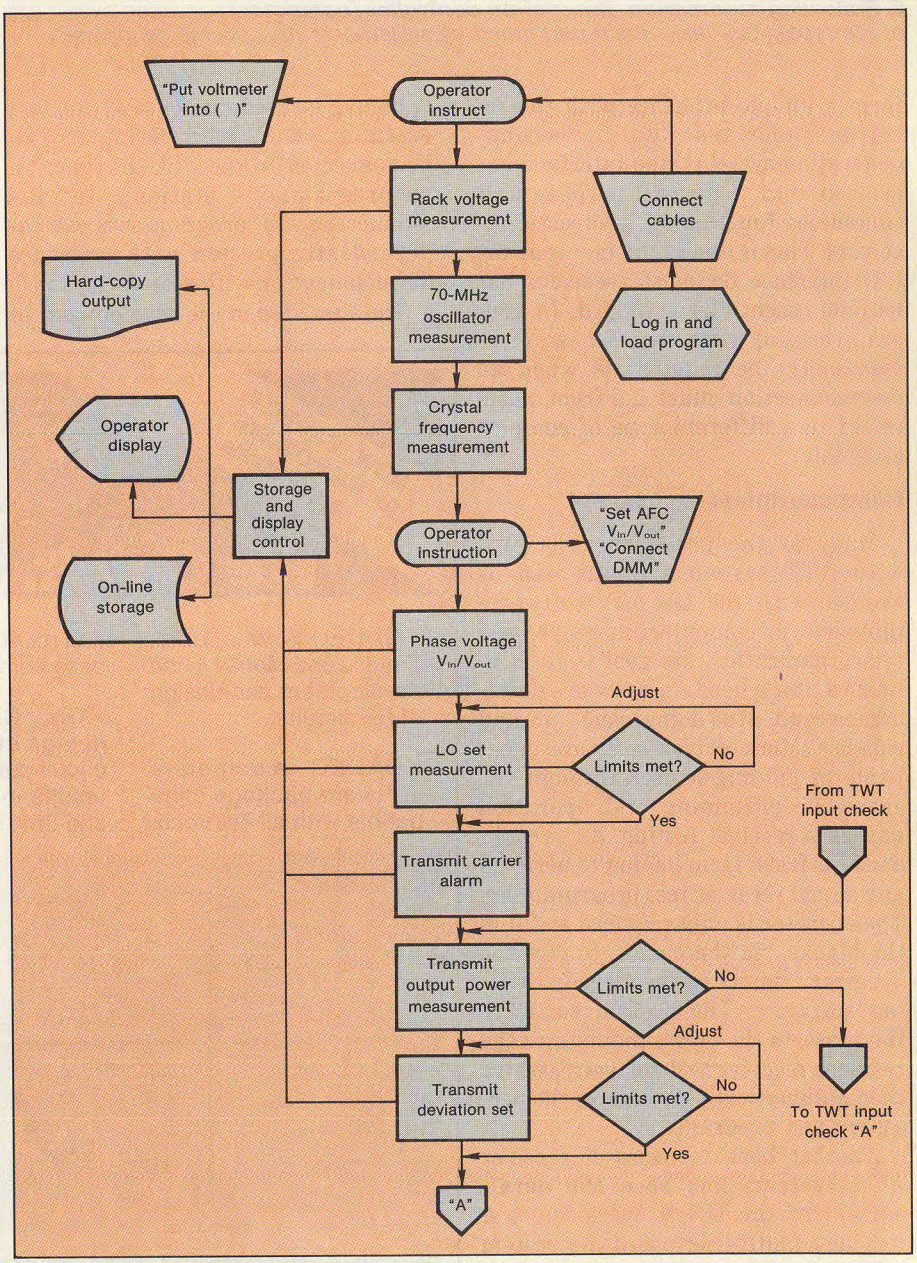
Typically, after the initial connections have been made, an operator will make all preparations concerning the UUT according to instructions provided by the ATE system. Then, the operator must identify the UUT to the test system for data storage purposes. After the test program is initiated, a series of tests are run and data are taken until an adjustment is required. At this time, an audible or visual command will provide an indication of which action is required by the operator.

The test system will identify the required adjustment, monitor performance, and signal the operator audibly or visually when the adjustment has been reached. The system checks on how an adjustment affects other measurements and continues to perform a given series of tests until an "out of specification" measurement is made. When this occurs, the operator will be alerted as to which section of the UUT to test. This may require disconnection of part of the radio for subsequent reconnection to the test system. Even so, instructions for reconnection are provided by the ATE system's menu. This continual operator prompting makes certain the test is performed the same each time and reduces the skill level required. More tests will be conducted until the fault is isolated and repaired. At this point, the system will return to its original test parameter configuraton and the test that initially failed will be repeated in order to check for acceptable specification limits.

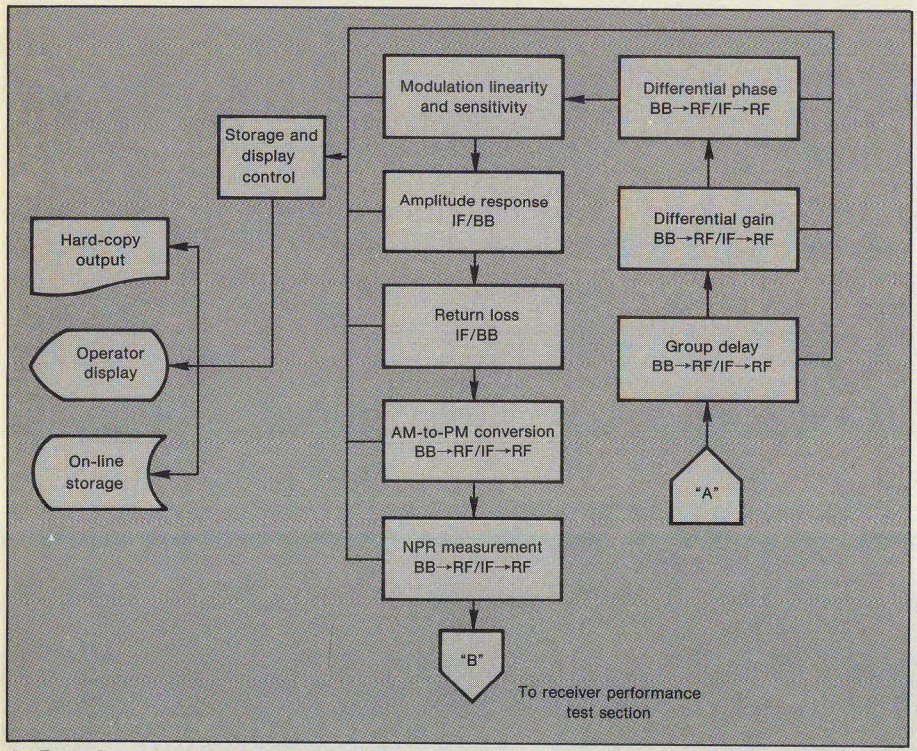
Automatic test procedures are usually partitioned to save as much time as possible. For example, when a radio is checked for alignment, a great deal of operator interaction is required because of the number of adjustments that must be made. A typical case is the alignment flow diagram for a radio transmitter (Fig. 5). On the other hand, performance testing calls for little or no operator intervention, in



4. The multi-user ATE configuration *makes the most cost-effective and efficient use of the test system's overall computing power.*



5. This flow diagram for a radio alignment test *indicates the amount of operator interaction required for this type of testing.*



***6. Receiver performance testing** is performed almost exclusively by the system controller, preempting the need for operator intervention and attention.*

Tests that can be made on an ATE system

Analog tests	Digital tests
AC volts	Noise margin
DC volts	Truth table
Current	Delay
Resistance	Fan out
Pulse	Rise/fall time
(amplitude, width, delay, rise/fall time)	Propagation delay
Period	Delay
Frequency	Race conditions
Phase distortion	Load variations
	Signature evaluation
	Stimulus word generation
	Power dissipation

RF/microwave/receiver tests	
Frequency accuracy	Noise figure
Bandwidth	Selectivity
Passband ripple	Frequency resettability
Incidental FM	IF/image rejection
Signal linearity	LO radiation
Spurious-free dynamic range	Recovery time
RF/IF gain	Spurious response
FM/PM/AM demodulation	Third-order intermodulation
Sampled LO power	Pulse-modulation fidelity
Demodulation bandwidth	Audio/video output
AM/FM sensitivity	FM quieting
RF/IF range/linearity	AFC range/linearity
Intermodulation intercept point	Internally generated spurs
AGC response	Tuning accuracy
Reciprocal mixing	

Note: All tests in each area may or may not be included in a single ATE system.

which case the ATE system can essentially work on its own (see the flow diagram in Fig. 6).

Once the specifications of a receiver have been gathered and analyzed, troubleshooting and diagnosis may be necessary for any out of tolerance units. This test step can be automated in two ways. It is possible to create a mechanical interface to the internal circuitry of the receiver and trace a signal through the receiver, although the necessary interface may require extensive engineering as well as additional costs, and may alter the performance of the UUT to the point that the tests are invalid. A far less painful approach is to rely on the experience of the technician/operator, who should be able, from the acquired specifications, to identify the cause of the radio's failure. Much of this diagnostic capability of a skilled operator can be transferred to the software of the ATE system. Additional software analysis of the specifications can help to speed this diagnostic process.

The versatility of an ATE system is demonstrated by the contents of the table. Most digital, RF, and microwave measurements can be made automatically. Of course, system calibration can be a critical factor, especially for RF and microwave tests. For measurements that run baseband/baseband, IF/IF, or RF/RF, system self-calibration techniques can usually be employed. It is a matter of initially creating a calibration vector that can be algebraically added to subsequent measurements. When tests are at a different level from one another—for example, RF/IF—it's not possible to use an absolute selfcalibration technique. Rather, a tolerance or uncertainty must be used to verify that the system adds only minimal and predictable errors to any measurements.

Any RF cables that are used can be calibrated by routing the cable from the RF stimulus port to the RF measurement port. A swept response is performed and the insertion loss versus frequency is stored in the controller's memory as the calibration vector. The results are later used to provide the necessary correction data for any power measurements. It's possible to calibrate for errors due to group delay, differential gain, differential phase, and other RF factors in a similar manner.

It is possible to set up a remote

(concluded on p. 114)

Snap Varactors Prove Useful In High-Factor Multipliers

Ordinary varactor diodes make good frequency multipliers up to a factor of about four. Above that limit, snap varactors, or step-recovery diodes, can handle the job.

Banmali Rawat, Dept. of Elec. Eng., Univ. of North Dakota, Grand Forks, N.D. 58202

THE nonlinear—capacitance characteristics of reverse-bias p-n junction diodes have proven very useful in frequency multiplier applications. Varactor multipliers are desirable at microwave frequencies because these circuits provide sufficient power output while offering high reliability, small size, and low power consumption. However, at multiplying factors greater than four, the efficiency and power output of ordinary varactor diodes decreases rapidly. This problem has been overcome by the use of step-recovery varactor diodes, or snap varactors.

The step-recovery or charge-storage characteristics of varactor diodes are obtained by driving the devices in the forward-bias region. Under certain conditions, power-handling capacity can be increased with little change in the power-conversion efficiency. A snap varactor is an epitaxial-diffused varactor that stores a charge when conducting in the forward direction. Under reverse bias it conducts for a short time until this charge is swept out by the drive. Conduction then ceases very abruptly.

The microstrip design of the snap varactor multiplier described in this article is quite attractive due to its light weight, low cost, ruggedness, high reliability, and small size. Since detailed theory analysis and performance information is readily available,[1,2,3,4] we will concentrate on the design of a practical microstrip doubler circuit. The following parameters were chosen for the doubler:

Input frequency (f_i) = 2.2 to 2.5 GHz

Input power (P_i) = 27 dBm (≈500 mW)

Output power (P_o) = 20 dBm (≈100 mW)

Output frequency (f_o) = 4.4 to 5 GHZ

Selecting the diode

Snap varactors are suitable for high-efficiency, narrow-bandwidth applications in both low- and high-order multipliers and comb generators, and they exhibit very little change in capacitance at reverse bias beyond zero. The choice of the varactor depends on the input frequency, output frequency, power required, and circuit medium (i.e., coaxial, stripline, or waveguide).

The important parameters to be optimized in the selection of the varactor for the multiplier can be summarized as follows:[5]

Capacitance (C_T)—The capacitive reactance of the diode at the operating bias and output frequency should be a minimum of 30 Ω and preferably 60 Ω. This capacitance also must be compatible with the required thermal impedance. The thermal resistance is an inverse function of the capacitance.

Snap time (T_S)—The transition time, or snap time, is the time the diode takes to switch from the conducting to the nonconducting state. Snap time should be less than the reciprocal of the output frequency.

Lifetime (T_L)—The lifetime is the time required for the stored charge to be recovered. It must be long enough to permit RF current to reach a negative peak before the diode snaps. The lifetime should be a minimum of 10 times the reciprocal of the input frequency. A T_L of 20 to 30 times $1/f_i$ is a better choice.

Package parasitic (L_p, C_p)—The diode's package parasitics should be small enough that the series and parallel resonances are well above the maximum operating frequency.

Thermal resistance (θ_{jc})—The thermal resistance of the diode must be small enough to allow the diode to remain within the maximum operating temperature. In addition, it must be commensurate with the power to be dissipated—i.e.,

$$\theta_{jc} = \frac{T_{max} - T_A}{P_{diss.}} \qquad (1)$$

where,

θ_{jc} = thermal resistance in °C/W

T_{max} = maximum allowable diode temperature in °C

T_A = heatsink temperature in °C

$P_{diss.}$ = power dissipated under worst-case conditions (i.e., $P_i - P_o$) in watts

Breakdown voltage (V_B)—The minimum breakdown voltage required of the varactor can be obtained by:

$$V_B = K\sqrt{2P_o/f_iC_{TR}} \qquad (2)$$

where,

P_o = output power at the output frequency in watts

f_i = input frequency in Hz

C_{TR} = total capacitance in farads at 6 V

K = 0.8 for N≤4

K = 1.5 for N>4

N = multiplication factor

Based on these factors, the most suitable snap varactor chip for the doubler circuit is the MA-43031 (Microwave Associates, Burlington, MA), which has the following characteristics:

Chip system: 132

Suggested output frequency range: 3 to 7 GHz

Junction capacitance at 6 V: 1.6 pf (min), 2.4 pf (max)

Breakdown voltage: 45 V (min)
70 V (max)

The characteristics of the diode package are:

Model: MA-43002

(continued on next page)

Case style: 91
Output power: 1.5 W min
Input power: 5 W max
f_o : 6 GHz
f_i : 2 GHz
Breakdown voltage: 45 V min
70 V max

Junction capacitance at 6 V: 1.6 pf min, 2.4 pf max

Minority carrier lifetime: 75 ns min, 225 max

Snap time: 250 ps (max)

Thermal resistance: 25°C/W max

This varactor chip is quite suitable for series mounting on the microstrip configuration used for the doubler circuit (Fig. 1). The substrate used is alumina with gold cladding and a dielectric constant, ϵ_r, of 9.6, and thickness, H = 0.635 mm (25 mil).

Before going into the details of the circuit design, the input and output resistances of the diode should be calculated:

$$R_i = A/\Omega_i C_j \qquad (3)$$
$$R_o = B/\Omega_i C_j$$

where,

ω_i = input frequency in radians
C_j = junction capacitance

A and B are constants that can be determined by tables.[1] Assuming a graded junction with an elastance-voltage exponent, γ, of 0.333 and a drive of 1.6 for higher efficiency, A = 0.126 and B = 0.172. Thus, R_i = 42.7 Ω and R_o = 58.2 Ω.

Once the required characteristics of the varactor are decided and the device selected, the multiplier design can proceed with the typical input, output, and bias circuits.

Designing to meet requirements

A bandpass filter is used at the doubler's output to suppress the unwanted harmonics. The filter was designed with three elements,[6] and the results obtained are summarized below. Figure 1 shows the filter, whose characteristics include:

Pass band: 4.4 to 5.0 GHz
Center frequency: 4.7 GHz
Rejection: 40 dB at 3.4 GHz and 6.0 Ghz
Fractional bandwidth: 13 percent

The input of the doubler includes a low-pass filter that improves the circuit's performance (Fig. 1). The filter was designed with five elements,[6] and to the following characteristics:

Cut-off frequency: 2.5 GHz
Insertion loss: 0.1 dB
Rejection: 40 dB at 5 GHz

Proper biasing of the diode is important. The circuit chosen (Fig. 1) uses λ/4 lines and assumes a high impedance (100 Ω) for the inductive component and a low impedance (20 Ω) for the capacitive component. The bias voltage can be calculated by:

$$V_o = \phi + (V_B - \phi)V_{no} \qquad (4)$$

where,

Vo = DC bias voltage corresponding to selected drive level
ϕ = barrier potential
V_B = breakdown voltage
V_{no} = normalized voltage

Using Eq. 4 and the appropriate tables,[1] for γ = 0.333 and a drive of 1.6, the bias voltage is −19.27 V.

Since the biasing is being provided from the output side, the bias voltage must bypass the output leakage signal to ground. Thus the bias circuit must be designed around a center frequency of 4.7 GHz, as was the bandpass filter.

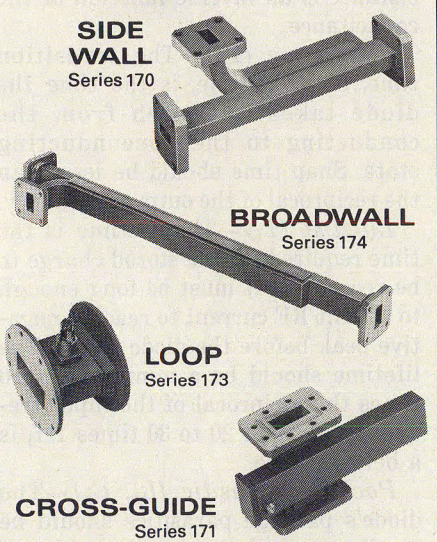
In order to get the maximum output

WAVEGUIDE
Couplers

PRICE: Unbeatable from $99.95
(Series 171X; Quantity 75-100)
DELIVERY: Stock to 30 days
CALL: 516/420-9000

Struthers directional couplers satisfy exacting specifications and environmental requirements in radar and satellite communications systems. PLUS unconditional guarantees assured by a tight, independent quality-control system. PLUS computerized design techniques to offer you custom configured components. PLUS 25 years experience in the manufacture and design of MIL Spec microwave components.

To find out more about Struthers complete product line, write or call for comprehensive catalog. Let our engineering staff review your particular requirements.



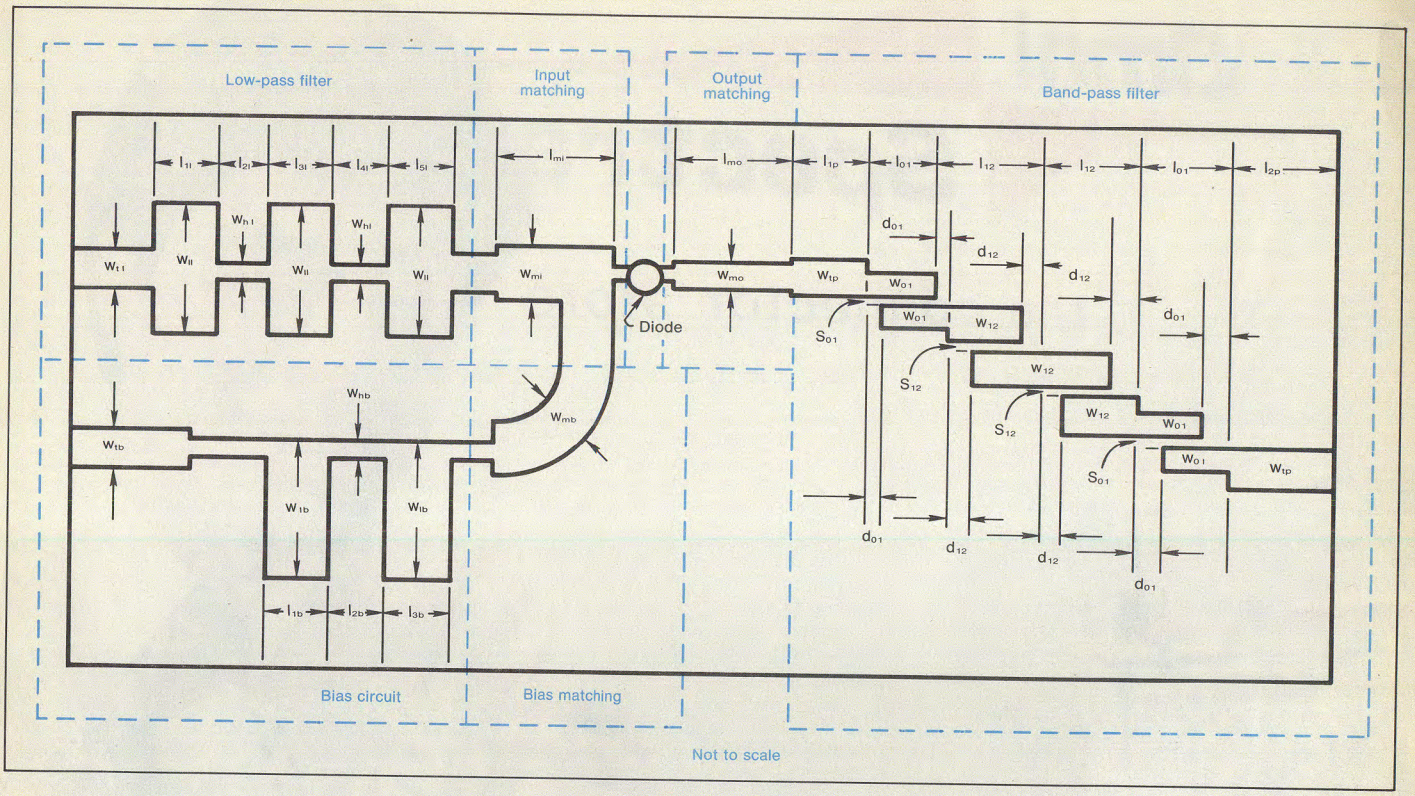
- Frequency Range 1 to 40 GHz
- Available in SMA, Type N, and APC connectors
- Coaxial and waveguide outputs
- Uni- and bi-directional units
- High directivity, Low VSWR
- Ultra Flat Coupling .25DB
- Unconditionally guaranteed

& WAVEGUIDE-TO-COAXIAL ADAPTERS
Series 101



Struthers®
Struthers Electronics Corporation, 4 Dubon Court, Farmingdale, NY 11735 • 516/420-9000 • TWX 510-224-6112

READER SERVICE NUMBER 63



The following dimensions were used in the varactor doubler designed for an output of 4.4 to 5 GHz at 100 mW:

Low-pass filter

w_{tl} = 0.61 mm w_{ll} = 2.80 mm w_{hl} = 0.10 mm
$l_1 = l_5$ = 3.14 mm $l_2 = l_4$ = 6.00 mm l_3 = 5.41 mm

Input matching network

w_{mi} = 0.78 mm l_{mi} = 11.80 mm

Bandpass filter

w_{tp} = 0.68 mm w_{01} = 0.45 mm w_{12} = 0.61 mm
S_{01} = 0.19 mm S_{12} = 0.78 mm d_{01} = 0.21 mm
d_{12} = 0.21 l_{01} = 6.17 mm l_{12} = 6.07 mm
l_1p = 2.00 mm l_{2p} = 5.00 mm

Output matching network

w_{mo} = 0.54 mm l_{mo} = 6.25 mm

Bias circuit

w_{tb} = 0.61 mm w_{lb} = 2.80 mm w_{hb} = 0.10 mm
$l_{1b} = l_{3b}$ = 5.72 mm l_{2b} = 6.59 mm

Bias matching network

w_{mb} = 0.16 mm l_{mb} = 6.56 mm

from the doubler, the impedances of the different parts of the circuit must be matched. That includes matching diode input impedance to the low-pass filter and output impedance to the bandpass filter, as well as matching the bias circuit to the bandpass filter on the output side and to the 50-ohm line on the input side. Microstrip lines of $\lambda/4$ were used. The matching impedance is related to the input and output impedances by:

$$Z_m = Z_i Z_o \qquad (5)$$

where,

Z_m = matching line impedance
Z_i = input impedance
Z_o = output impedance

Note that the matching line between the bias circuit and the bandpass filter was given a round shape to reduce reflections.

The design data for the microstrip doubler are summarized in the table above.

Fabrication considerations

The dimensions of the strips are quite small, especially in the low-pass filter and bias circuit. Therefore, fabrication requires the use of a coordinatograph with a resolution of 0.001 mm. Extreme care must be exercised in the photoetching process to make the undercuts negligible.

If the efficiency of the doubler circuit is less than 95 percent, the dissipated power will be quite appreciable and will require a suitable heatsink. If the circuit losses can be reduced, its efficiency will be increased. ●●

Acknowledgements

The author wishes to express his thanks to Professors John D. Dixon and Alan G. Fletcher for their advice and encouragement.

References

1. C.B. Burckhard, "Analysis of varactor frequency multiplier for arbitrary capacitance variation and drive level," *Bell System Tech. Jour.*, (April 1965), p. 675.
2. P. Penfield and R.R. Rafuse, *Varactor Applications*, MIT Press, (1962), p. 337.
3. A.I. Grayzel, "The bandwidth of the abrupt-junction varactor frequency doubler," *IEEE Trans. on Circuit Theory*, Vol. CT-13, No. 1, (March 1966), p.52.
4. A.I. Grayzel, "Design parameters for overdriven varactor frequency doublers using punch-through or bimode varactors," *IEEE Trans. on Microwave Theory Tech.*, Vol. MTT-17, No. 6, (June 1969), p. 345.
5. Microwave Associates USA, *Microwave Semiconductor Handbook*, (1971), p. 174.
6. G.L. Matthaei, et al., *Microwave Filters, Impedance Matching Networks, and Coupling Structures*, McGraw-Hill, (1964).

TI-59 Program Simplifies Complex-Number Arithmetic

Owners of the TI-59 calculator now have a program that performs the basic arithmetic functions on complex numbers. The program is straightforward and easy to remember.

Darko Kajfez, Professor, Dept. of Electrical Engineering, University of Mississippi, University, Mississippi 38677

COMPLEX numbers are an essential part of many microwave network measurements, including those involving semiconductors and amplifier circuits. Some engineers use a TI-59 programmable, handheld calculator equipped with an EE module to make arithmetic calculations with complex numbers.[1] Use of the EE module can be quite awkward, however, since it is easy to forget the sequence of commands required to perform the necessary operations. Because of the complexity of the EE module, the user must frequently consult the instruction manual while executing the commands.

The program described in this article is an alternative to the EE module. The routine enables users of the TI-59 calculator to perform the four basic arithmetic operations on complex numbers without the need for any additional modules. The program has 114 steps and requires only four registers (26 through 29) and four flags (1 through 4).

One of the benefits of the new program is that the instructions are easy to memorize, since the standard keys are used. For example, the "+" key is used for addition and the "1/X" key is used for inversion. Memory storage and recall are accomplished by means of the standard keys for these operations ("STO" and "RCL"). Thus, rules for operating the program are fairly simple, eliminating the "search-the-manual" syndrome that can occur with the EE module.

How it works

Either the rectangular or the polar coordinate forms can be used to enter a complex number into the TI-59. The rectangular form of a complex number, such as (2 + j5), can be entered by pressing the following keys:

2 x ≷t 5

The storage operates by keeping the complex number's real part in the T register and its imaginary part in the display register. To change (2 + j5) into the polar form, press the following keys:

INV 2nd P→R

It's important to remember two things when using the new program. When two numbers are to be added or subtracted, they must be entered in the rectangular form. When multiplication, division, or inversion are to be performed, the numbers must be entered in the polar form.

Commands are entered in much the same fashion as if real numbers were involved, except that the "SBR" key must be pressed *before* each operation (=, +, −, ÷ , × , or 1/X).

Examining some examples

The four examples that follow illustrate the ease with which complex arithmetic can be performed with the new program. Suppose that a calculation requires the addition of two complex values. In rectangular coordi-

(concluded on next page)

Program listing

000	92	RTN	029	42	STO	058	00	00	087	32	X:T
001	76	LBL	030	29	29	059	85	85	088	43	RCL
002	85	+	031	32	X:T	060	22	INV	089	28	28
003	86	STF	032	92	RTN	061	44	SUM	090	81	RST
004	01	01	033	76	LBL	062	28	28	091	76	LBL
005	61	GTO	034	95	=	063	32	X:T	092	35	1/X
006	00	00	035	87	IFF	064	22	INV	093	94	+/-
007	26	26	036	01	01	065	44	SUM	094	32	X:T
008	76	LBL	037	00	00	066	29	29	095	35	1/X
009	75	-	038	52	52	067	61	GTO	096	32	X:T
010	86	STF	039	87	IFF	068	00	00	097	92	RTN
011	02	02	040	02	02	069	85	85	098	76	LBL
012	61	GTO	041	00	00	070	44	SUM	099	42	STO
013	00	00	042	60	60	071	28	28	100	42	STO
014	26	26	043	87	IFF	072	32	X:T	101	27	27
015	76	LBL	044	03	03	073	49	PRD	102	32	X:T
016	65	×	045	00	00	074	29	29	103	42	STO
017	86	STF	046	70	70	075	61	GTO	104	26	26
018	03	03	047	87	IFF	076	00	00	105	32	X:T
019	61	GTO	048	04	04	077	85	85	106	92	RTN
020	00	00	049	00	00	078	22	INV	107	76	LBL
021	26	26	050	78	78	079	44	SUM	108	43	RCL
022	76	LBL	051	81	RST	080	28	28	109	43	RCL
023	55	÷	052	44	SUM	081	32	X:T	110	26	26
024	86	STF	053	28	28	082	22	INV	111	32	X:T
025	04	04	054	32	X:T	083	49	PRD	112	43	RCL
026	42	STO	055	44	SUM	084	29	29	113	27	27
027	28	28	056	29	29	085	43	RCL	114	92	RTN
028	32	X:T	057	61	GTO	086	29	29			

nate form, the operation would be expressed as:

$$(10 + j2) + (8 - j2) = (18 + j0)$$

In order to use the TI-59 in the calculation, press the following keys:

10 x ≷t 2 SBR + 8 x ≷t 2 ± SBR =

The display will then show the imaginary part of the result (0). To view the real part (18), press the x ≷t key. It is important to realize that, because the x ≷t key has now been engaged, the complex number is now stored improperly: the real part is in the display register, while the imaginary part is in the T register. To use the value in any further computations, it must be stored properly. This can be done by pressing the x ≷t key again.

Multiplication is handled in a different manner than addition. The complex values must be entered in their polar forms. In order to compute the following,

$$(10 \angle 90°) \times (0.5 \angle -90°) = (5\angle 0°)$$

press the following keys:

10 x ≷t 90 SBR × .5 x ≷t 90 ± SBR =

The phase angle of the result (0) will appear in the display, with the absolute value (5) stored in the T register.

When the complex numbers to be operated upon are not in the form desired, the proper conversion operation should be performed to make the number suitable for use in the program. Such a case would be necessary in

$$(10 + j10) \times (.5 - j.5) + (2 + j2) = (12 + j2)$$

where two complex numbers are multiplied and the result added to a third complex number. The solution requires the use of both rectangular and polar forms, since addition and multiplication are being performed. Proceed in the following manner:

Enter the first number in rectangular form, convert it to the polar form, and start the multiplication operation:

10 x ≷t 10 INV 2nd P→R SBR ×

Next, enter the second number, convert it, and complete the multiplication process with:

.5 x ≷t .5 ± INV 2nd P→R SBR =

Before the addition of the third number can be executed, it is necessary to make a conversion to the rectangular form:

2nd P→R SBR + 2 x ≷t 2 SBR =

The resulting value shows the imaginary part (2) in the display register, and the real part (12) in the T register.

One last example is included to demonstrate how to attack a problem in which mixed operations are to be performed and, thus, intermediate storage of values is necessary. Suppose that the reflection coefficient must be computed:

$$\Gamma = Z - Z_0/Z + Z_0$$

with values of $Z = 35 - j10$ and $Z_0 = 50$. First, solve for the numerator and store this result in the polar form:

35 x ≷t 10 ± SBR − 50 x ≷t 0 SBR = INV 2nd P→R SBR STO

The display will show 213.69, the angle, in degrees, of the numerator. Next, compute the denominator and express this value in the polar form:

35 x ≷t 10 ± SBR + 50 x ≷t 0 SBR = INV 2nd P→R

The display will show the angle of the denominator as −6.709 degrees. The last step is to take the inverse of the denominator and multiply it by the numerator:

SBR 1/X SBR × RCL SBR =

The result is 2.106∠ 220.399 degrees, which in rectangular coordinates is T = (−0.1604 − j0.1365).

A faster way of completing this last exercise would be to perform the addition and subtraction of Z_0 by inspection, and divide the numerator by the denominator in the following manner:

15 ± x ≷t 10 ± INV 2nd P→R SBR: ÷85±x ≷t 10±INV 2nd P→R SBR=

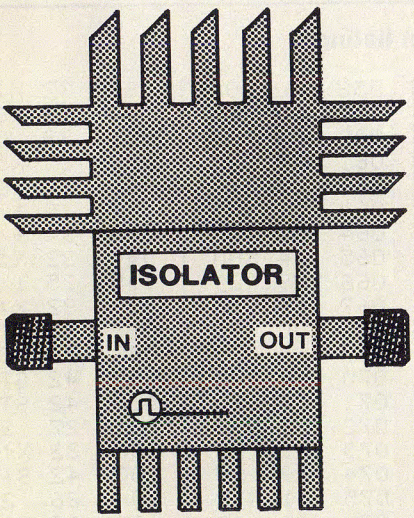
The result will be the same as obtained previously, in polar coordinates.

As demonstrated by these four program examples, the complex arithmetic operations are fairly straightforward, relying on a logical data-entry procedure. The program requires only 114 steps, leaving more than adequate memory space for other programs. ••

Reference

1. *TI Programmable 58/59 Electrical Engineering*, Texas Instruments, p. 17, 1979.

HIGH POWER



ISOLATORS
CIRCULATORS
R.F. LOADS
ATTENUATORS
POWER SPLITTERS

100 TO 3,000 MHz
500,000 WATTS PEAK
2,000 WATTS cw
5% and 30% BANDWIDTH
CHOICE OF CONNECTORS

MOST DELIVERIES MADE WITHIN 2 WEEKS ARO

PLEASE CONTACT:

FERRITE CONTROL CO. DIVISION
MICON INC.
1105 Industrial Parkway, Brick, New Jersey 08723
(201) 458-3333 Telex 642-651 Micon Inc Bktn

READER SERVICE NUMBER 65

power; define the exact duty cycle; sample and store the peak pulse voltages at several sites; and derive the peak power with reference to any one, or an average of all, time sites.

CW power is available to almost 20W through the TWTA. Input pulse power of 20 to 200 W is served through the narrow-pulse amplifier. However, the dynamic range of the subsystem is a problem. Saturated operation must be maintained by varying the voltage of a power supply together with the TWTA input power (a more versatile pulse amplifier would simplify matters).

Amplitude analysis is performed by a fast-sampling voltmeter that has a 1.5-μs "window." A digitizing oscilloscope, at considerable additional cost, is under consideration as a more versatile approach. Time domain information is derived from a counter with a 0.5-GHz time base (Fig. 3).

Despite these limitations, SIFT III operates with repeatability that is at least three times better than that of any manually operated synchronous detection scheme previously tried. The dynamic range of the narrow-pulse amplifier represents an important improvement over the manual systems. The transistors used are designed for uniform class-C output conditions and operate within a restricted duty-cycle range (Fig. 4).

Another automatic test system, called SIFT IV, has been designed for the evaluation of class-A linear devices. As soon as it became operational, it took on the added function of testing class-C transistors at low power. Class-C devices require an input-power-setting resolution of 0.1 dB, but SIFT IV's resolution is 1 dB since that is adequate for testing class-A devices. To improve resolution, the frequency synthesizer DC-coupled AM input is connected to a digital-to-analog converter under bus control. Input power is controlled by looping the input power meter through the DAC. The converter's program restricts the linear amplitude to a specific linear region of the synthesizer's operating curve. This demonstrates the inherent flexibility of a system having common-control building blocks. ••

Moving?

1. For FASTEST service you must attach old mailing label in space below.

If mailing label is not available print your old Company name and address in this box

Please allow 6 weeks for change to take effect

2. Print your NEW business address here

NAME_____ TITLE_____

COMPANY _____

ADDRESS _____

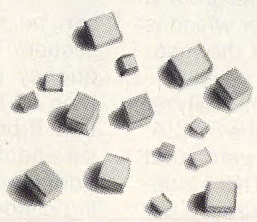
CITY_____ STATE_____ ZIP_____

3. Mail to:

MicroWaves
P.O. Box 1419
Riverton, NJ 08077 USA



MICROWAVE CHIP CAPACITORS



TRUST! For twenty-eight years Microwave Circuit Designers have trusted Pyrofilm to deliver the highest quality microwave components. Now, when Pyrofilm, a leader in microwave film technologies, offers a microwave monolithic chip capacitor, you know that this trusted experience goes into every chip. DELIVERY! Equally as important, Pyrofilm delivers from stock. PERFORMANCE! Pyrofilm capacitors offer superior performance in microwave applications. "Q" factors are greater than 10,000 and the devices offer very low noise figures and insertion loss characteristics. These capacitors are designed to meet the requirements of Mil-C-55681.

KDI PYROFILM

For Additional Information - Call TOLL FREE - **(800) 221-0357**

60 S. Jefferson Road, Whippany, N.J. 07981 • (201) 887-8100 • TWX (710) 986-8220

P 83-5

Cover Feature

Integration arms receiver with low noise floor

A measurement receiver that combines the features of a sensitive power meter, a modulation analyzer, and an audio analyzer performs power measurements down to −127 dBm. Some new tricks were needed to keep the noise at bay.

Mike McNamee, Development Engineer, Hewlett-Packard Co., 1620 Signal Dr., TAF C-34, Spokane, WA 99220

The model 8902A Measuring Receiver offers an alternative to the existing avenues of low-level power measurement. It handles input signals from 150 kHz to 1300 MHz and combines the features of a wide-dynamic-range (157-dB) power meter, a tuned modulation analyzer, and an audio analyzer.

Such an instrument is useful in a variety of applications. The 8902A's primary purpose is to calibrate signal generators, but its combinaton of functions allows it to replace larger, more complex multicomponent systems. It can also serve as an attenuation measurement center with a 127-dB dynamic range. Its relative power measurement accuracy is not limited by the need to make an absolute reference calibration. And in transmitter testing, the model 8902A can replace many of the components typically used to measure power, modulation, and audio distortion.

Perhaps the most valuable feature of the 8902A is its tuned RF level measurement capability, which allows power readings to be taken down to −127 dBm (0.1 μV into 50 ohms), with linearity better than 0.5 dB. The fundamental measurement accuracy derives from a model 436A type power meter which is integrated into the circuitry of the measuring receiver.

A model 8901A modulation analyzer has also been integrated into the 8902A. It measures AM depths to 99 percent at rates as high as 100 kHz. The modulation analyzer can also measure FM deviations as high as 400 kHz at rates up to 200 kHz, both with an accuracy of better than ±1 percent. The third type of modulation handled by the modulation analyzer section is phase, at peak deviations up to 400 radians and rates up to 20 kHz, with an accuracy of ±3 percent. Demodulated signals are supplied to a front-panel RF connector for further processing.

Audio measurements of either the demodulated RF signal or an external input can be made with the audio analyzer section. This section features audio frequency counting of signals at better than 50-kHz rates, with six-digit resolution. It provides for true RMS level measurements of signals up to 50 kHz. In addition, it has the capability of analyzing distortion levels down to −54 dB at the standard calibration frequencies of 400 and 1000 Hz.



1. The 8902A Measuring Receiver *works in conjunction with the 11722A sensor module to make power measurements down to −127 dBm.*

Single-conversion receiver

The 8902A is basically a single-conversion receiver with detectors at several key locations (Fig. 2). In most cases, a measurement is made by connecting a model 11722A sensor module to the signal under test. The sensor module contains a thermocouple sensitive to relative power levels; an input signal can be routed into this thermocouple or, through a specially designed RF cable, into the input section of the 8902A. Once in the measuring receiver, the signal is attenuated or amplified to an optimum level for downconversion to an IF of either 455 kHz or 1.5 MHz.

Several measurements are made in the receiver's IF section. A signal is simultaneously amplitude and frequency (or phase) demodulated, and the recovered audio signal is made available at front and rear panel output ports. High-pass and low-pass filters, as well as selectable de-emphasis filters, can be switched in when signal processing is required. And depending on the measurement, peak, RMS, and average detectors are available.

Another component in the IF section

is a new tracking synchronous detector. It provides very linear relative level measurements under extremely noisy conditions. The detector has a wide dynamic range, using 60 dB of variable IF gain as well as the available RF gain and attenuation to achieve that range.

The 455-kHz frequency of the 8902A was chosen to allow the use of common components and electronic switching. As a result, a high degree of accuracy in the IF gain steps was possible, and it was achieved without expensive, elaborate attenuation standards.

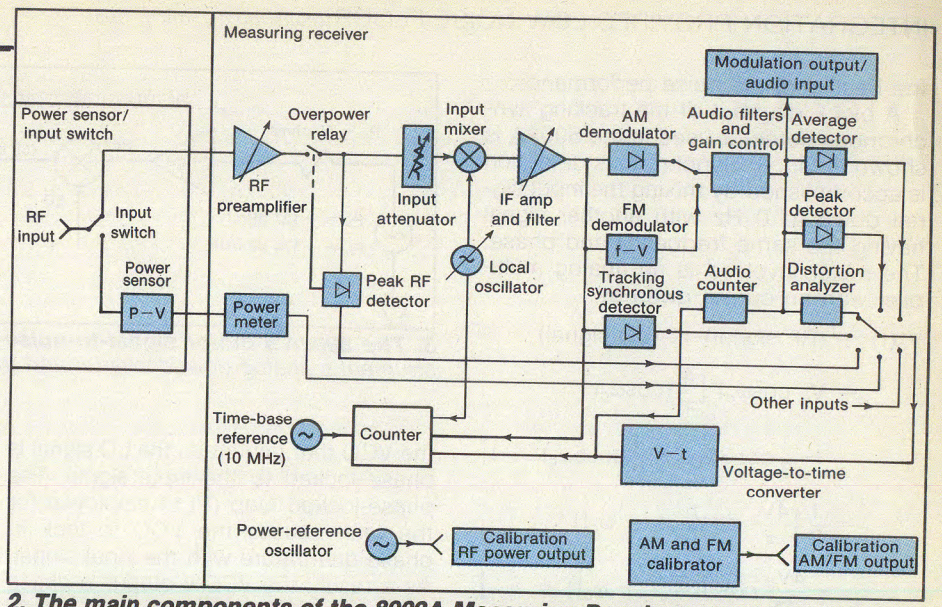
All measurements performed by the 8902A are ultimately made by the frequency counter section. The RF frequency is indirectly read by counting the LO and IF signals and determining the difference frequency, LO − IF. The frequency counter, together with a voltage-to-time converter, doubles as a voltmeter, measuring the outputs of the internal detectors. The voltages are converted into a result that is displayed, with the appropriate units of measurement, on the 8902A's front panel.

The dynamic range of the 8902A is broken down into several measurement ranges. Two measurement modes are used: RF power (which relies on the power sensor in the model 11722A) and tuned RF level (which depends on the IF tracking synchronous detector). The calibration factors for the sensor in the 11722A module are printed on the back of the device. These can be entered into the memory of the 8902A for automatic correction of power sensor frequency response.

The internal power meter is set to the zero point and calibrated by connecting the 11722A to a 0-dBm power reference output from the 8902A's front panel. When an operator presses the "zero" key, the 11722A disconnects the power sensor and the 8902A subtracts any offset in the power metering circuitry under zero-input conditions. When the operator presses the "calibrate" key, the power sensor is switched in and the reference output is turned on. When the "save cal" key is engaged, the output voltage from the power metering circuitry is read by the measuring receiver's internal voltmeter, and the instrument controller equates that voltage to a power level of 0 dBm. From that point on, all readings will be compared to this reference calibration point, and all subsequent measurements can be traced to this initial calibration. (This accuracy is essentially equal to that of the model 436A power meter.)

Ranges rely on TSD

The tuned RF level ranges rely on the tracking synchronous detector (TSD). Each range is obtained by extending the



***2. The main components of the 8902A Measuring Receiver** are shown here. The newly developed tracking synchronous detector appears in the center.*

TSD's basic 15-dB range via 60 dB of IF gain in 10-dB steps. The three overlapping ranges result from three different gain/attenuation configurations in the RF section. The highest range corresponds to 50 dB of RF attenuation, the middle range to 10 dB of attenuation, and the lowest range represents 24 dB of RF gain. This gain is achieved with a broadband, thick-film microcircuit amplifier specifically designed for low input SWR or high input return loss and minimum noise figure.

A high degree of relative accuracy is maintained within each range. The nonlinearity over the 15-dB range of the TSD is only about 0.003 dB, while the 10-dB IF gain step accuracy is approximately ± 0.02 dB.

The overlapping of the RF and tuned RF bands allows for cross-calibration between the ranges. This calibration information is used to achieve absolute calibration to the 0-dBm reference.

In order to calibrate the tuned RF level ranges for measurements to −127 dBm, the following procedure is practiced. First, the RF power measurement range is calibrated with the 0-dBm reference output. Then, the source under test, perhaps a signal generator, is set to the frequency of interest at a level lying in the overlap region between the RF power range and the first tuned RF range. Next, the 11722A sensor module is connected to the source under test, and the tuned RF level mode is selected. The 8902A will automatically tune to the signal. The operator at this point presses the "calibrate" key, which switches the 8902A to the RF power mode. It takes a calibrated level reading using the power sensor, switches back to the tuned RF level mode, and takes another level reading using the tracking synchronous detector. (Through all this, the source under test should be maintained at a constant output power level.) The 8902A then defines the tracking detector output to correspond to the power level just read by the power sensor. Now, the first tuned RF level range is absolutely calibrated. All absolute RF and IF losses are effectively calibrated out at that frequency. In addition, any mismatch errors due to complex impedance differences between the two internal configurations of the power sensor module are also calibrated out.

The other tuned RF ranges are calibrated similarly. Each time a lower range is calibrated, the source under test is simply set to an output level that corresponds to the overlap region between the two ranges of interest.

The calibration data that are obtained by this method are valid for signals within 5 percent of the calibration frequency.

Considering instrument noise

Attempts to accurately measure signal levels as low as −127 dBm are invariably complicated because of the degradation of the predetection signal-to-noise ratio (SNR) by thermal noise. Figure 3 illustrates the major noise-influencing components of the 8902A receiver. The basic level of kTB noise power at −174 dBm/Hz results in an input SNR of 47 dB in a 1-Hz bandwidth. This SNR decreases by the 8902A's double-sideband noise figure of 10 dB, which includes noise from the front end as well as image noise from the single-balanced mixer. An equivalent noise bandwidth of 30 kHz in the IF further decreases the SNR by a value of 10log(30 kHz) or 45 dB. As a result, the SNR in the IF is −8 dB.

Because the SNR is so low, standard signal detection methods are meaningless. For this reason, the synchronous detector unit was developed to provide

(continued on next page)

the best possible noise performance.

A block diagram of the tracking synchronous detector used in the 8902A is shown in Fig. 4. Synchronous detection is accomplished by mixing the input signal down to 0 Hz with another signal having the same frequency and phase. The mixer involved is an analog multiplier with an output given by

$$V_o(t) = (\text{RF signal}) \times (\text{LO signal})$$

$$= V_s \cos\omega_c t \left[\frac{4}{\pi}(\cos\omega_c t - \frac{1}{3}\cos 3\omega_c t + \frac{1}{5}\cos 5\omega_c t \ldots)\right]$$

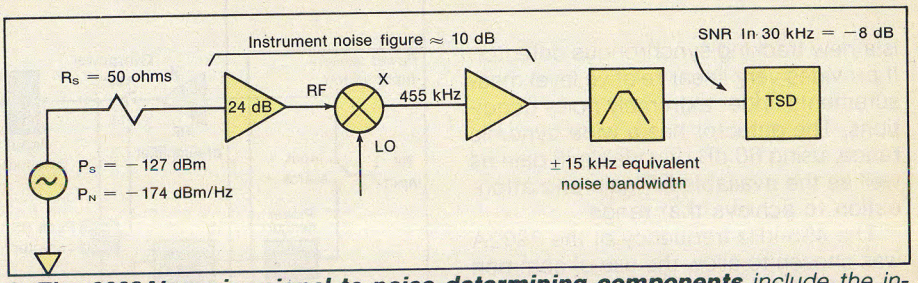
$$= \frac{1}{2}\left[\frac{4V_s}{\pi}\cos(\omega_c t \pm \omega_c t) - \frac{4V_s}{3\pi}\cos(3\omega_c t \pm \omega_c t) + \ldots\right]$$

$$= \frac{2V_s}{\pi} + \frac{2V_s}{\pi}\cos 2\omega_c t - \frac{2V_s}{3\pi}\cos 2\omega_c t + \text{higher frequency terms} \quad (1)$$

This output is processed through a low-pass filter, leaving $2V_s/\pi$, a DC component proportional to the input signal level. If the input signal happens to be amplitude modulated, the demodulated audio will also appear at the output of the synchronous detector.

At high input SNRs, detection linearity is determined by the switching multiplier. As a result, nonlinearities as small as approximately 0.003 dB for each 10-dB input change are possible. Complications arise, however, when the SNR is reduced; in this case, significant nonlinearities can result.

Most of the TSD's circuitry is used to generate the high-level LO input signal required by the mixer. This signal must be in phase with the test input signal and must be capable of tracking an input that may be drifting over several kilohertz. In order to accomplish this, the VCO that generates the LO signal is phase locked to the input signal. The phase-locked loop (PLL) employed for the task causes the VCO to lock in phase quadrature with the input signal. As a result, the VCO's output is phase shifted by 90 degrees in order to create the proper zero-degree phase relationship between the LO and the input signal. The synchronous detector error, as well as the overall loop response, is determined by the PLL filter.



***3. The 8902A's major signal-to-noise-determining components** include the instrument's analog downconverter and the tracking synchronous detector (TSD).*

Synchronous detection offers considerable improvement in noise performance over conventional envelope detection techniques. For example, assume an input signal consists of an unmodulated carrier at 455 kHz surrounded by ±15 kHz additive noise. The noise can be separated into two independent in-phase and quadrature components: $\eta_i(t)$ and $\eta_q(t)$. These components are uncorrelated stochastic signals, limited in bandwidth to 15 kHz. As a result, the composite input signal looks like:

$$V_i(t) = A\cos\omega_c t + \eta_i(t)\cos\omega_c t - \eta_q(t)\sin\omega_c t \quad (2)$$

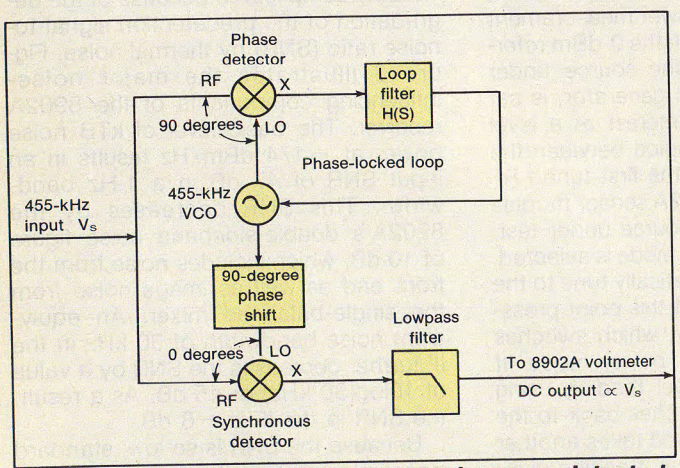
To simplify this form, consider an ideal LO signal, $2\cos\omega_c t$, and perform basic linear analog multiplication. Equation 2 then becomes:

$$v_o(t) = 2\cos\omega_c t\,[A\cos\omega_c t + \eta_i(t)\cos\omega_c t - \eta_q(t)\sin\omega_c t]$$

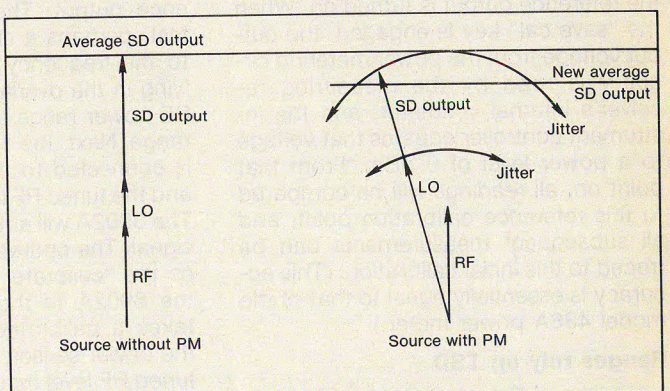
$$= A\cos(\omega_c t \pm \omega_c t) + \eta_i(t)\cos(\omega_c t \pm \omega_c t) - \eta_q(t)\sin(\omega_c t \pm \omega_c t)$$

$$= A + \eta_i(t) + [A + \eta_i(t)]\cos 2\omega_c t - \eta_q(t)\sin 2\omega_c t \quad (3)$$

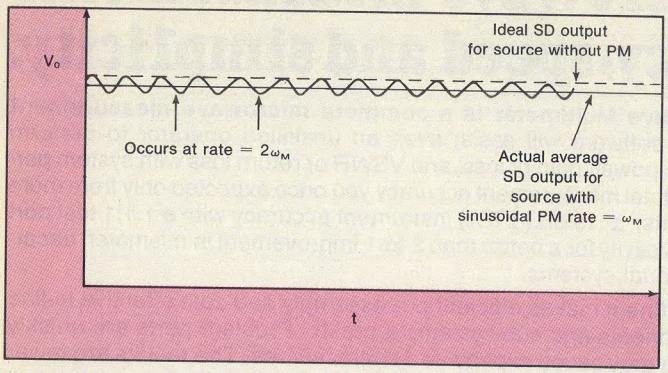
This result highlights two advantages to the use of synchronous detection. For one thing, the noise is additive at the output. It isn't multiplied onto the input signal as in envelope detection. As a result, the desired signal can always be recovered. Output noise can be reduced whenever necessary simply by adding low-pass filtering to the output. It should be noted, however, that filtering adds delay to the response time and should be used only when the noise level absolutely must be lowered. The second advantage in using synchronous detection is that only the in-phase noise component is translated to DC; the quadrature component is rejected. When downconverted, the noise sidebands on each side of the input carrier "fold over" and add in power level, since the two sidebands are uncorrelated. In contrast, the peak value of the input signal is translated directly to the output, due to the synchronization of the LO with the carrier. The power in the desired output component is related to the peak of the



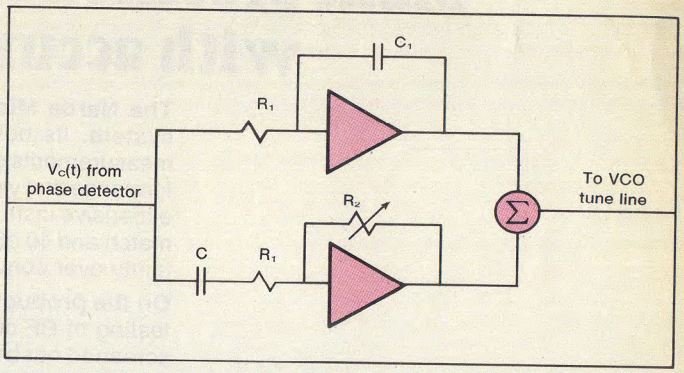
***4. This closeup of the tracking synchronous detector's hardware** reveals how the VCO locks in phase quadrature to the 455-kHz input signal.*



***5. The inputs to the synchronous detector can be represented as phasors.** The ideal case (left), a source with no phase modulation, is compared to an actual case (right).*



6. Phase modulation on the output of the synchronous detector *causes a level that fluctuates below the ideal case.*



7. This phase-locked loop filter *was implemented to correct for phase errors in the synchronous detector.*

input signal voltage. The undesired noise output power is related to the RMS noise input voltage.

Unfortunately, these two advantages hold only for ideal synchronous detection, where the LO signal is exactly in phase with the input signal. Most problems associated with implementing synchronous detectors stem from the inability of the PLL to provide an LO signal with exactly the right phase.

One of the realities faced by designers of synchronous detectors is the unavoidable existence of residual phase modulation on the input signal. The synchronous detector is specifically designed for use with CW signals. When there are fluctuating phase conditions at the input signal, the PLL will attempt to follow and track out the phase modulation. If the bandwidth of the PLL were large enough to accept all the phase-modulated sidebands contained with the input signal, the VCO would track the incoming signal's phase perfectly, and the two inputs of the synchronous detector would be exactly in phase. However, due to noise constraints, the bandwidth of the PLL must be narrow.

The synchronous detector inputs can be viewed as phasors that are multiplied together (Fig. 5). The synchronous detector's output is proportional to the cosine projection of the input phasor on the LO phasor. The maximum output occurs when the two phasors line up exactly. The slight PLL mistracking caused by residual input phase modulation produces the relative phase jitter between the inputs. This jitter causes the average output level to fluctuate below the ideal maximum output level.

The effect of having the actual synchronous detector output at a lower than ideal level can be illustrated by the

(continued on p. 107)

Editorial call

SAW design competition

The editors of **Microwaves & RF** invite you to enter a design competition for new surface acoustic wave applications.

Articles must be received by August 1, 1983.

Articles should be five to eight typewritten pages (double-spaced) with a maximum of two illustrations.

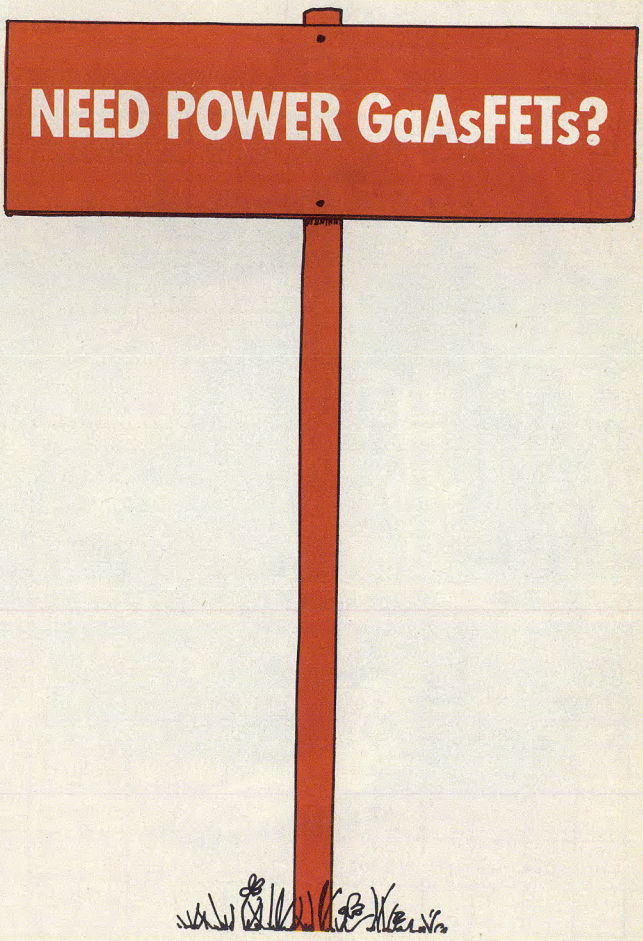
All authors who submit articles to the competition will receive a special token of appreciation.

Authors selected for publication will receive an honorarium and become eligible for the competition.

Judging will be by reader poll.

Send manuscripts to:

"I SAW it in Microwaves & RF"
c/o Ms. Cathleen Fedele
50 Essex Street
Rochelle Park, NJ 07662



following example. Suppose that the input signal has a small amount of sinusoidal pulse modulation at a rate of ω_m, with a peak deviation of β radians. Relying on an analysis similar to that which led to Eq. 1, the synchronous detector output can be shown to be

$$v_o(t) = \frac{2V_s}{\pi} \cos [\beta\cos\omega_m t - \beta'\cos(\omega_m t + \theta)] + \text{higher frequency terms} \quad (4)$$

where β is the equivalent peak LO phase deviation in radians, and θ is the phase error between the two inputs. If ω_m is much less than the PLL bandwidth, the VCO will track the input signal almost perfectly. This ideal case produces a synchronous detector output of $2V_s/\pi$.

When ω_m is much greater than the PLL bandwidth, the VCO will track very little of the incoming phase modulation, and the detector output can be approximated by:

$$v_o(t) \simeq \frac{2V_s}{\pi} \cos (\beta\cos\omega_m t) \quad (5)$$

This can be expanded with the Bessel series representation of

$$\cos (x\cos\phi) = J_o(x) - 2J_2(x)\cos 2\phi + 2J_4(x) \cos 4\phi \ldots \quad (6)$$

which yields

$$v_o(t) = \frac{2V_s}{\pi} [J_o(\beta) - 2J_2(\beta)\cos 2\omega_m t + \ldots] \quad (7)$$

where the J terms are Bessel coefficients.

For small β deviations, the synchronous detector output can be approximated by the first two terms shown above, a DC and an AC term. Since the term $J_0(\beta)$ is less than or equal to 1, which indicates that suppression of the DC term is taking place, there will be errors for inputs with phase modulation, as shown in Fig. 6.

If the phase errors as a percentage of DC output were constant, they would cancel in any relative measurement. Unfortunately, the percentage of error changes with the input level. Because of the design of the PLL phase detector, the equivalent loop bandwidth is proportional to the input level. This changing bandwidth causes different amounts of input phase modulation to be tracked out by the VCO as the input level changes. Assuming that the input signal's spectral purity remains constant as the signal level varies, the change in PLL tracking produces a change in the percent error in the synchronous detector's DC output. The end result is a nonlinearity in relative level measurements.

The solution adopted in the 8902A for these phase-induced nonlinearities was to implement the PLL filter shown in Fig. 7. The approach is relatively standard, with the exception that the AC gain path has been made variable. Gain is controlled by a multiplying digital-to-analog converter that changes the effective value of resistor R_2. If capacitor C is large enough, the transfer function of this loop filter will be:

$$H(s) = -\left[\frac{R_2}{R_1} + \frac{1}{sC_1R_1}\right] \quad (8)$$

This loop filter allows the PLL bandwidth to be held constant, regardless of input signal level, thereby eliminating the PM-induced error. The second major problem that must be overcome when using a tracking synchronous detector is additive noise at the input. This error will occur regardless of the spectral purity of the input carrier. It depends only on the input additive noise level. The error increases as the input SNR decreases.

Additive noise errors are caused by phase modulation of the VCO. In a

(continued on next page)

Moving?

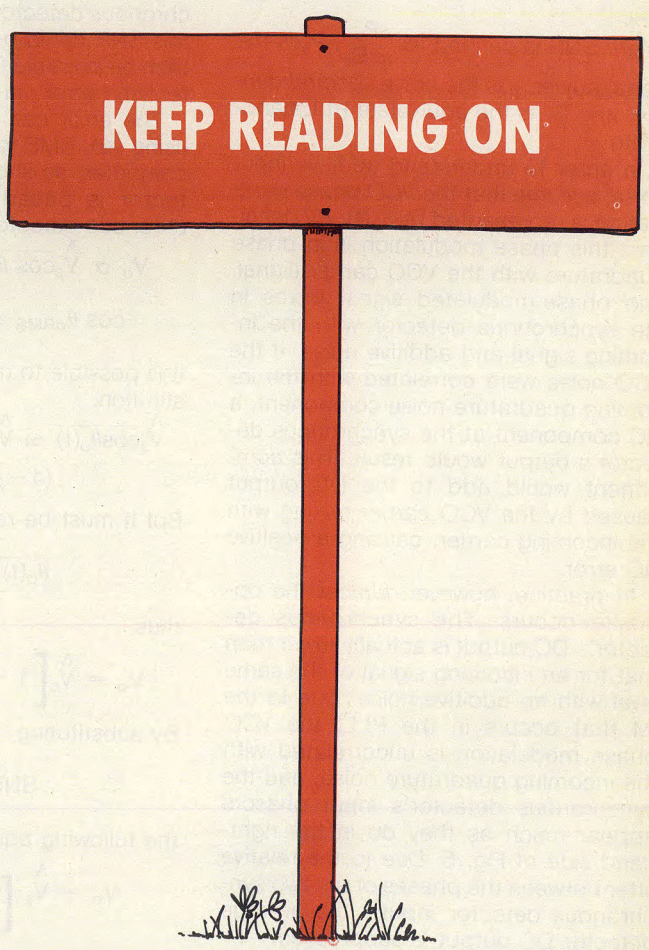
1. For FASTEST service you must attach old mailing label in space below.

Please allow 6 weeks for change to take effect

If mailing label is not available print your old Company name and address in this box

2. Print your NEW business address here
NAME_____TITLE_____
COMPANY_____
ADDRESS_____
CITY_____STATE_____ZIP_____

3. Mail to:
MicroWaves
P.O. Box 1419
Riverton, NJ 08077 USA



mathematical analysis, assume that the input with the additive noise looks like

$$v_i(t) = V_s\cos\omega_c t + \eta_i(t)\cos\omega_c t - \eta_q(t)\sin\omega_c t \quad (9)$$

while the VCO signal appears as

$$2\sin(\omega_c t + \theta_o(t))$$

Since the phase detector is essentially a switching mixer like the synchronous detector, the phase detector output can be given by:

$$v_e(t) = V_s\sin\theta_o(t) + \eta_i(t)\sin\theta_o(t) - \eta_q(t)\cos\theta_o(t) \quad (10)$$

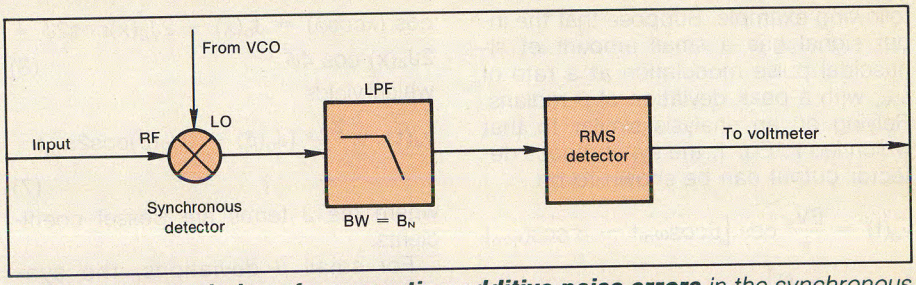
which does not include higher-frequency terms removed by the loop filter. In order to find the error caused by the VCO's phase modulation, the term $\theta_o(t)$ must be determined. Unfortunately, due to intermodulation (IM) in the PLL between the VCO phase modulation quadrature sidebands, and in-phase and quadrature components on the incoming additive noise, this determination is not straightforward. The best solution lies in a statistical representation of the magnitude of $\theta_o(t)$. Previous analyses have shown that a relationship exists between $\overline{\theta_o(t)^2}$ and the SNR in the loop[1]:

$$\overline{\theta_o(t)^2} \simeq \frac{1}{2SNR} \quad (11)$$

where SNR is defined as $\frac{P_s}{\eta 2B_L}$, P_s is the signal power, η is the noise spectral density, and B_L is the equivalent PLL bandwidth.

In order to understand additive input noise, assume that the VCO phase modulation is represented by $\theta_o(t)$. By definition, this phase modulation is in phase quadrature with the VCO carrier signal. The phase-modulated signal mixes in the synchronous detector with the incoming signal and additive noise. If the VCO noise were correlated with the incoming quadrature noise component, a DC component at the synchronous detector's output would result. This component would add to the DC output caused by the VCO carrier mixing with the incoming carrier, causing a positive DC error.

In practice, however, almost the opposite occurs. The synchronous detector's DC output is actually lower than that for an incoming signal of the same level with no additive noise. Due to the IM that occurs in the PLL, the VCO phase modulation is uncorrelated with the incoming quadrature noise, and the synchronous detector's input phasors appear much as they do in the right-hand side of Fig. 5. Due to the relative jitter between the phases of the two synchronous detector inputs, the average detector DC output is suppressed.



8. This is one technique for correcting additive noise errors *in the synchronous detector. It relies on using an RMS detector as an analog computer.*

Since the detector's DC output is proportional to the average cosine projection of the input phasor on the VCO phasor, the detector output error can be calculated from the SNR in the loop. The procedure is as follows:

$$v_o(t) \propto \overline{\cos\theta_o(t)} \simeq \cos\theta_{oRMS} \quad (12)$$

$$\theta_{oRMS} = \sqrt{\overline{\theta_o^2}} \simeq \sqrt{\frac{1}{2SNR}} \quad (13)$$

$$\text{Error (dB)} = 20\log\cos\theta_{oRMS} = 20\log\cos\left[\frac{1}{\sqrt{2SNR}}\right] \quad (14)$$

If this error were a constant percentage of the input signal level, it would cancel, since the level measurements are relative. However, the error is a function of the SNR, which varies with changes in the input level, resulting in a synchronous detector output nonlinearity. If this SNR could be determined, it would then be possible (in the software) to correct the error via Eq. 14.

The error can also be corrected by using an RMS detector in an analog computer, as shown in Fig. 8. This detector is based on the known synchronous detector output of

$$V_o \propto \hat{V}_s\overline{\cos\theta_o(t)} \simeq \hat{V}_s\cos\theta_{oRMS}$$

$$\cos\theta_{oRMS} \simeq 1 - \frac{\theta_{oRMS}^2}{2} \quad (15)$$

It is possible to make the following substitution:

$$\hat{V}_s\overline{\cos\theta_o(t)} \simeq \hat{V}_s\left(1 - \tfrac{1}{2}\theta_{oRMS}^2\right) = \hat{V}_s\left(1 - \tfrac{1}{2}\overline{\theta_o(t)^2}\right) \quad (16)$$

But it must be remembered that

$$\overline{\theta_o(t)^2} = \frac{1}{2SNR}$$

thus,

$$V_o = \hat{V}_s\left[1 - \tfrac{1}{2}\left(\frac{1}{2SNR}\right)\right] \quad (17)$$

By substituting

$$SNR = \frac{P_s}{2\eta B_L}$$

the following equivalency is obtained:

$$V_o = \hat{V}_s\left[1 - \tfrac{1}{2}\left(\frac{1}{\frac{2P_s}{\eta 2B_L}}\right)\right] = \hat{V}_s\left(1 - \frac{1}{4}\frac{2\eta B_L}{P_s}\right) \quad (18)$$

Building upon this equation, the RMS detector input (V_i) can be written as:

$$V_i = V_{DC} + V_{AC} - V_s\left(1 - \tfrac{1}{4}\frac{2\eta B_L}{P_s}\right) + \hat{V}_s\frac{V_n}{\hat{V}_s}(\text{in } B_N);$$

$$\overline{V_i^2} = \overline{(DC + AC)^2} = \overline{DC^2} + \overline{AC^2} + \overline{2DC\cdot AC} = \overline{DC^2} + \overline{AC^2} \quad (19)$$

where the synchronous detector AC input (the noise voltage) is represented by V_n. By substituting the AC and DC voltage terms into this last equation, the following form results:

$$\overline{V_i^2} = \hat{V}_s^2\left(1 - \tfrac{1}{4}\frac{2\eta B_L}{P_s}\right)^2 + \hat{V}_s^2\left[\frac{V_n(\text{in } B_n)}{\hat{V}_s}\right]^2 = \hat{V}_s^2\left[1 - \tfrac{1}{2}\frac{2\eta B_L}{P_s} + \frac{1}{16}\left(\frac{2\eta B_L}{P_s}\right)^2\right] + \hat{V}_s^2\frac{V_n^2(\text{in } B_N)}{\hat{V}_s^2}$$

$$\simeq \hat{V}_s^2\left(1 - \tfrac{1}{2}\frac{2\eta B_L}{P_s}\right) + \hat{V}_s^2\left[\frac{P(\text{in } B_N)}{\hat{V}_s^2}\right] \quad (20)$$

where P is the average power.

Since

$$\frac{P.(\text{in } B_N)}{\hat{V}_s^2} = \frac{\text{Power In Noise Out Of SD}}{2 \times P_s \text{ In The IF}} = \frac{2\eta B_N}{2P_s} \quad (21)$$

by substituting into Eq. 20, the final result appears as:

$$\overline{V_i^2} = \hat{V}_s^2\left(1 - \tfrac{1}{2}\frac{2\eta B_L}{P_s}\right) + \hat{V}_s^2\frac{2\eta B_N}{\hat{V}_s^2} = \hat{V}_s^2\left(1 - \tfrac{1}{2}\frac{2\eta B_L}{P_s} + \tfrac{1}{2}\frac{2\eta B_N}{P_s}\right) \quad (22)$$

This last equation shows that by setting $B_N = B_L$, the last two terms will cancel, leaving $\overline{V_i^2} = \hat{V}_s^2$, so that the error due to additive noise has been effectively cancelled. Of course, this technique relies on a fixed value of B_L. Still, this has been already guaranteed by the technique used to correct for phase modulation on the source.

(concluded on p. 119)

SAW oscillators feature low phase noise

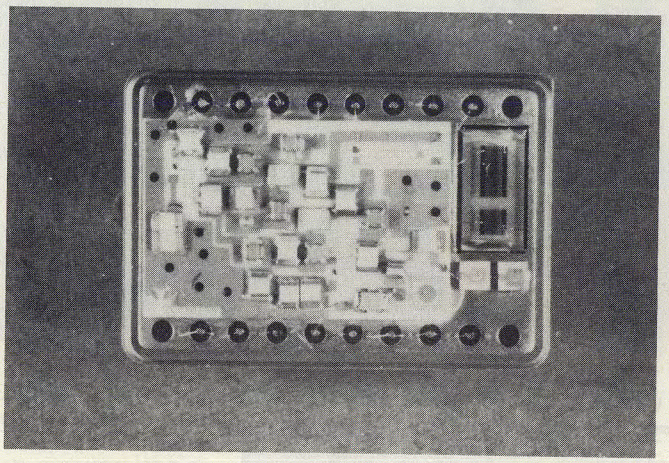
Surface acoustic wave components are starting to shed their "laboratory curiosity" status of several years back. SAW filters are already providing stable rejection performance in some commercial video receiver applications. And with the introduction of the SR series, SAW technology continues to advance in the area of RF oscillators.

The SR series includes SAW oscillators at fixed frequencies from 100 to 600 MHz. The sources feature an outstanding noise floor of −160 dBc/Hz at offsets of 2 kHz from a 100-MHz carrier or 60 kHz from a 600-MHz carrier. For applications where even this phase-noise performance is inadequate, devices can be supplied with a noise floor of −175 dBc/Hz. The harmonic content of an oscillator's output is typically −30 dBc.

These low-noise oscillators are capable of producing output levels from 0 to +26 dBm. They will operate over a temperature range of 0 to 50°C with a maximum temperature stability of 40 PPM/°C. The stability is a remarkable 0.3 PPM/°C at 25°C.

The SR-series oscillators, which measure only 1.1 × 0.8 in. represent one segment of a line of SAW products manufactured by the French firm Thomson-CSF that is now available in this country. The sources run on a typical supply line of +12 VDC and consume no more than 80 mA current. P&A: $525 to $825 (depending on frequency); 120 days. **Phonon Corporation, 7 Herman Dr., P. O. Box 549, Simsbury, CT 06070. (203) 651-0211, telex: 294705.**

CIRCLE NO. 157



The SR series of SAW oscillators *covers frequencies from 100 to 600 MHz with extremely low phase noise.*

INTEGRATION PROVIDES LOW NOISE FLOOR (*continued from p. 108*)

In viewing this technique qualitatively, note that the VCO power is constant. When the PLL transfers phase noise onto the VCO, the power in the VCO carrier is reduced by the amount of power that goes into the phase noise sidebands. Since the synchronous detector output is proportional only to the VCO carrier, the output will be suppressed by this amount. If $B_N = B_L$, the RMS detector will add a voltage based on the same amount of noise power that was taken from the VCO carrier line. P&A: 8902A, $21,000; 11722A, $1900; 90 days. **Inquiries Manager, Hewlett-Packard Co., 1507 Page Mill Rd., Palo Alto, CA 94304. (415) 857-1507. CIRCLE NO. 158**

Acknowledgments

The author would like to acknowledge the enormous contributions of Stuart Carp and Andrew Naegeli of Hewlett-Packard Co. for their work on the theoretical and hardware techniques described in the article.

References

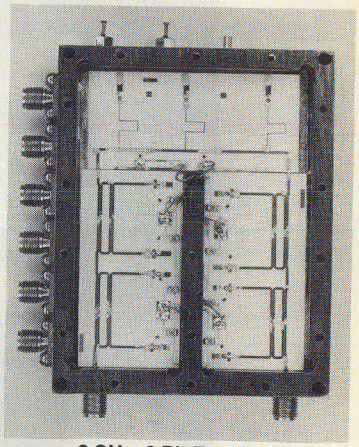
1. F.M. Gardner, *Phaselock Techniques*, 2nd ed. (Wiley, New York, 1979), p. 32.
2. A.B. Carlson, *Communication Systems*, 2nd ed. (McGraw-Hill, New York, 1975).

STATE-OF-THE-ART MICROWAVE

Digital Frequency Translators

Doppler Simulators

- High Carrier and Sideband Suppression
- MIC Construction
- Small Size—Low Weight
- High Reliability



2 GHz, 6-Bit Translator

Frequency, F_0	UHF to X-Band
Bandwidth	Up to 2:1
No. of Bits, N	3-7
Carrier and Sideband Suppression	Up to 40 db
RF Loss	2-6 dB (depends on F_0 & N)
RF Power	Up to +30 dBm
Translation	0 to ±200 kHz (6-bit)
Control	Binary TTL or VCO
DC	+5 V and −15 V
RF Connectors	SMA

VMC is widely recognized for expertise in Digital Frequency Translators (Serrodyne) for use in deceptive-jamming ECM systems and Doppler simulators. Units feature highest carrier and sideband suppression, low loss, high power capability, small size and convenient binary TTL control, or internal VCO clock and decoder. Their rugged MIC construction assures high stability and reliability in military airborne environments. VMC's experience in MIC signal processing circuits results in the highest performance/cost ratio in the industry.

- Digital Phase Shifters, Low and High Power 3-7 Bits, TTL Control, High Accuracy
- Digital Attenuators, Programmable or binary, High Resolution, up to 100 dB Range
- PSK and QPSK Modulators
- PIN Diode Switches, Modulators, Attenuators
- Mixers, Balanced, Image-Reject, Quadrature IF
- Monopulse Converters and Feed Networks
- Integrated Front Ends, Custom MIC Modules

Also: Microstrip Couplers, Hybrids, Power Dividers/Combiners, Video Detectors, Metalized and Etched Substrates.

VMC

VECTRONICS MICROWAVE CORPORATION

P.O. Box 70—276 Lincoln Blvd. Middlesex, N.J. 08846 (201) 356-2377

READER SERVICE NUMBER 72